NON-LINEAR EFFECTS IN THE EVOLUTION OF GALAXY CLUSTERING

Stephen James Dodds

Presented for the Degree of Doctor of Philosophy at the

University of Edinburgh

1995

DECLARATION

This thesis is my own composition, with the exception of Section 2.4 and parts of Subsection 2.3.2, which have been taken from the published paper Peacock & Dodds (1994).

Stephen Dodds

21st June 1995

Contents

List of Figures

List of Tables

ABSTRACT

A review of the cosmological observations and theory necessary for an understanding of the formation and evolution of cosmic large-scale structure is presented in Chapter 1.

The evolution of large-scale structure in the Universe is well understood in the linear regime, where the density is close to the mean density. Where the density contrast is large, the linearization of the equations of motion is no longer valid, and new techniques are needed. To this end, analytic arguments are combined with n-body simulations in Chapter 2, resulting in an analytic correction for the non-linear evolution of clustering. This method, and models of bias and redshift-space distortion, are then applied to a number of observational power spectra, in order to reconstruct the linear power spectrum of cosmic mass fluctuations. Constraints are put on the values of bias parameters, and a high degree of redshift-space distortion is required, $\Omega^{0.6}/b_{IRAS} = 1.0 \pm 0.2$. A Cold Dark Matter power spectrum can be fitted to the data, provided $\Omega h = 0.255 \pm 0.017$.

Chapter 3 is concerned with the formation of galaxy clusters through gravitational collapse. The non-linear techniques developed in Chapter 2 are used to set up the initial conditions for numerical n-body simulations such that the final power spectra are nearly the same for two different cosmological models, $\Omega = 1$ and $\Omega = 0.2$. Galaxy clusters formed in these simulations are identified, and a mean density profile calculated. It is shown that although differences in power spectra have been largely eliminated, significant differences remain in the density profile under different cosmological conditions.

In Chapter 4, the angular correlation function, $w(\theta)$, of faint blue galaxies is considered. Simple models of the evolution of clustering are unable to reproduce the observed $w(\theta)$ of the faint galaxies, over-predicting the amplitude of $w(\theta)$ by nearly an order of magnitude.

The non-linear evolution model of Chapter 2 is applied to the present epoch correlation function, and it is found that the agreement with the observations is significantly improved, and that the model predictions are consistent with the observations, provided that the faint blue galaxies lie at the highest redshift allowed by the observations. Low Ω models are disfavoured, as they are unable to reproduce the observed shape of $w(\theta)$, approximately described by a power-law. A Cold Dark Matter model, with $\Omega = 1$, is able to reproduce this shape well.

Chapter 1

INTRODUCTION

The work of this thesis is concerned with understanding and modelling the growth of large-scale structures in the Universe. In order to achieve this, a general familiarity with some areas of cosmology and a more thorough knowledge of others is required. Section 1.1 reviews briefly the so-called 'Standard Model' of cosmology, the observational consequences of which are described in Section 1.2. The content of the Universe, luminous matter, dark matter, radiation and the implications of its existence on cosmic mass measurements are considered in Section 1.3. The inflationary theories invoked to explain some troublesome features of the Hot Big Bang model are considered in Section 1.4. The statistical techniques used to describe large-scale structure, as well as theories of its origin and evolution are reviewed in Section 1.5. A brief description of the rest of this thesis in the context of this review of cosmology is given in Section 1.6.

1.1 Hot Big Bang Cosmology

1.1.1 The Cosmological Principle

The Cosmological Principle (CP) which constrains theory (and indeed reduces the number of possible models to a manageable number) is simply this:

The Universe is isotropic about every point,

which implies that the Universe is also homogeneous. There is no evidence to support the claim that the Earth exists in a special place in the Universe, or that there exist any special places. This principle is maintained, philosophically, because it is the simplest, and practically, because it greatly simplifies the possible cosmological models. On scales below 100 Mpc, the Universe is clearly neither homogeneous nor isotropic about the Earth. However, there is evidence (such as the decline in the amplitude of galaxy clustering on large scales, see Section 1.5) to suggest that on larger scales, the CP is valid. Certainly, it is justified to maintain the CP until strong evidence opposing it is produced.

1.1.2 Cosmological Geometry

Consider a four-dimensional space-time. At every point in this space time, an observer can, in principle, be placed in a locally inertial frame of reference. The nature of these hypothetical observers can be chosen such that their motion is not influenced by non-gravitational physical processes. In this case, the observers will remain inertial, and their motions will follow the evolution of the space-time, defining a spatial coordinate system known, for this reason, as comoving. These observers are known as *fundamental* observers. The fundamental observers can then be issued with identical clocks, with which to measure their proper times, and the instruction to start their clocks when the local density of the Universe reaches some chosen value. In this way, a cosmological time coordinate can be established, which, in a homogeneous cosmology, can be identified with the proper time of the fundamental observers. There are, *ab initio*, an infinite number of possible geometries for a four-dimensional space-time. However, the Cosmological Principle reduces the range of possibilities to three, as investigated variously by Friedmann, Lemaître, Robertson and Walker (FLRW). A thorough derivation of the FLRW metric is given by Weinberg (1972), but it will suffice here to comment briefly on the application of the CP to the metric. Consider a metric equation

$$\mathrm{d}s^2 = g_{\mu\nu}\mathrm{d}x^\mu \mathrm{d}x^\nu, \tag{1.1}$$

where Greek indices run from 0 to 3, and the Einstein summation convention is followed. From the CP, it is clear that $g_{\mu\nu}$ must be independent of position, x^{μ}. In order that the time variable, x^0, and definitions of simultaneity based on it, agree with the locally valid Lorentz frame of Special Relativity, the time-space cross terms, g_{0i}, must vanish, and the time-time coefficient should be simply the c^2 of Minkowski spacetime. (Here Roman indices cover the three spatial dimensions, running from 1 to 3). Isotropy then implies that any time dependence in the spatial-spatial coefficients should be the same for all, and can be factored out into a scale factor, $a(t)$. Weinberg (1972) shows that spaces described by such a metric are spaces of constant curvature, and also that any two such metrics with the same curvature constant can be related by a coordinate transformation. One conventional coordinate choice, with the dimensions contained in the scale factor $R(t)$, and using an angular diameter distance can be written

$$\mathrm{d}s^2 = c^2\mathrm{d}t^2 - R^2(t)\left[\frac{\mathrm{d}r^2}{1-kr^2} + r^2(\mathrm{d}\theta^2 + \sin^2\theta\mathrm{d}\phi^2)\right]. \tag{1.2}$$

Also used is the dimensionless scale factor, normalised to be unity at some reference time, usally the present epoch, $a(t) \equiv R(t)/R(t_0)$. Since the coordinate system labels fundamental observers, the radial coordinate, r, is a comoving coordinate. The curvature constant, k, can, by a suitable rescaling of r, be constrained to take values of -1, 0, or $+1$. Then the spatial metric is hyperbolic, flat, or spherical, respectively. This radial coordinate, r, is described as a 'comoving angular diameter distance' because in these units, the diameter of an object subtending angle $\mathrm{d}\phi$ at the observer is $r\mathrm{d}\phi$ whatever the geometry of the cosmology. It can be written in terms of the 'ruler distance', $\hat{r}$, by, depending on the geometry, $r = \hat{r}$ if $k = 0$ (flat), $r = \sin\hat{r}$ if $k = 1$ (spherical, or closed), or $r = \sinh\hat{r}$ if $k = -1$.

In the Robertson-Walker metric, the cosmological scale-factor, $a(t)$, is unconstrained. Clearly, if it increases with time, the Universe is expanding, and vice-versa. The equations governing the evolution of $a(t)$ are discussed in Section 1.1.4 below. Observationally, it is found that $a(t)$ is an increasing function of time; the Hubble parameter, $H = \dot{a}/a$, is found today to be approximately $40 - 100\ \mathrm{kms}^{-1}\mathrm{Mpc}^{-1}$ (Peebles 1993; see also Pierce *et al.* 1994, and Freedman *et al.* 1994, for recent estimations). This figure is the subject of much debate; for this reason, the Hubble parameter is usually written

$H = 100\,h\ \mathrm{kms}^{-1}\mathrm{Mpc}^{-1}$, where the dimensionless parameter h can be retained explicitly in any calculation.

1.1.3 Radiation and Thermodynamics

Probably the most important observational consequence of the expansion of the Universe is the cosmological redshift. Consider light emitted by a source at position r_e and observed at the origin, $r = 0$. Since photons travel along null geodesics, it follows from the metric, Eqn.(1.2), that

$$\int_0^{r_e} \frac{dr}{\sqrt{1-kr^2}} = \int_{t_e}^{t_o} \frac{dt}{a(t)}. \tag{1.3}$$

If we associate this pair of emission and observation times with one wave-crest of the light, the propagation of the next crest, emitted at time $t_e + \Delta t_e$ and observed at time $t_o + \Delta t_o$, will satisfy

$$\int_0^{r_e} \frac{dr}{\sqrt{1-kr^2}} = \int_{t_e+\Delta t_e}^{t_o+\Delta t_o} \frac{dt}{a(t)}. \tag{1.4}$$

Then since the rate of expansion of the Universe is much slower than the cycle rate of the light, it follows that

$$\frac{\Delta t_e}{a(t_e)} = \frac{\Delta t_o}{a(t_o)}, \tag{1.5}$$

demonstrating that the interval between wave crests gets longer for a photon travelling in an expanding Universe. It is trivial to show, using the definition of redshift, $z = (\lambda_o - \lambda_e)/\lambda_e$, that

$$z = \frac{a(t_o)}{a(t_e)} - 1. \tag{1.6}$$

If the contents of the Universe are modelled as uniform gases, then writing the First Law of Thermodynamics ($\mathrm{d}U = -p\mathrm{d}V$) in terms of cosmic scale factor a, and comoving density ρ gives

$$c^2 \frac{\mathrm{d}\rho}{\mathrm{d}a} + 3\left(\frac{p + \rho c^2}{a}\right) = 0. \tag{1.7}$$

It remains to determine the equation of state for the gas. For non-relativistic particles,

$$p_g = \frac{1}{3}\rho_g c_s^2, \tag{1.8}$$

where c_s is the sound speed in the gas. Substituting into Eqn. (1.7), and using the fact that $c^2 \gg c_s^2$ gives

$$\rho_g \propto a^{-3},\ p_g \propto a^{-5} \propto \rho_g^{5/3}. \tag{1.9}$$

This is understood easily, since ρ_g is just the rest mass density, and so decreases by the same factor that the volume increases. For relativistic particles,

$$p_r = \frac{1}{3}\rho_r c^2, \tag{1.10}$$

which in turn gives

$$\rho_r \propto p_r \propto a^{-4}. \tag{1.11}$$

Here, an additional factor of a^{-1} is introduced due to the redshifting of the photons. A final case to consider is that of a false vacuum, such as is postulated in the inflationary models discussed below. Here the energy density is just the difference between the false vacuum energy and the true vacuum energy; i.e. it is constant. Eqn. (1.7) then gives

$$p_v = -\rho_v c^2. \tag{1.12}$$

Of particular importance is the effect of cosmic expansion on a black-body radiation spectrum. The Planck function for the energy density of a black-body radiation field at temperature T_0 when the cosmic scale factor $a_0 = 1$, is

$$u_0(\nu_0)\mathrm{d}\nu_0 = \frac{8\pi h}{c^3}\frac{\nu_0^3 \mathrm{d}\nu_0}{\exp\left(\frac{h\nu_0}{kT_0}\right) - 1}. \tag{1.13}$$

In a given comoving volume the number of photons of a given mode will be unchanged as the Universe expands. Using this, and applying the mapping $\nu_0 \rightarrow \nu(1+z)$, where z is the redshift at some time at which the radiation field is to be calculated, the energy density at redshift z is found to be

$$u(\nu)\mathrm{d}\nu = \frac{8\pi h}{c^3}\frac{\nu^3 \mathrm{d}\nu}{\exp\left(\frac{h\nu}{kT}\right)-1}, \tag{1.14}$$

where $T = (1+z)T_0$, i.e. a black body spectrum at a different temperature.

1.1.4 General Relativity and the Friedmann Equations

Using the CP, uncertainty in the metric has been reduced to the evolution of the scale factor, and whether the Universe is open, closed, or flat. In order to go further, one needs to known the way in which spacetime is curved by the presence of mass. To do this one invokes the theory of General Relativity (GR). It is interesting to note that using Newton's theory of gravitation, one can construct a spherically symmetric model, the evolution of which agrees with the relativistic Friedmann equations (below), provided that one identifies a constant of integration in the Newtonian model with the curvature constant, k.

The Einstein field equations of General Relativity are

$$R_{\mu\nu} - \frac{1}{2}Rg_{\mu\nu} + \Lambda g_{\mu\nu} = \frac{8\pi G}{c^2}T_{\mu\nu}. \tag{1.15}$$

This equation deserves some explanation. $R_{\mu\nu}$ is the Ricci tensor, and is related ultimately to the metric tensor, $g_{\mu\nu}$, and its derivatives. The Ricci scalar, R, is found by contracting $R_{\mu\nu}$. Einstein, motivated by a desire to produce a static cosmological model, introduced the constant term, $\Lambda g_{\mu\nu}$, but dropped this after the discovery by Hubble (1925) that the Universe was expanding. The cosmological constant, Λ, has recently found favour again, as a means to ensure the flatness of the Universe, and to explain clustering statistics. On the right hand side of the equation is Newton's gravitational constant, G, and the stress-energy tensor $T_{\mu\nu}$. For a perfect fluid, this takes the form

$$T_{\mu\nu} = (\rho + p/c^2)u_\mu u_\nu + pg_{\mu\nu}, \tag{1.16}$$

where p is the pressure, ρ the density, and u_μ the four-velocity of the fluid. Isotropy implies that there can be no three-velocity with respect to the fundamental observer, and since the frame of reference is locally Minkowskian, this reduces to

$$T_{\mu\nu} = \mathrm{diag}(\rho c^2 + 2p, -p, -p, -p). \tag{1.17}$$

It remains only to combine the FLRW metric with $T_{\mu\nu}$ in the field equation, yielding the following two equations, known as the Friedmann equations:

$$\left(\frac{\dot{a}}{a}\right)^2 + \frac{kc^2}{a^2} = \frac{8\pi G}{3}\rho + \frac{\Lambda c^2}{3}, \tag{1.18}$$

and

$$2\left(\frac{\ddot{a}}{a}\right) + \left(\frac{\dot{a}}{a}\right)^2 + \frac{kc^2}{a^2} = -\frac{8\pi G}{c^2}p + \Lambda c^2. \tag{1.19}$$

Taking the difference of these two equations gives the Raychaudhuri equation:

$$\frac{\ddot{a}}{a} = -\frac{4\pi G}{3c^2}(\rho c^2 + 3p) + \frac{\Lambda c^2}{3}. \tag{1.20}$$

Inspection of the first Friedmann equation, Eqn.(1.18), reveals that, in the absence of a cosmological constant, a flat Universe, $k = 0$, obtains if, and only if,

$$\rho = \frac{3}{8\pi G}\left(\frac{\dot{a}}{a}\right)^2 \equiv \rho_c. \tag{1.21}$$

The density of the Universe is then expressed in units of this critical density, and denoted Ω, where

$$\Omega \equiv \frac{\rho}{\rho_c}. \tag{1.22}$$

Writing the cosmological constant as a vacuum energy density, Ω can be expressed as a sum of components, the dependence of which on scale-factor is determined by the equations of state given above:

$$\rho = \rho_{\mathrm{m}} a^{-3} + \rho_{\mathrm{r}} a^{-4} + \rho_{\mathrm{v}}. \tag{1.23}$$

Substituting this into the first Friedmann equation (1.18), and using $\Omega - 1 = kc^2/(H^2a^2)$ yields, after some manipulation

$$\Omega(a) - 1 = \frac{\Omega_0 - 1}{a^2\Omega_v + a^{-1}\Omega_m + a^{-2}\Omega_r - \Omega_0 + 1}, \tag{1.24}$$

where $\Omega_0, \Omega_v, \Omega_m$, and Ω_r are all present epoch values. The negative powers of $a(t)$ in the denominator for all density components except Ω_v mean that if one considered the model at arbitrarily small scale factors, the Universe approaches the $\Omega = 1$ flat model in the absence of a cosmological constant. Some implications of this equation are discussed below in Section 1.4.

Ω then determines the evolution of the Universe; in the absence of any vacuum energy density, if $\Omega = 1$ the Universe will continue to expand indefinitely, but with the expansion rate tending asymptotically to zero; if $\Omega \leq 1$ the expansion will continue for ever, never stopping, and if $\Omega > 1$ the Universe will expand to a maximum size, and then recollapse to a 'Big Crunch'. The FRLW models predict a singularity at time zero, and also at a later time for closed models, at which the laws of physics no longer apply. In order to avoid this, many theorists believe that effects due to the quantization of gravity will prevent the singularity from being reached. Others prefer to include a cosmological constant, the effect of which is also to avoid singularities by causing the Universe to start expanding again after a minimum, non-zero, size is reached.

The evolution of the scale factor is particularly simple in an Einstein-de Sitter ($\Omega = 1$) model, being simply $a \propto t^{2/3}$, from which it is easily shown that the Hubble parameter $H(t) = 2/(3t)$. Not surprisingly, all cosmological calculations are noticeably easier in a flat, Einstein-de Sitter model, and this is one reason why this model is the preferred choice of many workers. Another reason is that of all possible values of Ω, only one stands out, in that the geometry does not change with time, namely $\Omega = 1$. For this reason, it is felt by many to be unlikely that the Universe should choose some undistinguished values of Ω rather than this one. Furthermore, a cosmological model with $\Omega = 1$ is at a point of unstable equilibrium with respect to Ω. If Ω is slightly less than the critical value $\Omega = 1$, then evolution will cause Ω to get smaller with time. Similarly, if Ω starts off greater than one, it will become ever larger. Present estimates of the density of the

Universe suggest that $\Omega > 0.2$. If the Universe is this close to being flat, then it has been calculated that at the Planck time (the natural unit of time derived from the fundamental constants of physics, before which it is thought that quantum gravity should dominate) $\Omega - 1 \leq 10^{-55}$. It is argued that it is unlikely that the Universe should be this close to being flat, but not quite flat (but see below for a discussion of inflationary theories and their explanation for this).

In models where the Universe was dominated at early times by matter or radiation, but not in models where vacuum energy density prevailed, *particle horizons* are shown to occur. A particle horizon about one fundamental observer is the locus of other fundamental observers from whom a light signal, emitted at the moment of the Big Bang, has just reached that first observer. No point in space beyond the particle horizon could possibly have influenced the fundamental observer at that time. Of course, as the Universe continues to expand, signals from ever more distant regions of space will reach the observer, extending the particle horizon. In a closed dust Universe, where the expansion is eventually turned around into a contraction, the particle horizon encompasses the entire Universe at the moment of turn-around.

A second type of horizon, known as an *event horizon*, can be shown to exist in closed models, and models dominated by vacuum energy density at late times, but not in flat or open models with no cosmological constant. Events beyond this horizon will never be able to influence an observer at the origin. The time taken for the signal to travel from such an event to the observer is the upper limit on the integral on the right-hand side of

$$\int_0^r \frac{\mathrm{d}r}{\sqrt{1-kr^2}} = \int_0^t \frac{c\mathrm{d}t}{a(t)}, \tag{1.25}$$

deduced from the metric equation. For these events, $t \to \infty$ or $t = t_{\mathrm{collapse}}$ (in a closed model) without satisfying this equation.

1.2 Observational Consequences of the Hot Big Bang

A number of astronomical observables depend on the cosmological model. Consider the flux of energy from a source at redshift z. In order to see the effects of cosmological

models (i.e. the geometry) it is convenient to change to a new, dimensionless, radial coordinate, χ, with the dimensions contained in a dimensional scale factor, $R(t)$. The new coordinate, χ, is

$$\chi = \int \frac{\mathrm{d}r}{\sqrt{1-kr^2}} = \begin{cases} \sin^{-1} r & \text{for } k = +1, \\ r & \text{for } k = 0, \\ \sinh^{-1} r & \text{for } k = -1. \end{cases} \tag{1.26}$$

With this transformation, the metric becomes

$$\mathrm{d}s^2 = c^2\mathrm{d}t^2 - R^2(t)[\mathrm{d}\chi^2 + f^2(\chi)(\mathrm{d}\theta^2 + \sin^2\theta\mathrm{d}\phi^2)], \tag{1.27}$$

where

$$f(\chi) = \begin{cases} \sin\chi & \text{for } k = +1, \\ \chi & \text{for } k = 0, \\ \sinh\chi & \text{for } k = -1. \end{cases} \tag{1.28}$$

In this notation, the surface area of a sphere becomes $4\pi R^2(t)f^2(\chi)$. In order to determine the geometric dilution of radiation from a point source in such cosmologies as described by the metric above, one need only substitute this area for the more familiar $4\pi r^2$ of flat space, to which it reduces in the case $k = 0$. However, there are also redshift factors to consider. Each photon arriving at the observer is redshifted, so its energy drops by a factor $1 + z$. The same process causes the rate of arrival of photons to drop by the same factor, so the flux of energy received varies as $(R^2(t)f^2(\chi)(1+z)^2)^{-1}$. Radiation emitted in a band of frequency of width $\delta\nu$ will arrive at the observer compressed into a band of width $\delta\nu(1+z)$, so the flux density, which is the energy received per unit time per unit frequency interval, will vary as $(R^2(t)f^2(\chi)(1+z))^{-1}$. The surface brightness, the flux per unit solid angle, also suffers the $(1+z)^2$ reduction due to redshift that the flux does. In addition, the factor $R^2(t_e)/R^2(t_o)$ that arises from taking the ratio of the surface ares of spheres centred on the source and the observer, leads to another factor of $(1+z)^2$, which gives a total dependence on redshift of $(1+z)^4$.

1.3 The Content of The Universe and Ω_0

A standard estimate (but somewhat uncertain because the surveys have not to date been large enough to include many large structures) of the mean luminosity density of the universe, derived from Efstathiou *et al.* (1988), is

$$\langle \mathcal{L} \rangle = 2 \pm 0.7 \times 10^8 h \mathrm{L}_\odot / \mathrm{Mpc}^3. \tag{1.29}$$

Dividing this by the critical density (Eqn. 1.21) gives a value for the critical mass-to-light ratio, which in terms of the solar mass-to-light, gives

$$\left(\frac{M}{L} \right)_{\mathrm{crit}} = 1500 \pm 500. \tag{1.30}$$

Mass-to-light ratios for the visible parts of galaxies are typically in the range $2 \leq M/L \leq 10$, implying a contribution to the cosmic density

$$\Omega_{\mathrm{L}} \sim 0.003 h^{-1}. \tag{1.31}$$

Diffuse intergalactic gas in rich galaxy clusters is detected through its X-ray emission. How much of this gas there is away from rich clusters, where it is expected to be at lower temperatures and harder to detect, is uncertain. However, since no scattering of light from quasars by the Lyman-α line of atomic hydrogen is detected, an upper limit can be placed on the present day (the clouds are at redshift $z \sim 2$) density. The estimated density of gas depends on the geometry of the Universe (i.e. Ω); for $\Omega = 1$, the contribution from the diffuse gas is (Steidel & Sargent 1987)

$$\Omega_{\mathrm{diff}} \leq 1.5 \times 10^{-8} h^{-1}. \tag{1.32}$$

Absorption by discrete clouds of neutral hydrogen is detected, though. The nature of these clouds varies, but they are typically comparable in size to spiral galaxies. The density inferred directly from observations is (Wolfe 1989)

$$\Omega_{\mathrm{clouds}} \approx 0.002 h^{-1}. \tag{1.33}$$

Both these measurements are made at redshift of order 2. Observations at lower redshifts of neutral hydrogen in nearby galaxies yield density contributions an order of magnitude smaller. It is possible that the temperature of the gas has risen sufficiently that the gas has become transparent, or that it has been turned into stars.

In addition to these visible contributions to the density of the Universe, there is evidence that substantially more matter is present but not directly observable; its existence is inferred from its gravitational effects on visible matter. Some of the principal observations are recounted here, along with the contributions to Ω that they imply.

The speed of rotation of spiral galaxies can be measured through the consequent redshift of the light it emits. It is found from neutral hydrogen emission regions that the speed of rotation persists at a roughly constant level out to two or three times the radius of the luminous disc, suggesting the presence of a dark, massive halo extending to these radii (e.g. Binney & Tremaine 1987), implying $\Omega_{\rm halo} \sim 0.02$. Furthermore, observations of spiral galaxies are dominated by flat discs of stars in roughly circular orbits. Numerical simulations of such systems show that they are unstable, collapsing into bar-like structures. Ostriker & Peebles (1973) argued that such a system of stars could be stabilized by a roughly spherical halo sufficiently massive to dominate the motions of the stars. Attempts to detect light from the outer regions of these dark halos have been unsuccessful, placing a lower limit on the mass to light ratio of the dark matter at $M/L > 1000$.

Groups and clusters of galaxies are in approximate dynamical equilibrium, and so the virial theorem can be used to infer their masses. The simplest galaxy groups are binaries, analysis of which gives $\Omega = 0.02 - 0.07$. It was realised as early as 1933 by Zwicky that the masses of the galaxies alone were unable to account for the dynamics of the Coma cluster. Due to its size and proximity, the Coma cluster still provides the best evidence for the existence of dark matter on large scales. Estimates of the mass of dark matter can be made by assuming that the observed galaxies should be in equilibrium with the potential well of the cluster, or by assuming its X-ray emitting atmosphere is in hydrostatic equilibrium. A detailed analysis is found in White *et al.* (1993) and White (1990), quoting $\Omega \sim 0.2$. More recently the effect of the gravitational potential on the images of objects behind the cluster have been analysed (Kaiser & Squires 1993,

Fahlman *et al.* 1994, and references therein), although the techniques developed have been limited by the quality of observational data available. Fahlman *et al.* find a mass per galaxy in the cluster MS 1224.7+2007 of about $8 \times 10^{12} h^{-1} \mathrm{M}_{\odot}$. If this is typical of the Universe as a whole, then the somewhat surprising result $\Omega \approx 2$ is obtained. One can obtain an estimate of Ω on yet larger scales if one studies the large-scale mass flows of the Local Supercluster of galaxies centred on the Virgo cluster (Davis & Peebles 1983), giving $\Omega = 0.1-0.4$. If cosmic structure formed as small fluctuations in a primordial density, and subsequently grew through gravitational instability, one can relate the peculiar motions of galaxies to the density field. Here, the distribution of gravitating matter is compared with the distribution of luminous matter; it is uncertain whether the two should be the same or not. If the overdensity of galaxies is proportional to the overdensity of matter, with the constant of proportionality labelled b, then what one measures in these analyses is $\Omega^{0.6}/b$, which is found to be typically ~ 0.5 for surveys of optical galaxies. For IRAS galaxies, a figure close to unity is found. Bias is discussed further below. The velocity of the local group of galaxies with respect to the microwave background (deduced from its dipole moment) can be compared with the galaxy density field of the IRAS survey, resulting in $\Omega^{0.6}/b = 0.5 - 1.0$ (Dekel 1994).

The dark matter thus inferred could take several forms, ranging from hypothetical exotic particles such as axions to black holes. One suggested explanation is that the dark matter is made up of brown dwarfs, stars too small to carry out the nuclear reactions that cause larger stars to shine, although the models of nucleosynthesis discussed below limit the baryonic content of the Universe to $\Omega < 0.2$. Hawkins (1993) has attributed variations in the brightness of quasars to the effect of compact halo objects in our galaxy microlensing the quasar image, although this result is disputed (Baganoff & Malkan 1995). Microlensing of stars in the Large Magellanic Cloud has also been detected by several groups (Alcock *et al.* 1993, Auborg *et al.* 1993). However, brown dwarfs have yet to be observed directly (Jones 1995). A slightly more exotic possibility is that the dark matter is made up by a population of white dwarf stars, neutron stars, or perhaps black holes. One would expect stars such as white dwarfs or neutron stars to have left their mark in the form of a greater abundance of heavy elements than is observed. A population of very massive stars might have collapsed into black holes, taking the heavy

elements they produced with them. Another possibility is that a population of primordial black holes exists today, although such a solution seems somewhat arbitrary. However, white dwarfs and neutron stars have both been subject to confirmed observation.

Even more exotic explanations have been suggested. Weakly Interacting Massive Particles (WIMPs), such as a massive neutrino, gave rise to the Hot Dark Matter (HDM) model of structure formation. The failure of the HDM model to reproduce the observed clustering statistics on small scales led to the creation of the Cold Dark Matter (CDM) model, where the WIMPs have initially much lower thermal velocities than the HDM particles. Possible candidates for the CDM particles include axions and the lightest supersymmetric particles.

One population of relativistic particles has been known to exist in the Universe for three decades now. The Cosmic Microwave Background Radiation (CMBR) was first detected by Penzias & Wilson (1965), although its existence had been predicted on theoretical grounds as early as Gamow (1948). The COBE satellite has measured the spectrum of the microwave background, and confirms and refines earlier, terrestrial, measurements. The agreement with a blackbody spectrum is extremely good, with a best fit temperature (Mather *et al.* 1994)

$$T = 2.726 \pm 0.010\mathrm{K}. \tag{1.34}$$

The contribution to the cosmic density from the microwave background is $\Omega_{\mathrm{r}} \approx 2.5 \times 10^{-5} h^{-2}$, considerably higher than any other known radiation field, while considerably lower than the dark matter density inferred from galaxy clusters, where $\Omega_{\mathrm{DM}} \sim 0.2$. The ratio of number of baryons to the number of photons, η, can also be estimated, leading to

$$\eta \approx 2.8 \times 10^{-8} \Omega_{\mathrm{b}} h^2. \tag{1.35}$$

An explanation for this very small number of baryons per photon is a major goal of those working on the theory of baryogenesis, and is the reason that the standard model of cosmology is called the Hot Big Bang. It is also very important when one comes

to consider the origin of the chemical elements, below. The COBE satellite has also measured the degree of anisotropy in the CMBR, and in broad agreement with later work finds the *rms* temperature fluctuations, $\Delta T/T \sim 10^{-5}$ (after subtracting the dipole contribution due to the motion of the Earth with respect to the CMBR). The more detailed measurements of the CMBR anisotropies, made by COBE, are discussed below in Section 1.5.

The physics of the Universe at the earliest times is rightly the preserve of particle physics, although any theories modelling this have implications for cosmology, and their predictions can be tested against cosmological observations. One example of such a prediction might be the existence of WIMPs, or other relic particles, such as magnetic monopoles or primordial black holes. Another example, discussed in Section 1.5, below, is the origin of density fluctuations in the early Universe.

The production in the early Universe of light nuclei, from deuterons to ^{7}Li, as the radiation field cooled to well below the nuclear binding energies, has been extensively modelled, first by Wagoner, Fowler & Hoyle (1967). The high photon to baryon ratio of the Universe, means that sufficient photons populate the high energy, Wien tail of their thermal distribution at temperatures slightly below the nuclear binding energies that nucleosynthesis does not take place until much later, when the temperature drops to $T \leq 10^9$K, at time $t > 10^2$s. By time $t \sim 10^3$s, the thermal energies of the nuclei drop below the Coulomb potential barrier between the positively charged nuclei, and nucleosynthesis stops. The seminal work of Wagoner *et al.* has been improved upon only slightly as more accurate measurements of reaction rates have become available (see Smith *et al.*, 1993, for a review). Elements heavier than ^{7}Li are not produced in primordial nucleosynthesis, since there are no stable mass-5 or mass-8 nuclei which can be produced by two-body interactions in the (low-density) early Universe. Without these nuclei being present, heavier nuclei can only be formed by many-body interactions, which are prohibitively unlikely. In the (very dense) cores of stars, however, the stable mass-5 and mass-8 nuclei can be produced by three-body interactions, and the subsequent recycling of matter from old stars into new stars can account for the observed abundances of heavier elements. Elements heavier than ^{56}Fe require an input of energy if produced by fusion, and are believed to be synthesized in supernova explosions. Of particular interest

in the context of the Standard Big Bang model is the restriction placed on the density of baryons in relation to the critical density. Comparison of the model with observed abundances of light elements imply $0.010 \leq \Omega_{\rm b} h^2 \leq 0.035$ (Boesgaard & Steigman 1985). Taking $0.4 \leq h \leq 1$ as the range of measurements of h gives $0.010 \leq \Omega_{\rm b} \leq 0.22$. Since the density of luminous matter is found to be $\Omega_{\rm L} \sim 0.003 h^{-1}$, and the largest visible contribution, from clouds of neutral hydrogen, is $\Omega_{\rm clouds} \approx 0.002 h^{-1}$, then the models of nucleosynthesis imply at least some baryonic matter is dark, while at the same time placing a strong upper limit on the baryon content of the Universe.

If one is to reconcile the measurement of $\Omega \approx 0.2$ from the study of galaxy clusters with the results on larger scales which show a larger Ω, and with the theoretical preference for $\Omega = 1$, then one must conclude that the cluster measurements are not typical of the Universe. One way to deal with this is to hypothesize that the distributions of luminous matter and dark matter are not the same. This is known generically as *bias*, and could reflect a tendency for galaxies to form at peaks of the linear density field (see Bardeen *et al.* 1986), and thus tend to be grouped together, or perhaps stars are formed more readily in a high density environment, making galaxies there more easily detectable.

The simplest model is based on the assumption that there is a linear relationship between the densities,

$$\frac{\delta \rho_{\rm g}}{\rho_{\rm g}} = b \frac{\delta \rho_{\rm m}}{\rho_{\rm m}}, \tag{1.36}$$

where b is called the bias parameter. An analysis of the data in Peebles (1990) shows that if, indeed, $\Omega = 1$, then $b \approx 1.2$. An understanding of the processes involved in galaxy formation is necessary to model this accurately, and, unfortunately, such an understanding is not available. Cen & Ostriker (1992,1993) have carried out numerical N-body simulations modelling dissipational physical processes as well as gravity. Using what they describe as 'heuristically plausible' criteria for galaxy formation, they claim the following bias relationship

$$\log_{10}\left(\frac{\rho_{\rm g}}{\langle \rho_{\rm g} \rangle}\right) = A + B \log_{10}\left(\frac{\rho_{\rm m}}{\langle \rho_{\rm m} \rangle}\right) + C \left[\log_{10}\left(\frac{\rho_{\rm m}}{\langle \rho_{\rm m} \rangle}\right)\right]^2 . \tag{1.37}$$

The parameters, A, B, & C, were found to be dependent on the scale on which the density fields were smoothed. In all cases, $|B| > |C|$, by an order of magnitude. Thus, a simpler approximation might be a power-law, $\rho_g \propto \rho_m^B$. Cen & Ostriker found that B ranged from 2.00 on scales of $1h^{-1}$Mpc, to $B = 1.40$ on scales of $20h^{-1}$Mpc. If, when deduced from galaxy clusters, $\Omega = 0.2$, a simple power-law bias scheme requires $B \approx 1.4$, if Ω is to be unity globally, somewhat smaller than the Cen & Ostriker models predict on cluster-sized scales. This field is still in its infancy; only recently has sufficient computing power been widely available for these studies. Furthermore, our knowledge of the physical processes involved is patchy, forcing models to make sometimes dubious assumptions.

The situation, deduced from attempts to measure Ω, is presently this; Ω is almost certainly greater than 0.1, with some observations suggesting that it be as high as 1. If Ω is as large as 1, then significant amounts of dark matter must be present. Whatever Ω is, the existence of some baryonic dark matter can be inferred from nucleosynthesis models and observations of luminous baryonic matter. The possibility that Ω be greater than 1 is discounted in the face of a lack of any evidence to suggest this. Many workers believe that Ω will turn out to be identically unity, but are forced to introduce possibly dubious biasing schemes to accommodate this. Although a low Ω model has some attractions from the point of view of fitting the data, such a model poses theoretical and philosophical problems.

1.4 Inflation

A number of problems exist within the Standard Big Bang model which have led to a period of rapid exponential expansion at some time in the early history of the Universe being hypothesized, first by Guth (1981). The 'Flatness Problem' is discussed above, where the Universe is so close to being flat today that, in the Standard Big Bang model, Ω at the Planck time should differ from unity by less than 1 part in 10^{-55}, if one takes a conservative limit of $0.01 \leq \Omega \leq 1$. Such fine tuning is considered unlikely. Another problem is often called the 'Horizon Problem', and relates to the near isotropy of the CMBR. When electrons and protons first combined to produce atomic hydrogen, the Universe

became transparent to the CMBR, as it decoupled from the matter content. After this time, at redshift $z \approx 1000$, the pattern of the CMBR was effectively frozen in, and has remained unchanged to the present day. In a standard big bang cosmology, the different regions of space at this redshift observed in the CMBR would be outside their particle horizons. This begs the question 'How did the different regions of the Universe know the mean temperature of the CMBR to such accuracy?' Furthermore, measurements of the clustering statistics of the CMBR, discussed below, imply small, but significant, correlations of the temperature over scales which had not been in causal contact before the matter and radiation decoupled. At some stage in the past, the standard big bang model implies that the temperature was above the threshold at which Grand Unification of the four fundamental interactions is expected to take place ($\sim 10^{15}$GeV). Theory suggests that as the temperature drops through this threshold, magnetic monopoles will be created with a density of roughly one per horizon (at that time) volume. This would close the Universe many times over, in contrast with observations.

During an inflationary period, the Universe is dominated by vacuum energy density, implying that $\dot{a}/a$ is constant, and $\ddot{a} > 0$. This solution to the field equations, in which the scale factor increases exponentially with time, is known as the de Sitter model. It is suggested that at some time in the past the Universe passed through a phase change (perhaps with the breaking of Grand Unification), but got stuck in a state of false vacuum (analogous to supercooled steam), i.e. with non-zero vacuum energy. The consequent exponential expansion provides solutions to the horizon problems above, in that scales observed today were very much smaller in the past than they would be in the Standard Big Bang model. The number density of magnetic monopoles would be sufficiently greatly reduced by the expansion that there would be no conflict with observation. In a model dominated by vacuum energy, Eqn. (1.24) reduces to

$$\Omega(a) - 1 = \frac{\Omega_0 - 1}{a^2 \Omega_v - (\Omega_0 - 1)}. \tag{1.38}$$

From this equation it can be seen that at late times, when $a(t)$ is large, the Universe will tend asymptotically towards the $k = 0$ flat model. Thus the flatness problem can be resolved if, during inflation, the Universe expands by a factor 10^{28} or so. However, this introduces another problem: if the expansion factor exceeds the required value by

only a small amount, $\Omega_0 \approx 1$, requiring further fine tuning if, as some observations suggest, $\Omega_0 = 0.2$. Another problem with inflation is the mechanism through which the expansion stops. This problem is known as the 'Graceful Exit Problem', and has led to many revisions of the original model, although none as yet have proved entirely successful. The inflationary hypothesis has another weakness in that it is somewhat arbitrary; it assumes the presence of a fundamental field yet to be discovered, and which is not introduced for any other reason. However, the inflationary hypothesis makes concrete, testable predictions for the origins and nature of large-scale structure, which are discussed below.

1.5 Origins and Growth of Large-Scale Structure

The work of this thesis is concerned with the growth of large-scale density perturbations in the Universe, particularly when, in the matter dominated, later stages of the Universe's history, the density in perturbations on scales of a few megaparsecs becomes large compared to the mean density. The origins of density perturbations are discussed briefly, followed by a review of the effects of physical processes on these perturbations, prior to redshift $z \sim 100$, after which processes other than gravity become negligible. This marks the beginning of the linear theory regime, when the first order perturbation theory described below becomes valid. Once the perturbations become non-linear, this approximation fails. The Zel'dovich approximation agrees with linear theory in the linear regime, but can still be used after the linear theory approximation breaks down. The Zel'dovich approximation is included here, as it is used in setting up the initial conditions of N-body simulations (Chapter 2). A model for the non-linear evolution of clustering statistics is given in Chapter 2.

1.5.1 Clustering Statistics

In quantifying the statistical properties of large-scale structure, it is the deviations from the mean density that are of interest, so the density field, $\rho(\mathbf{x}, \mathbf{t})$, is often written

$$\rho(\mathbf{x}, t) = \bar{\rho}(t)(1 + \delta(\mathbf{x}, t)), \tag{1.39}$$

where $\bar{\rho}(t)$ is the mean density. The first statistical measure to consider is the two-point autocorrelation function (or just correlation function, for short) of this overdensity field, δ, and is given by

$$\xi(\mathbf{x}) = \langle \delta(\mathbf{x}+\mathbf{x}')\delta(\mathbf{x}') \rangle, \tag{1.40}$$

where an ensemble average is being taken. Clearly, we do not have access to an ensemble of universes over which to take an average, so here it is assumed that the density is ergodic, implying that a spatial average is equivalent to an ensemble. Since the Universe is assumed to be statistically isotropic (and there is some evidence to support this), the correlation function is taken to be a function of separation only, $\xi(x)$.

The density field may be subjected to a Fourier transform,

$$\delta(\mathbf{x},t) = \sum_{\mathbf{k}} \delta_{\mathbf{k}} e^{i\mathbf{k}.\mathbf{x}}, \tag{1.41}$$

$$\delta_{\mathbf{k}}(t) = \frac{1}{V} \int \delta e^{-i\mathbf{k}.\mathbf{x}} \mathrm{d}^3 x, \tag{1.42}$$

and another statistic composed of the amplitudes of the Fourier components. This is the power spectrum,

$$P(k) = \langle \mid \delta_k \mid^2 \rangle, \tag{1.43}$$

and is simply the Fourier transform of the correlation function,

$$\xi(x) = \frac{V}{2\pi^2} \int_0^\infty P(k) \frac{\sin kx}{kx} k^2 \mathrm{d}k. \tag{1.44}$$

For a Gaussian random field, it can be shown (Adler 1981) that the field is ergodic. Furthermore, the correlation function (or, equivalently, the power spectrum) then contains all statistical information about the density field. For non-Gaussian fields, further quantities are needed to determine completely the properties of the field. In the real-space

representation, these are the hierarchy of n-point correlation functions, starting at the three-point.

The power spectrum, as defined above, depends on the choice of Fourier convention. This uncertainty can be eliminated by using a dimensionless form,

$$\Delta^2(k) = \frac{V}{2\pi^3} 4\pi k^3 \mid \delta_{\rm k} \mid^2 . \tag{1.45}$$

Another quantity often considered is the *r.m.s.* fractional overdensity fluctuation in cells of a given size and shape. The most commonly used window for this is a spherical top-hat, then the *r.m.s.* fluctuation, $\sigma_{\rm R}$ is

$$\sigma_{\rm R}^2 = \int \Delta^2(k) \frac{{\rm d}k}{k} \frac{9}{(kR)^6} [\sin kR - kR\cos kR]^2 , \tag{1.46}$$

where radius $R = 8h^{-1}$Mpc is commonly used; observational measurements give σ_8 of order unity for measurements of galaxy number counts.

1.5.2 The Origins of Density Fluctuations

Currently, the most popular model for the origins of density fluctuations is one where quantum fluctuations in the very early Universe were subsequently blown up and frozen in (as their length scale crossed the horizon) by an inflationary period. A detailed discussion of the inflationary models may be found in Brandenberger (1990); it will suffice here to note that most inflationary models predict that the power spectrum of these fluctuations be a power-law, $P(k) \propto k$. Such a spectrum is known as a Harrison-Zel'dovich spectrum, after its early proponents. This spectrum was introduced since the *r.m.s.* overdensity in a sphere the size of the horizon, is independent of time if $P(k) \propto k$. If this were not the case, it would be possible to single out the time at which the horizon-volume overdensity was unity, thus introducing a preferred time, such as does not exist in an Einstein-de Sitter cosmology. For this reason, and also since the *r.m.s.* perturbations in the gravitational potential are independent of scale for this spectrum, the Harrison-Zel'dovich spectrum is also known as *scale-invariant*. The perturbations

produced in such inflationary theories are known as *adiabatic*; the matter and radiation components are perturbed equally. *Isocurvature* perturbations are perturbations where the matter density perturbation is offset by a radiation density perturbation of opposite sign, thus keeping the total density, and therefore, curvature, constant. The number of photons per baryon then changes from place to place, and for this reason isocurvature perturbations are also known as *entropy* perturbations. Pure isocurvature perturbations are unstable in that as they evolve, they produce radiation perturbations, thus mixing in adiabatic modes. Models producing isocurvature fluctuations are more contrived than the inflationary models leading to adiabatic perturbations, and for this reason adiabatic perturbations are favoured. The effects of the form of the perturbation are calculated in the transfer function, described below. The amplitude of the density fluctuations is not predicted in these theories, and remains a free parameter. Other sources of primordial density fluctuations include cosmic strings and other topological defects. All of these produce non-Gaussian density fields. To date, no firm observational evidence has been produced to suggest that the primordial density field should not be Gaussian, so this simplest hypothesis is adopted here.

1.5.3 Types of Matter and Transfer Functions

Between the formation of primordial density perturbations and the beginning of the matter-dominated, linear regime, physical processes can vary not just the amplitude, but also the shape of the power spectrum of mass fluctuations. These effects are grouped together in the *transfer function*, T_k, where $\delta_k \propto T_k \delta_k^P$, and the superscript P denotes the primordial fluctuation. Since the amplitude of the primordial spectrum is a free parameter, it is usual to normalize $T_k \to 1$ as $k \to 0$. For an adiabatic Hot Dark Matter model, where the Universe is dominated by a species of massive neutrino, Bond & Szalay (1983) find the transfer function to be well fitted by

$$T_k \propto 10^{-2(k/k_\nu)^{3/2}}, \tag{1.47}$$

where

$$\lambda_\nu = \frac{2\pi}{k_\nu} \approx 41\,(m_\nu 30\mathrm{eV})^{-1}\,\mathrm{Mpc}. \tag{1.48}$$

Thus in a Hot Dark Matter model, the power spectrum is truncated at even modest values of k, which comes about because any fluctuations on scales smaller than the horizon when the neutrinos are relativistic will be erased by the free-streaming of the neutrinos. The adiabatic Cold Dark Matter model produces a very different transfer function (Bardeen *et al.* 1986)

$$T_k = \frac{\ln(1+2.34q)}{2.34q} \times [1 + 3.89q + (16.1q)^2 + (5.46q)^3 + (6.71q)^4]^{-1/4}. \tag{1.49}$$

where $q = k/(\Omega h^2)$.

Some workers (e.q. Holtzman 1989; Taylor & Rowan-Robinson 1992) have considered a composite model, containing both hot and cold dark matter. Holtzman (1989) gives parametric fits to the transfer function for a range of models; they are not reproduced here. Figure 1.1 shows the linear power spectra derived from a Harrison-Zel'dovich spectrum in the Cold Dark Matter and Hot Dark Matter (with $m_\nu = 30\mathrm{eV}$) models given above, with $\Omega h = 0.255$, and a Mixed Dark Matter model with one species of massive neutrino and $\Omega h = 0.5$. All these spectra have been normalised to the COBE result (see below), and are for adiabatic perturbations. As will be seen in Chapter 2, the CDM model is able to fit the observations reasonably well. The MDM model, having more free parameters, can be made to fit the data, but is for this reason a weaker model. The HDM disagrees fatally with the data. One consequence of these differing transfer functions is that in HDM, large-scale structures form first, whereas in CDM, small-scale structures form first.

1.5.4 Linear Perturbation Theory

Once the radiation CMBR has cooled sufficiently so that it has negligible effect on the matter content of the Universe, at redshift $z \approx 100$, the evolution of density perturbations

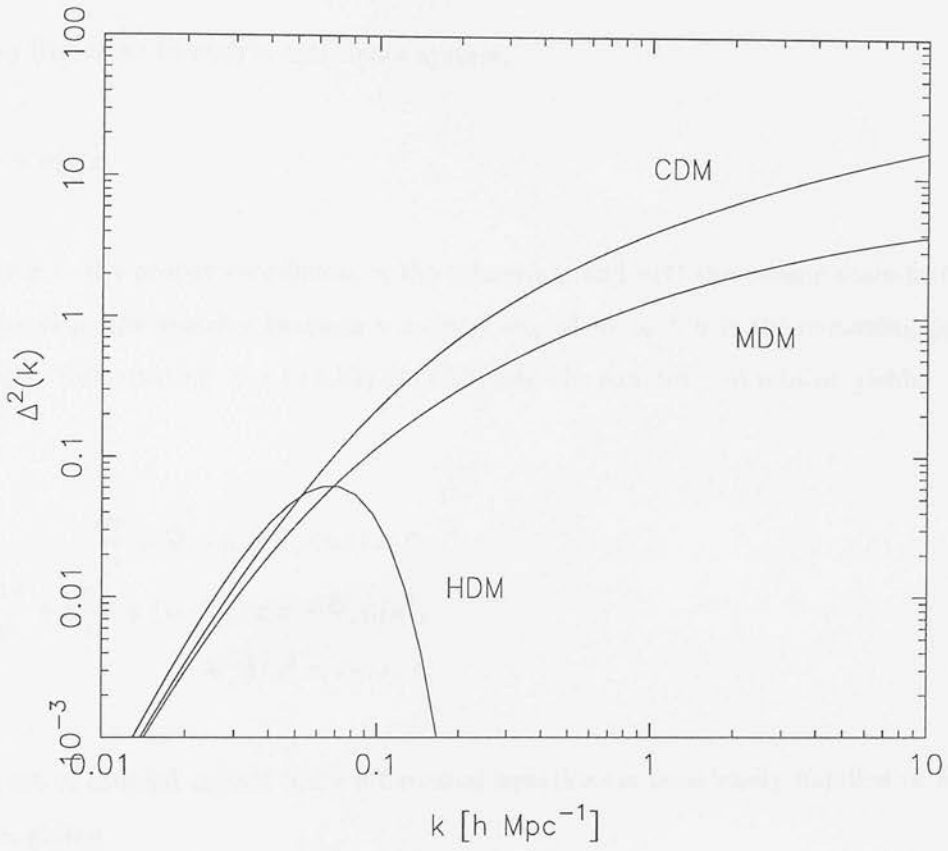

Figure 1.1: Power spectra obtained from a Harrison-Zel'dovich spectrum using CDM, HDM, and MDM transfer functions.

is dominated by gravitational interactions, and can be treated as a pressureless fluid. The Newtonian equations of motion for such a fluid interacting under its own gravity are well known;

$$\frac{\partial \rho}{\partial t} + \nabla \cdot (\rho \mathbf{v}) = 0, \tag{1.50}$$

$$\frac{\partial \mathbf{v}}{\partial t} + (\mathbf{v} \cdot \nabla)\mathbf{v} = -\nabla \phi, \tag{1.51}$$

$$\nabla^2 \phi = 4\pi G \rho, \tag{1.52}$$

being the continuity equation, Euler's equation, and Poisson's equation, respectively. It is convenient in cosmology to work in comoving coordinates, to account for the expansion

of the Universe. In such a coordinate system,

$$\mathbf{r} = a(t)\mathbf{x}, \tag{1.53}$$

where $\mathbf{r}$ is the proper coordinate, $\mathbf{x}$ the comoving, and $a(t)$ the cosmic scale-factor. In this system, the velocity becomes $\mathbf{v} = \dot{a}\mathbf{x} + a\dot{\mathbf{x}}$, where $\dot{\mathbf{x}} \equiv \mathbf{u}$ is the comoving peculiar velocity. Substituting Eqn.s (1.53) & (1.39) into the equations of motion yields

$$\frac{\partial \delta}{\partial t} + \nabla_{\mathrm{x}} \cdot \mathbf{u} + \nabla_{\mathrm{x}} \cdot (\mathbf{u}\delta) = 0, \tag{1.54}$$

$$\frac{\partial \mathbf{u}}{\partial t} + 2\frac{\dot{a}}{a}\mathbf{u} + (\mathbf{u} \cdot \nabla_{\mathrm{x}})\mathbf{u} = -\nabla_{\mathrm{x}}\hat{\phi}/a^2, \tag{1.55}$$

$$\nabla_{\mathrm{x}}^2 \hat{\phi}/a^2 = 4\pi G\bar{\rho}\,\delta. \tag{1.56}$$

This set of coupled second order differential equations is most easily handled in Fourier space, giving

$$\frac{\mathrm{d}\delta_{\mathrm{k}}}{\mathrm{d}t} + i\mathrm{k} \cdot \mathbf{u}_{\mathrm{k}} + \sum_{\mathrm{k}'} i\delta_{\mathrm{k}'}(\mathrm{k} \cdot \mathbf{u}_{\mathrm{k}-\mathrm{k}'}) = 0, \tag{1.57}$$

$$\frac{\mathrm{d}\mathbf{u}_{\mathrm{k}}}{\mathrm{d}t} + 2\frac{\dot{a}}{a}\mathbf{u}_{\mathrm{k}} + \sum_{\mathrm{k}'} i\left[\mathbf{u}_{\mathrm{k}'} \cdot (\mathrm{k} - \mathrm{k}')\right]\mathbf{u}_{\mathrm{k}-\mathrm{k}'} = i\frac{\mathrm{k}}{\mathbf{a}^2}\hat{\phi}_{\mathrm{k}}, \tag{1.58}$$

$$\frac{\hat{\phi}_{\mathrm{k}}}{a^2} = -4\pi G\bar{\rho}\,\frac{\delta_{\mathrm{k}}}{k^2}. \tag{1.59}$$

If one is prepared to assume that the terms in these equations that couple modes with wavevectors k and k' are small, then the equations can be linearized and solved. That this is justified has never been established rigorously, but results from N-body simulations support the assumption. Plausibility arguments to this effect are given in Peebles (1980). The linearized equation of motion for δ_{k} is then

$$\frac{\mathrm{d}^2\delta_{\mathrm{k}}}{\mathrm{d}t^2} + 2\frac{\dot{a}}{a}\frac{\mathrm{d}\delta_{\mathrm{k}}}{\mathrm{d}t} - 4\pi G\bar{\rho}\,\delta_{\mathrm{k}} = 0. \tag{1.60}$$

Heath (1977) showed that the growing mode solution, when the Universe is dominated by matter and vacuum energy, is given by

$$\delta_{\rm k} \propto \frac{X^{1/2}}{H_0^2 a} \int_0^a X^{-3/2}\, {\rm d}a', \tag{1.61}$$

where $X \equiv 1 + \Omega_{\rm m}(a^{-1} - 1) + \Omega_{\rm v}(a^2 - 1)$. For an Einstein-de Sitter model this becomes

$$\delta_{\rm k} \propto a(t). \tag{1.62}$$

In general, the growth of perturbations is suppressed, when compared to the Einstein-de Sitter model, by a factor (Carroll, Press, & Turner 1992; Lahav *et al.* 1991; Lightman & Schechter, 1990)

$$g(\Omega_{\rm m}, \Omega_{\rm v}) = \frac{5}{2}\Omega_{\rm m} \int_0^1 \left(\frac{{\rm d}a'}{{\rm d}t}\right)\, {\rm d}a', \tag{1.63}$$

which can be well approximated by

$$g(\Omega_{\rm m}, \Omega_{\rm v}) \approx \frac{5}{2}\Omega_{\rm m} \left[\Omega_{\rm m}^{4/7} - \Omega_{\rm v} + (1 + \Omega_{\rm m}/2)(1 + \Omega_{\rm v}/70)\right]^{-1}. \tag{1.64}$$

When calculating the linear growth rate, γ, between, say, $t = t_{\rm i}$ and $t = t_{\rm f}$, for models other than Einstein-de Sitter, the amplitude at $t_{\rm i}$ must first be converted to the amplitude that would have resulted in an Einstein-de Sitter model by application of Eqn (1.64), using the value of $g(\Omega_{\rm m}, \Omega_{\rm v})$ at time $t_{\rm i}$, and then converted using the value of $g(\Omega_{\rm m}, \Omega_{\rm v})$ at time $t_{\rm f}$, thus;

$$\gamma = \frac{a(t_{\rm f})}{a(t_{\rm i})} \frac{g(\Omega_{\rm m,f}, \Omega_{\rm v,f})}{g(\Omega_{\rm m,i}, \Omega_{\rm v,i})}. \tag{1.65}$$

Since both the correlation function and the power spectrum depend on the density contrast to second order, the effect on the linear evolution is to increase the amplitude by a factor γ^2.

1.5.5 The Zel'dovich Approximation

Zel'dovich (1970) proposed a simple analytic approximation for non-linear evolution. The motion of a test particle was assumed to depend on its initial position and time, independently, thus

$$\mathbf{x} = \mathbf{q} + b(t)\mathbf{p}(\mathbf{q}), \tag{1.66}$$

where $\mathbf{q}$ is the initial position of the particle. Differentiating with respect to time gives the peculiar velocity:

$$\mathbf{u} = \dot{b}(t)\mathbf{p}(\mathbf{q}). \tag{1.67}$$

The perturbed density is then given by the Jacobian of the transformation:

$$\rho(\mathbf{q},t) = \bar{\rho}\left|\frac{\partial q_{\mathrm{j}}}{\partial x_{\mathrm{k}}}\right| = \bar{\rho}\left|\delta_{\mathrm{jk}} + b(t)\frac{\partial p_{\mathrm{k}}}{\partial q_{\mathrm{j}}}\right|^{-1}, \tag{1.68}$$

which is, to first order in the perturbation $b(t)\mathbf{p}(\mathbf{q})$,

$$\rho(t) \approx \bar{\rho}\left[1 - b(t)\nabla_{\mathrm{q}}.\mathbf{p}(\mathbf{q}) + \ldots\right], \tag{1.69}$$

implying

$$\frac{\delta\rho}{\rho} \approx -b(t)\nabla_{\mathrm{q}}.\mathbf{p}(\mathbf{q}). \tag{1.70}$$

Comparing this with linear theory allows $b(t)$ to be found; it is simply the factor γ determining the linear growth rate. The position-dependent factor can also be found for each plane wave component:

$$\mathbf{p}(\mathbf{q}) = \sigma_{\mathrm{k}}\frac{i\mathbf{k}}{k^2}A_{\mathbf{k}}\exp\left(i\mathrm{k}.\mathrm{q}\right). \tag{1.71}$$

This can then be substituted into the Jacobian, Eqn. (1.68), which can then be diagonalized, and the density found at any point in space:

$$\rho(\mathbf{q},t) = \frac{\bar{\rho}}{[1-b(t)\lambda_1(\mathbf{q})][1-b(t)\lambda_2(\mathbf{q})][1-b(t)\lambda_3(\mathbf{q})]}, \tag{1.72}$$

where the λ_i are the eigenvalues of the matrices $\partial \mathbf{p_k}/\partial \mathbf{q_j}$. showing that, since, for Gaussian fields, in general the eigenvalues will be different (Doroshkevich, 1970; Bardeen *et al.* 1986), one axis will collapse before the other two. Zel'dovich used this to argue that sheet-like structure should be the first non-linear structures to form. The Zel'dovich approximation breaks down after such structures formed, because the approximation will carry the particles onwards in the direction of their initial velocity, whereas gravity will in fact turn them around. A more detailed review of the Zel'dovich approximation can be found in Shandarin & Zel'dovich (1989).

The shell-crossing that causes the eventual breakdown of the Zel'dovich approximation is clearly difficult to model analytically, although N-body simulations can do this with ease. In Chapter 2, N-body simulations are used to develop an analytic approximation to the non-linear evolution problem, extending to over-densities greatly in excess of the limit of the Zel'dovich approximation.

1.5.6 The Effects of Bias on Clustering Statistics

The effects of the linear bias model, described above, on clustering statistics are easier to calculate. The density contrast is enhanced linearly, $\delta_g = b\delta_m$, implying that both the correlation function and the power spectrum, which contain δ^2 terms, are enhanced by a factor b^2 on all scales. The effects of the model of Cen & Ostriker (1993), expressed in Eqn. (1.37), cannot be calculated analytically, but those of a power-law bias scheme can (Peacock, Mann, & Heavens 1995), giving $1+\xi_g = (1+\xi_m)^{B^2}$. These bias models are discussed in the context of the deprojected APM power spectrum in Chapter 4.

1.5.7 Implications from Anisotropies in the Microwave Background

Measurements of the dimensionless power spectrum, $\Delta^2(k)$, from galaxy and cluster surveys at the present epoch show variations in amplitude of up to one and a half orders of magnitude, presumably due to the effects of non-linear evolution, bias, and redshift-space distortions. For this reason, it is difficult to use such measurements to determine the amplitude of the spectrum (which is a free parameter). Chapter 2 describes an attempt to reconcile these observations in terms of an underlying, linear power spectrum and thus determine the amplitude observationally.

A better way to normalize the spectrum is to make use of the measurements of the anisotropy in the CMBR made by the COBE satellite (Smoot *et al.* 1992). A number of effects have caused the CMBR to deviate from an isotropic black-body radiation field. The largest is simply the Doppler shift due to the motion of the observer relative to the CMBR rest-frame. After the motions of the Earth relative to the Sun, the Sun relative to the Galaxy, and the Galaxy relative to the Local Group of galaxies, have been subtracted, the CMBR dipole implies that the Local group is moving at a speed of $627 \pm 22 \mathrm{kms}^{-1}$ relative to the CMBR. On the last scattering surface, at redshift $z \approx 1000$ depending on cosmological model, where the CMBR was last in thermal equilibrium with the matter content of the Universe, a number of effects can lead to anisotropies. The Sachs-Wolfe effect (Sachs & Wolfe 1967) dominates for angles larger than $\theta_{\mathrm{H}} = 1^o$, the angular size of the Hubble radius, as photons gain or lose energy due to the gravitational redshift effect of potential perturbations. On intermediate scales, the Doppler shift caused by the motions of the emitting matter at the last scattering surface is more significant. On smaller scales, the perturbations in the photon density at last scattering dominate. For adiabatic perturbations, the enhanced photon density in regions of high matter density implies a higher temperature, which in turn leads to a later recombination time, at lower redshift, raising the apparent temperature of the CMBR. In regions of low matter density, the reverse is true. The effect of isocurvature fluctuations is to reduce the photon density in, and thus the CMBR temperature in the direction of, regions of high matter density, and vice-versa. On arcminute scales, the physical scales are comparable to the thickness of the last scattering surface, and so anisotropies tend to be washed

out. Once the radiation is free of the last scattering surface, it is still subject to the Sunyaev-Zel'dovich effect (Sunyaev & Zel'dovich 1972). Photons passing through rich clusters of galaxies are scattered by the hot intergalactic plasma that exists there, and so the temperature of the radiation is raised.

On the scales measured by COBE, at the surface of last scattering, $z \approx 1000$, the power spectrum is expected to be a Harrison-Zel'dovich spectrum, free from the effects of bias, non-linear evolution, and the non-gravitational physical processes expressed in the transfer function. The first two years of COBE data gives the slope of the primordial power spectrum as $n \approx 1.5 \pm 0.5$ (Bennett *et al.* 1994; Wright *et al.* 1994), consistent with a Harrison-Zel'dovich spectrum, $n = 1$. A more recent analysis by Górski *et al.* (1994) has produced a slope $n = 1.10 \pm 0.32$ if the quadrupole is included, and $n = 0.87 \pm 0.36$ if it is not. The calculations have been done with and without the observed quadrupole moment because it is somewhat unreliable since it is subject to a large uncertainty due to cosmic variance. A better estimate of the quadrupole can be found by fitting a power-law power spectrum to the higher-order multipoles, and extrapolating to the quadrupole. Górski *et al.* found $Q_{\rm rms-PS} = 17.0 \mu K$ including the observed quadrupole, and $Q_{\rm rms-PS} = 20.0 \mu K$ excluding it. This quantity should be used to normalize a power spectrum only if the spectrum in question is that for which $Q_{\rm rms-PS}$ was calculated. If the dimensionless version of a Harrison-Zel'dovich power spectrum is written in the form

$$\Delta^2 = \frac{4\epsilon^2}{9} \left(\frac{ck}{H_0} \right)^4, \tag{1.73}$$

(Peacock 1991) then the parameter ϵ, can be related to the COBE $Q_{\rm rms-PS}$, assuming a spatially flat cosmology, by

$$\epsilon^2 = \frac{108}{5} \left(\frac{Q_{\rm rms-PS}}{T_0} \right)^2 \Omega_0^{-1.54}, \tag{1.74}$$

where T_0 is the mean temperature of the CMBR. Then the quadrupole-excluded $Q_{\rm rms-PS}$ of Górski *et al.* gives $\epsilon = 3.5 \pm 0.5$.

It is, in principle, possible to determine Ω by comparing the power spectrum at the present epoch with that of the microwave background at $z \approx 1000$ using linear theory,

in which the rate of growth is dependent on Ω. Unfortunately, at present this would require a model-dependent (i.e. the power spectrum on large-scales) extrapolation over an order of magnitude in wavenumber, precluding such a measurement. However, as galaxy surveys become ever larger, the power spectrum on large-scales will become better known, permitting a determination of Ω

The study of the CMBR is a rapidly developing field, with work continuing on the COBE data, and new experiments being conducting with great frequency. It is to be hoped that within the next few years, the parameters discussed here will be constrained much more tightly than at present.

1.6 A Brief Overview

The Standard Hot Big Bang model of cosmology has been introduced, along with the inflationary models that have attempted to resolve some of its problems. The attempts to determine observationally the cosmic density parameter Ω have been reviewed. The currently popular belief that large-scale structure formed from quantum fluctuations, and models of its subsequent growth have been put forward.

In Chapter 2, a new model for non-linear evolution of large-scale structure is developed, combining analytic and numerical results, yielding a convenient, analytic approach. This approach is the first to be able to model non-linearities over a wide range of density contrasts, and is immensely useful in the study of large-scale structure. The power spectrum of mass fluctuations has been observed on scales at which it is non-linear; in order to test model predictions, the non-linearities must be included in any calculations. This has been done in Chapter 2 (taken from the paper Peacock & Dodds 1994, which is appended to this thesis), where the linear power spectrum of cosmic mass fluctuations is reconstructed and compared with the CDM model of structure formation.

In Chapter 3, the non-linear evolution model is used to set up the initial conditions for N-body simulations designed to investigate the density profiles of galaxy clusters. Previous N-body simulations of cluster formation have erred in breaking one of the fundamental rules of experimental science: they have changed more than on parameter at once. Using

the non-linear evolution model, it is possible to produce the same final power spectrum in simulations with different Ω, thus isolating the effect of Ω on the clusters. This work has shown that the mean density profiles of galaxy clusters are dependent on Ω, thus holding forth the possibility of a new observational determination of Ω.

A population of galaxies, known as Faint Blue Galaxies (FBGs), have to date defied attempts to explain their clustering properties in terms of an underlying mass fluctuation spectrum from which all structure evolves, because prior to this work, it has not been possible to model the non-linear effects in the evolution of the angular correlation function. This has now been done, and is presented in Chapter 4, where the clustering of the FBGs (at redshift $z \sim 0.5$) is reconciled with the clustering of optical galaxies from the APM survey, observed at much lower redshift ($z \sim 0.1$).

In Chapter 5, the achievements of this thesis are reviewed. Possible refinements of the work here, and applications of the non-linear evolution model to other areas of cosmology are discussed.

Chapter 2

NON-LINEAR EVOLUTION OF CLUSTERING STATISTICS

2.1 Introduction

It is widely believed that the large-scale structures observed in the Universe today grew from density fluctuations in the early Universe through gravitational collapse. The linear theory of the growth of density fluctuations in a pressureless fluid, due to gravitational interactions, has been described in Chapter 1. This theory breaks down when the density contrast, $\delta = \rho/\bar{\rho} - 1$, becomes of order unity. However, the power spectrum of cosmic density fluctuations becomes non-linear well within the observed range of scales. In order to understand these observations, models for the non-linear evolution of density fluctuations are needed. One way to study non-linear evolution is to carry out particle simulations using a computer. This has the advantage that the simplifying approximations of analytic theories are not needed, although the computation has its own draw-backs, in terms of both time and accuracy. Unfortunately, such simulations take a long time to run, and it is not possible to set up non-linear final conditions to be evolved backwards, since the relation between density and velocity fields is only calculable in the linear regime. Furthermore, when the sign of the time step is changed, the equations of motion become chaotic: very small uncertainties in the final positions and velocities

would change greatly the inferred initial conditions. The basic techniques of N-body simulations are described in Section 2.2.

Baugh & Efstathiou (1994) have compared the predictions of second order perturbation theory with N-body simulations, finding in general an improvement over linear theory. However, the improvement is slight, and is limited to mildly non-linear regimes. Furthermore, the calculations involved in this method are cumbersome and inconvenient.

Much progress can be made towards understanding non-linear evolution of galaxy clustering with analytic methods. Hamilton *et al.* (1991, hereafter HKLM) combine some of these techniques with the results of numerical simulations to develop an analytic correction to the linear theory for an Einstein-de Sitter model. The arguments of HKLM are reviewed in section 2.3, and extended to open cosmological models. Also described are the numerical simulations carried out to confirm and extend the results of HKLM.

If, indeed, all types of large-scale structure formed through gravitational collapse from primordial density fluctuations, then it should, in principle, be possible to determine the underlying power spectrum. The non-linear correction was applied to the power spectrum of a number of different classes of galaxies and clusters of galaxies in order to reconstruct the linear power spectrum of mass fluctuations from which they evolved. It was also necessary to correct for the effects of bias and redshift space distortions. The methods used, and the results are obtained, are given in Section 2.4, adapted from the scientific paper, Peacock & Dodds (1994), which is appended to this thesis.

2.2 N-Body Simulations

2.2.1 Equations of Motion

In the standard model of cosmology, the Universe is assumed to be isotropic and homogeneous on large scales, with local perturbations on smaller scales. The expansion of the Universe can therefore be expressed as a global expansion of coordinates onto which local, peculiar, motions are superimposed. This can be expressed most conveniently if one works in a coordinate system that is expanding with the Universe, i.e. is comoving.

Such a coordinate, $\mathbf{x}$, can be defined as

$$\mathbf{x} = \mathbf{r}/a(t), \tag{2.1}$$

where $a(t)$ is the scale-factor of the Robertson-Walker metric, and obeys the Friedman equation, which in the absence of a cosmological constant is

$$\ddot{a} = -\frac{4}{3}\pi G\bar{\rho}a(t) \tag{2.2}$$

governing the expansion of the Universe. The mean density, $\bar{\rho}$, is related to the density at some reference time, $t = 0$, through

$$\bar{\rho}(t) = \bar{\rho}(0)/a^3(t). \tag{2.3}$$

Substituting Eqn. (2.3) into Eqn. (2.2), we find

$$\ddot{a} = -\frac{4}{3}\pi\frac{G\bar{\rho}(0)}{a^2(t)} \tag{2.4}$$

The Newtonian equations of motion in terms of the proper coordinate, $\mathbf{r}$, subject to a potential field ϕ are

$$\ddot{\mathbf{r}} = -\nabla_r\phi, \tag{2.5}$$

where the subscript on the gradient operator indicates that it is the gradient with respect to the proper coordinate, $\mathbf{r}$, and

$$\nabla_r^2\phi = 4\pi G\rho(\mathbf{r}, t). \tag{2.6}$$

Substituting Eqn. (2.1) into Eqn. (2.5), and writing the Hubble parameter $H = \dot{a}/a$, one obtains

$$\ddot{\mathbf{x}} + 2H(t)\dot{\mathbf{x}} = -\frac{1}{a}\nabla_r\phi - \frac{\ddot{a}}{a}\mathbf{x}. \tag{2.7}$$

By noting that $\nabla_r \phi = a^{-1} \nabla_x \phi$, and $\nabla_x \mathbf{x}^2/2 = \mathbf{x}$, it is possible to write the right-hand side of Eqn. (2.7) in the form of the gradient of a potential ϕ',

$$\ddot{\mathbf{x}} + 2H(t)\dot{\mathbf{x}} = -\frac{1}{a^3}\nabla_x \phi' \tag{2.8}$$

where

$$\phi' = a\phi + \frac{a^2 \ddot{a}}{2}\mathbf{x}. \tag{2.9}$$

This expression for the potential ϕ can be substituted into Eqn. (2.6), which after some manipulation gives,

$$\nabla_x^2 \phi' = 4\pi G \rho a^3 + 3\ddot{a}a^2. \tag{2.10}$$

Using Eqn. (2.4), this can be written in terms of the density at the reference time and the comoving density at time t, $\rho_x = a^3 \rho$, to give

$$\nabla_x^2 \phi' = 4\pi G[\rho_x(\mathbf{x}, t) - \bar{\rho}(0)]. \tag{2.11}$$

Eqns. (2.8) and (2.11) constitute the equations of Newtonian motion in comoving coordinates. It can be seen that Eqn. (2.8) contains a viscous-drag term absent in the proper coordinate equations, reflecting the fact that as the Universe expands, a given physical velocity will become ever smaller when expressed in comoving coordinates. The right-hand side of Eqn. (2.11) depends on the difference between the comoving density and the (constant) comoving mean density, and not the density itself. The total *charge*, i.e. $\rho_x - \bar{\rho}(0)$, then, in any sufficiently large volume of space will be zero. In simulating a volume of space, it is computationally convenient to apply triply periodic boundary conditions, in which case Poission's equation has solutions only if the total charge in any volume is zero.

In N-body simulations, a small number of point particles are used to represent an effectively infinite number of fundamental particles (dark matter, such as axions) that

interact only through gravity. In making this representation, a smoothly varying potential is replaced by one which exhibits high peaks on small scales. This leads to two-body interactions between the point particles that the dark matter would not exhibit. An order of magnitude estimate for this effect can be derived: following Binney & Tremaine (1987), consider a particle passing another. Assume that one particle is fixed in position, and that the perturbation in the other's velocity is small, so that it can be considered to move along a straight line. If the perpendicular distance from the fixed particle to the trajectory of the moving one is b, then the perpendicular force on the moving one is

$$F_\perp \approx \frac{Gm^2}{b^2}\left[1+\left(\frac{vt}{b}\right)^2\right]^{-3/2}, \tag{2.12}$$

where m is the particle mass, and v the velocity of the moving particle. But by Newton's laws, $m\dot{\mathbf{v}}_\perp = \mathbf{F}_\perp$, which gives, on integrating with respect to time,

$$|\delta\mathbf{v}_\perp| \approx \frac{Gm}{bv}\int_{-\infty}^{\infty}(1+s^2)^{-3/2}\,\mathrm{d}s = \frac{2Gm}{bv}. \tag{2.13}$$

Consider now an aggregation of N particles. In crossing such an aggregation, a particle will suffer

$$\delta n = \frac{N}{\pi R^2}\,2\pi b\,\delta b = \frac{2N}{R^2}\,b\delta b, \tag{2.14}$$

encounters with impact parameter between b and $b+\delta b$ (here, R is the typical scale of the aggragation). Although the perturbations are randomly oriented around $\mathbf{v}$, and so the mean perturbation will be zero, by summing the squares of the perturbations, it can be seen that $\delta v_\perp^2$ changes by an amount

$$\delta v_\perp^2 \approx \left(\frac{2GM}{bv}\right)^2\frac{2N}{r^2}\,b\delta b. \tag{2.15}$$

The approximation of a straight-line trajectory breaks down if $|\delta\mathbf{v}_\perp| \approx v$, i.e. when $b < b_{\min} \equiv Gm/v^2$. Then integrating over all values of b between $b_{\min}$ and the maximum possible, $b = R$, gives

$$\Delta v_\perp^2 \approx 8N\left(\frac{Gm}{Rv}\right)^2\ln\Lambda, \tag{2.16}$$

where

$$\ln \Lambda \equiv \ln \left(\frac{R}{b_{\min}} \right). \tag{2.17}$$

The typical speed of a particle in the aggregation can be estimated by considering kinetic and potential energies, giving $v^2 \approx GNM/R$, which can be substituted into Eqn. (2.16) to yield

$$\frac{\Delta v_{\perp}^2}{v^2} \approx \frac{8 \ln \Lambda}{N}. \tag{2.18}$$

Then the number of crossings a particle must make in order that its velocity change by of order itself is

$$n_{\text{relax}} = \frac{N}{8 \ln \Lambda}, \tag{2.19}$$

Then the time taken for a particle to 'relax' and lose information about its original trajectory is $t_{\text{relax}} = n_{\text{relax}} \times t_{\text{cross}}$, where t_{cross} is the time the particle takes to cross the aggregation. The parameter Λ can be found from the above relations, reducing to $\Lambda \approx N$. Thus the relaxation time, $t_{\text{relax}} \approx N/8 \ln N$. In dark matter simulations, there should be no such relaxation, so clearly making the relaxation times as long as possible is advantageous. The simplest way to do this is to increase the number of particles, which, if the density in the simulation is fixed, implies an increase in mass resolution. The other contributory factor in the relaxation time is the integration of the r^{-2} force law along the fixed trajectory. Since the particles are simulating an effectively continuous distribution, it seems reasonable to modify the force law to treat the particles as extended objects, i.e. large clumps of dark matter moving in one direction. This results in a weakening of the force at small separations, known as force softening, which increases the contribution to the relaxation time due to the integral along the trajectory. A commonly used softened force law is the Plummer law,

$$\mathbf{F}_{ij} = -Gm^2 \frac{\mathbf{r}_{ij}}{(r_{ij}^2 + \epsilon^2)^{3/2}}, \tag{2.20}$$

where ϵ is the characteristic length of the softening, known as the softening length. Another undesirable effect of the use of point charges and finite integration step is that two particles may end a time-step very close to each other, and thus the force between them will be very large. This large force will be applied, incorrectly, to the particles for the duration of one time-step, resulting in extremely large accelerations. This process can lead to 'evaporation' of particles from bound groups. A softened potential reduces this difficulty, since the force at small separations is much smaller than for an r^{-2} force law. However, softening also reduces the potential around a particle, so preventing tightly bound objects from forming. This effect is noticeable in the density profiles of simulated clusters in Chapter 3.

In addition to the equations of motion derived above, it is useful to adapt the energy equations to comoving coordinates. Layzer (1963) and Irvine (1961) find

$$\frac{d}{dt}(a^4 T) + a\frac{dW}{dt} = 0 \tag{2.21}$$

where the kinetic and potential energies are, respectively,

$$T = \sum_i \frac{m_i a^2 \dot{x}_i^2}{2}, \tag{2.22}$$

and

$$W = \sum_i m_i \phi'(\mathbf{x}_i). \tag{2.23}$$

2.2.2 Time Integration

In order to integrate numerically the equations of motion described above, it is necessary to convert the differential equations to finite difference equations. Let subscript n denote evaluation at time t_n, and subscipt $n+\frac{1}{2}$ denote evaluation halfway between t_n and t_{n+1}. Then $\mathbf{x}$ can be calculated approximately using

$$\mathbf{x}_{n+1} = \mathbf{x}_n + \dot{\mathbf{x}}_{n+\frac{1}{2}}\delta t. \tag{2.24}$$

Here $\dot{\mathbf{x}}$ is evaluated at the half-step to give the best estimate of the integral of $\dot{\mathbf{x}}$ over the range $t, t+\delta t$. To evaluate $\dot{\mathbf{x}}$, the equation of motion, Eqn. (2.8) is written in difference form,

$$\frac{\dot{\mathbf{x}}_{n+\frac{1}{2}} - \dot{\mathbf{x}}_{n-\frac{1}{2}}}{\delta t} + 2H(t_n)\frac{\dot{\mathbf{x}}_{n+\frac{1}{2}} + \dot{\mathbf{x}}_{n-\frac{1}{2}}}{2} = \mathbf{F}'_n, \tag{2.25}$$

where $\mathbf{F}'_n = -\nabla^2\phi'(t = t_n)$ is the comoving force on the particle at $\mathbf{x}$ at time t_n. The dependence of the accuracy of this "leapfrog" scheme on the size of time step can be estimated by comparing the calculated force with the force derived from the true (but unknown) solution to the equation of motion. Rewriting the time derivatives in Eqn. (2.25) as finite differences, and replacing $\mathbf{x}_n$ with the true solution, $\mathbf{X}(t_n)$, gives

$$\frac{\mathbf{X}(t_{n+1}) - 2\mathbf{X}(t_n) + \mathbf{X}(t_{n-1})}{(\delta t)^2} + H(t_n)\frac{\mathbf{X}(t_{n+1}) - \mathbf{X}(t_{n-1})}{\delta t} = \mathbf{F}'_n. \tag{2.26}$$

Writing $\mathbf{X}(t_{n+1})$ as a fourth order Taylor expansion about $\mathbf{X}(t_n)$, and setting $\mathbf{F}'_n = \mathbf{F}'(t_n) + \delta\mathbf{F}'$, the equation of motion, Eqn. (2.8) can be used to rewrite Eqn. (2.26), giving

$$\delta\mathbf{F}' = (\delta t)^2\left(\frac{1}{12}\frac{\mathrm{d}^4 X}{\mathrm{d}t^4} + \frac{H(t_n)}{3}\frac{\mathrm{d}^3 X}{\mathrm{d}t^3}\right), \tag{2.27}$$

demonstrating that, to lowest order in δt, the force error, $\delta\mathbf{F}' \propto (\delta t)^2$. Higher order finite difference approximations can be used, but the additional computation time and memory requirements make it preferable simply to reduce the time interval. A problem that arises because of the finite time-step is that of relaxation. Consider a particle orbiting through a group of particles. In each orbit, an error will be introduced into the particle's velocity due to the finite integration scheme. If the particle crosses the group enough times that the error in its velocity is comparable to the average velocity within the group, the structure and evolution of the group will not be modelled accurately. The size of this effect can be monitored by noting the effect of changing the size of the time-step.

Rearranging the Eqn. (2.25) gives,

$$\dot{\mathbf{x}}_{n+\frac{1}{2}} = \frac{1 - H(t_n)\,\delta t}{1 + H(t_n)\,\delta t}\dot{\mathbf{x}}_{n-\frac{1}{2}} + \frac{\mathbf{F}'_n\,\delta t}{1 + H(t_n)\,\delta t}. \tag{2.28}$$

Initially, $\mathbf{x}_0$ and $\dot{\mathbf{x}}_{\frac{1}{2}}$ are known. Eqn. (2.24) then determines $\mathbf{x}_{n+1=1}$, which is in turn used to find $\dot{\mathbf{x}}_{n+\frac{1}{2}=\frac{3}{2}}$ from Eqn. (2.28). This process is repeated as many times as desired.

The accuracy to which the Layzer-Irvine equation (2.21) is satisfied as the integration proceeds is a useful test of the accuracy of the integration itself, although not a complete one. The finite difference form of it is

$$\frac{a_{n+1}^4 T_{n+1} - a_n^4 T_n}{\delta t} + \frac{a_{n+1} W_{n+1} - a_n W_n}{\delta t} - W_{n+1} \dot{a}_{n+1} = 0, \tag{2.29}$$

which can be summed to give

$$a_m^4 T_m^4 + a_m W_m - \sum_{n=1}^{m} \delta t \, W_n \dot{a}_n = C, \tag{2.30}$$

where the constant of integration, C, must be adjusted to fit the initial conditions, i.e.

$$C = a_0^4 T_0 + a_0 W_0. \tag{2.31}$$

2.2.3 Force Evaluation

To evaluate the force on a given particle, the comoving version of Poisson's equation given in the previous Section must be solved. Clearly, for a set of point particles, the potential ϕ' at the same position as a particle is undefined. This problem disappears when a Particle-Mesh algorithm, described below, is used. The force at one mesh point then depends only upon the charges at other mesh points.

The problem of divergent potentials can be avoided by calculating the force as a direct sum analagous to Newton's inverse square law. One proceeds as follows. Integrating Eqn. (2.11), one obtains,

$$\phi'(\mathbf{x}) = -G \int d^3x' \, \frac{[\rho - \bar{\rho}(0)]}{|\mathbf{x}' - \mathbf{x}|} \tag{2.32}$$

which gives

$$\mathrm{g}(\mathrm{x}) = -\frac{\nabla\phi'}{a^3} = -\frac{G}{a^3}\int d^3x'[\rho - \bar{\rho}(0)]\frac{\mathrm{x}' - \mathrm{x}}{|\mathrm{x}' - \mathrm{x}|^3}, \tag{2.33}$$

where g is the acceleration on a particle due to gravity. By choosing to carry out the integration over angle first, it can be seen that the term in $\bar{\rho}(0)$ vanishes, leaving the familiar Newtonian form (except for the factor a^{-3}), which for a collection of point particles is

$$\mathrm{g}(\mathrm{x}_i) = -\frac{G}{a^3}\sum_{j\neq i} m_j \frac{\mathrm{x}_j - \mathrm{x}_i}{|\mathrm{x}_j - \mathrm{x}_i|^3}. \tag{2.34}$$

It is evident that the number of floating point operations needed to evaluate Eqn. (2.34) will be proportional to $n(n-1)$, where n is the number of particles.

A commonly used technique, in fields such as plasma physics as well as cosmology, designed to reduce the computational time required to evaluate the force on each particle is the Particle-Mesh (PM) algorithm. The basic idea is simple; the density field composed of the particles is approximated by charges on an evenly spaced mesh. If the mesh size is fixed, then the dependence of the time requirement is reduced to first order (as the particles are assigned to the mesh, and the forces read off). The price paid for this reduction in computational time is a clearly a loss of resolution. When optimised for performance, the PM algorithm becomes somewhat more complex. The algorithm can be broken down into four stages:

1. assignment of charge to the mesh,
2. solution of Poisson's equation on the mesh,
3. differencing the potential on the mesh to find the force,
4. and finally interpolation of the mesh forces to particle positions.

The charge assignment can be made as refined as one likes, by employing ever higher-order schemes. In the lowest order scheme, Nearest Grid Point (NGP), the entire charge

of one particle is assigned to the nearest mesh point, a zeroth-order scheme, in which both the charge assigned and its first derivative with respect to the distance of the particle from the mesh point vary discontinuously. The first order scheme is called Cloud In Cell (CIC), and is a linear interpolation between the nearest mesh points, and ensures continuity of charge. To ensure the continuity of the first derivative, a second-order interpolation, known as Triangular-Shaped Cloud (TSC) is employed. The drawback of higher-order schemes is that they are computationally more expensive; in three dimensions, charge is assigned to one mesh point in the NGP scheme, but to twenty-seven if TSC is used. TSC is commonly used as a compromise between accuracy and expense. The solution of Poisson's equation on the mesh is best performed in Fourier space, owing to the existence of the Fast Fourier Transform (FFT), which enables the transformation of an array with N elements to be performed for a cost proportional to $N \log N$, and not N^2. Another advantage of Fourier space is that the force law is effectively the convolution of the density field with the Green's function representing that force law (r^{-2} for the inverse-square law). The Green's function can be optimized to reduce the effects of the mesh, such as translational and directional variations and non-central forces, for a given charge assignment scheme and potential differencing operator. A detailed discussion of this process is given in Hockney & Eastwood (1981). The optimal Green's function is usually calculated once for a given mesh, and then stored. Since no wave with a frequency greater than the Nyquist frequency (corresponding to a wavelength of two mesh spacings) can be represented on a mesh, the force resolution of a PM cycle is limited to about two mesh spacings, dropping off for separations of this size or smaller. Provided that the same scheme is used for the force interpolation as for the charge assignment, and that the differencing operator used to derive the mesh force from the mesh potential is antisymmetric, then the PM cycle conserves momentum, an important property.

The force resolution can be improved upon (although at the expense of a greater time requirement) by performing a direct sum for particles at small separations, as is done in the Particle-Particle Particle-Mesh (P^3M) algorithm. A mesh, typically two or three times courser than the PM mesh, called the chaining mesh, is used to identify which particles should be included in the direct sum for any given particle. A list is created of

the memory addresses of the positions of all the particles in a given chaining cell. For any given particle, all particles in the same chaining cell and in the adjacent cells are included in the direct sum, which in three dimensions amounts to twenty-seven cells. The force law used requires careful consideration, since although the PM force between two particles will be lower than the true force, it will not be zero. For this reason, it is essential in a P^3M code that the Green's function be optimised so that the short range force needed to take into account the PM force errors be a function of separation only, and not of position relative to the mesh or of direction. Even still, the short range force is not a simple function of separation, but determined by comparing the true force with an averaged PM force, and so is usually calculated once and stored. The short range force must be truncated at some cut-off separation, or else the direct sum will need to be performed for all particles. At the cut-off separation, a step arises in the force law. Clearly then, there is a play-off between minimising the force inaccuracies and computational time. Efstathiou *et al.* (1985) find that with a cut-off at 2.7 times the mesh spacing, the force discontinuity amounts to 2.4%. One feature of P^3M codes is that as the particles become more clustered, the code slows down greatly, as the direct sum comes to dominate the cycle.

The computational cost of a given level of accuracy in the force evaluation can be further reduced, at the expense of a more complicated code, by treating the most overdense regions with a refined PM calculation rather than a direct sum. This Adaptive Particle-Particle Particle Mesh (AP^3M) algorithm is due to Couchman (1991). It can be broken down into three steps:

1. regions of high density are identified,
2. a P^3M cycle is carried out, but particle pairs in the same high density region are excluded from the direct sum,
3. and a refined P^3M cycle is performed on each of the identified high density regions.

For convenience, the regions on which a refined P^3M cycle is performed are chosen to be non-overlapping cubes composed of a whole number of chaining cells. This is not optimal for asymmetric particle distributions, such as two groups of particles merging, but the

added complexity of non-cubic, overlapping refinements would make this difficult to put into practice. The refined PM cycle is fundamentally different to the base PM cycle, in that periodic boundary conditions do not apply. In this case, the region of space is considered to be isolated, since the forces between particles inside it and outside it have been calculated in the base P^3M cycle. The refinement region is placed at the centre of a mesh extending to twice the physical size of the refinement region, and the mesh points outside the region are assigned zero charge in a process known as zero-padding (Eastwood & Brownrigg, 1979). Clearly, the three force estimations must be matched in the same way as the direct sum and the mesh forces are matched in the P^3M algorithm. The AP^3M algorithm goes further yet; the code is not restricted to one level of refinement, but further refined P^3M cycles can be performed on the high density regions within refinements. The AP^3M code of Hugh Couchman uses a TSC charge assignment/force interpolation scheme, and a 10-point differential operator for the potential. The true force is softened using a cloud with a density dropping off linearly to zero density at a specified radius.

2.2.4 Adaptation of AP^3M Code to more General Cosmologies

The original AP^3M code, kindly supplied by Hugh Couchman, was modified for this work in order to carry out simulations of open cosmological models, and flat models where a significant fraction of the closure density is provided by vacuum energy. The equation of motion, in the notation of Couchman (1991), is

$$\frac{\mathrm{d}^2\mathbf{x}_i}{\mathrm{d}t^2} + 2\frac{\dot{a}}{a}\,\frac{\mathrm{d}\mathbf{x}_i}{\mathrm{d}t} = -G\,\frac{\mathbf{F}_i}{a^3}, \tag{2.35}$$

where

$$\mathbf{F}_i = \sum_{j\neq i} m_j \frac{\mathbf{x}_i - \mathbf{x}_j}{|\mathbf{x}_i - \mathbf{x}_j|^3}. \tag{2.36}$$

In these equations, the comoving physical coordinate is $\mathbf{x} = \mathbf{r}a_\mathrm{i}/a$ (having dropped the index on the coordinate for clarity; subscript i now refers to the initial epoch of the simulation). It is convenient to set $a_\mathrm{i} = 1$. The computational coordinate is $y = xL/D$,

where L is the size of the base mesh, D the physical comoving size of the simulation box, and the computational time unit is $\tau = t/t_{\rm i}$. In these units, the equation of motion becomes

$$\frac{{\rm d}^2{\rm y}}{{\rm d}\tau^2} + 2t_{\rm i}\frac{\dot{a}}{a}\frac{{\rm d}{\rm y}}{{\rm d}\tau} = -t_{\rm i}^2\left(\frac{L}{D}\right)^3\frac{G}{a^3}\,{\rm F}. \tag{2.37}$$

Now consider the matter content of the model, i.e. the particles. The matter density in the simulation is then

$$\rho = \frac{Nm}{a^3D^3}, \tag{2.38}$$

where m is the mass of one particle. The matter density is related to cosmological parameters through

$$\rho = \frac{3H^2\Omega_{\rm m}}{8\pi G}, \tag{2.39}$$

which can be combined with Eqn. (2.38) to give

$$\frac{Gm}{a^3} = \frac{3}{8\pi}\frac{D^3}{N}H^2\,\Omega_{\rm m}, \tag{2.40}$$

and for convenience, m is taken to be unity. Substituting this expression for the gravitational constant into the computational equation of motion, Eqn. (2.37), gives

$$\frac{{\rm d}^2{\rm y}}{{\rm d}\tau^2} + 2Ht_{\rm i}\frac{{\rm d}{\rm y}}{{\rm d}\tau} = -\Omega_{\rm m}[Ht_{\rm i}]^2\frac{3L^3}{8\pi N}\,{\rm F}. \tag{2.41}$$

Additional felxibility can be introduced into the time integration scheme by changing to a new time variable $p = 3a^\alpha/2\alpha$. For an Einstein-de Sitter model, this corresponds to $p = t/t_{\rm i}$ for the case $\alpha = 3/2$; setting t_i simplifies the expression for p as well as the equation of motion. In terms of this new time variable, the equation of motion becomes

$$\frac{{\rm d}^2{\rm y}}{{\rm d}p^2} + \left[\frac{1}{p} + \frac{2}{\alpha p} + \frac{1}{Ht_{\rm i}}\frac{{\rm d}Ht_{\rm i}}{{\rm d}p}\right]\frac{{\rm d}{\rm y}}{{\rm d}p} = -\frac{\Omega_{\rm m}}{(\alpha p)^2}\frac{3L^3}{8\pi N}\,{\rm F}. \tag{2.42}$$

It is now clear where the equations of motion evaluated by the AP^{3}M code are dependent on cosmological model; in the derivative with respect to p in the viscous drag term on the left hand side of Eqn. (2.42), and in $\Omega_{\rm m}(p)$ on the right hand side. These changes correspond to changes in the function $H(t)$ and the gravitational constant, G, in the leapfrog integration scheme, discussed in Subsection 2.2.2. One futher change must be made: the velocities in the initial conditions, as determined from the Zel'dovich approximation, must be multiplied by the linear theory velocity suppression factor, $f(\Omega) \approx \Omega^{0.6}$.

With these changes made, it was now possible to run AP^{3}M simulations for a wide range of cosmological models.

2.2.5 Initial Conditions

The techniques neeeded to integrate the equations of motion of a large number of particles interacting under their own gravity are given above; it remains to determine the initial positions and velocities of the particles. In cosmological simulations, we are interested in clustering statistics such as the power spectrum, so it is natural to use as initial conditions a realisation of a particular power spectrum. Firstly, the Fourier transform of the density field is set up, with each of the real and imaginary parts being an independent Gaussian random variate with zero mean and variance $P(k)(\Delta k)^3/2$, where $P(k)$ is the power spectrum. In the linear regime, the density field, δ, is related to the displacement field Ψ by

$$\delta = -\nabla \cdot \Psi, \tag{2.43}$$

$$\nabla \times \Psi = 0, \tag{2.44}$$

by conservation of mass and circulation. Fourier transforming these equations yields the following expression for the transformed displacement field, Ψ_k, in the j-th coordinate direction,

$$\Psi_k = -\frac{ik_j}{k^2}\delta_k, \tag{2.45}$$

for $j = 1, \ldots, 3$. Ψ_k is then transformed back to real space. In order to create a realisation of the power spectrum with an ensemble of particles, the particles are first placed on a uniform grid throughout the computational volume, and then displaced using the Zel'dovich approximation, as discussed in Chapter 1. Alternative methods for the initial distribution of the particles exist, such as placing them randomly throughout the volume, or in a pseudo-random way such as a So'bol sequence. Another way in which the particles may be distributed nearly uniformly, but with particles avoiding each other, due to Simon White, is to run a simulation with repulsive gravity. Baugh (1994) explores three of these possiblilies; random, grid-based, and repulsive gravity distributions, and concludes that simulations with randomly placed particles are impaired by significant Poisson noise, which persists in influencing the power spectrum well into the non-linear regime. In this work, the grid-based distribution is used, being as accurate (as far as has been tested) as the pseudo-random techniques, but far simpler. The initial velocities of the particles are also given by the Zel'dovich approximation.

2.2.6 Limitations

Several limitations exist on the accuracy of N-body simulations. Clearly, one wishes to have as many particles as possible, but this is limited by the desire to restrict computational time, and because of the finite memory available. The more particles one has, the better one is able to measure statistical properties. If one wishes to study the statistical properties of, say, galaxy clusters, one needs to have a large number of clusters, and also sufficient particles in each cluster to accurately simulate the cluster. A similar problem arises in the calculation of the forces; clearly, one would like the forces to be calculated as accurately as possible, but also that the simulation take a reasonable length of time. Both of these effects manifest themselves on small scales. Similarly, the choice of the size of time step is restricted to computationally feasible values. The most powerful computer available for this work, and the one on which the majority of simulations were carried out, was an Alpha AXP 3000/400, with 196Mb RAM. The code was compiled to run with a maximum array size of 128^3, and 64^3 particles, which produced an executable requiring 125Mb. Further increases in size would have resulted in extensive swapping of memmory from RAM to hard disk, slowing down the code prohibitively.

The code estimated force errors, and comparing this figure with a maximum permitted error, then decided on whether to continue with further refinements, or to accept the forces as calculated. This parameter was set to 6%, corresponding approximately to two levels of refinement. The computational time taken to evolve 64^3 particles through one integration step was found to be about 70s at the start of the simulation, when the integration and base mesh force calculations dominated. As the clustering evolved, the time required rose to around 200s. With these timings, a simulation expanding in scale through a factor of around 10, and taking 300 time-steps, took approximately 10 hours, a manageable time. The time required clearly depends linearly on the number of steps taken, so it was feasible to double the number of steps to estimate the accuracy of the time integration.

More subtle considerations exist. In particular, Fourier methods assume periodic boundary conditions. When there is little clustering on the same scale as the period of the Fourier transform, this is not a problem, but as the large wavelength modes become non-linear, they cease to be independent, and mode-mixing occurs. If periodic boundary conditions are used, there is an upper limit to wavelength, so large wavelength modes will not be able to mix properly. One way to avoid the problem of periodic boundary conditions, and the problems of matching short and long range forces, is to use what is known as a tree-code (e.g. Barnes & Hut, 1986). Here, particles far from the particle for which the acceleration is to be calculated are considered as a single, 'super particle', and so only one inverse square law calculation is required. However, tree codes are not used in this work.

2.3 An Analytic Description of Non-Linear Evolution

2.3.1 The *Ansatz* of Hamilton *et al.* (1991)

Hamilton *et al.* (1991, hereafter HKLM) considered the non-linear evolution of the mean interior correlation function,

$$\bar{\xi}(r) = \frac{3}{r^3}\int_0^r \xi(x)x^2dx, \tag{2.46}$$

where $\xi(r)$ is the usual correlation function, in a spherical collapse approximation. The mean interior correlation function therefore gives a measure of the average overdensity in regions on scales of r. Such a region, with density contrast $1+\delta$, can be thought of as arising through collapse by a factor of $(1+\delta)^{1/3}$ in radius. Thus, it seems that when considering the non-linear mean interior correlation function, $\bar{\xi}_{\rm NL}$, the related linear quantity is the linear mean interior correlation function, $\bar{\xi}$, on a linear scale,

$$r_{\rm L} = [1+\bar{\xi}_{\rm NL}(r_{\rm NL})]^{1/3} r_{\rm NL}. \tag{2.47}$$

It still remains to relate $\bar{\xi}_{\rm NL}(r_{\rm NL})$ to $\bar{\xi}_{\rm L}(r_{\rm L})$. HKLM proposed that there exists a universal function to do this,

$$\bar{\xi}_{\rm NL}(r_{\rm NL}) = f_{\rm NL}[\bar{\xi}_{\rm L}(r_{\rm L})]. \tag{2.48}$$

Clearly, in the linear regime, where $\bar{\xi}_{\rm L}$ is small, $f_{\rm NL}(x) = x$. In this regime, the length scale is mapped onto itself. In the extreme non-linear regime, where the clustering is fixed in proper coordinates, $\bar{\xi}_{\rm NL} \propto a^3$, where a is the scale factor. Since $\bar{\xi}_{\rm L} \propto a^2$, it can be seen that the functional form tends asymptotically to $f_{\rm NL} \propto x^{3/2}$. Using the N-body simulations of Efstathiou *et al.* (1988, hereafter EFWD), with 32^3 particles and a force resolution of $L/200$, where L is the side of the computational box, HKLM were able to determine that the constant of proportionality should be 11.68, and to derive a rational function to represent $f_{\rm NL}$ over the entire range of $\bar{\xi}_{\rm L}$. They were able to show negligible dependence of $f_{\rm NL}$ on the slope of $\bar{\xi}_{\rm NL}$, for power-laws with indices -2, -3, -4 (equivalent to $n = -1, 0, 1$ for power spectra, $P(k) \propto k^n$). The non-linear function, $f_{\rm NL}$, deduced by HKLM is given by

$$f_{\rm NL}(x) = \frac{x + 0.358x^3 + 0.0236x^6}{1 + 0.0134x^3 + 0.00202x^{9/2}}, \tag{2.49}$$

the inverse of which is approximated to within 1% over its entire range by

$$f_{\rm NL}^{-1}(y) = y\left(\frac{1 + 0.0158y^2 + 0.000115y^3}{1 + 0.926y^2 - 0.0743y^3 + 0.0156y^4}\right)^{1/3}. \tag{2.50}$$

2.3.2 A Power Spectrum Implementation

However, the mean interior correlation function, $\bar{\xi}(r)$, is not a commonly used measure of clustering. More often used is the dimensionless power spectrum, $\Delta^2(k)$. In words, $\Delta^2(k)$ is the contribution to the fractional density variance per bin of $\ln k$. Following Peebles (1980),

$$\Delta^2 \equiv \frac{\mathrm{d}\sigma^2}{\mathrm{d}\ln k} = \frac{V}{(2\pi)^3} 4\pi k^3 P(k), \tag{2.51}$$

where $P(k)$ is the usual power spectrum. One advantage of $\Delta^2(k)$ is that it is independent of Fourier convention. The HKLM method can be used to evolve $\bar{\xi}(r)$, which can then be translated into the corresponding $\Delta^2(k)$. In principle, the translation between $\bar{\xi}(r)$ and $\Delta^2(k)$ is straightforward, but it is not so easy to obtain stable numerical results. One route is to use the relations between $\bar{\xi}(r)$ and $\xi(r)$

$$\bar{\xi}(r) = \frac{3}{r^3} \int_0^r \xi(x)\, x^2\, \mathrm{d}x, \tag{2.52}$$

$$\xi(r) = \frac{\mathrm{d}\left[r^3 \bar{\xi}(r)\right]}{\mathrm{d}[r^3]}, \tag{2.53}$$

followed by the Fourier relations between $\xi(r)$ and $\Delta^2(k)$:

$$\xi(r) = \int_0^\infty \Delta^2(k) \frac{\sin kr}{kr} \frac{\mathrm{d}k}{k}, \tag{2.54}$$

$$\Delta^2(k) = \frac{2k^3}{\pi} \int_0^\infty \xi(r) \frac{\sin kr}{kr}\, r^2\, \mathrm{d}r. \tag{2.55}$$

This approach is not so attractive. To obtain the non-linear power spectrum from the linear one requires two numerical integrations, followed by differentiation, followed by one further integration. It is possible to do a little better by manipulating the above equations to relate $\Delta^2(k)$ and $\bar{\xi}(r)$ directly

$$\bar{\xi}(r) = \int_0^\infty \Delta^2(k) \frac{\mathrm{d}k}{k} \frac{3}{(kr)^3} [\sin kr - kr \cos kr], \tag{2.56}$$

$$\Delta^2(k) = \frac{2k^3}{3\pi} \int_0^\infty \bar{\xi}(r)\, r^2\, \mathrm{d}r\, \frac{1}{(kr)}[\sin kr - kr\cos kr], \tag{2.57}$$

where the last relation holds provided that $\bar{\xi}(r) \to 0$ faster than r^{-2} at large r (i.e. a spectrum which asymptotically has $n > -1$, a valid assumption for spectra of practical interest). This looks better, since there are now only two integrations required, and, furthermore, efficient methods exist for dealing with integrations with sin and cos weightings in the integrand. However, because the window function consists of the difference of two such terms, the transformation remains difficult: evaluating the two parts of the integral separately gives a result as a difference of two large numbers, which is thus generally of low accuracy. The most satisfactory practical procedure seems to be a mixture of the two possibilities: (i) evaluate a table of $\bar{\xi}_{\rm L}(r)$ values for a given linear power spectrum by evaluating the oscillatory integral directly; (ii) transform to a table of $\bar{\xi}_{\rm NL}(r)$ values using the HKLM procedure; (iii) fit splines to the result and differentiate to get $\xi_{\rm NL}(r)$; (iv) Fourier transform to get $\Delta^2_{\rm NL}(k)$. The accuracy of the result can be improved in the final step by transforming $\xi_{\rm NL}(r) - \xi_{\rm L}(r)$, which vanishes rapidly at large r, and then adding $\Delta^2_{\rm L}(k)$ to the answer.

The HKLM method is couched in terms of the mean interior correlation function, $\bar{\xi}(r)$. It would clearly be very useful to develop a technique for non-linearizing $\Delta^2(k)$ directly, rather than follow the laborious process of transformation described above. Eqn. (2.56), gives $\bar{\xi}(r)$ as an integral over k of $\Delta^2(k)/k$ multiplied by a window function, $3[\sin kr - kr\cos kr]/(kr)^3$. Expanded to second order in kr, this window function takes the form $1 - k^2/\sigma^2$, where $\sigma^2 = 10/r^2$, which form is also the expansion to second order for a Gaussian, $\exp[-k^2/\sigma^2]$. Using this approximation, and changing variables to $l = k/\sigma$, Eqn. (2.56) becomes

$$\bar{\xi} \approx \int_0^\infty \Delta^2(\sigma l) \exp -l^2\, \frac{dl}{l}. \tag{2.58}$$

For a power-law, $\Delta^2(k) = (k/k_0)^{(3+n)}$, this gives

$$\bar{\xi} \approx \frac{1}{2}\Delta^2(\sigma)\Gamma(\frac{3+n}{2}), \tag{2.59}$$

which, taking the constant factor into the power-law Δ^2, yields

$$\bar{\xi} \approx \Delta^2(k_{\rm eff}), \tag{2.60}$$

$$k_{\rm eff} = \left[\frac{\Gamma(\frac{3+n}{2})}{2}\right]^{\frac{1}{3+n}} \frac{\sqrt{10}}{r}, \tag{2.61}$$

This approximation is accurate to within a few percent provided that $\Delta^2(k)$ is shallower than $n \approx 0$. In most circumstances, then, he HKLM method can be applied directly to $\Delta^2(k)$:

$$\Delta^2_{\rm NL}(k_{\rm NL}) = f_{\rm NL}[\Delta^2_{\rm L}(k_{\rm L})], \tag{2.62}$$

$$k_{\rm L} = [1 + \Delta^2_{\rm NL}(k_{\rm NL})]^{-1/3} k_{\rm NL}. \tag{2.63}$$

The n-dependence of the effective wavenumber is weak; over the range $-2 \leq n \leq 0$ it is $2.4/r$ to within 20%. This becomes significant when $\Delta^2(k)$ is not a power-law (such as when a power-law is subject to non-linear evolution). What matters then is that the constant relating $k_{\rm eff}$ and $\frac{1}{r}$ should not vary much between $r_{\rm NL}$ and $r_{\rm L}$. When one applies this approximation, one is effectively fitting a power-law to the power spectrum over this range. So long as the power spectrum is a fairly smooth, monotonic, function, as is usually the case in cosmology, and the spectra involved are not very flat, $n \leq -2$, the approximation works well. A power spectrum derived from a pure baryon model could not be treated with this method; the spectrum exhibits oscillatory features. Figure 2.1 compares the this approximation with direct integration of the HKLM method, for CDM models with (lower panel) and without (upper panel) a short wavelength filter. It is apparent that the approximation works well for the CDM models except where the linear power spectrum is very flat, and for the filtered models up to the point where the linear spectrum is cut-off. Since the method compares wavenumbers related through Eqn. (2.63), if the amplitude of the linear power spectrum is high, the non-linear spectrum over a large range of $k_{\rm NL}$ will depend only on the linear spectrum over a much smaller range of $k_{\rm L}$, and at lower wavenumber. This is seen in Figure 2.1 in the greater success of the approximation for those models with greater power. Also

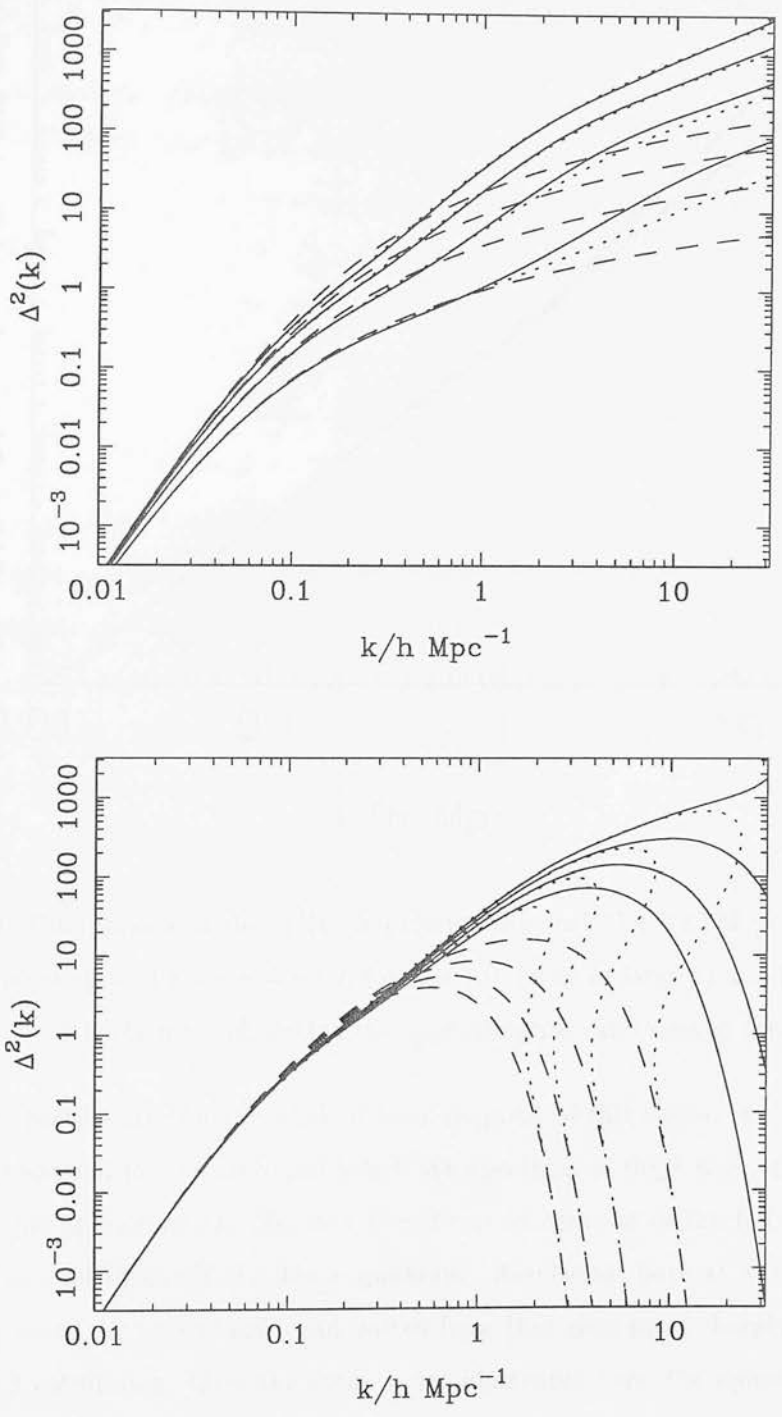

Figure 2.1: Non-linear CDM power spectra according to the HKLM method (solid line), and the direct approximation presented here (dotted line). In the lower panel, the spectra have been filtered. Linear spectra are shown dashed.

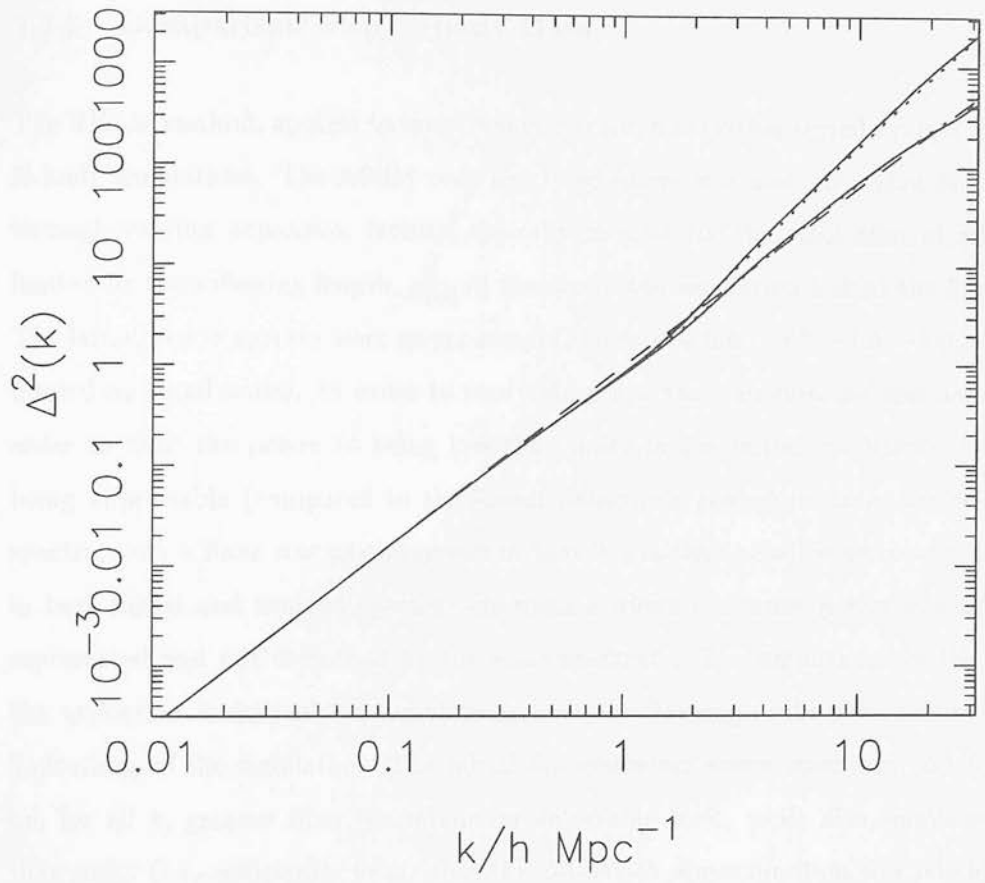

Figure 2.2: Comparison of the $\Delta^2(k)$ approximation with the HKLM procedure, for a canonical power-law of slope $n = -1.2$, for $\Omega = 1.0$ (lower at large k) and $\Omega = 0.2$. Solid lines show the HKLM method, dotted the approximation, and dashed the linear theory.

of interest, particularly for the work of later chapters of this thesis, is the accuracy of this approximation for the canonical power-law spectrum of slope $n = -1.2$. Figure 2.2 compares this approximation (dotted) with direct integration of the HKLM procedure (solid). The dashed line is the linear spectrum. Results for both $\Omega = 1$ and $\Omega = 0.2$ are shown here: the pair of solid and dotted lines that rises most sharply at large k is the $\Omega = 0.2$ calculation. Over the entire range illustrated here, the approximate power spectrum agrees with the HKLM spectrum to within 10%.

2.3.3 Comparison with N-body Data

The HKLM method, applied to the power spectrum, was further tested against numerical N-body simulations. The AP3M code described above was used to evolve 64^3 particles through varying expansion factors, typically around 10, the resolution of which was limited by the softening length, $\frac{1}{1280}$ of the size of the simulation box at the final epoch. The initial power spectra were power-laws of slopes $n = 0.0, -0.5, -1.0, -1.5, \text{and} -2.0$, filtered on small scales. In order to study steep spectra, this filtering was necessary in order to limit the power to being less than unity in the initial conditions, while also being appreciable (compared to the lowest detectable power) on large scales. For all spectra, such a filter was advantageous in that it was then possible to clearly delineate, in both initial and evolved spectra, the regions where the input power was accurately represented and not disturbed by the noise spectrum. The amplitudes of the spectra, the expansion factors of the simulations, and the filtering scale were decided by the limitations of the simulation. The initial dimensionless power spectrum, $\Delta_{\rm i}^2(k)$ had to be, for all k, greater than the minimum detectable level, while also significantly less than unity (i.e. sufficiently linear that the Zel'dovich approximation was reliable). The final conditions had to be sufficiently non-linear so as to be interesting, but still linear on the fundamental mode, $k = 2\pi$ in units where the simulation volume is unity. As a consequence of this, simulations with spectra with $n = -2.0$, only covered a relatively small range of $\Delta_{\rm NL}^2(k)$. For all spectra care had to be exercised when choosing initial conditions and expansion factors. When deducing the non-linear function from the N-body data, the power spectra at wavenumbers higher than $k = 400$ (in units where the simulation box has width unity) were discarded, as the (particle) resolution limit of the simulations was being reached.

The output of the simulations was recorded at the final expansion factor, and two intermediate stages. The non-linear functions, $f_{\rm NL}(x)$, deduced from the N-body data are shown in Figure 2.3, along with $f_{\rm NL}(x)$ (unbroken lines), as deduced by HKLM. It is apparent that for slopes $n \geq -1.5$ the agreement is very good, especially when one considers that the model covers three or more orders of magnitude in $\Delta_{\rm NL}^2(k)$. It appears that for $n = -2.0$, the agreement between model and data is not as good as for steeper

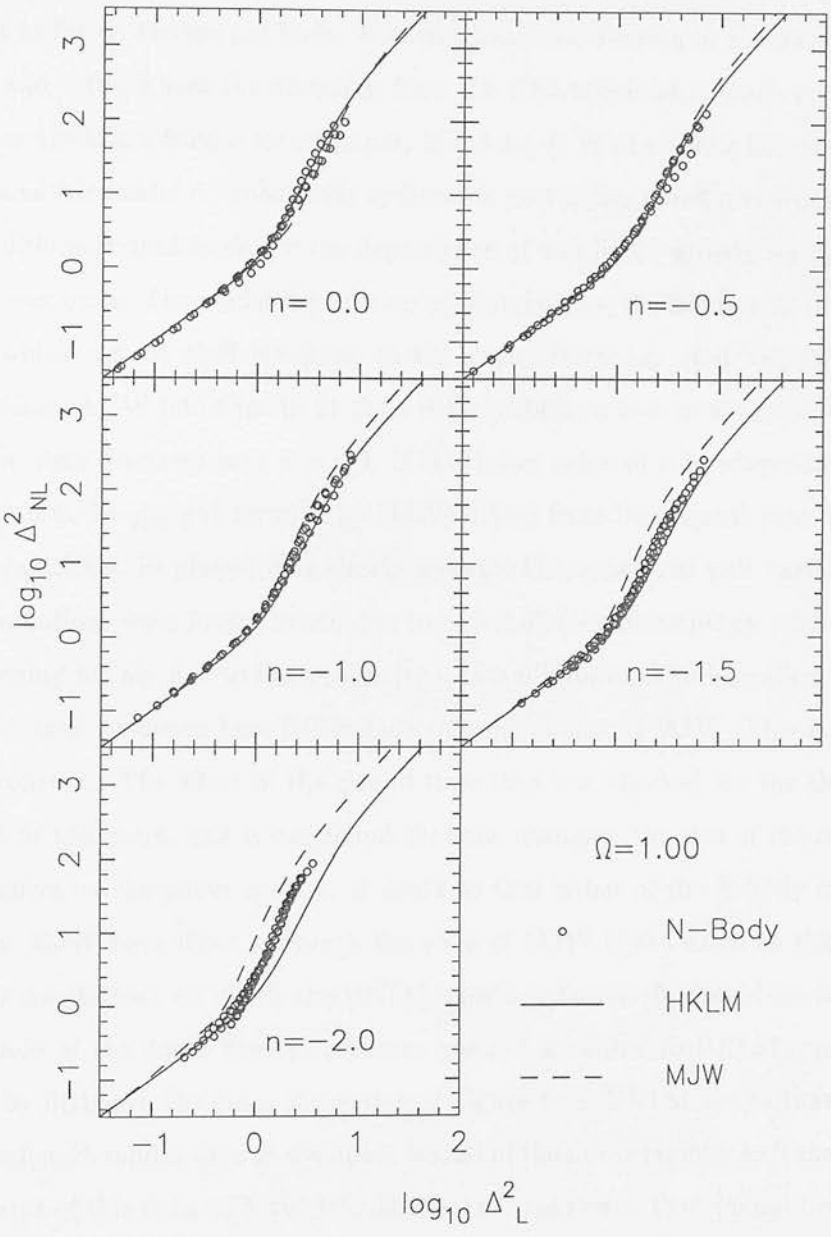

Figure 2.3: Non-linear growth function, f_{NL}, deduced from N-body simulations (circles), the HKLM model (solid lines), and the MJW model (dashed lines).

spectra. The data clearly follow a trend away from the model function, in the direction of, but not as far as, the dashed lines. This trend can also be seen in the data for slopes $n = -1.0$ and -1.5, where the deviation from the HKLM model is much smaller. The dashed lines are taken from a recent paper, Mo, Jain, & White (1995, hereafter MJW), where an analytic model for spherically symmetric gravitational collapse from Gaussian initial conditions is used to derive the dependence of non-linear growth on the slope of the power spectrum. The model depends on a parameter, α, the fraction of turn-around radius at which a mass shell virializes, to the sixth power, i.e. it is very sensitive to this parameter. MJW find that to fit their N-body data, $\alpha = 1$ to within two percent, whereas the virial theorem says $\alpha = 0.5$. If this latter value of α is adopted, $\Phi(x)$ (the alternative form for $f_{\rm NL}$ put forward by MJW) differs from its original form by several orders of magnitude in places; it is clearly wrong. The conserved pair surfaces in the EFWD simulations were found to collapse to $\alpha = 0.55$ (the discrepency with the virial theorem arising mainly due to force softening). In addition to this theoretical difficulty, the N-body data produced here fail to bear out the claims of MJW. This is, in itself, cause for concern. The effect of the size of time step was checked for the simulations carried out in this work, and it was found that the changing the size of the step had a negligible effect on the power spectra. It could be that either of the N-body codes used here and in MJW have flaws, although the code of MJW is the same as that used in the EFWD simulations on which the HKLM ansatz is based. It should be noted that the amplitude of the linear theory spectrum was not available to HKLM, and a value was found by fitting to the data. Inspection of Figure 1. in HKLM shows that even the largest wavelength modes were at the upper bound of the linear regime, so it may be that the agreement of this data with the HKLM ansatz is spurious. The simulations used by MJW used between 3.8 and 8 times as many particles as the AP^3M simulations, lending more weight to their data. Although the data here suggest that the non-linear function is not entirely independent of the slope of the power spectrum, the modifications of the HKLM model introduced by MJW overshoot the required correction. Furthermore, it is intrinsically difficult to carry out simulations for spectra as shallow as $n = -2$, where the biggest discrepancies occur. Certainly, for the power spectra slopes modelled in later chapters of this thesis, where $n \approx -1.2$, and on the basis of the N-body data presented here, the HKLM method appears to work well. The accuracy of the HKLM method can

be estimated from Figure 2.3; for slopes $n \leq -1.5$, going from linear to non-linear, the HKLM method underestimates the power by about 40%, while going from non-linear to linear the power is overestimated by only 30%. The same figures for the $n = -2.0$ slope are 150% and 60% respectively. These estimates are for $\Delta^2_{\rm NL} \approx 1$; clearly, closer to the linear regime the errors in the HKLM method decrease. There is some evidence in the data that the deduced non-linear function is tending to the stable clustering asymptote of HKLM, but at the wavenumbers in question the power spectrum is close to the resolution limit of the simulations. In Chapter 4, a non-linear spectrum is linearized, its amplitude adjusted as per linear theory, and then non-linearized to give the non-linear spectrum at abitrary redshift. Clearly, if the shift in amplitude is very small, the errors will likewise be small, as the process is inverting itself, returning very nearly the input non-linear spectrum. If the shift is very large, the non-linearization will have very little effect, and the errors will be simply those involved in the linearization. In between these regimes, the error should lie between these two estimates, since the non-linearization is no longer the inverse of the linearization.

2.3.4 Extension of the Model to $\Omega < 1$

The usefulness of this technique would be greatly enhanced if it could be extended to cosmological models where $\Omega \neq 1$. The linear theory of density perturbation growth is valid for $\Omega \leq 1$, differing from the Einstein-de Sitter case in that the linear growth rate is suppressed by a factor $g(\Omega)$, which can be well approximated (Carroll, Press, & Turner, 1992), by

$$g(\Omega) = \frac{5}{2}\Omega_{\rm m}\left[\Omega_{\rm m}^{4/7} - \Omega_{\rm v} + (1+\Omega_{\rm m}/2)(1+\Omega_{\rm v}/70)\right]^{-1}, \tag{2.64}$$

where the subscripts refer to matter (m) and vacuum (v) density contributions. For the remainder of this Chapter, Ω will be taken as being synonymous with $\Omega_{\rm m}$. As in the Einstein-de Sitter case, non-linear correlations will grow as a^3 when stable clustering has been achieved. If it is assumed that objects collapse at high redshift when $\Omega \approx 1$, then the constant of proportionality, 11.68 in the HKLM model, will be unchanged. However, the amplitude of the linear theory correlations when compared with the $\Omega = 1$ linear

theory correlations will be reduced by a factor $[g(\Omega)]^2$. Then, for $x \gg 1$ the function $f_{\rm NL}$ becomes asymptotically

$$f_{\rm NL}(x) \rightarrow 11.68\,[g(\Omega]^{-3}\,x^{3/2}. \tag{2.65}$$

For flat models with non-zero cosmolgical constant, i.e. $\Omega_{\rm m}+\Omega_{\rm v}=1$, $g(\Omega)$ is only weakly dependent on the composition of the total Ω, and is well approximated by $g(\Omega) \approx \Omega_{\rm m}^{0.2}$. This suggests that non-linear effects in such a model should be similar to those in an Einstein-de Sitter model.

The behaviour of the non-linear growth function between these two regimes was investigated with further numerical simulations, carried out for $\Omega = 0.5$, 0.2, and 0.1, which, in addition to the $\Omega = 1$ simulations already mentioned, are plotted as circles in the Figure 2.4. Power spectra with slopes $n = -1.0$ and -1.5 were used for this study, since they are the most interesting cosmologically, being close to the canonical observed spectrum with slope $n = -1.2$. Also, it was found that the non-linear growth model was more successful for these spectra than for steeper or shallower ones, as can be seen in Figure 2.6. It is apparent that the data display a gradual steepening in the intermediate regime as Ω decreases. The following analytical form was found to fit the low-Ω data while reproducing the original HKLM function when $\Omega = 1$:

$$f_{\rm NL}(x) = x\,\left[\frac{1+0.2\beta x+(Ax)^{\alpha\beta}}{1+([Ax]^{\alpha}g^3(\Omega)/[11.68x^{1/2}])^{\beta}}\right]^{1/\beta}, \tag{2.66}$$

where the parameters are $A = 0.84[g(\Omega)]^{0.2}$, $\alpha = 2/[g(\Omega)]$, and $\beta = 2g(\Omega)$, and is shown alongside the data in Figure 2.4. The deviation of the data to the left of the model line which was seen for the $\Omega = 1$ data is also present in the $\Omega = 0.5$ data, but to a lesser degree. The very low density models, $\Omega = 0.1$, 0.2, do not display this feature and agree extremely well with the numerical data. It is apparent from the data that non-linear effects are more severe in low density models.

The dependence of the non-linear growth function on the slope of the linear power spectrum was investigated for the case $\Omega = 0.2$, and the N-body results are plotted in Figure 2.6. The agreement with the model (solid lines) for slopes $n = -1.0$ and -1.5,

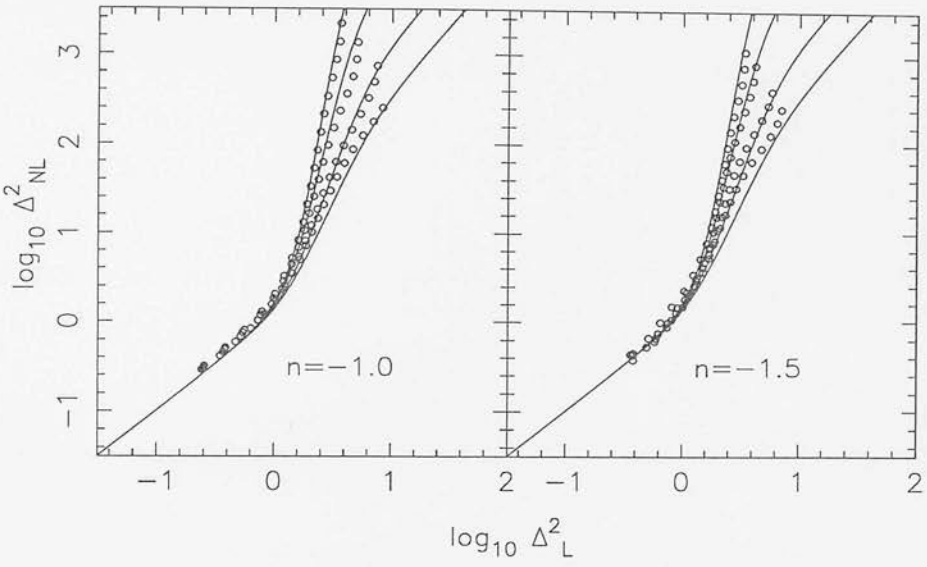

Figure 2.4: The generalization of the HKLM function relating non-linear power to linear power. The lowest curve is the original HKLM function for $\Omega = 1$; in ascending order the other curves are $\Omega = 0.5$, 0.2, and 0.1.

is very good, being accurate on the whole to within 10% for both the linear to non-linear mapping and the non-linear to linear. As was seen in the case of an Einstein-de Sitter cosmology, the model is less successful for very flat spectra, $n = -2.0$, predicting significantly less non-linear power than is observed in the N-body simulations. The linear power deduced from a non-linear spectrum is over-estimated by about 30%, while the non-linear prediction form the linear spectrum is again a factor of 2.5 too small.

The model described here makes predictions for the non-linear growth of not just matter dominated models, but also models with significant vacuum energy. The growth is expected to depend only on the linear theory growth factor, $g(\Omega_m, \Omega_v)$, and not on Ω_m and Ω_v directly. This hypothesis was tested against N-body simulations, considering flat models with $\Omega_m = 0.2$ and $\Omega_v = 0.8$ at the final epoch. The linear growth factor at this epoch was $g \approx= 0.703$, equivalent to a matter-only model with $\Omega_m = 0.55$. (At the

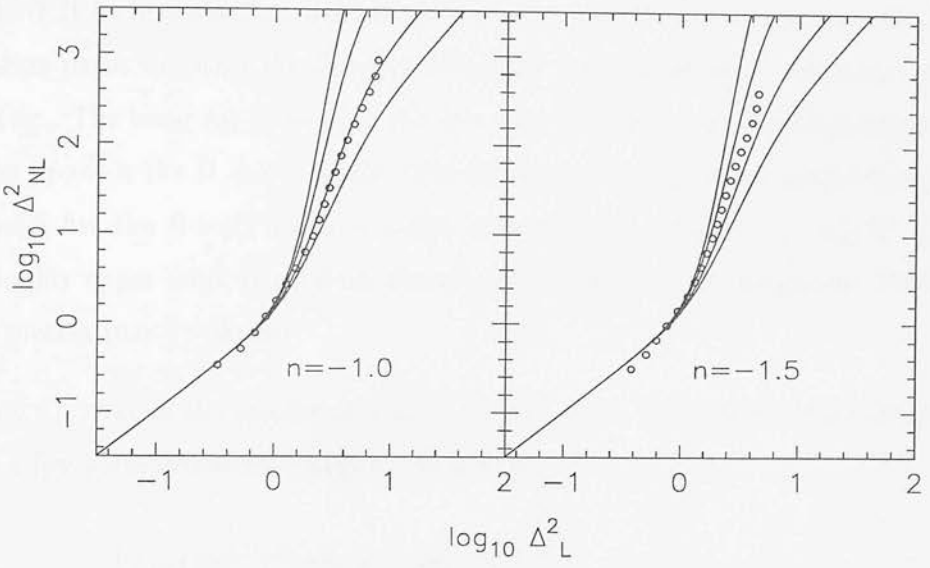

Figure 2.5: Non-linear growth function plotted against N-body data with $\Omega_m = 0.2$ and $\Omega_v = 0.8$. The curves are matter-only models; in ascending order, $\Omega = 1$, 0.5, 0.2, and 0.1. The non-linear growth model depends only on the linear growth factor, which is equivalent to matter-only $\Omega_m = 0.55$.

initial epoch, this simulation was very close to Einstein-de Sitter, with $g \approx 0.999$). Due to time limitations, only two power spectra were simulated, namely, power-laws with slopes $n = -1.0$ and $n = -1.5$, for the same reasons as discussed above. The results are shown in Figure 2.5. The agreement between model and data for the $n = -1.0$ simulation is very good, but less so for the $n = -1.5$ model. This is qualitatively similar to the Einstein-de Sitter model; a steepening of the non-linear growth function, $f_{\rm NL}$, is observed for shallower spectra. Furthermore, Figure 2.4 shows that the effects of steepening the spectrum decrease for low-density models. The data here seem to lie between the Einstein-de Sitter case, and the matter-only $\Omega \sim 0.2$. The cause of this effect is at present not known, but is a worthy topic for further inevstigation. This aside, the N-body data suggest that non-linear growth model works for non-zero vacuum energy

models, as well as more conventional, matter only models.

Figure 2.7 shows the non-linear power spectra evolved from initial spectra with $n = -1.0$ using both N-body simulations and the non-linear model. The circles represent the $\Omega = 1$ simulation data, the stars the $\Omega = 0.2$ data, and the dashed line is the linear theory prediction. The lower (at large k) of the two solid lines is the $\Omega = 1$ non-linear model, and the upper is the $\Omega = 0.2$ model. The success of the non-linear model is evident; the model fits the N-body data to within 30% over the range $0.2 \leq \Delta^2_{\rm NL}(k) \lesssim 500$. Indeed, this upper limit arises from the resolution limit of the simulation, where the power spectra turn up sharply.

The exact inverse of the non-linear growth function Eqn. 2.66 can be approximated to within a few percent over the range of interest by

$$f^{-1}_{\rm NL}(y) = y \left[\frac{1 + (By^{\gamma - 1/3}[g^3(\Omega)/11.68]^{2/3})^{\delta}}{1 + 0.2\delta y + (By^{\gamma})^{\delta}} \right]^{1/\delta}, \tag{2.67}$$

where $B = 0.96[g(\Omega)]^{0.07}$, $\gamma = 1.03 - 0.39[g(\Omega)]^{0.5}$, and $\delta = 5[g(\Omega)]^{0.3}$, allowing the linear power spectrum to be reconstructed from the non-linear, as is done in Section 2.4. To illustrate, the linear power spectrum has been reconstructed from a canonical $n = -1.2$ spectrum for a range of values of Ω, and is shown in Figure 2.8. Again, the increased severity of non-linear effects in the low-Ω models is apparent, resulting in very flat spectra.

2.4 Reconstructing the Linear Power Spectrum of Cosmological Mass Fluctuations

The interest that the linear power spectrum presents is described above in Section 2.1. In order to reconstruct the linear power spectrum of mass fluctuations, correction must first be made for the effects of bias and redshift-space distortion.

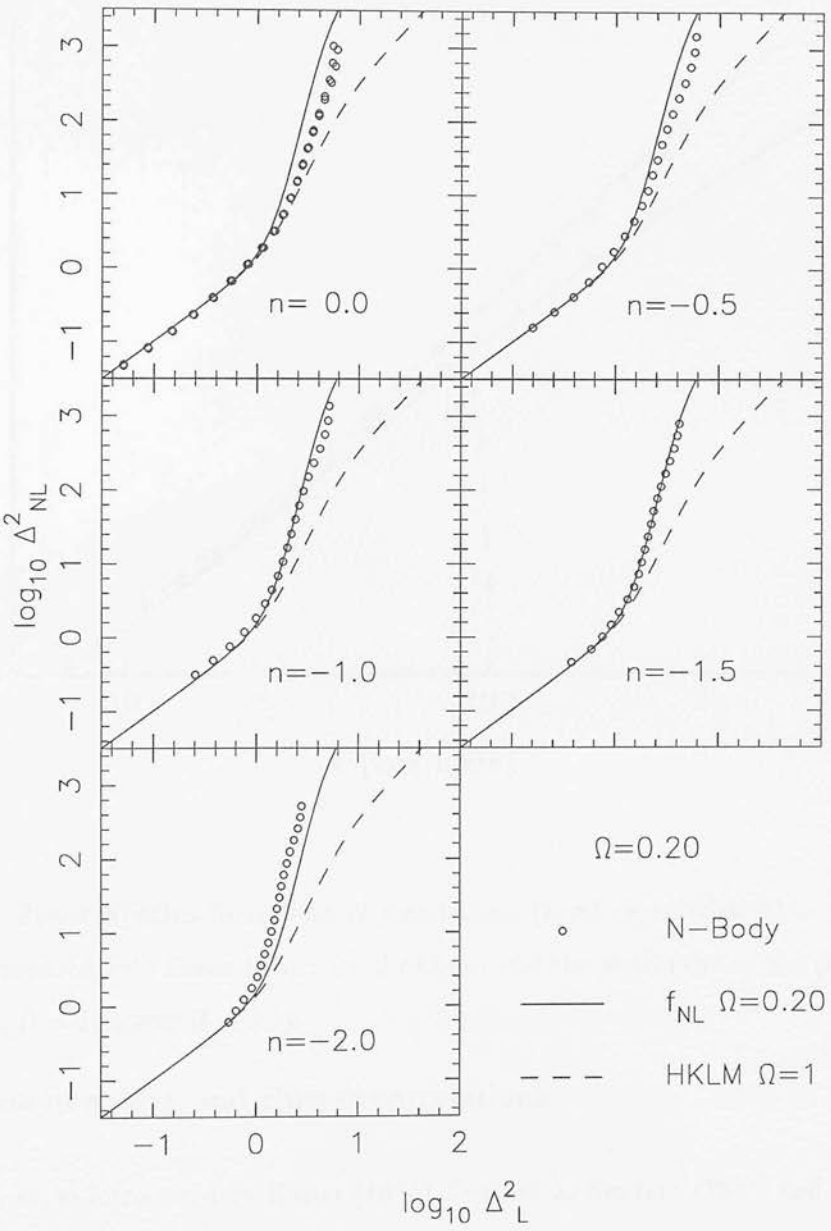

Figure 2.6: Non-linear growth function, f_{NL}, deduced from N-body simulations (circles), and the analytic fit for $\Omega = 0.2$ (solid lines) and $\Omega = 1$ (dashed).

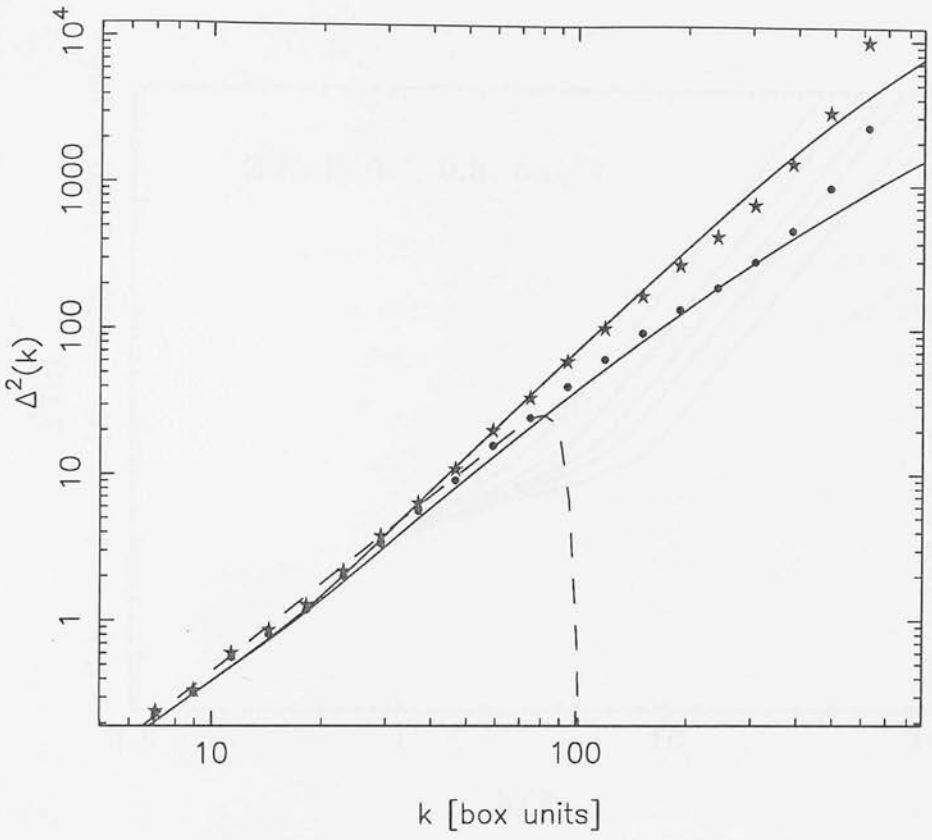

Figure 2.7: Power Spectra from N-body simulations (symbols: circles, $\Omega = 1$; stars, $\Omega = 0.2$) compared with linear theory (dashed line) and the non-linear model (two solid lines: lower, $\Omega = 1$; upper $\Omega = 0.2$).

2.4.1 Bias in galaxy and cluster correlations

If one assumes, as introduced by Kaiser (1984), Peacock & Heavens (1985) and Bardeen et al. (1986; BBKS), that the sites of massive objects such as clusters can be identified at early times as high peaks in the linear density field, then the power spectrum, $\Delta^2(k)$, for a given class of galaxy system can be related, in the linear regime, to the spectrum of the underlying density field through

$$\Delta^2(k) = b^2 \, \Delta^2_{\rm mass}(k). \tag{2.68}$$

For all practical power spectra, the restriction to the linear regime is equivalent to a restriction to large wavelengths. Such a scheme might be termed Lagrangian bias, and

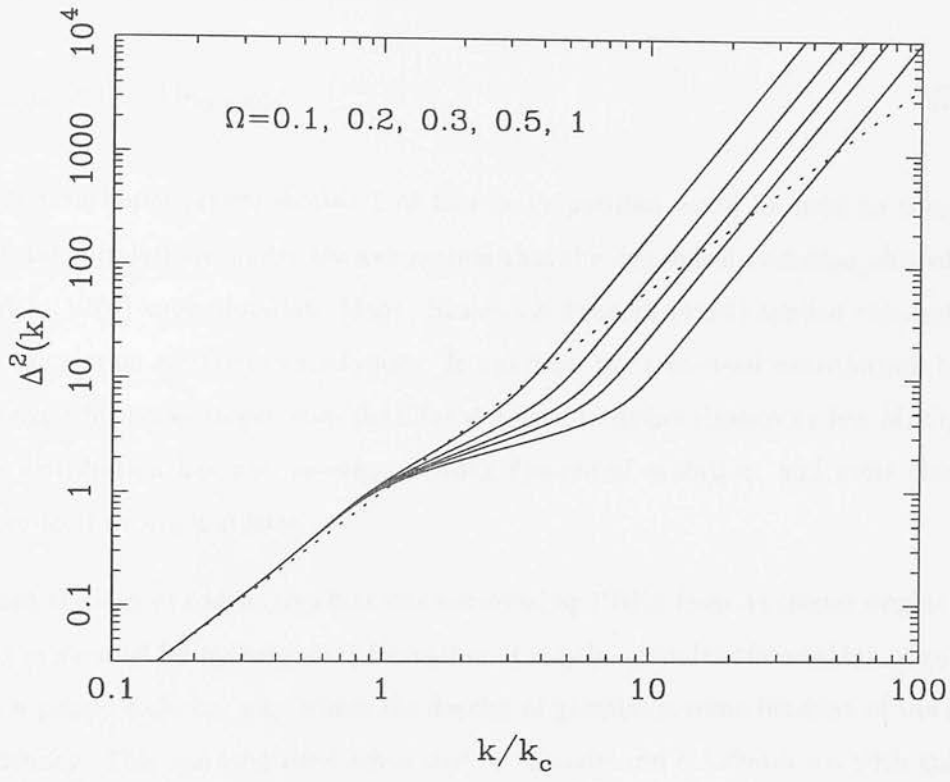

Figure 2.8: The inverse of the generalized HKLM procedure, as applied to a power-law power spectrum (show dotted) $\Delta^2(k) = (k/k_c)^{1.8}$ (in correlation-function terms, $r_0 = 0.945/k_c$). Open models with $\Omega = 1, 0.5, 0.3, 0.2, 0.1$ are considered.

b is called a bias parameter. Some confusion exists over the definition of bias: it can mean a situation where light does not trace mass. However, galaxy clusters would still be more strongly correlated than galaxies, even if light did trace mass. Here bias is taken to mean the enhanced correlations of clusters.

As the density field evolves, the initial statistical clustering in Lagrangian coordinates is supplemented as dynamics moves objects from their initial sites. Owing to the equivalence principle, all objects move in the same way, so that the overall observed clustering in Eulerian coordinates is

$$1 + \delta_{\rm Euler} = (1 + \delta_{\rm Lagrange})(1 + \delta_{\rm dynamics}). \tag{2.69}$$

In the linear regime, we therefore have

$$\delta_{\rm Lagrange} = (b-1)\delta_{\rm dynamics}. \tag{2.70}$$

Bond & Couchman (1988) showed how this decomposition could be used to compute exact total correlations, under the assumption that the dynamical evolution obeyed the Zeldovich (1970) approximation. Mann, Heavens & Peacock (1993) applied this method to the calculation of cluster correlations. In practice, the statistical contribution tends to dominate for scales larger than the filter size used to define clusters (a few Mpc); the cluster distribution has not undergone strong dynamical evolution, and most clusters are close to their original sites.

Although the idea of Lagrangian bias was borrowed by BBKS from its cluster origins and applied as a model for biased galaxy formation, it may be more fruitful to think of galaxy bias in a purely Eulerian way, where the density of galaxies is some function of the final mass density. This has long been advocated by Einasto and collaborators, with galaxy formation being suppressed in low-density regions (Einasto, Joeveer & Saar 1980). More recently, studies of the operation of dissipation in numerical simulations have produced a more direct physical justification for relating the galaxy and mass density fields through a single non-linear function (Cen & Ostriker 1992).

These contrasting views of the origin of cluster and galaxy bias lead to rather different approaches when attempting to use clustering data to infer the mass fluctuations. For clusters, the statistical bias is dominant, and it may be assumed that the clusters reflect mainly the initial conditions. Conversely, it is reasonable to believe that galaxies come close to tracing the mass. Many studies have indicated that different classes of galaxy follow the same 'skeleton' of voids, filaments, walls and clusters, while differing most markedly in regions of high density (e.g. Babul & Postman 1990, Strauss et al. 1992). This last effect may not be so important: despite having densities differing by factors of close to 10 in rich clusters, it shall be seen below that *IRAS* and optical galaxies have bias factors within about 30 per cent of each other. This is analogous to the findings of Cen & Ostriker (1992): even though their model has a highly non-linear dependence of galaxy density on mass density for high densities, the power spectra are proportional on

most scales, even down to the point where $\Delta^2(k) \sim 1$. In any case, it is important to keep in mind that the exact way in which a given class of galaxy does or does not follow the density field are not of interest here: a variety of different bias schemes could give the same galaxy power spectrum, even though the light distributions would be model dependent.

The above discussion motivates the assumptions used below to make estimates of the linear power spectrum. The extreme approximations that the cluster distribution contains information only about the linear power spectrum, whereas the galaxy distribution mainly measures the non-linear density field, are adopted:

$$\Delta^2_{\rm C} = b^2_{\rm C}\Delta^2_{\rm L}, \tag{2.71}$$

$$\Delta^2_{\rm G} = b^2_{\rm G}\Delta^2_{\rm NL}. \tag{2.72}$$

A further way of understanding this distinction is to consider the following illustrative model, in which we populate the Universe with identical spherical protocluster perturbations. At some critical time, these will turn round and virialize, producing a large excess of small-scale power in the non-linear density field. However, at this time, the cluster centres will still be weakly perturbed: the existence of the small-scale power is what allows us to say that clusters are present, but there is no reason to expect this power to manifest itself in many close pairs of cluster centres. Ultimately, the hypothesis must submit to the test of numerical simulation, but for the present it should certainly be closer to the truth to say that clusters respond to the linear power spectrum, rather than to the non-linear one.

Although the above bias factors are calculable given a specific bias model, they are treated here as unknowns to be determined from the data. It is clear that the assumption of constant bias factors cannot be exact, and will certainly break down at small scales. To some extent, the domain of validity can be found empirically, by seeing whether it is possible to make a consistent picture in this way from all the available data. Only data at wavenumbers $k \lesssim 0.6\,h\,{\rm Mpc}^{-1}$, i.e. wavelengths $\lambda \gtrsim 10\,h^{-1}{\rm Mpc}$ (as usual, $h \equiv H_0/100\,{\rm km\,s^{-1}Mpc^{-1}}$), so only the large-scale mass distribution is considered.

There is a third way in which the mass power spectrum may be inferred, which is to use cross-correlation data from two catalogues, in addition to the respective autocorrelations. In this case, it is not so obvious whether the linear or non-linear correlations are more nearly measured. The above restriction to data on large scales means that the distinction will not be so important; for simplicity, a relation to linear theory is assumed

$$\Delta^2_{\rm CG} = b_{\rm C} b_{\rm G} \Delta^2_{\rm L}. \tag{2.73}$$

This provides a useful consistency test of the assumptions made here: the cluster-galaxy cross-correlation should be the geometrical mean of the separate auto-correlations.

2.4.2 Redshift-Space Distortions.

With the exception of surveys where angular data are deprojected to obtain an estimate of the spatial power spectrum, three-dimensional clustering data generally involve redshift surveys where the radii are distorted by peculiar velocities. There are two effects to consider. On large scales, a linear analysis should be valid and so the anisotropic effect noted by Kaiser (1987) should occur:

$$\delta_k \rightarrow b\,\delta_k\,(1 + f\mu^2/b), \tag{2.74}$$

where μ is the cosine of the angle between the wavevector and the line of sight. The function $f(\Omega) \simeq \Omega^{0.6}$ is the well-known velocity-suppression factor due to Peebles, which is in practice a function of $\Omega_{\rm m}$ only, with negligible dependence on the vacuum density (Lahav et al. 1991). The anisotropy arises because mass flows from low-density regions onto high density sheets, and the apparent density contrast of the pattern is thus enhanced in redshift space if the sheets lie near the plane of the sky. If this anisotropic effect is averaged by integrating over a uniform distribution of μ, the net boost to the power spectrum is

$$|\delta_k|^2 \rightarrow b^2\,|\delta_k|^2\,\left(1 + \frac{2}{3}[f/b] + \frac{1}{5}[f/b]^2\right). \tag{2.75}$$

On small scales, this is not valid. The main effect here is to reduce power through the radial smearing due to virialized motions and the associated 'finger-of-God' effect. This is hard to treat exactly because of the small-scale velocity correlations. A simplified model was introduced by Peacock (1992) in which the small-scale velocity field is taken to be an incoherent Gaussian scatter with 1D rms dispersion σ. This turns out to be quite a reasonable approximation, because the observed pairwise velocity dispersion is a very slow function of separation, and is all the better if the redshift data are afflicted by significant measurement errors (which should be included in σ). This model is just a radial convolution, and so the k-space effect is

$$\delta_k \rightarrow \delta_k \exp[-k^2\mu^2\sigma^2/2]. \tag{2.76}$$

This effect in isolation gives an average isotropic factor of

$$|\delta_k|^2 \rightarrow |\delta_k|^2 \frac{\sqrt{\pi}}{2} \frac{\mathrm{erf}\,(k\sigma)}{k\sigma} \tag{2.77}$$

and produces only mild damping (one power of k at large k).

Some workers (e.g. Fisher et al. 1992; Kofman, Gnedin & Bahcall 1993) have combined the above two effects simply by multiplying the two power correction factors to achieve a total distortion. However, this is not correct: both terms are anisotropic in k space and they interfere before averaging: $\langle A^2B^2\rangle \neq \langle A^2\rangle\langle B^2\rangle$. For the present paper, it is also interesting to consider the case of cross-correlation where each of two catalogues gives a different measure of the same underlying density field. The model for the effect in k space of cross-correlation is then the product of two separate factors of the above form:

$$\begin{aligned} |\delta_k|^2 \rightarrow & b_1 b_2 |\delta_k|^2 (1 + f\mu^2/b_1)(1 + f\mu^2/b_2) \\ & \times \exp[-k^2\mu^2(\sigma_1^2 + \sigma_2^2)/2]. \end{aligned} \tag{2.78}$$

The overall effect is obtained by averaging over μ, and looks more complicated than it really is:

$$|\delta_k|^2 \rightarrow b_1 b_2 |\delta_k|^2 \, G(y, \alpha_1, \alpha_2), \tag{2.79}$$

where

$$y^2 \equiv k^2(\sigma_1^2 + \sigma_2^2)/2, \tag{2.80}$$

$$\alpha \equiv f(\Omega)/b, \tag{2.81}$$

$$G(y, \alpha_1, \alpha_2) = \frac{\sqrt{\pi}}{8}\frac{\mathrm{erf}\ y}{y^5}[3\alpha_1\alpha_2 + 2(\alpha_1 + \alpha_2)y^2 + 4y^4] - \frac{\exp(-y^2)}{4y^4}[\alpha_1\alpha_2(3 + 2y^2) + 2(\alpha_1 + \alpha_2)y^2]. \tag{2.82}$$

This simplifies a little in the case of autocorrelations, where indices 1 and 2 are equivalent. The interesting aspect of this formula is that the linear boost is lost at large k, where the result is independent of Ω (as is obvious from the anisotropic form: the main contribution at large k comes from small μ). The true damping at large k is thus more severe than would be obtained by multiplying the power corrections prior to angular averaging. The simulations of Gramann, Cen & Bahcall (1993) show a good level of agreement with the above formula in the autocorrelation case. The result is reassuringly insensitive to the assumed form for the small-scale velocity distribution function; if an exponential is taken instead of a Gaussian, we find the same result at small k:

$$G(y, \alpha_1, \alpha_2) \simeq \left(1 + \frac{\alpha_1 + \alpha_2}{3} + \frac{\alpha_1\alpha_2}{5}\right) - \left(\frac{1}{3} + \frac{\alpha_1 + \alpha_2}{5} + \frac{\alpha_1\alpha_2}{7}\right) y^2, \tag{2.83}$$

and the large-y limit becomes $G \to \pi/(2^{3/2}y)$ instead of $G \to \pi^{1/2}/(2y)$.

In practice, the relevant value of σ to choose is approximately $1/\sqrt{2}$ times the pairwise dispersion $\sigma_{||}$ seen in galaxy redshift surveys. According to the most recent compilation of velocity results by Mo, Jing & Börner (1993b), this corresponds to the figure (adopted hereafter) of

$$\sigma \simeq 300\ \mathrm{km\,s^{-1}}. \tag{2.84}$$

To this, any errors in measured velocities should be added in quadrature . The relatively low value of this dispersion is of course a significant problem for some high-density models. Gramann et al. (1993) argue that redshift-space power spectra of CDM models fit observation very well, mainly because the predicted pairwise dispersion is so high in

these models. As will be seen below, such an unrealistically large dispersion would spoil the agreement between data sets in real and in redshift space.

2.4.3 Data

The above tools can now be applied to some of the more recent results on the clustering power spectrum. Eight distinct sets of data are considered, which fall into several distinct classes.

1. Real-space clustering of galaxies. Baugh & Efstathiou (1993) have applied a de-projection procedure to the angular clustering of the APM galaxy survey to infer the non-linear power spectrum of optically selected galaxies without redshift-space distortions. This paper considers the large-scale power spectrum, and we have thus used the APM data at $k < 1\,h\,\mathrm{Mpc}^{-1}$ only. To allow comparison with other data sets, a lower limit of $k > 0.015\,h\,\mathrm{Mpc}^{-1}$ must be set.

2. Redshift-space clustering of galaxies. The following three data sets are used: Feldman, Kaiser, & Peacock (1994, hereafter FKP) for *IRAS* galaxies (the QDOT sample); Loveday et al. (1992) for the Stromlo/APM survey; Vogeley et al. (1992) for the CfA survey. The last paper quotes results for two separate subsets; a straight mean of the two sets of data is used here. The *IRAS* data of Fisher et al. (1993), which are systematically lower than those of FKP, are not used. As discussed by FKP, this seems most likely to be a local sampling effect. In any case, it is the deeper QDOT sample used by FKP which also appears in cross-correlation analyses (see iv below).

3. Redshift-space clustering of groups and clusters of galaxies. The power spectrum for $R \geq 1$ Abell clusters from Peacock & West (1992) is used, and also that for radio galaxies from Peacock & Nicholson (1991), on the assumption that the strongly enhanced clustering of these latter objects may be attributed to their location in moderately rich environments.

4. Lastly, the cross-correlation between *IRAS* galaxies and Abell clusters or radio galaxies from Mo, Peacock & Xia (1993a), is used.

Not all of the above data are available directly in power-spectrum form. In cases where what is published is a cell variance or a measure of $\bar{\xi}(r)$, the notion of an effective wavenumber is applied, as discussed above and in Peacock (1991). The treatment of errors requires some discussion. Only FKP give a full realistic error covariance matrix for their data; the other data sets give errors ranging from Poisson estimates to field-to-field errors, but with no discussion of the independence of the measurements at different k. For consistency, a fraction of the FKP data, spaced widely enough to be roughly independent, is used. Any imprecision in this procedure, plus unrecognized systematics, will become apparent once the various data sets are compared with each other.

The raw power-spectrum data are plotted in Figure 2.9. There is a wide range of power measured, ranging over perhaps a factor 20 between the real-space APM galaxies and the rich Abell clusters. We now have to see to what extent these measurements are all consistent with one Gaussian power spectrum for mass fluctuations.

2.4.4 Implications for bias and Ω

The reconstruction analysis has available eight data sets containing 91 distinct $k - \Delta^2$ pairs. The modelling has available five free parameters in the form of Ω and the four bias parameters for Abell clusters, radio galaxies, optical galaxies and *IRAS* galaxies ($b_{\rm A}$, $b_{\rm R}$, $b_{\rm O}$, $b_{\rm I}$). The model is optimized by making independent determinations of $\Delta^2_{\rm L}(k)$ for each data set and then comparing them. This was done in practice by dividing the range $0.01 < k < 0.1\,h\,{\rm Mpc}^{-1}$ into 20 bins, and evaluating a weighted mean power and a χ^2 for each bin. The likelihood of the model is given in terms of the summed χ^2 values:

$$\mathcal{L} \propto \exp -\chi^2/2. \tag{2.85}$$

At this stage, the question arises of whether the errors are realistic, which may be judged from whether the overall χ^2 matches the number of degrees of freedom: in fact, it does not. A procedure that ensures the required match is to add some constant rms error ϵ in quadrature to the existing errors. In practice,

$$\epsilon = 23 \text{ per cent} \tag{2.86}$$

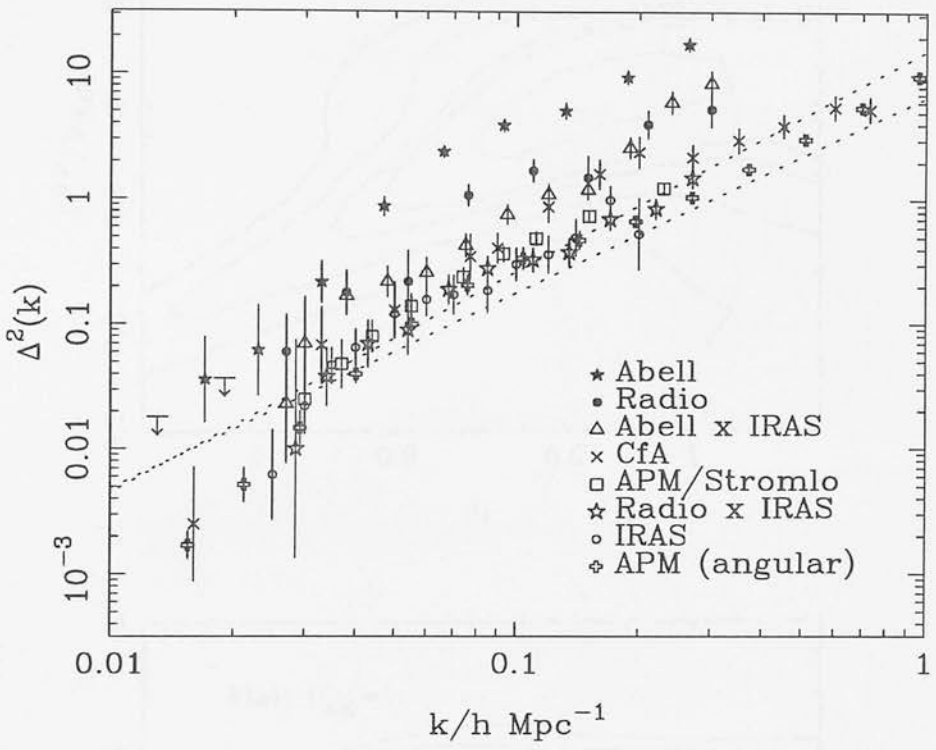

Figure 2.9: The raw power-spectrum data used in this analysis. All data with the exception of the APM power spectrum are in redshift space. The two lines shown for reference are the transforms of the canonical real-space correlation functions for optical and *IRAS* galaxies ($r_0 = 5$ and $3.78\ h^{-1}$ Mpc and slopes of 1.8 and 1.57 respectively).

is required for the best-fitting model. Such a fudge is unsatisfactory and indicates a failure of understanding of the data errors. However, there are grounds for suspecting that some of the published errors are too low, so ϵ is not a surprisingly large correction. There may be excessive democracy here, in that the formally most accurate data sets are penalized most strongly by this procedure. On the other hand, these may be the ones most likely to 'detect' small residual systematics; it seems conservative to distribute the blame for any small disagreement uniformly. One might also query whether this correction should be applied at all k; for many models, the disagreement is worst at high k. The simplest procedure is adopted here, since the quoted errors are usually much larger at low k.

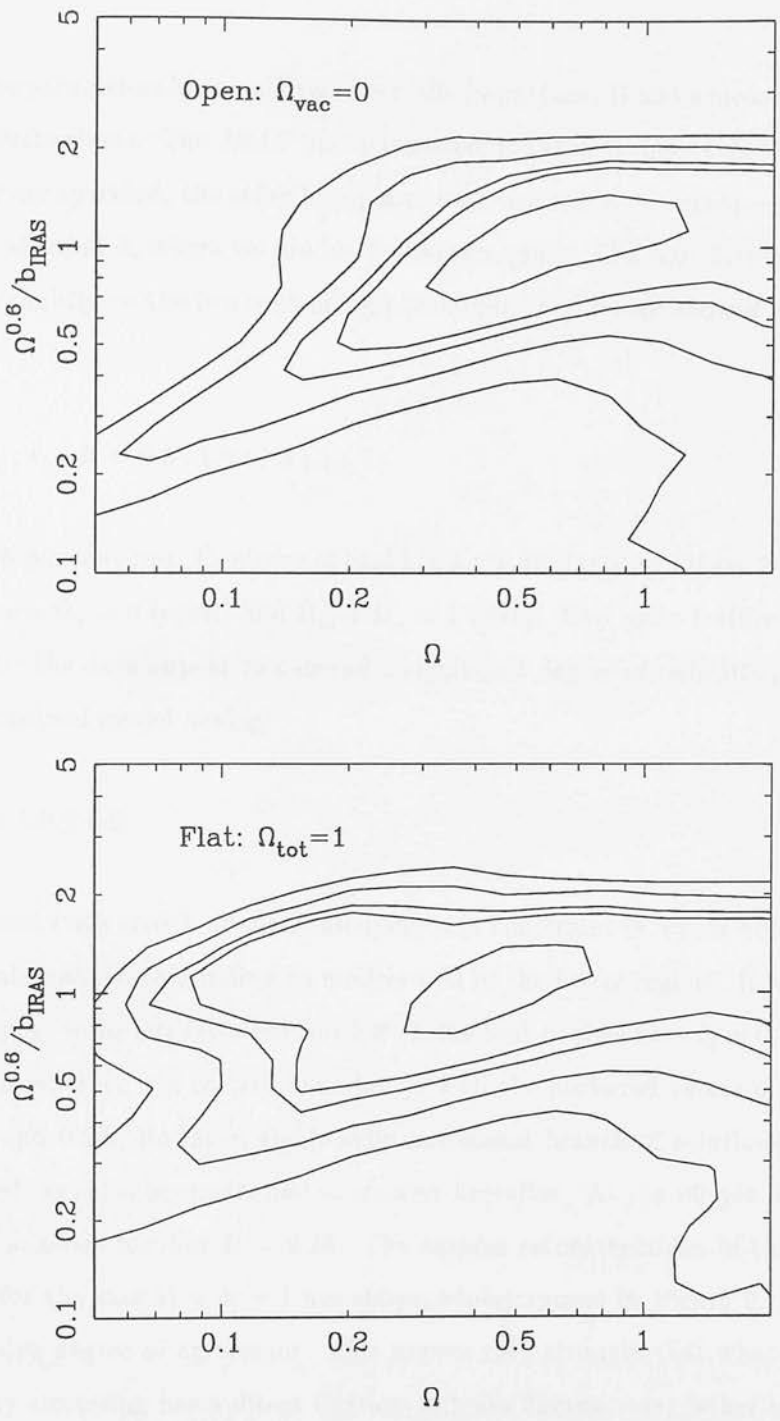

Figure 2.10: Contours of relative likelihood based on the degree of agreement of the various estimates of linear power spectra. At each $(\Omega, b_{\rm I})$ point, the other bias factors have been optimized. The cases $\Omega_{\rm v} = 0$ (open) and $\Omega_{\rm m} + \Omega_{\rm v} = 1$ (flat), are distinguished. Contours are plotted at what would be the 50, 90, 95, 99, 99.5 per cent confidence levels in a two-dimensional Gaussian (i.e. $\Delta \ln \mathcal{L} = 0.69, 2.3, 3.0, 4.6, 5.3$).

Of the free parameters here, only two are really important: Ω and a measure of the overall level of fluctuations. The *IRAS* bias parameter is taken to play this latter role. Once these two are specified, the other bias parameters are well determined – principally from the data at small k, where we are in the linear regime. The best-fitting values depend only very slightly on the two controlling parameters, and for all allowed models are close to

$$b_{\rm A} : b_{\rm R} : b_{\rm O} : b_{\rm I} = 4.5 : 1.9 : 1.3 : 1, \tag{2.87}$$

to within 6 per cent rms. Contours of likelihood are displayed in Figure 2.10, distinguishing the cases $\Omega_{\rm v} = 0$ (open) and $\Omega_{\rm m} + \Omega_{\rm v} = 1$ (flat). Two main features are visible on these plots: the data appear to demand a significant degree of redshift-space distortion, with the optimal model having

$$\frac{\Omega^{0.6}}{b_{\rm I}} = 1.0 \pm 0.2 \tag{2.88}$$

in both cases (rms error). Models satisfying this constraint in which both Ω and $b_{\rm I}$ are large are allowed, corresponding to models well in the linear regime. However, low-bias models appear to be less favoured: for low Ω, the best models have $b_{\rm I} \simeq 0.8$. For the case of flat models, there is a certain bimodality, with the preferred values of $b_{\rm I}$ for $\Omega = 0.1$ being 0.8 and 0.25. However, the heavily antibiased branch of solutions can probably be excluded on other grounds, and is ignored hereafter. At the 90 per cent confidence level, this analysis requires $\Omega > 0.14$. The various reconstructions of the linear power spectrum for the case $\Omega = b_{\rm I} = 1$ are shown superimposed in Figure 2.11, and display an impressive degree of agreement. This argues very strongly that what one measures with galaxy clustering has a direct relation to mass fluctuations, rather than the large-scale clustering pattern being an optical illusion caused by non-uniform galaxy-formation efficiency (Bower et al. 1993). If this were the case, the spectrum inferred from clusters should have a very different shape at large scales, contrary to observation.

The detection of redshift-space distortions is based largely on the inclusion of the APM survey, since it is the only real-space measurement used here. If this data set is removed from the analysis, small values of $\Omega^{0.6}/b_{\rm I}$ are no longer excluded. An upper limit at

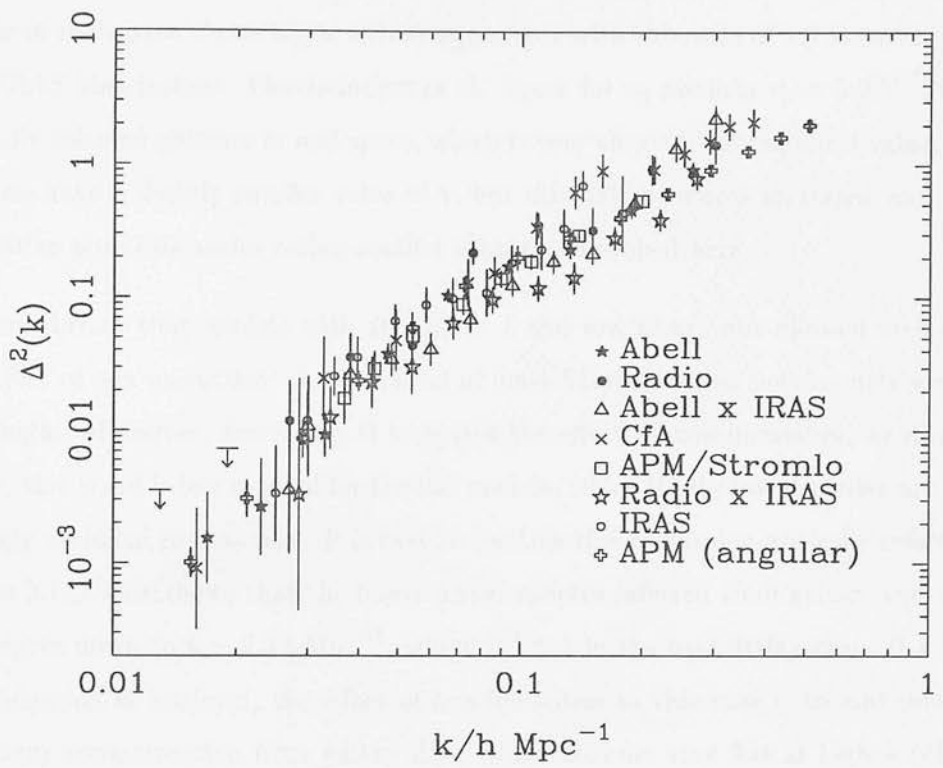

Figure 2.11: The power-spectrum data, individually linearized assuming $\Omega = b_{\rm I} = 1$. There is an excellent degree of agreement, particularly in the detection of a break around $k = 0.03h$.

$\Omega^{0.6}/b_{\rm I} \lesssim 2$ can still be set; this comes primarily from the cross-correlation data. In real space, the cross-correlation should be the geometric mean of the two auto-correlation results. Because of the different effects of the redshift-space mapping, however, this is no longer true when redshift-space distortions become large. The observed cross-correlations thus set a limit to how strong the distortion can be. Some independent confidence in the detection of non-zero distortion can be gained from the work of Saunders, Rowan-Robinson & Lawrence (1992). They deduced the real-space correlation function for *IRAS* galaxies: $\xi(r) = (r/r_0)^{-\gamma}$, with $r_0 = 3.78 \pm 0.14\,h^{-1}$Mpc and $\gamma = 1.57 \pm 0.03$. This is converted to a power spectrum, it lies lower than the QDOT results of FKP by a factor 1.61 ± 0.26 over the range $0.05\,h < k < 0.15\,h$ Mpc^{-1}. This corresponds to $\Omega^{0.6}/b_{\rm I} = 0.75 \pm 0.25$, in good agreement with the figure deduced above, and provides

independent evidence for the detection of significant redshift-space distortion. This lower degree of real-space clustering is also in agreement with the ratio of 1.3 between optical and *IRAS* bias factors. The Saunders et al. figure for r_0 predicts $r_0 = 5.3\,h^{-1}$Mpc for optically selected galaxies in real space, which is very close to the canonical value. *IRAS* galaxies have a slightly smaller value of γ, but this only produces an important change in relative power on scales rather smaller than those probed here.

The conclusion that models with $\Omega^{0.6}/b_{\rm I} \simeq 1$ and low Ω are not allowed stems from the effect of non-linearities: the true level of mass fluctuations in such models would be very high. Moreover, decreasing Ω increases the effect of non-linearities, as discussed above; this trend is less marked for the flat models, which is why low densities are not so strongly excluded in that case. It is easy to see how this conclusion arises by referring to Figure 2.11. This shows that the linear power spectra inferred from galaxy and cluster data agree down to $k \simeq 0.3\,h\,{\rm Mpc}^{-1}$, where $\Delta^2 \simeq 1$ in the best-fitting case. If a higher normalization is assumed, the effect of non-linearities in this case is to add power, so the linear reconstruction from galaxy data would become very flat at high k (cf. Fig. 2.8). However, this would disagree with the cluster data, which would still indicate a steep power spectrum, since it has been assumed that the clusters give the linear result directly. This is a general problem with highly evolved models: since non-linearities change the shape of the power spectrum at $\Delta^2 \simeq 1$, and especially so for low densities, it requires something of a conspiracy for the non-linear power spectrum to be a featureless power law (see Gott & Rees 1975). However, on the present assumptions, extreme non-linear evolution should steepen the galaxy correlations faster than those for clusters, and yet they empirically have much the same slope. The easiest way of understanding this is to say that the degree of non-linearity is only mild. This is certainly an issue which merits further investigation, and a detailed simulation of cluster formation in a highly non-linear low-density model would be most valuable. In the meantime, it is interesting to note that the constraints drawn here on density and bias are very similar to those obtained in a completely independent way by the POTENT group in their analysis of the peculiar-velocity field (Dekel et al. 1993).

Table 1 gives the final data for the mean reconstructed power spectrum, for the case $\Omega = b_{\rm I} = 1$. The data have been averaged in bins of width 0.1 in $\log_{10}$(wavenumber)

and the errors quoted are standard errors. These numbers are plotted in Fig. 2.12, and will be compared with models in the next Section; as will be shown there, the data are consistent with a smooth and featureless power spectrum, despite the small size of the errors. One of the pleasant features of the result is that the power spectrum is only weakly dependent on model parameters. For $\Omega = 1$, the power is not so sensitive to b, because in redshift space (the majority of the data) one measures

$$\Delta_z^2 \propto b^2 \left(1 + \frac{2}{3}[f/b] + \frac{1}{5}[f/b]^2\right). \tag{2.89}$$

The overall power correction factor thus scales only as $b^{10/7}$ for b close to unity. This can be used to rescale the 'standard' result to some other desired value of b, given $\Omega = 1$. For low densities, an empirical formula for the scaling of the linear mass spectrum in the present analysis is

$$\Delta_{\rm L}^2 \propto \Omega^{-0.3}. \tag{2.90}$$

It is convenient to be able to compare the results here with another common measure of the amplitude of linear mass fluctuations. This is σ_8: the linear-theory rms density contrast when averaged over spheres of radius $8\,h^{-1}$ Mpc:

$$\sigma_R^2 = \int \Delta^2(k)\,\frac{{\rm d}k}{k}\,\frac{9}{(kR)^6}[\sin kR - kR\cos kR]^2. \tag{2.91}$$

The squared window function weighting the power spectrum is very close to a Gaussian $W_k^2 = \exp[-k^2R^2/5]$, and so σ_R^2 is just $\Delta^2(k)$ at some effective wavenumber:

$$\sigma_R^2 = \Delta^2(k_R), \tag{2.92}$$

$$\tag{2.93}$$

$$k_R = \left[\frac{([n+1]/2)\,!}{2}\right]^{1/(n+3)}\frac{\sqrt{5}}{R}, \tag{2.94}$$

where n is the effective power-law index of the power spectrum. As before, this approximation is within a few per cent of the exact integration provided that $n \lesssim 0$. On the scales of interest, the effective index is close to -1.5 and so the effective wavenumber for σ_8 is $k = 0.20$. Using the above scalings, it is found that

$$\sigma_8 = 0.75\,\Omega^{-0.15}, \tag{2.95}$$

$k/h\,\mathrm{Mpc}^{-1}$	$\Delta^2(k)$	$\pm$
0.014	0.0010	0.0003
0.018	0.0013	0.0008
0.022	0.0032	0.0009
0.028	0.0087	0.0023
0.035	0.0196	0.0037
0.045	0.0312	0.004
0.056	0.052	0.008
0.071	0.107	0.011
0.089	0.146	0.017
0.112	0.211	0.027
0.141	0.33	0.033
0.178	0.43	0.051
0.224	0.73	0.095
0.282	1.14	0.13
0.355	1.63	0.27
0.447	1.61	0.41

Table 2.1: The linear power-spectrum data, assuming $\Omega = b_{\mathrm{I}} = 1$. To scale the data to other values of these parameters, see text.

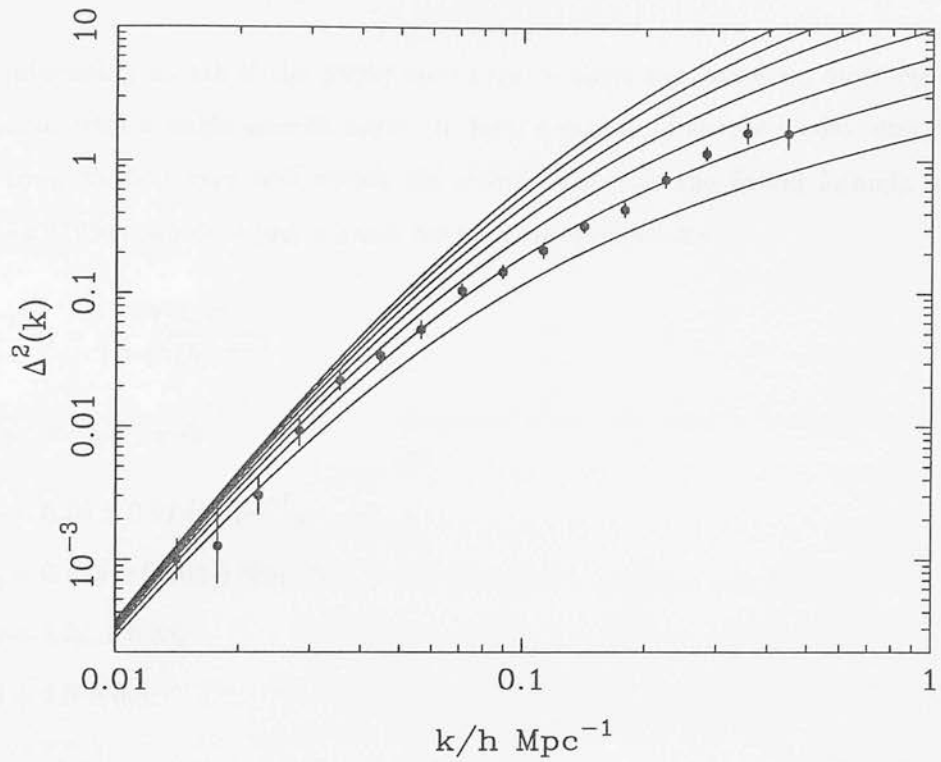

Figure 2.12: The linearized data averaged over bins of width 0.1 in $\log_{10} k$. This plot assumes $\Omega = b_{\rm I} = 1$. Also shown are a number of CDM models with the same large-wavelength normalization. Different values of the fitting parameter $\Omega h = 0.5$ (highest power), 0.45, ...0.25, 0.2 (lowest power) are shown.

with a formal rms uncertainty of 13 per cent.

The significance of $8\,h^{-1}$ Mpc as a normalization scale is that σ_8 is of order unity and thus its value can be probed by observations of weakly non-linear structures such as galaxy clusters. White, Efstathiou & Frenk (1993) discuss this constraint, and deduce $\sigma_8 = 0.57\,\Omega^{-0.56}$ for spatially flat models (although the scaling should be very similar for open models), to within a tolerance of roughly ± 10 per cent. The precise meaning of their uncertainty is hard to quantify, but it seems intended to give hard limits, rather than an rms. The agreement with the results here is very good; the Ω dependence is steeper, but the disagreement in σ_8 is only a factor 1.4 even for $\Omega = 0.2$.

2.4.5 CDM-like models

It is interesting to ask if the power spectrum contains any features, or whether it is consistent with a single smooth curve. In fact, a variety of simple models describe the data from Table 1 very well within the errors. Consider the fitting formula used by Peacock (1991), which is just a break between two power laws:

$$\Delta^2(k) = \frac{(k/k_0)^\alpha}{1+(k/k_c)^{\alpha-\beta}}. \tag{2.96}$$

This works well, with

$$k_0 = 0.29 \pm 0.01\ h\,\mathrm{Mpc}^{-1}, \tag{2.97}$$

$$k_1 = 0.039 \pm 0.002\ h\,\mathrm{Mpc}^{-1}, \tag{2.98}$$

$$\alpha = 1.50 \pm 0.03, \tag{2.99}$$

$$\beta = 4.0 \pm 0.5. \tag{2.100}$$

A value of $\beta = 4$ corresponds to a scale-invariant spectrum at large wavelengths.

A more physical alternative is the CDM power spectrum, which is $\Delta^2(k) \propto k^{n+3}T_k^2$. The transfer function for a CDM model is well approximated by:

$$T_k = \frac{\ln(1+2.34q)}{2.34q} \times[1+3.89q+(16.1q)^2+(5.46q)^3+(6.71q)^4]^{-1/4}, \tag{2.101}$$

where $q \equiv k/[\Omega h^2\ \mathrm{Mpc}^{-1}]$ (BBKS). Since observable wavenumbers are in units of $h\,\mathrm{Mpc}^{-1}$, the shape parameter is the apparent value of Ωh. This scaling applies for models with zero baryon content, but there is an empirical scaling that can account for the effect of baryons. If the scaling

$$T_k(k) = T_{\mathrm{BBKS}}(k/[\Omega h^2 \exp(-2\Omega_{\mathrm{B}})]), \tag{2.102}$$

is used, then the BBKS transfer function can be used to approximate the true transfer functions in the presence of baryons (Holtzman, 1989) Making use of this scaling, the term 'Ωh' can be taken to refer to the BBKS fitting parameter for the present work, on the understanding that it means the combination $\Omega h \exp(-2\Omega_{\mathrm{B}})$. The results here

will hence differ slightly from those of Efstathiou, Bond & White (1992), who defined a parameter Γ which is almost Ωh. Unfortunately, they scaled to a 'standard' CDM model with $\Omega_{\rm B} = 0.03$, with the result that $\Gamma = 1.06\Omega h$.

Fitting the CDM model to the data also results in a satisfactory χ^2 and requires the parameters

$$\Omega h = 0.255 \pm 0.017 + 0.32(1/n - 1), \tag{2.103}$$

in agreement with many previous arguments suggesting that a low-density model is needed. The fit of this and other models is illustrated in Fig. 2.12. It should be noted that the popular choice of $\Omega = 0.2$ (e.g. Kauffman & White, 1992) will produce too low a value of Ωh. For any reasonable values of h and baryon density, a high-density CDM model is not viable. Even a high degree of 'tilt' in the primordial spectrum (Cen et al. 1992) does not help reach the required $\Omega h \simeq 0.75$. The simplest conclusion that can be drawn from this is that the CDM model is largely correct, and that $\Omega \leq 1$. If a high density CDM model is to be reconciled with the data, then it must be assumed that the physical processes modelled in the calculation of the transfer function are incomplete, and that some other mechanism is responsible for making the transfer function look like a low density model. Since the parameter Ωh comes from the horizon size at matter-radiation equality, a decaying particle that would boost the radiation density would do the trick (although it would have to decay after nucleosynthesis takes place, or the model would disagree with observed primordial abundances). A third option is to abandon the CDM model altogether. The Mixed Dark Matter model (MDM: Holtzman 1989; van Dalen & Schaefer 1992; Taylor & Rowan-Robinson 1992; Davis, Summers & Schlegel 1992; Klypin et al. 1993; Pogosyan & Starobinsky 1993) produces a spectrum that bends much more sharply that the data, and is much flatter on small scales. Another option is to invoke gravitational waves as a means to alter the shape of the Hot Dark Matter transfer function, although the absence of detailed predictions make this somewhat unproductive.

An important general lesson to be drawn from this Section is the lack of large-amplitude features in the power spectrum. This is a strong indication that collisionless matter is deeply implicated in forming large-scale structure. Purely baryonic models contain

large bumps in the power spectrum around the Jeans length prior to recombination ($k \sim 0.03\,\Omega h^2\ \mathrm{Mpc}^{-1}$), whether the initial conditions are isocurvature or adiabatic (e.g. Section 25 of Peebles 1993). It is hard to see how such features can be reconciled with the data.

2.4.6 Summary of Results

A compilation of recent studies of galaxy clustering has been analysed, and, under the assumption that large-scale structure formed from primordial Gaussian density fluctuations, the linear power spectrum of mass fluctuations has been recovered. The principal results are these:

1. The relative bias factors for Abell clusters, radio galaxies, optical galaxies and *IRAS* galaxies must be in the ratios $b_{\mathrm{A}} : b_{\mathrm{R}} : b_{\mathrm{O}} : b_{\mathrm{I}} = 4.5 : 1.9 : 1.3 : 1$, to within 6 per cent rms.

2. The data require a significant degree of redshift-space distortion: $\Omega^{0.6}/b_{\mathrm{I}} = 1.0 \pm 0.2$.

3. Low values of Ω and bias are disfavoured because non-linear evolution would spoil the agreement in shape between galaxy and cluster power spectra. Both this and the previous conclusion are in good agreement with independent studies based on peculiar-velocity fields.

4. The linear power spectrum is smooth and featureless, and is well described by a zero-baryon CDM model with $\Omega h = 0.25$.

Chapter 3

DENSITY PROFILES OF GALAXY CLUSTERS

3.1 Introduction

Clusters of galaxies are typically concentrations of mass on scales of a few megaparsecs, and are so large that, except in the very innermost regions, only a few crossing times have elapsed in one Hubble time. The implication of this is that clusters should still preserve information (such as Ω and the linear power spectrum) about the evolutionary history of the universe as they were forming. This realisation has led cosmologists to investigate the processes of cluster formation in order to learn something of the evolution of the cosmos. Two specific features have been identified as most likely to contain information of cosmological interest, namely mass density profiles and substructures (Forman & Jones 1982; Quinn, Salmon & Zurek 1986; Fitchett & Webster 1987; West, Dekel & Oemler 1987; Richstone, Loeb & Turner 1992; Evrard *et al.* 1993).

Attempts have been made to model analytically the formation of galaxy clusters, and these are reviewed in section 3.2. These methods are severely limited by the degrees of symmetry that must be assumed to make the problem tractable. N-body simulations are not bound by this constraint, and have been used extensively by many workers to study cluster formation (section 3.3). Also described in that section are N-body simulations

whose initial power spectra were set up using the non-linear growth approximation of Chapter 2, in order to isolate Ω as a free parameter. In this work, in contrast with the work of Crone *et al.* (1994), the final power spectra of the simulations were largely independent of Ω. The criteria used to identify clusters in these simulations are discussed in section 3.4. In section 3.5, the cluster density profiles are measured and their mean determined. Finally, a discussion of the significance of these results is given in section 3.6.

3.2 Analytic Models

The analysis of a spherically symmetric density perturbation in a uniform density field is considerably simplified if a Newtonian approximation can be made. Consider an infinite, uniform density field which is expanding with the Universe. Now remove all the matter, radiation, etc., in a spherical region. Birkhoff's theorem (see Rindler, 1977) tells us that the metric inside this region will be a Schwarzschild metric

$$\mathrm{d}s^2 = \left(1 - \frac{2Gm}{rc^2}\right) c^2 \mathrm{d}t^2 - \left(1 - \frac{2Gm}{rc^2}\right) \mathrm{d}r^2 - r^2(\mathrm{d}\theta^2 + \sin^2\theta \mathrm{d}\phi^2), \tag{3.1}$$

with $m = 0$ (i.e. zero mass), which is simply the Minkowski metric. Now place some matter in the sphere, again in a spherically symmetric distribution. Then the metric will be perturbed from the Minkowskian form to the Schwarzchild form, with perturbations of order $2Gm/rc^2$. If these curvature perturbations are to be small, $r \ll c/\sqrt{G\rho}$, where ρ is the mean interior density. The Hubble time, $t_0 \equiv H_0(t) = \sqrt{3/8\pi G\rho}$, so the condition becomes $r \ll ct_0$. Observationally, this quantity is approximately 3×10^3Mpc, so the evolution of galaxy clusters (of order 1Mpc across) can be studied using a Minkowski metric. Provided that the velocities involved are much less than the speed of light, the Newtonian approximation to Special Relativity can be used. The largest velocities considered are of order the Hubble velocity across the spherical perturbation. This corresponds to the condition $v = H_0 r \ll c$, which implies $r \ll ct^0$, the same condition as for the General Relativistic effects. Hence, galaxy clusters can be studied using Newtonian mechanics and gravity.

The motion of a spherically symmetric density perturbation was first studied in detail by Gunn & Gott (1972), with further elaborations in Gott (1975) and Gunn (1979). Gunn & Gott considered a spherical region of uniform density, embedded in an unbounded region of constant, but different, density, subject to an unperturbed Hubble law expansion. If a shell of matter has initial radius r_i, and the radius at later times is written $r(r_i, t) = r_i a(r_i, t)$, then the evolution of the local scale factor, a, is governed by the Newtonian differential equation,

$$\dot{a}^2 = \frac{8\pi G}{3a}\bar{\rho}_i(r_i) + \frac{8\pi G}{3}(\rho_{ci} - \bar{\rho}_i), \tag{3.2}$$

where dots denote differentiation with respect to time, $\bar{\rho}_i$ is the mean density within radius r_i at the initial time, t_i, and ρ_{ci} is the critical density of the universe at time t_i. This equation has parametric solutions of the same form as the Friedman equation for open, closed, and flat cosmological models. Which one of these provides the correct solution depends on the difference between the density of the region within radius r_i, and the critical density of the universe at the same time. Clearly, if the interior density is greater than the critical density, then the shell will eventually cease to expand, turn around and collapse. If the density is less than the critical value, the region will continue to expand indefinitely, and if the density is exactly the critical value, the motion of the spherical region will be poised between the two scenarios, with the rate of expansion getting ever slower, but never quite stopping. From the point of view of the study of galaxy clusters, we need only concern ourselves with the first of these cases, galaxy clusters being regions of considerable overdensity. However, as pointed out by Bertschinger (1985), the analysis of such a scenario is very similar to the analysis of the evolution of cosmic voids, with a change of sign in the differential equations leading to hyperbolic, not circular, parametric solutions. It should be noted that the change in sign has a major effect in the case of aspherical perturbations; overdensities become more aspherical (Zel'dovich, 1970), while voids become more spherical.

The solutions, then, to the equations of motion of a spherical overdensity, are, in their simplest form,

$$r = ar_i = A(1 - \cos\theta) \tag{3.3}$$

$$t = B(\theta - \sin\theta), \tag{3.4}$$

where $A^3 = GMB^2$, and M is the mass interior to the shell under consideration.

Gott (1975) used this and other results to estimate the density profile of such a mass distribution. By assuming that a shell expands to its maximum radius, and is then artificially held there, it can be shown that a $\rho \propto r^{-2.25}$ profile results. However, the shells will fall back in, and since the shells accelerate as they fall in, and also since the mass is compressed into a shell of smaller volume, the mass will be more centrally condensed than this simple model. Hence the profile of such an object should lie between this lower limit and the upper limit of r^{-4} (where a finite overdensity collapses) derived numerically (Gott 1973). Gunn (1977) suggested that the infall process may become self-similar, i.e. unaffected in form by a rescaling of lengths, the obvious choice for which being the radius of the shell currently turning around. Gunn argued that, averaged over time, the shells should satisfy the virial theorem, and tend to a mean radius one half of the maximum radius for that shell. This provided support for the assumption of Gott that the shells be artificially held at a fixed fraction of their turnaround radius, and so lent weight to the $r^{-2.25}$ profile.

Filmore & Goldreich (1984, hereafter FG) derived self-similar solutions for the collapse of cold, collisionless matter around perturbations in an Einstein-de Sitter cosmology. They considered perturbations with planar, cylindrical and spherical symmetry. The Newtonian equations of motion were expressed in a scale invariant form, having expressed the mass excess as a power-law function of the interior mass. The non-dimensional equations of motion can then be solved numerically to arbitrary accuracy, and the most important result in the context of this work was that the density profile derived in the spherically symmetric scenario was a power-law, $\rho \propto r^{-2.25}$, for radial positions small compared to the current turnaround radius. Nearer the turnaround point, the density profile became dominated by caustics. These could be understood as one outgoing shell shortly before turnaround catching up with another slightly ahead of it and starting to turn around, with a concertina effect on the mass shells in between. FG found that if the initial slope of the density profile, i.e. the slope of the linear correlation function (see Hoffman & Shaham below), was shallower than $n = -1$, the analysis leading to

the $r^{-2.25}$ profile failed. This analysis included the assumption that an infalling mass shell makes only a small perturbation to the mass interior to an already collapsed shell. For shallow profiles, where the density at large radius is still comparable to the density nearer the centre, this is not the case. FG also found that initial profiles shallower than $n = -2$ produce virialised halos with profile r^{-2}, independent of the initial slope.

Bertschinger (1985b) considered three spherically symmetric scenarios in an Einstein-de Sitter cosmology; collapse and subsequent infall onto a central black hole, collisional collapse leading to shocks, and collisionless infall. Since gravity has no intrinsic scale, the solutions at a late time when the process is dominated by the infall of shells far from the initial overdensity should be self-similar, since the radius, R_i, of the initial overdensity takes on ever decreasing significance. In the expectation of self-similar solutions, the physical variables were couched in dimensionless terms, and this choice was subsequently justified by the finding of such solutions.

The first of these scenarios is the simplest; the boundary conditions implied by the central black hole permit an analytic solution. Bertschinger found that the density diverges near the origin as $\lambda^{-3/2}$, where λ is the radius divided by the radius of the shell currently turning around. This is in poor agreement with observations, and also with other analytic and numerical (see below) models. However, much of the analysis is used in the solution of the second case: shocked infall. The fluid variables (velocity, density, pressure and interior mass) are written in non-dimensional form, and then the fluid equations (continuity, Euler, adiabatic and mass) are expressed in terms of these variables. The pressureless infall solutions of the first scenario are used to provide pre-shock boundary conditions, and the inner boundary conditions are taken to be, at zero radius, zero infall velocity and zero interior mass. The asymptotic behaviour of the fluid equations can be factored out, and the resulting equations solved numerically. A density profile, $\rho \propto r^{-2.25}$ is obtained, in agreement with that found by Gott. The solutions also show that a given shell is halted by the shock at a constant fraction of its turnaround radius, the fraction depending on the ratio of the specific heats of the fluid. This feature explains the agreement with Gott's profile. The collisionless model is complicated by the fact that the mass interior to a given shell is no longer constant, but variable, due to shell crossing. However, Bertschinger (1985a) was able to express

the interior mass as a sum over all mass shells in dimensionless coordinates, and this equation, coupled with the equation of motion can be then solved iteratively, using a first guess solution. The singular behaviour of the solutions at the origin require special treatment. Bertschinger found that the best method was to introduce a small amount of angular momentum, producing a repulsive force $\propto r^{-3}$ which excludes shells from the origin. The amount of angular momentum needed was found to be sufficiently small so as to have negligible effect on shells outside two percent of the present turnaround radius. This produced oscillatory solutions for the radius of a given shell, with the amplitude of the oscillations decreasing asymptotically to a constant fraction (roughly 80%) of the first turnaround radius. The oscillations, their pattern fixed as expected from self-similarity, were of decaying period. The interior mass was found to dip at each point corresponding to the maximum extent of an oscillation. Since the derivative at these dips was infinite, caustics were implied in the density field, as found by FG. More interestingly, the density at radius $r \ll r_{ta}$ was found to obey a power-law relationship, again $\rho \propto r^{-2.25}$, in agreement with the result of FG.

Hoffman & Shaham (1985, hereafter HS) examined the formation of structure around local density extrema. The mean density profile around such extrema, they claimed, was given by

$$\delta(r) = \delta(0)\frac{\xi(r)}{\xi(0)}, \tag{3.5}$$

where $\delta(r)$ is the mean overdensity at radius r, and $\xi(r)$ the correlation function. Since for any correlation function, $\xi(r) \propto r^{-(3+n)}$, $n > -3$ implies that the rms density perturbations increase as one looks on smaller scales, it is necessary to smooth the density field on some scale, r_c, in order to identify peaks. The authors proceeded to consider the evolution of a spherical perturbation possessing the mean density profile. The authors applied the standard techniques of collisionless infall, and assumed that the time averaged radius of a given shell would tend to a constant fraction of its turn-around radius. This is clearly valid for an Einstein-de Sitter cosmology, which is scale-invariant, and this was verified numerically by Bertschinger, above. However, in an open model, a natural scale is introduced, namely the radius of the shell which is just bound. So long

as the radius of the shell currently turning around is much smaller than the outermost bound shell, the system will be approximately scale invariant.

In the first case, the radius of the shell which is just bound is much larger than the filtering scale, and the density profile is then given by

$$\rho(r) \propto r^{-3(3+n)/(4+n)}. \tag{3.6}$$

This case corresponds to an Einstein-de Sitter cosmology, where the radius of the critical shell is infinite, and in an open cosmology, where the objects collapsed at some time in the past when curvature effects were small. The second case is when the radius of the critical shell is slightly larger than the smoothing radius. Here, the initial radius of a shell of interest must be $\leq r_0$ but greater than r_c, which results in a density profile

$$\rho \propto r^{-4}. \tag{3.7}$$

This case corresponds to objects forming at late times in an open cosmology when the curvature has become significant. These results do not work for $n \leq -1$, for the reasons discussed above. It will be seen later that the initial correlation function needed to produce a final one of the desired slope ($n = -1.2$ to approximate present epoch observations), is very much shallower than $n \leq -1$, and so while the analysis of HS is enlightening, its results cannot be applied to the simulations considered here.

The state of analytic models of cluster formation is this: the collapse of a spherical overdensity is well understood, and attempts have been made to apply this statistically to an ensemble of such objects. The collapse of objects possessing cylindrical or planar symmetry has also been calculated. The three omissions in the theory are these: the effects of asymmetry have not been modelled, the effects of environment (such as tidal forces) are not considered, and the evolution of the mean density profile has not been calculated statistically. An N-body simulation is able to include all these considerations, by using a large enough simulation volume to include many collapsed objects.

3.3 Numerical Models

Some early attempts at simulating shells falling onto a core were able to support qualitatively the conclusions of the analytical models (Gott 1975; Dekel, Kowitt & Shaham 1981; Pryor 1982). More recent, and sophisticated, simulations, having an advantage over the analytical models in that they do not need to assume spherical symmetry, have been unable to verify the analytical results quantitatively. Quinn, Salmon & Zurek (1986) were able to demonstrate a link between the slope of the halo density profile and the slope of the power spectrum on the relevant (i.e. Mpc) scale. In their $\Omega = 1$ simulations, they found that only a power spectrum with spectral index $-3 \leq n \leq -1$ could reproduce the observed flat rotation curves. In contrast with this result is the work of West, Dekel, & Oemler (1987) who found no connection between the slope of the initial power spectrum and the density profile for $\Omega = 1$. The slope of the profiles was found to steepen in the inner regions for $\Omega = 0.2$. Supporting the work of Quinn, Salmon, & Zurek, Efstathiou *et al.* (1988) found that the density profiles in their simulations steepened with increasing spectral index. Finally, Warren *et al.* (1992) reproduced the results of Efstathiou *et al.*, but used $\sim 10^6$ particles, compared to the 32^3 of Efstathiou *et al.*.

A recent paper by Crone, Evrard & Richstone (1994) has attempted to clarify the situation, and carry out a systematic study of the effect of Ω and the initial power spectrum on the density profiles of galaxy clusters. They use a P^3M code (see Chapter 2 for details) with 64^3 particles to model the growth of clusters in $\Omega = 1.0, 0.2, 0.1$ models, and an $\Omega = 0.2, \lambda = 0.8$ model. The spectrum of initial conditions has power law form, with slopes $n = -2, -1, 0$. The great virtue of this work is that the dependence of cluster profiles on cosmological parameters is explored systematically, identifying the dependence of the mean profile on Ω and n. The authors find a significant difference in the slopes of the density profiles in the different Ω models, with low Ω models exhibiting steeper profiles. Furthermore, the slope also steepens as n increases, with this effect being most pronounced in the flat models. Some degeneracy of the slope with model was, however, found, limiting the scope of cosmological determinations from this result, but coupled with some other measurement of Ω, Λ or n, the determination of the unknown parameter

remains a possibility.

However, there is one major flaw in the methodology of this work, in that while the final power spectra of all the simulations are the same in the linear regime, non-linear growth leads to significant differences on the non-linear, cluster scales. Since the power on these scales is likely to play a pivotal rôle in the growth of clusters, it is necessary to eliminate differences in the power spectrum before examining the effect of Ω and the slope of the power spectrum on the density profiles. In essence, one should vary only one parameter at a time, which the authors have done in all other respects. The purpose of the work detailed in this chapter is to determine whether the differences in power spectra could account for the observed differences in the density profiles, rather than to examine systematically the effects of Ω and n.

For this work, the Adaptive Particle-Particle Particle-Mesh code detailed in Chapter 2 was used to evolve 64^3 particles, through varying expansion factors. Two sets of simulations were carried out, with $\Omega = 1.0, 0.2$ respectively, in which the initial conditions (i.e. power spectrum) were chosen such that at the end of the expansion period, the power spectrum of the simulation was close to a power-law of slope $n = -1.2$. This form was chosen as a convenient approximation to the measured power spectrum on the scales of galaxy clusters (see Chapter 2).

The shape of the initial power spectrum was determined using the linear reconstruction technique described in Chapter 2, and are shown in Figure 3.1. The amplitude was adjusted so that the power spectrum signal was above the background noise due to the finite number of particles, while still being less than unity, in order that the Zeldovich approximation be valid. A third set of simulations, with the initial power spectrum being a power-law of slope $n = -1.2$, was used as a control to determine the influence of the final power spectrum on the mean density profiles. This set of control simulations is denoted by the letters NC. No control was carried out for the $\Omega = 1.0$ model since for a power-law of this slope, the non-linear effects are very small. For each $\Omega = 1.0$ simulation, an $\Omega = 0.2$ and a control simulation were carried out, using the same random numbers to determine the initial placement of particles, and the phases of the Fourier modes of the potential. The three sets of simulations, then, modelled the same volumes

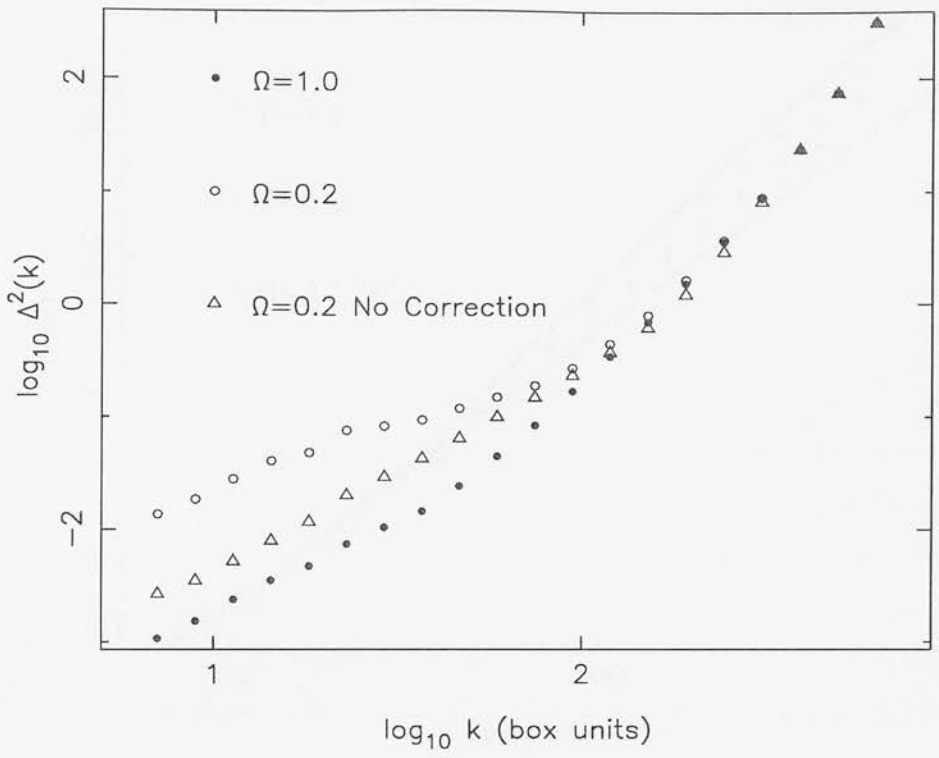

Figure 3.1: Initial Power Spectra of Galaxy Cluster Simulations. The amplitude of the $\Omega = 0.2$ corrected spectrum was initially higher than for the other spectra, in order to raise the very flat portion of the spectrum above the noise. The noise spectrum of the initial conditions is not simply Poisson noise; no attempt has been made to subtract this noise.

of space, save with different initial power spectra and different Ω.

The final power spectra are shown in Figure 3.2. It can be seen that while the two bona-fide simulations' power spectra deviate from a power law on small scales, they are very similar on typical cluster scales, whereas the uncorrected control simulation's spectrum is significantly different from the two others. The two lines show the power law of slope $n = -1.2$ towards which the two principal simulations were aimed, and the predicted non-linear power spectrum obtained from power-law initial conditions in an $\Omega = 0.2$ model. It can be seen that the aim of a power-law power spectrum at the end of the simulation was only approximately realised.

To the extent that the final power spectra were power-laws, i.e. scale invariant, this scaling was irrelevant; the simulations were scale-invariant with respect to the size of the box. In the open model simulations the radius of the outermost bound shell is

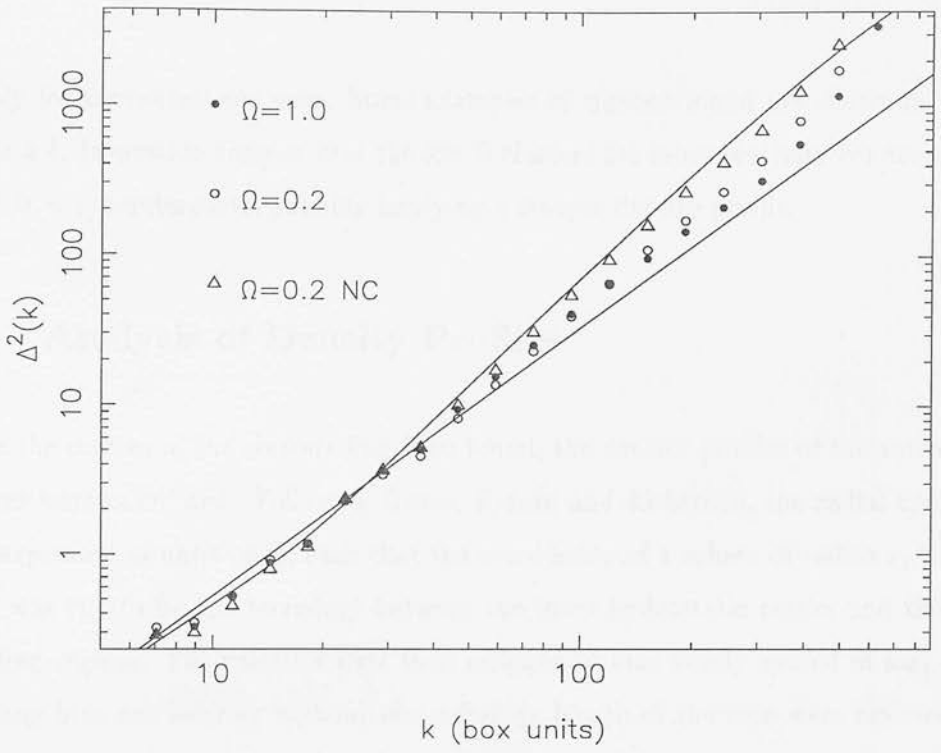

Figure 3.2: Final Power Spectra of Galaxy Cluster Simulations. Poisson noise has been subtracted from these spectra.

introduced. This length scales in the same way as the equations of motion of the clusters, being derived from them.

3.4 Detection of Galaxy Clusters

The particles were first binned up into a 128^3 array, which was then smoothed with a Gaussian filter ($\sigma_1 = 0.02$, in units of the box size). Peaks in this density field were identified, with those possessing overdensity of less than 150 being rejected. All particles within $2\sigma_1$ of the peaks were then binned up into another array, and were this time smoothed on a scale of $\sigma_2 = \sigma_1/10$. An overdensity of 10000 on this scale was considered to be indicative of a cluster core, and so local peaks satisfying these criteria were taken as such. The smoothing scale parameters were chosen as a compromise between having a large number of particles in each object, and there being many such objects in a simulation. The overdensity cut-off's were chosen to reflect the somewhat subjective criteria for what constitutes a galaxy cluster. A two-step process was used

simply for computational ease. Some examples of clusters found are shown in Figures 3.3 & 3.4. Inspection suggest that the low Ω clusters are more centrally condensed than their $\Omega = 1$ counterparts, possibly implying a steeper density profile.

3.5 Analysis of Density Profiles

Once the centres of the clusters had been found, the density profiles of the surrounding matter were calculated. Following Crone, Evrard and Richstone, the radial coordinate was expressed in units of r_δ, such that the overdensity of a sphere of radius r_δ was 300. This was felt to be the boundary between the inner hydrostatic region and the outer, infalling regions. The particles were then assigned to bins evenly spaced in $\log_{10}(r/r_\delta)$, and any bins not entirely without one softening length of the core were rejected. The profiles for the $\Omega = 1$, $\Omega = 0.2$, and $\Omega = 0.2$ NC simulated clusters are plotted in Figs. 3.5, 3.6, and 3.7, respectively.

A weighted geometric mean of the profiles was then calculated. The error in each bin of the measured profiles was taken as the fractional Poisson error, $1/\sqrt{N}$, where N is the number of particles in each bin . However, the profiles also exhibited scatter due not to the measurement errors, but to an underlying "cosmic" variance. It is possible to estimate the mean of such a population, minimising the error on the mean. The appropriate weighting (see Prestage, 1985, for a derivation), w_i, for a given measurement, x_i, should be

$$w_i \propto \frac{1}{\sigma^2 + \sigma_i^2}, \tag{3.8}$$

where σ is the cosmic variance, and σ_i the estimated error on each measurement. The best estimate of the mean is then

$$\overline{x} = \left(\sum_i \frac{x_i}{\sigma^2 + \sigma_i^2} \right) / \left(\sum_i \frac{1}{\sigma^2 + \sigma_i^2} \right) \tag{3.9}$$

with 1σ uncertainty

$$\pm \left(\sqrt{\sum_i \frac{1}{\sigma^2 + \sigma_i^2}} \right) / \left(\sum_i \frac{1}{\sigma^2 + \sigma_i^2} \right). \tag{3.10}$$

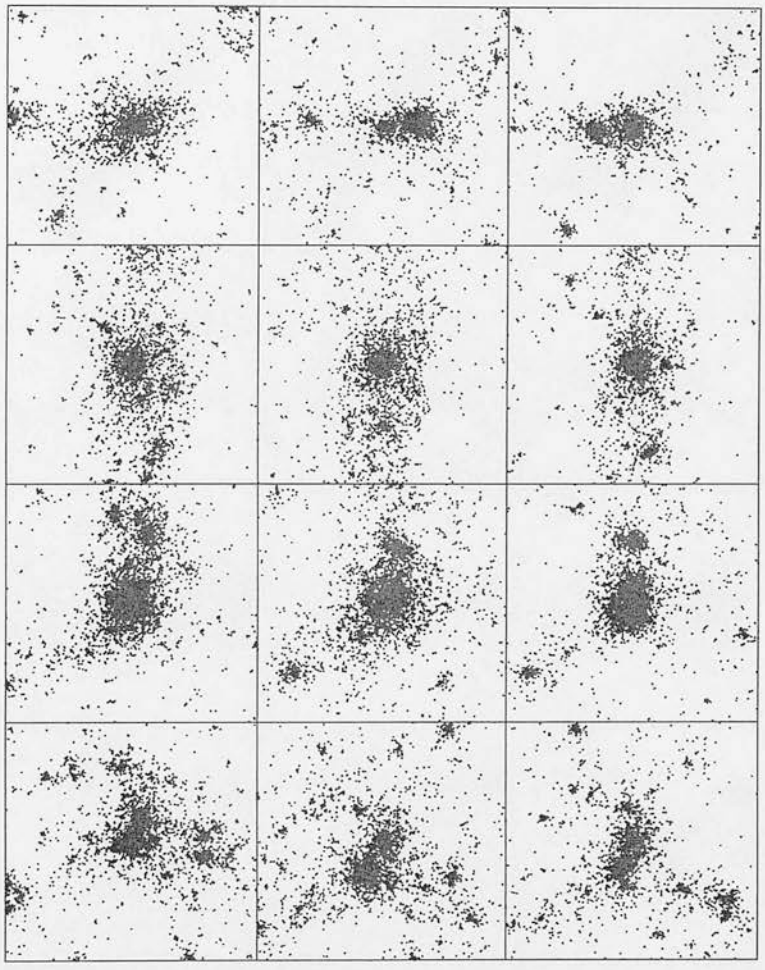

Figure 3.3: Sample galaxy clusters from the three simulation runs; left hand column, $\Omega = 1$, centre column, $\Omega = 0.2$, right hand column, $\Omega = 0.2$ NC.

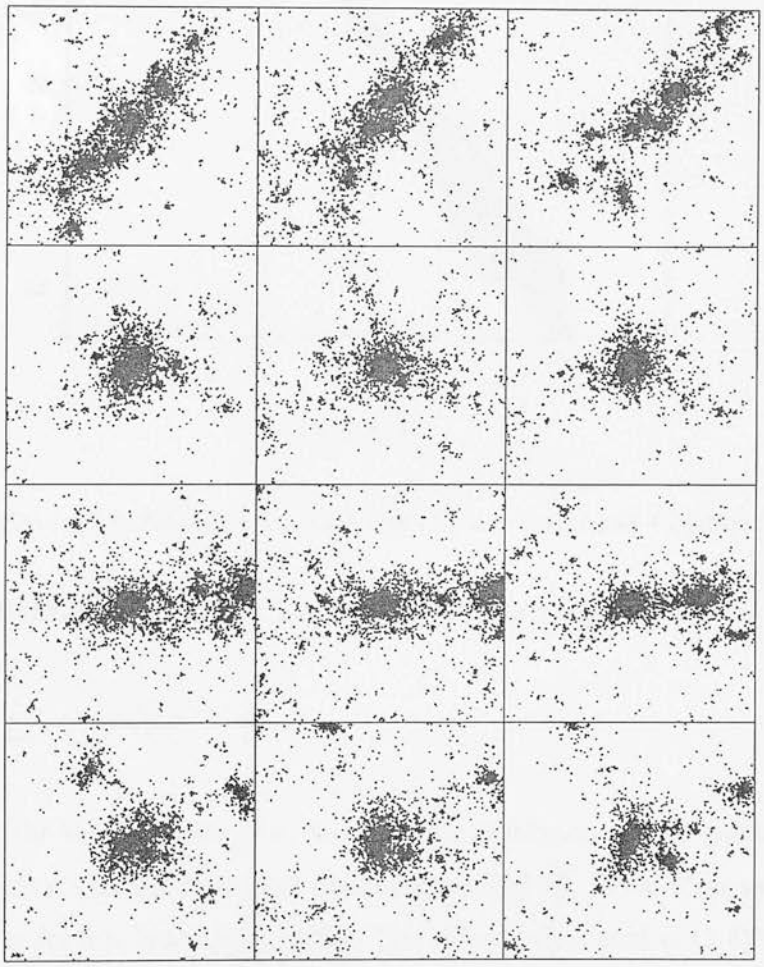

Figure 3.4: More sample galaxy clusters from the three simulation runs; left hand column, $\Omega = 1$, centre column, $\Omega = 0.2$, right hand column, $\Omega = 0.2$ NC.

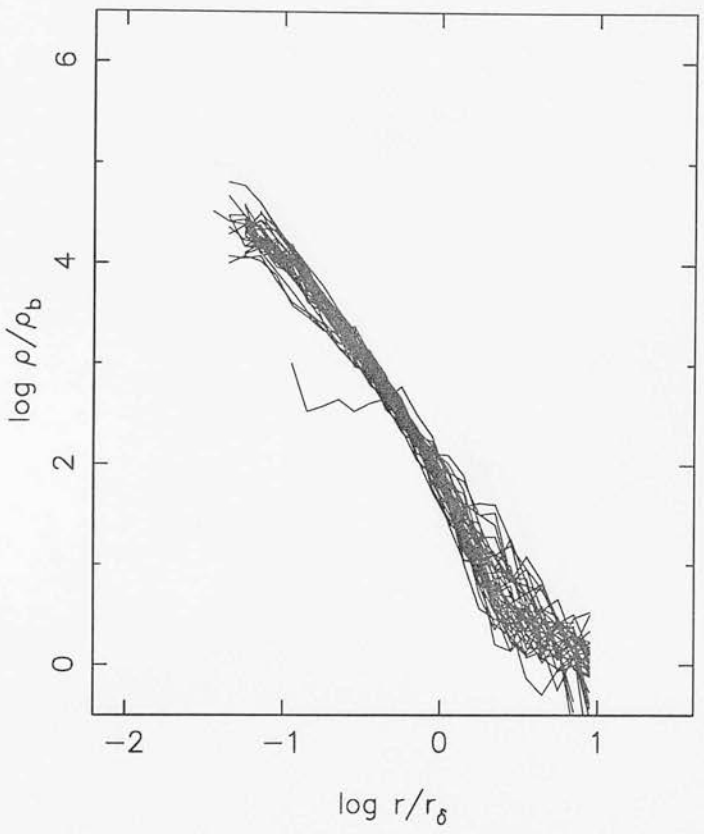

Figure 3.5: Density Profiles for the $\Omega = 1$ Simulated Clusters.

However, σ is unknown. Prestage (1985) shows that the weighted r.m.s. is given by

$$< \overline{x^2} >= \sum_i (w_i - w_i^2)(\sigma^2 + \sigma_i^2). \tag{3.11}$$

To determine the best estimate of σ, one proceeds as follows. A first guess is made for the set of weights, which is then used to calculate $\overline{x}$ and $\overline{x}^2$. Using $\overline{x}^2$ as an estimate of $< \overline{x}^2 >$, a value for σ is found from (3.11). This value is then used in (3.8) to determine a new set of weights, and the whole procedure is repeated until σ converges. (3.9) and (3.10) are then used to determine the mean and associated error. It is possible that this algorithm will converge to a negative value of σ^2, because the errors suggest that there should be more scatter in the data than is evident. This may be purely chance, or it may be (more likely) that the errors are overestimated. This dominance of σ_i^2 over σ^2 can be included in the calculations by setting $\sigma = 0$ for the bins in question.

To calculate a geometric mean of the profiles using this method, the profile densities were converted to logarithmic quantities, with the measurement error being the fractional

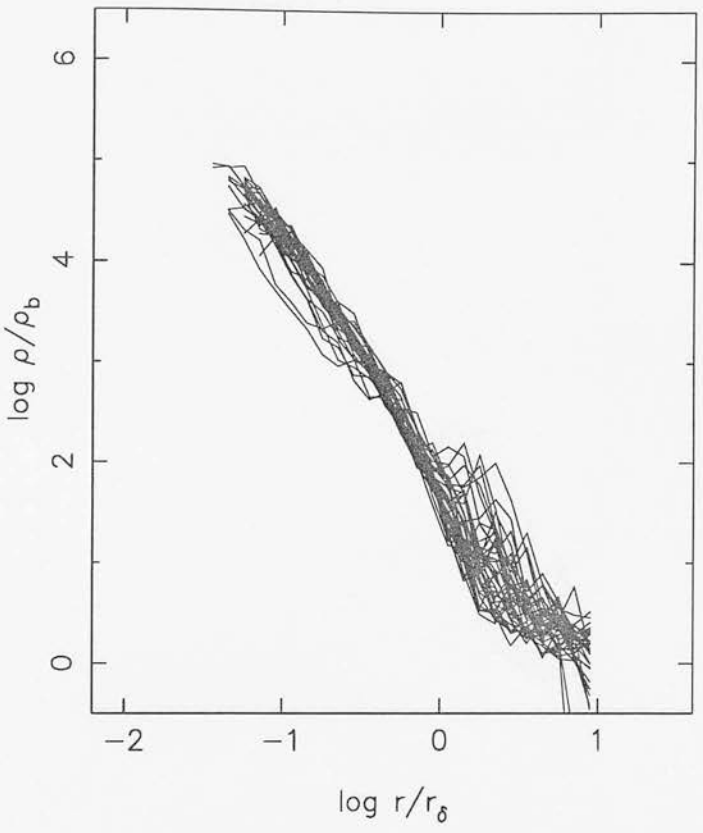

Figure 3.6: Density Profiles for the $\Omega = 0.2$ Simulated Clusters.

uncertainty implied by shot noise in the profile bins, $\sigma_i = 1/\sqrt{N}$.

The mean profiles are plotted in Figure 3.8. The notation 'NC' applied to one profile indicates that no correction for non-linear growth was made for that profile. All three profiles appear qualitatively similar; each starts with a shallow curve, steepening at $\log_{10}(r/r_\delta) \approx -1$, steepening again at $\log_{10}(r/r_\delta) \approx -0.4$, and flattening out towards constant (background) density at $\log_{10}(r/r_\delta) \approx 0.5$. An obvious feature is that the $\Omega = 1$ mean profile flattens out more than the others as one moves from $\log_{10}(r/r_\delta) \approx -0.8$ inwards. While the individual profiles were truncated at one softening length, some effects of softening will persist to separations of about two softening lengths. Close inspection of the individual spectra in Figs. 3.5, 3.6, and 3.7 shows that for the smallest clusters, two softening lengths amounts to $\log_{10}(r/r_\delta) \approx -0.8$, at roughly the same radius as that at which the flattening of the profiles becomes noticeable. For this reason, the apparent turn-over of the density profiles at small radii is probably an effect of smoothing. In order to study the cores of clusters, the cluster must therefore occupy a much larger portion of the simulation volume (and so contain many more particles) than

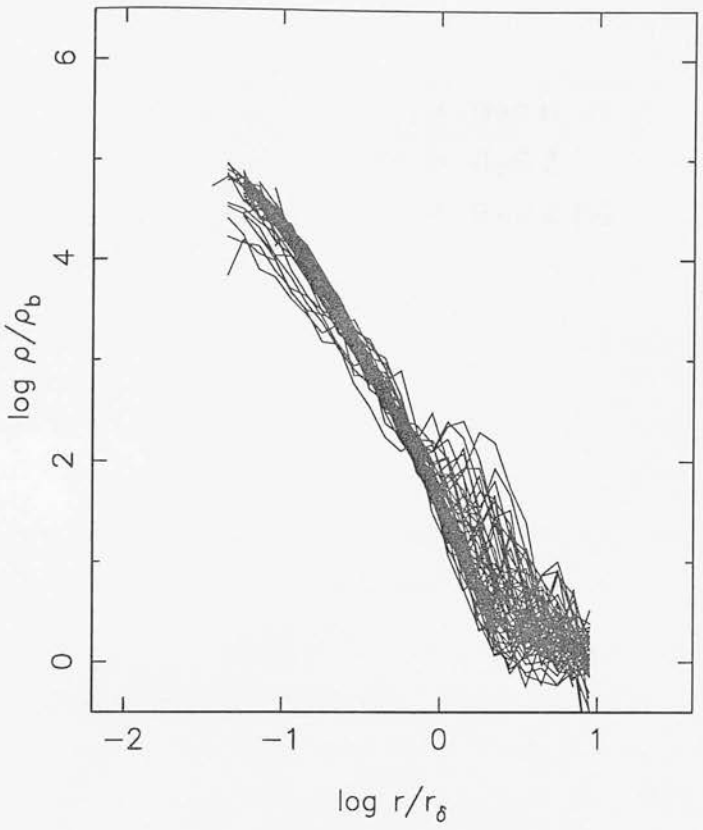

Figure 3.7: Density Profiles for the $\Omega = 0.2$ NC Simulated Clusters.

the clusters modelled here do. It is possible to constrain the initial density field in such a way as to place a cluster at the centre of each simulation volume (Bertschinger 1987; see also van Kampen 1994 for an implementation). The drawback of this is that only one, albeit well modelled, cluster is produced per simulation run. In this work, it is the outer regions of the cluster that are of interest, so such an approach is not necessary. It should be noted that the region of the profile to which a power-law is fitted does not extend to within two softening lengths of the centres of clusters. The two $\Omega = 0.2$ profiles are very similar to each other. Closer inspection reveals, however, that the low Ω profiles steepen rather more than the Einstein-de Sitter profile in the range $-0.8 \leq \log_{10}(r/r_\delta) \leq 0.0$.

A χ^2 fit of a power law, $\rho/\bar{\rho} = A\rho^\alpha$, to each mean profiles was made, considering only those points with density $100 \leq \rho/\bar{\rho} \leq 3000$, as this seemed to delimit the region were the profile follows an approximate power law. The parameters of the power law, the 1σ errors in the slope, and χ^2/ν, where ν is the number of free parameters, are given in Table 3.1. Inspection of the mean profiles by eye suggests that they do not follow a simple power-law, and the power-law analysis is provided only as a measure of steepness. The

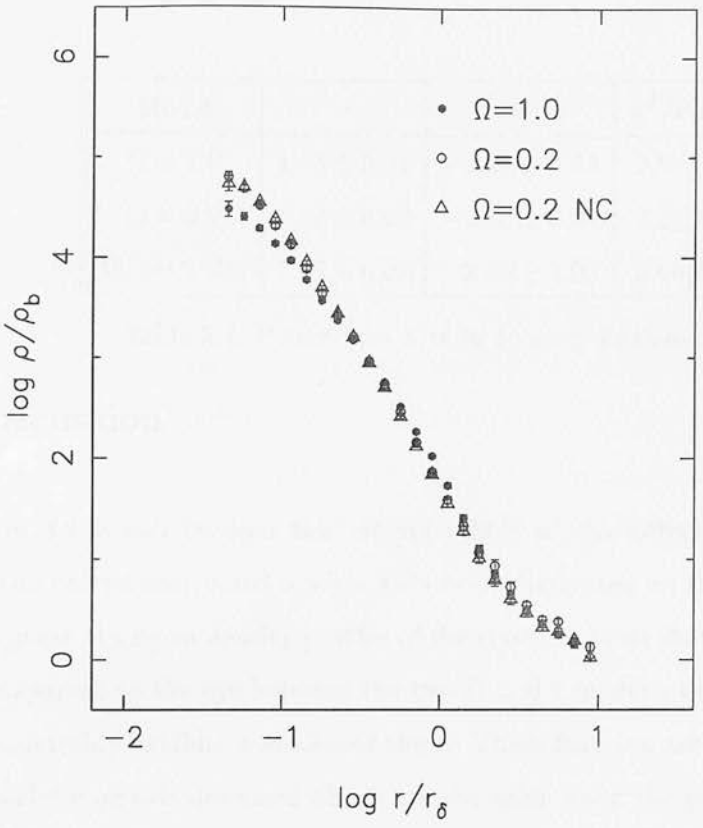

Figure 3.8: Mean Density Profiles

values of χ^2/ν reflect this. However, it can be seen that there are statistically significant differences between the slopes of the three profiles in the region under consideration. The $\Omega = 1.0$ slope is in good agreement with the results of Crone *et al.*, who find $\alpha = -2.33 \pm 0.04$, albeit for a power spectrum slope of $n = -1$. They find, too, that for a power spectrum slope of $n = -2$, $\alpha = -2.20 \pm 0.04$, suggesting that had they carried out a simulation with $n = -1.2$, they would have found $\alpha \approx -2.29$. The slope given in Table 3.1 for the low Ω model without the power spectrum correction is lower than that of Crone *et al.*, although only on the 1σ-level. The corrected low Ω slope is lower still, suggesting that some part of the observed difference in slope of the $\Omega = 1.0$, and $\Omega = 0.2NC$ models is due to the difference in power spectrum. However, the corrected $\Omega = 0.2$ model is still steeper than the $\Omega = 1.0$ model by 4σ. So although some of the difference between models has now been accounted for in terms of differences of power spectrum, a significant difference remains.

Model	A	α	$\chi^2/\nu[\nu]$
$\Omega = 1.0$	1.93 ± 0.01	-2.29 ± 0.03	2.86[5]
$\Omega = 0.2$	1.82 ± 0.02	-2.54 ± 0.05	3.25[4]
$\Omega = 0.2$ NC	1.75 ± 0.02	-2.66 ± 0.03	2.60[4]

Table 3.1: Power Law Fits to Density Profiles.

3.6 Discussion

From Figure 3.2 it can be seen that of order 80% of the differences in final power spectra of the two reconstructed models have been eliminated on the scales of interest. Figure 3.8 giving the mean density profiles of the clusters shows that while there is little difference apparent to the eye between the two $\Omega = 0.2$ models, the Einstein-de Sitter model demonstrably exhibits a shallower slope. These features are quantified in Table 3.1. The analytic models discussed above are not valid when the power spectrum is as shallow as considered here, although they do make qualitative predictions that the mean density profile should be steeper in low Ω models. The lack of quantitative analytic predictions for spectra close to the observed spectrum is a drawback. However, this gap in our knowledge can be, and has been, filled using N-body simulations. The many difficulties involved in modelling analytically (lack of symmetry, lack of scale-invariance, environmental effects, statistical variations) suggest that this is not the right approach; this is clearly the domain of the ever-improving N-body simulations.

It is commonly assumed that in the extremely non-linear regime, the correlation function is dominated by the density profiles of galaxy clusters. This idea, due to Peebles (1980), was used by Hamilton *et al.* (1991) when formulating their model for non-linear evolution, as described in Chapter 2. However, it is shown here that the mean density profile of clusters depends on Ω independently of the power spectrum (equivalently, the correlation function), demonstrating that the correspondence between density profiles and correlation function is less tightly constrained than was thought. Further investigation is needed to determine to what extent the stable clustering hypothesis is undermined. It would be interesting to examine the mean profile and correlation functions as simulations evolve.

The effects of non-vacuum energy have not been considered here; this would be a straightforward, although time-consuming, extension of this work. Unfortunately, if one is prepared to consider such models, a degeneracy is introduced into the linear growth factor, making it impossible to distinguish between matter-only and matter plus vacuum energy models, in the linear regime. It may be that in the non-linear regime, the mean density profile will break this degeneracy, although the studies of non-linear evolution of the power spectrum in such models (Chapter 2) found no evidence for this. Such a dependence of density profile on Ω_m and Ω_v is equivalent to saying that the correlation function - density profile correspondence of Peebles (1980) is dependent on the components of the cosmological density.

The effect of non-gravitational physics on the formation of galaxy clusters has not been studied here. Algorithms now exist for calculating the effects of gas dynamics alongside gravity, and could certainly be applied to this problem. At present, though, such effects are unknown.

The mean density profile of galaxy clusters has been shown to depend on Ω, even when the power spectrum is unchanged. An observational determination of the mean profile could provide a determination of Ω. The best hope for a measurement of dark matter (i.e. mass) profiles is held forth by those working on the use of gravitational lensing to infer matter distributions (Kaiser & Squires, 1993; Fahlman *et al.*, 1994; Broadhurst, Taylor, & Peacock, 1995). In principle, density profiles could be determined, and given sufficient observational effort, a mean calculated. How many profiles would be needed would depend on the accuracy of individual measurements, at present an unknown quantity. Still, the very exciting possibility of a new measure of Ω remains.

Chapter 4

THE ANGULAR CORRELATION FUNCTION OF FAINT BLUE GALAXIES

4.1 Introduction

The model for the non-linear evolution of clustering statistics developed in Chapter 2 can be applied to a model of structure formation, such as CDM, in order to calculate the power spectrum or correlation function at any given epoch. If the quantity in question is known observationally, then the models can be tested. The spatial correlation function and power spectrum have been measured for the present epoch, and can be used to test the linear power spectrum model simultaneously with the evolution model. If, for example, $\xi(r)$ can be measured at sufficiently high redshift, then the evolution model can be tested more directly. However, redshifts, particularly high ones, are difficult to measure, so redshift surveys with sufficient numbers for statistical purposes tend to be confined to low redshift. An alternative approach is to measure the angular correlation function, $w(\theta)$, requiring only positions, which can be measured automatically. The predictions of any particular model of clustering for $w(\theta)$ can be calculated if redshift distribution of the objects is known (which requires many fewer redshifts than a full survey), and

provided that the spatial correlation function for the model in question is known as a function of redshift. In this way it is possible to compare theory with observation for objects at relatively high redshift, giving more information on the evolution, and a better estimate of the linear correlations than shallow redshift surveys. One drawback is that the angular correlation function at a given angle is, in effect, an average of the spatial correlation function over a range of scales and redshifts, and thus some information is lost. Clustering statistics for a population of galaxies, known as the faint blue galaxies, have been extensively studied, and provide an excellent source of data against which to test the models discussed here.

At magnitudes fainter than about $B = 22$, the surface density of objects in regions of the sky away from the Galactic plane is dominated by faint galaxies. These galaxies are on average slightly redder than locally observed galaxies, but when allowance is made for the reddening due to redshift (k-correction), they are found to be significantly bluer than their local counterparts. For this reason, these galaxies are known as Faint Blue Galaxies (hereafter FBGs). There seems to be an excess of the FBGs, when compared with low-redshift optical galaxies, to account for which a number of theories have been put forward. The FBGs may be ordinary galaxies, but at higher redshifts ($z \geq 1$) than previously thought (Tyson 1988), which would make them faint. They may be proto-galaxies in the process of merging to form the galaxies we see today (Broadhurst, Ellis & Glazebrook 1992). Since it is thought likely that star formation is closely associated with the tidal forces that arise from close encounters between galaxies, this would explain the blueness of the FBGs. It has also been suggested (White & Frenk 1991; Babul & Rees 1992) that the FBGs comprise a population of luminous dwarf galaxies that have faded by the present epoch.

The angular correlation function, $w(\theta)$ of the faint blue galaxies has been well determined as a power-law $w(\theta) \propto \theta^{-0.8}$ over the range $0.001^\circ \leq \theta \leq 0.1^\circ$. Recent work by Infante & Pritchet (1995, hereafter IP95) suggests that at larger angular separations, $\theta \geq 0.1^\circ$, $w(\theta)$ starts to fall off more rapidly than such a power-law. The amplitude of $w(\theta)$ in the power-law region is lower than that predicted by simple models of clustering evolution by up to one order of magnitude (Efstathiou 1995). The angular correlation function of the FBGs indicates clearly that their power spectrum is non-linear. No attempt is

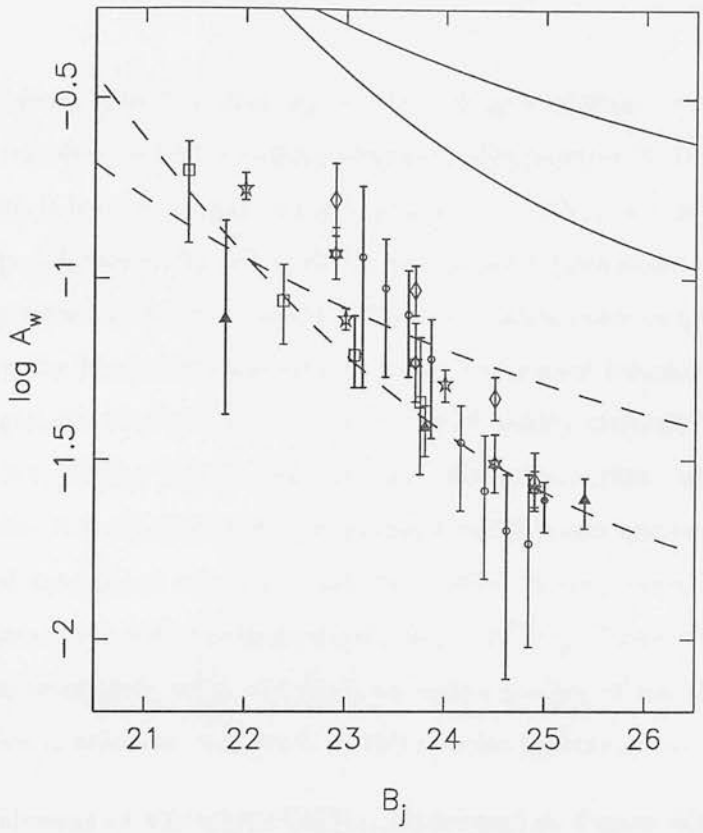

Figure 4.1: Angular correlation amplitude at $30''$ vs. limiting B magnitude.The models of Efstathiou (1995) are shown as solid lines for $r = 5.5\mathrm{h}^{-1}$Mpc and dashed for $r = 2\mathrm{h}^{-1}$Mpc. The data are: filled circle, Efstathiou *et al.* (1991); open circles Roche et al. (1993); open squares, Jones *et al.* (1991); filled triangles, Neuschaefer, Windhoerst & Dressler (1991); five-pointed stars, Pritchet & Infante (1992); rhombi, Couch, Jercevic & Boyle (1993, SGP data); Stars of David, Couch, Jercevic & Boyle (1993, F249 data); open cross, Baugh & Efstathiou (1993, APM).

made to account for non-linear evolution in the calculations of Efstathiou (1995). A method for doing this has been presented in Chapter 2, and is applied in this chapter. The discrepancy between the simple models and observations becomes larger as the limiting magnitude of the survey becomes fainter. Figure 4.1 shows the amplitude of the angular correlation function at $\theta = 30''$ plotted against limiting B-magnitude. Also shown are the predictions of the simple evolution models, as described below in section 4.4. The pair of solid lines show the predictions using a power law correlation function with correlation length $r = 5.5h^{-1}$Mpc, and the dashed lines the same models but with $r = 2.0h^{-1}$Mpc. Two different models of redshift distribution are used, hence

the pairs of lines, also described below. Of each pair of lines, the lower at any given magnitude represents a higher median redshift at that magnitude. On the grounds of this disagreement, it has been suggested (Efstathiou *et al.* 1991) that the faint blue galaxies comprise a population distinct from the typical L^* galaxies observed at the present epoch, which are intrinsically weakly clustered. However, recent work by Loveday *et al.* (1995) investigating the luminosity dependence of the correlation function of nearby galaxies found that galaxies fainter than L^* were only more weakly clustered than L^* galaxies by a factor of 2-4, smaller than is required here. Efstathiou (1995) carried out a number of dark-matter N-body simulations modelling a CDM power spectrum, and found that the observed correlation amplitude and the number density could be explained if the FBGs are associated with low-mass haloes, $M_{\rm H} \leq 10^{12}{\rm M}_{\odot}$. These simulations modelled gravitational interaction only, and until an understanding of the processes leading to star formation is achieved, such work as this remains speculative at best.

In the calculations of Efstathiou (1995), reproduced in Figure 4.1, the clustering of galaxies is assumed to be constant in comoving coordinates. This is clearly an over-simplification, and the agreement of this model with the observations only if $r_0 = 2h^{-1}$Mpc implies that if such a model be accurate, then the galaxies must lie at a redshift much higher than currently suggested by observations. A far better model for clustering evolution has been presented in Chapter 2, and in this chapter it is applied to the problem of the angular correlation function of the FBGs.

The angular correlation function is calculated using Limber's equation, described in section 4.2. Models for the redshift distribution of the FBGs, and the relationship between median redshift and limiting magnitude, are found from observations of these quantities (section 4.3). In section 4.4, a correlation function is derived from the CDM-like power spectrum described in Peacock & Dodds (1994, hereafter PD94), for different values of the cosmic density parameter, Ω. The normalization of the power spectrum, and the bias model are chosen such that the deprojected APM power spectrum of blue galaxies is recovered in the limit $z = 0$. A simple two power-law function is fitted empirically to the observed APM data. Non-linear evolution is also included in this model. In section 4.5 theoretical predictions are compared with observational measurements of $w(\theta)$.

4.2 Calculation of $w(\theta)$

If one knows the spatial correlation function, $\xi(r, z)$, for any redshift, z, it is possible to "project" this onto two-dimensions to determine the angular correlation function (Peebles 1980).

The the expected number density of galaxies with absolute magnitude between M and $M + \delta M$ in a randomly place volume element δV is

$$\delta P = \Phi(M)\delta M \delta V, \tag{4.1}$$

which defines the luminosity function Φ. Implicit in this definition is the assumption that neither the number density of galaxies nor their magnitudes changes with redshift. The probability that a galaxy with magnitude between M_1 and $M_1 + \delta M_1$ be found in volume element δV_1 and a second galaxy with magnitude between M_2 and $M_2 + \delta M_2$ be found in δV_2 at a distance r_{12} from the first is

$$\delta P = [\Phi(M_1)\Phi(M_2) + \Gamma(M_1, M_2, r_{12})]\, \delta V_1 \delta V_2 \delta M_1 \delta M_2. \tag{4.2}$$

This may be taken as a definition of Γ, which is the two-point correlation function of galaxies specified for different magnitudes. Φ is the number density of galaxies per unit magnitude interval. These two definitions can be stated more formally as

$$n = \int \Phi \, \mathrm{d}M, \tag{4.3}$$

and

$$n^2 \xi(r) = \int \Gamma(M_1, M_2, r) \, \mathrm{d}M_1 \, \mathrm{d}M_2. \tag{4.4}$$

where n is the spatial number density of galaxies, and ξ the spatial two-point correlation function, both these quantities being summed over all magnitudes.

Clearly, if the galaxies exhibit no correlation of positions, $\Gamma = 0$. The task now is to integrate Eqn.s (4.1) and (4.2) along a line of sight, in effect projecting the density field

onto the sky. The first problem to consider is that observations are not made in absolute magnitudes, but in apparent. Taking the curvature of space-time into consideration, the flux of energy received from an object with luminosity L at redshift z is

$$f = \frac{L}{4\pi a_0^2 x^2 (1+z)^2}, \tag{4.5}$$

where a_0 is the scale factor at the time of observation, and x is the comoving angular diameter distance to the object. Combining this with the definition of magnitude, and including a K-correction term, yields,

$$m - M = 5 \log_{10} [a_0 x(1+z)] + 25 + \kappa z, \tag{4.6}$$

where m is the apparent magnitude, and κz is the K-correction taking into account the effect of a shift in frequency when the detector is sensitive over fixed range in frequency. An element of solid angle, $\delta\Omega$, subtends proper area

$$\delta A = a(t)^2 x^2 \, \delta \, \Omega, \tag{4.7}$$

and a small increment, δx, in comoving coordinate x corresponds to proper radial increment

$$\delta r = a(t) \, \delta x / F(x), \tag{4.8}$$

where $F(x)$ is a factor accounting for non-Euclidean geometry when $\Omega \neq 1$, and is given by

$$F = \left[1 - (H_0 a_0 x/c)^2 (\Omega_0 - 1)\right]^{1/2}, \tag{4.9}$$

in the absence of a cosmological constant.The last three results can then be used to write a relativistic version of Equation (4.1):

$$\delta P = \delta\Omega \, \delta m \, \frac{\mathrm{d}N}{\mathrm{d}m}, \tag{4.10}$$

where

$$\frac{dN}{dm} = \int_0^\infty \frac{x^2}{F(x)}\, a^3\, \Phi(M,t)\, \mathrm{d}x. \tag{4.11}$$

Here the distance to the galaxy, in comoving coordinates, is x, and the apparent magnitude of the galaxy is m. Similarly, Equation (4.2) is modified to become

$$\delta P = \delta m_1 \delta m_2 \delta\Omega_1 \delta\Omega_2 \left[\frac{dN}{dm_1}\frac{dN}{dm_2} + g\right], \tag{4.12}$$

$$g = \int_0^\infty \mathrm{d}x_1 \int_0^\infty \mathrm{d}x_2\, \frac{x_1^2 x_2^2}{F_1 F_2}\, a_1^3 a_2^3 \Phi_1 \Phi_2\, \xi(x_1, x_2). \tag{4.13}$$

In this equation, ξ is properly a function of both x_1 and x_2, and thus a function of two cosmic times, corresponding to the two distances. However, ξ is known from observations to decrease rapidly with r, and this fact along with any realistic choice of Φ causes the integral in Eqn. (4.13) to be dominated by points at roughly the same cosmic time. Hence, in this small separation approximation, ξ can be taken to be a function of one epoch. Then the correlation function, g, becomes, after a change of variables,

$$g(m_1, m_2, \theta) = \int_0^\infty \frac{x^4 a^6 \Phi_1 \Phi_2}{F(x)^2}\, \mathrm{d}x \int_{-\infty}^\infty \mathrm{d}u\, \xi(r,t), \tag{4.14}$$

with

$$x \equiv \frac{1}{2}(x_1 + x_2), \tag{4.15}$$

$$r^2 = a\left(\frac{u^2}{F^2} + x^2\theta^2\right), \tag{4.16}$$

$$u = x_2 - x_1, \tag{4.17}$$

where it has been assumed that $\xi(r,t)$ is independent of the magnitudes of the galaxies. In a magnitude limited survey of galaxies brighter than limiting magnitude m_0, the probability that a galaxy at distance x is brighter than the cutoff is the selection function,

$$\phi(x) = \frac{1}{n}\int_{-\infty}^{M(x)} \Phi\, \mathrm{d}M, \tag{4.18}$$

where

$$M(x) = m_0 - 5\log_{10}[a_0 x(1+z)] - 25 - \kappa z. \tag{4.19}$$

If we assume that the number density of galaxies is not evolving, then

$$n(t) = n_0 \left[\frac{a_0}{a(t)}\right]^3 \tag{4.20}$$

Then we can write the angular number density (N) and the angular correlation function [$w(\theta)$] as

$$N = n_0 a_0^3 \int_0^\infty \frac{x^2 \phi}{F(x)}\, \mathrm{d}x, \tag{4.21}$$

and

$$w(\theta) = \frac{n_0^2 a_0^6}{N^2} \int_0^\infty \frac{x^4 \phi^2}{F^2} dx \int_{-\infty}^\infty \xi(r,t) du, \tag{4.22}$$

having integrated Eqn.s (4.10) and (4.13) over magnitude.

4.3 The Selection Function

The selection function, ϕ, in Eqn. (4.22) is clearly very important in the evaluation of $w(\theta)$. Because of the faintness that gives them their name, few redshifts are available for the FBGs (which is why this chapter is concerned with the angular correlation function, not the spatial), and as a result their redshift distribution is somewhat uncertain. The redshift distribution, i.e. the number of objects per unit interval in redshift, is related to the selection function by

$$\phi(x) = \frac{F(x)}{x^2} \frac{dz}{dx} \frac{dN}{dz}. \tag{4.23}$$

Before proceeding, it is worthwhile to consider a number of magnitude conventions in common use for observations of the FBGs. Now, b_J is the photographic analogue of the

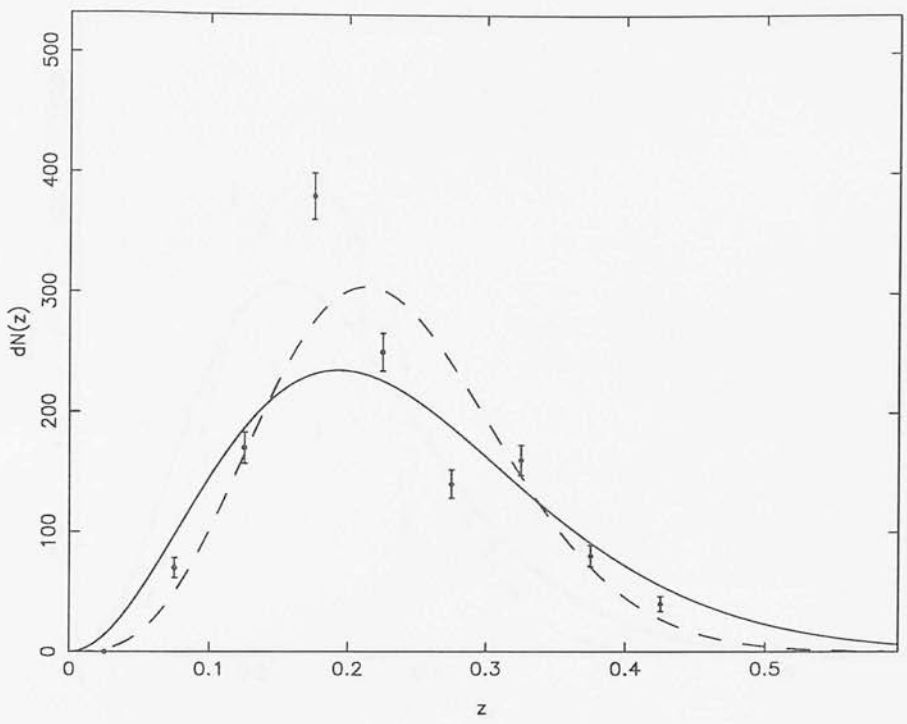

Figure 4.2: Redshift Distribution for $B \leq 21.5$ Baugh & Efstathiou (1993). Solid line shows the fit of BE93, dashed line a more peaked form described in the text.

standard Johnson B magnitude, and these two are easily related. Colless *et al.* (1993) relate standard Johnson B magnitudes to photographic $b_{\rm J}$, giving

$$B = b_{\rm J} + 0.16(b_{\rm J} - r_{\rm F}), \tag{4.24}$$

where $r_{\rm F}$ is a standard photographic red magnitude. The median $b_{\rm J} - r_{\rm F}$ found by Colless *et al.* for FBGs was approximately 1.5, giving $B \approx b_{\rm J} + 0.25$. Infante & Pritchet (1995) have measured the angular correlation function of galaxies selected in the J and F bands, down to limiting magnitudes of 24. Majewski (1992) gives relations between different magnitude systems, and on the basis of these, J magnitude can be related to B as

$$B = J + 0.195(J - F) - 0.005. \tag{4.25}$$

Infante & Pritchet have measured the colours (i.e. $J - F$) for the galaxy sample. For all their galaxies, $J - F \leq 2$, with a median value of approximately $J - F = 1.3$, which gives $B \approx J + 0.25$. This implies $b_{\rm J} = J$, which is reassuring, since $b_{\rm J}$ is the photographic

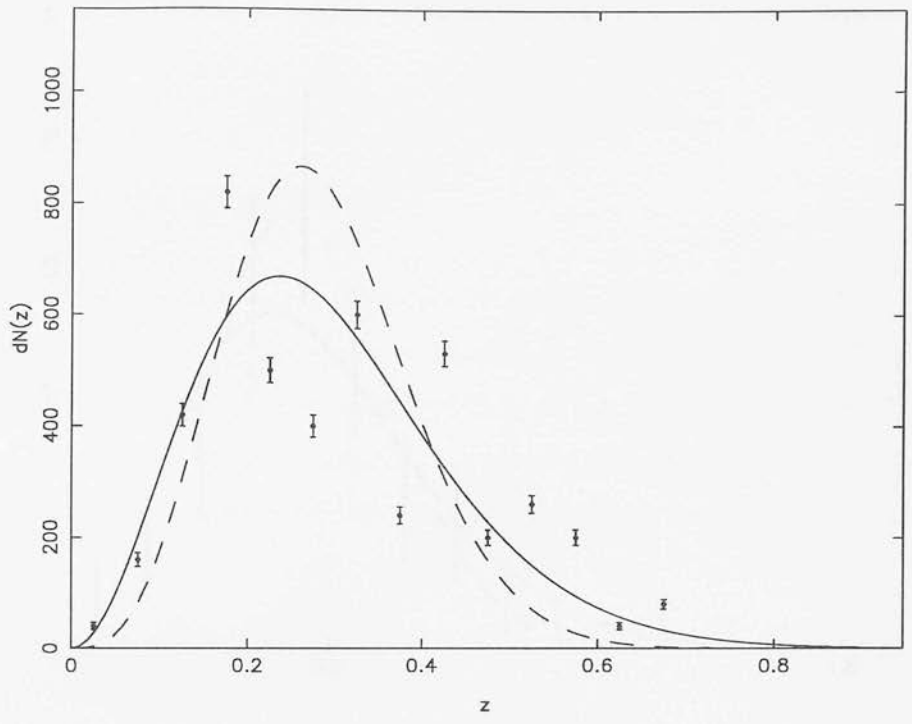

Figure 4.3: Redshift Distribution for $B \leq 22.5$ Baugh & Efstathiou (1993). Solid line shows the fit of BE93, dashed line a more peaked form.

Johnson blue magnitude as measured by the UK Schmidt Telescope, and J is the Kitt Peak equivalent.

In terms of the limiting magnitude of the survey, B_J, Efstathiou (1995) uses

$$\frac{dN}{dz} \propto z^2 \exp\left\{-\left[\frac{z}{z_c(b_J)}\right]^{3/2}\right\}, \tag{4.26}$$

where $1.412 z_c = z_m$, the median redshift. This form was chosen to fit the redshift data of Broadhurst *et al.* (1988) and Colless *et al.* (1990, 1993), as described in Baugh & Efstathiou (1993, hereafter BE93). These data and this distribution are shown in Figures 4.2 and 4.3.

Glazebrook *et al.* (1995) measured the redshifts of 73 galaxies, down to magnitude B=24. Figure 4.4 shows their data, along with the distribution of Eqn. (4.26). They estimate the completeness of this survey to be 73%. The galaxies that were not included in this catalogue were generally too faint for reliable identification and redshift measurement. Thus the incomplete fraction would tend to be at high redshift, suggesting that although

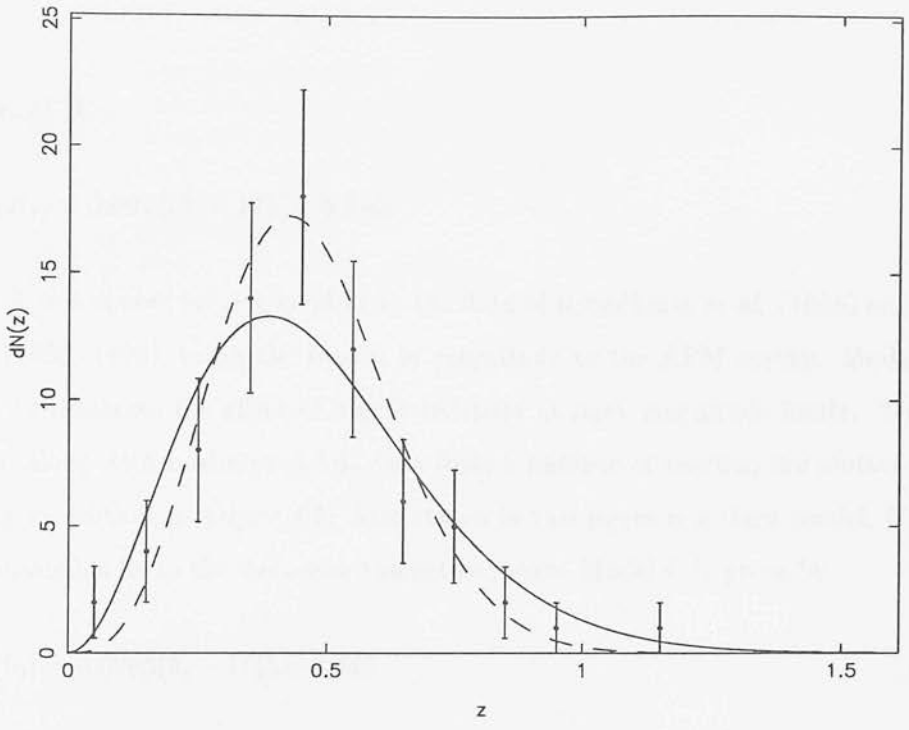

Figure 4.4: Redshift Distribution for $B \leq 24$ Glazebrook *et al.* (1995). Solid line shows the fit of BE93, dashed line a more peaked form.

the data seem more sharply peaked, and at lower mean redshift, than the distribution, the distribution is probably a better fit than it first appears. A more peaked distribution, with a lower median redshift, can be written as

$$\frac{dN}{dz} \propto z^3 \exp\left\{-\left[\frac{z}{z_c(b_J)}\right]^2\right\}. \tag{4.27}$$

The effect of using this distribution, rather than the one above, is typically to increase the amplitude of the angular correlation function by a factor largely independent of angle. For $B \leq 24$, this factor is about 1.3. The distribution of BE93 was used throughout the calculations of this chapter.

Efstathiou (1995) chose two models for the median redshift as a function of limiting magnitude, representing two possible extremes. He denotes these two models A and B, and this convention is followed here. Model A is

$$z_m(B_J) = 0.016(b_J - 17)^{1.5} + 0.046, \tag{4.28}$$

and model B,

$$z_{\rm m}(B_{\rm J}) = 0.0014(b_{\rm J} - 17)^3 + 0.046. \tag{4.29}$$

Model A was chosen to be a good fit to the data of Broadhurst *et al.* (1988) and Colless *et al.* (1990, 1993), being the closest in magnitude to the APM survey. Model B was chosen to illustrate the effect of higher redshifts at faint magnitude limits. These two models, along with median redshift data from a number of sources, are plotted against limiting magnitude in Figure 4.5. Also shown in this figure is a third model, C, chosen as a reasonable fit to the data over the entire range. Model C is given by

$$z_{\rm m}(b_{\rm J}) = 0.0085(b_{\rm J} - 17)^2 + 0.042. \tag{4.30}$$

If the redshift survey of Glazebrook *et al.* is indeed 73% complete, and those galaxies not included in the survey are at high redshift, as seems likely, an estimate of this effect on the median redshift can be made. If all the excluded galaxies are at redshift greater than the true median redshift, then the true median redshift is $z_{\rm median} = 0.55$, rather than 0.46, as estimated from the survey. This puts the data point for this survey in Figure 4.5 almost exactly on the line for model B. The possibility that the galaxies are at this deeper redshift is significant when one tries to compare theory with observation, discussed below.

It seems, then, that while model A provides a good fit at magnitudes $B \leq 22$, and model C is favoured for $B \geq 25$ (from the measurement of Knieb *et al.* 1994), model B may provide a better fit in between these two ranges. It should be borne in mind that Knieb *et al.* estimated the median redshift of a number of faint galaxies whose images were gravitationally lensed by a galaxy cluster, making an estimation of systematic errors very difficult.

4.4 The Spatial Correlation Function, $\xi(r, z)$

A simple model for the evolution of the correlation function has been proposed by Efstathiou *et al.* (1991). In this model the shape of the correlation function, taken to be a

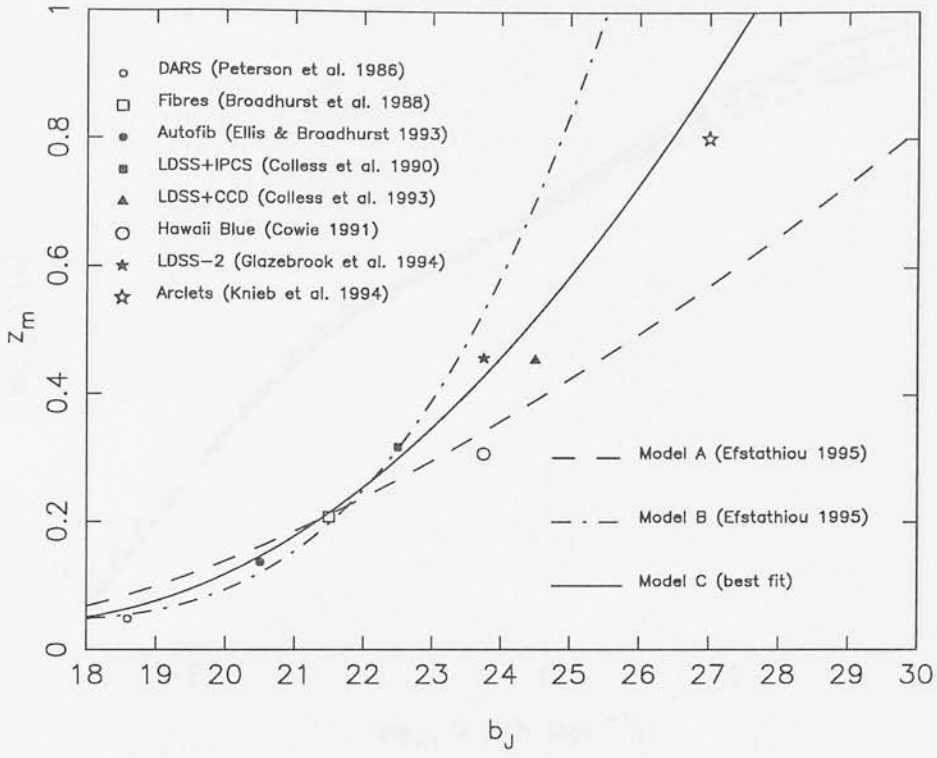

Figure 4.5: Median Redshift vs. Limiting Magnitude.

power-law of appropriate amplitude and index, does not evolve. Writing the correlation function (in terms of comoving separation and redshift)

$$\xi(r,z) = \left(\frac{r}{r_0}\right)^{-\gamma} (1+z)^{-(3+\epsilon-\gamma)} \tag{4.31}$$

it can be seen that the amplitude evolution is determined by the parameter ϵ. If the clustering pattern of galaxies is fixed in comoving coordinates, i.e. there is no $1+z$ dependence, than clearly $\epsilon = \gamma - 3$. Likewise, if the clustering is fixed in proper space, then $\epsilon = 0$. Efstathiou *et al.* choose $\gamma = 1.8$ as a fair representation of observations. These models are plotted in Figure 4.1, along with some observational data. The solid lines show the predictions for $\epsilon = -1.2$ (as chosen in Efstathiou 1995), with a scale length $r_0 = 5.5\mathrm{h}^{-1}\mathrm{Mpc}$; the upper is for redshift distribution A, the lower for distribution B. The dashed lines are for a scale length $r_0 = 2\mathrm{h}^{-1}\mathrm{Mpc}$, again with model A uppermost, chosen to be a good fit to the data. With $\epsilon = -1.2$, there is no evolution, and the effect then of Limber's equation is to effectively sample the correlation function through a window (the selection function) centered on the mean redshift. That the data are fit approximately by the $r_0 = 2\mathrm{h}^{-1}\mathrm{Mpc}$ model suggests that the FBGs are at a redshift

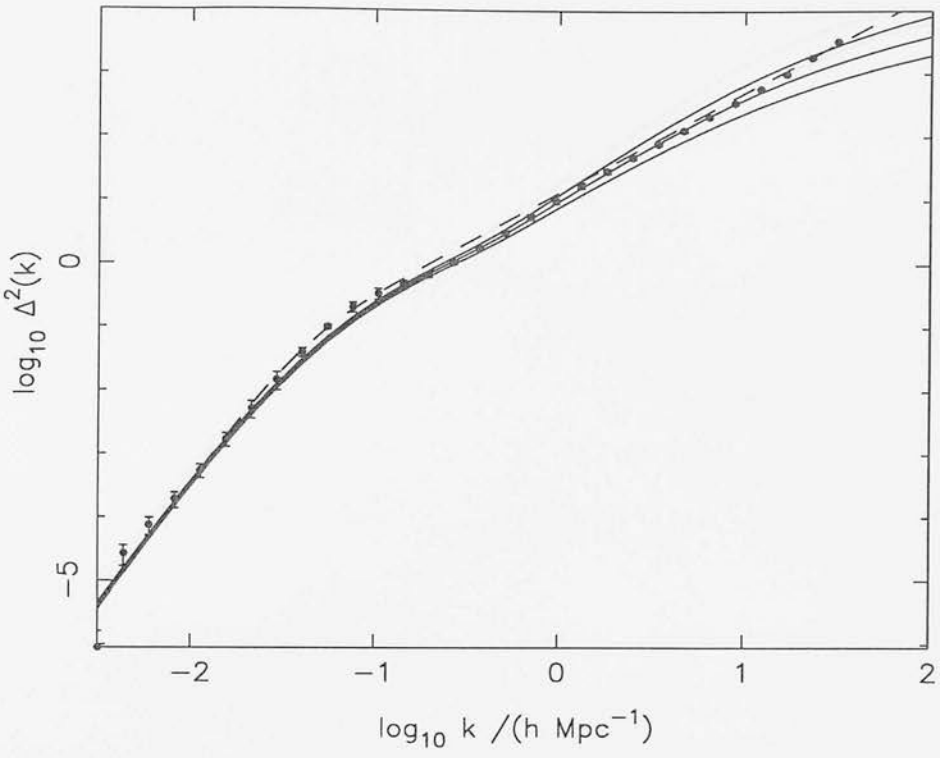

Figure 4.6: Deprojected APM power spectrum with CDM $\Omega = 1$, $\Omega h = 0.255$, $\sigma_8 = 0.75$, and power-law bias parameter (see text), $b = 1.0$, 1.15, 1.2 (solid lines, in ascending order), and empirical two-power-law fit (dashed).

where the correlation length is reduced to this value. A crude estimate of this redshift can be obtained by assuming that the correlation function evolves as per linear theory. For an $\Omega = 1$ model, this implies a mean redshift of about 0.7. Since the angular correlation function at $30''$ is influenced strongly by the non-linear part of the correlation function, this estimate is very rough, and is no substitute for the non-linear calculations done in this work.

Two models have been used in this work to described the $z = 0$ power spectrum of mass fluctuations, which were then subjected to the non-linear evolution model described in Chapter 2. The first, theoretically motivated, is the Cold Dark Matter linear power spectrum, reconstructed by PD94 from a number of different observations, including the deprojected APM spectrum of BE93. For $\Omega = 1$ models, PD94 find that the best fit is obtained with $\Omega h = 0.255$, and $\sigma_8 = 0.75$. The CDM power spectrum is calculated from these parameters using

$$\Delta^2 \propto k^{3+n} T_k^2 \tag{4.32}$$

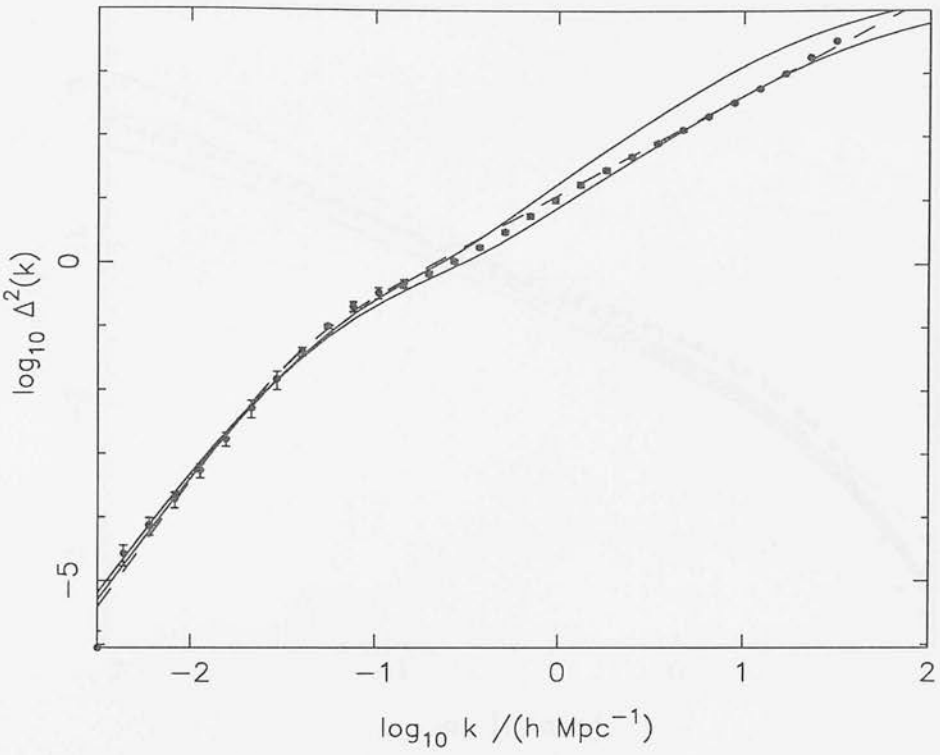

Figure 4.7: Deprojected APM power spectrum with CDM $\Omega = 0.2$, $\Omega h = 0.255$, $\sigma_8 = 0.95$ (upper solid line), $\Omega h = 0.2$, $\sigma_8 = 0.8$ (lower solid line), and empirical two-power-law fit (dashed).

and the approximate transfer function (Bardeen *et al.*, 1986)

$$T_{\rm k} = \frac{\ln(1+2.34q)}{2.34q}\left[1+3.89q+(16.1q)^2+(5.46q)^3+(6.71q)^4\right]^{-1/4}, \tag{4.33}$$

where $q \equiv k/[\Omega h^2 {\rm Mpc}^{-1}]$.

If $\Omega = 1$, then an analysis of the mass to light ratios of galaxy clusters (see, for example, Peebles 1990, and White 1990) require that the light distribution be biased. A power-law bias model (Peacock, Mann & Heavens, in preparation),

$$\frac{\rho_{\rm galaxies}}{\bar{\rho}_{\rm galaxies}} \propto \left(\frac{\rho_{\rm mass}}{\bar{\rho}_{\rm mass}}\right)^b, \tag{4.34}$$

is needed to match an $\Omega = 1$ CDM power spectrum to observations such as the deprojected APM power-spectrum of BE95. In the low density limit this reduces to the linear bias model, $\delta^2_{\rm galaxies} = b^2\delta^2_{\rm mass}$. Such a bias model leads to a biased correlation function,

$$(1+\xi_{\rm galaxies}) = (1+\xi_{\rm mass})^{b^2}. \tag{4.35}$$

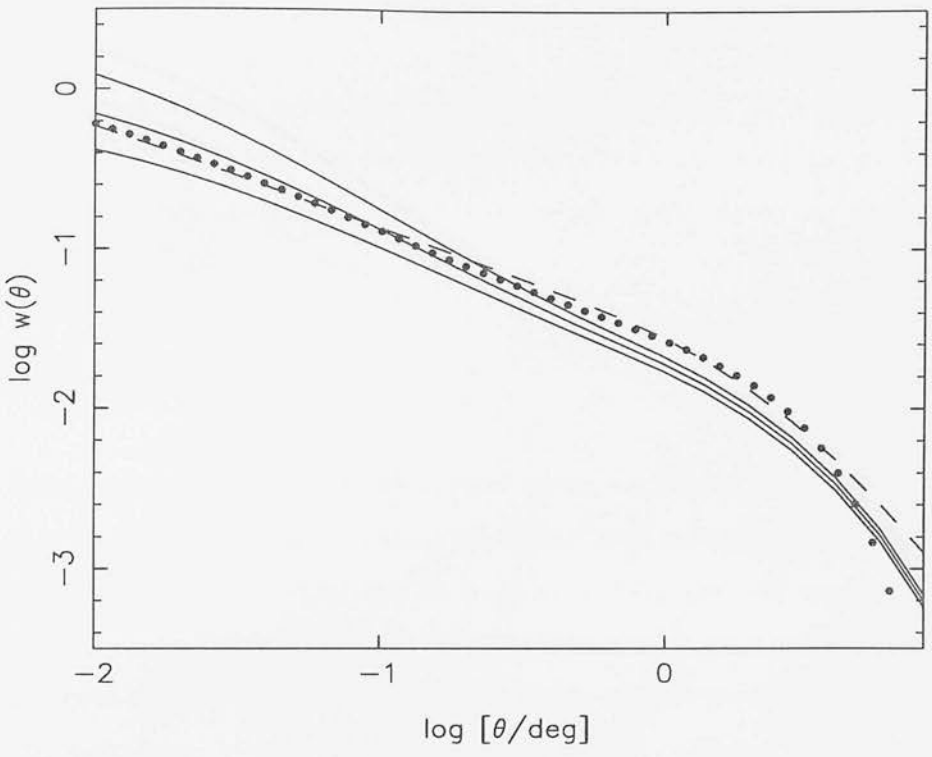

Figure 4.8: Parametric fit to APM angular correlation function from BE93 (filled circles), $\Omega = 1$ CDM models (solid lines), $b = 1.1$ (lowest), 1.15, and1.2 (highest), and two power-law model (dashed line).

It is illustrative to compare the model power spectrum with the APM deprojected spectrum. To do this, the bias model must be adapted to work in terms of the power spectrum. This cannot be done exactly without integrating the correlation function, but a rough approximation is possible. Clearly, in the linear regime, a biased power spectrum, $\Delta^2_{\rm galaxies} = b^2\Delta^2_{\rm mass}$ is implied. In the limit of $\xi \gg 1$,

$$\xi_{\rm galaxies} = \xi^{b^2}_{\rm mass}. \tag{4.36}$$

Thus if $\xi_{\rm mass}$ is an approximate power-law at small separations (where ξ is large), then so too will be $\xi_{\rm galaxies}$. A power-law ξ on small scales implies a power-law $\Delta^2(k)$ at large k, so a reasonable approximation for the biased power spectrum can be obtained using

$$1 + \Delta^2_{\rm galaxies} = (1 + \Delta^2_{\rm mass})^{b^2}. \tag{4.37}$$

However, this simple approach fails to consider the steepening of the slope of ξ when the bias is applied. This effect manifests itself in the constant of proportionality, β, in

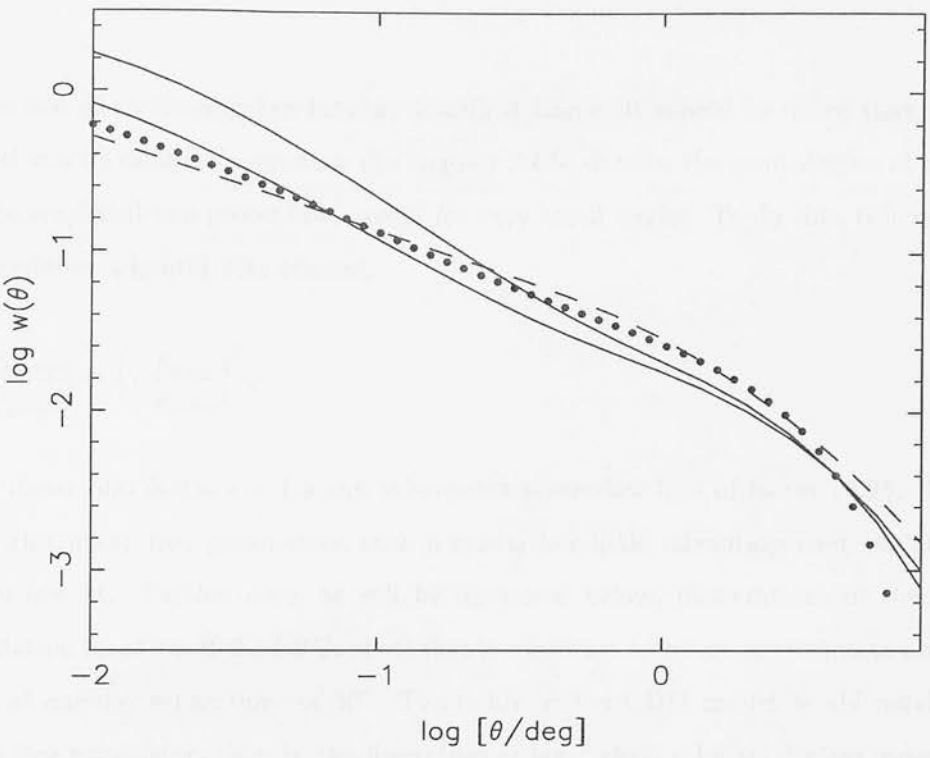

Figure 4.9: Parametric fit to APM angular correlation function from BE93 (filled circles), with models CDM $\Omega = 0.2$, $\Omega h = 0.255$, $\sigma_8 = 0.95$ (upper solid line), $\Omega h = 0.2$, $\sigma_8 = 0.8$ (lower solid line), and two-power-law model (dashed line).

$\Delta^2(k) = \beta(kr_0)^\gamma$, which relates the power spectrum to the (power-law) correlation function. The size of this effect can be determined by numerically integrating the equations relating ξ and $\Delta^2(k)$. For the range of bias parameters considered here (1.1 to 1.2) the result of using the approximation is to under-estimate the power spectrum by about 20%. This approximation was used only to illustrate the effects of bias on $\Delta^2(k)$; all the calculations leading to $w(\theta)$ were done using ξ.

If the observational measurements of Ω from galaxy clusters (see Chapter 1), i.e. $\Omega = 0.1 - 0.2$, are to be reconciled with an Einstein-de Sitter cosmology, then, in a power-law bias scheme,

$$\left(\frac{\rho_{\rm DM}}{\bar{\rho}_{\rm DM}}\right)^{b-1} \approx 5 - 10. \tag{4.38}$$

In clusters, $\rho_{\rm DM}/\bar{\rho}_{\rm DM} \approx 10^3 - 10^4$, implying $b \sim 1.2$. Figure 4.6 shows the deprojected APM data, along with three CDM models, with $b = 1.1$,, 1.15, and 1.2. The best fit is with $b = 1.15$, which was used in subsequent calculations. The dashed line is a two

power-law fit to the angular data, as described below. It should be noted that a 'CDM' model can be made to reproduce the angular APM data to the same degree of accuracy as the empirical two power-law, except for very small angles. To do this, it is necessary to introduce a hybrid bias scheme,

$$\frac{\rho_{\rm galaxies}}{\bar{\rho}_{\rm galaxies}} \propto \left(c\,\frac{\rho_{\rm mass}}{\bar{\rho}_{\rm mass}} \right)^{b}, \tag{4.39}$$

with linear bias factor $c = 1.3$ and subsequent power-law bias of factor 1.025. However, with this many free parameters, such a model has little advantage over the empirical power-law fit. Furthermore, as will be discussed below, observations of the angular correlation function of the FBGs show that it continues to be an approximate power-law even at angular separations of $30''$. To fit this with a CDM model would require even more free parameters than in the linear/power-law hybrid scheme. Unless independent evidence to support such a scheme is found, such a scheme will remain an empirical fit.

The canonical high-peaks bias scheme, where galaxies form first at the highest peaks in the density field predicts that biasing declines with time. However, the difficulty with the FBGs, as discussed above, and which remains to a small degree in the work below, is that the correlation amplitude of the models is too high, requiring the bias to increase with time if the model is to fit the data. Another possible bias model is one where the bias parameter is evolving with time. The simplest such model would be to abruptly turn on the biasing at a given redshift. So, for example, there would be no bias for $z \geq 0.5$. At this redshift, the amplitude of the correlation function would be reduced, and for a given angle one would be looking on ever larger scales, the biasing would behave as a linear scheme. Then the effect of this turn-off would be to reduce the amplitude of the correlations by b^2, for faint limiting magnitudes. For the preferred bias parameter, $b = 1.15$, this amounts to a 25% reduction in amplitude. This bias scheme was not used in the calculation of $w(\theta)$ for the two $\Omega = 1$ models, but since its effects are simple, it is easy to see the effect it would have on the predictions.

For an $\Omega = 0.2$ model, no bias is needed to account for the galaxy cluster data. PD94 find that for $\Omega = 0.2$, $\sigma_8 = 0.95$. This model is plotted in Figure 4.7, and is the higher of the two solid lines. A better fit to the data is obtained if $\Omega h = 0.2$ and $\sigma_8 = 0.8$, which

is the lower solid line. The dashed line is the two power-law fit described below.

Whatever the CDM model used, it is apparent that the observed APM power spectrum has significantly more power over the range $0.03 \leq k \leq 0.1$. This bump is visible also in the angular correlation function, and in the linearized power spectrum. The cause of this is unknown. In order to model the zero redshift correlations more accurately, a second, empirical model has also been used. The power spectrum can be well described by a two-power-law fit, such as

$$\Delta^2(k) = \frac{(k/k_0)^\alpha}{1 + (k/k_1)^{\alpha-\beta}} \tag{4.40}$$

The parameter β determines the power-law slope at small k, where the form of the primordial spectrum is preserved. For a Harrison-Zel'dovich scale-invariant spectrum, $\beta = 4$. The slope of the high k power-law is simply α. To match the APM angular correlation function (see BE93), $\alpha = 1.575$. The two wavenumbers, k_0 and k_1, determine the amplitudes of the two power-laws. Since the evolution of the power spectrum is Ω-dependent, so too will be the amplitudes of the power-laws. (The shape of the spectrum will evolve differently in different Ω models, but for a survey of the depth of the APM, $\bar{z} \approx 0.14$, this effect is very small). For $\Omega = 1$ the best fit is obtained with

$$k_0 = 0.195h\mathrm{Mpc}^{-1}, \qquad k_1 = 0.038h\mathrm{Mpc}^{-1}, \tag{4.41}$$

while for $\Omega = 0.2$, they were

$$k_0 = 0.210h\mathrm{Mpc}^{-1}, \qquad k_1 = 0.035h\mathrm{Mpc}^{-1}, \tag{4.42}$$

Inspection of the APM $w(\theta)$ data shows that it can only be approximated by a power-law at small angles to the level of about 25%.

These power spectra are shown in Figures 4.6 and 4.7, for $\Omega = 1$ and $\Omega = 0.2$, respectively. It is apparent that the amplitude of the power-laws at large k are slightly higher than the deprojected data. This is because, when calculating this spectrum, BE93 assumed a no-evolution model for the power-spectrum, thus under-estimating the power

by about 20% when compared with a simple evolution model $\Delta^2 \propto (1+z)^{-1.2}$, which is in rough agreement with the more complex model here. The effect is smaller for $\Omega = 0.2$, because of the growth suppression. It should be remarked that the spectrum used above was deprojected under the assumption of flat space. However, as measured by BE93, the effect of setting $\Omega = 0$ is to increase the deprojected power by about 20%, which explains why the power-law fit in Figure 4.7 for $\Omega = 0.2$ is close to the deprojected data.

For both the models, the linear mean interior correlation function (MICF) was found from the linear power spectrum by integrating,

$$\bar{\xi} = \int_0^\infty \Delta^2(k) \frac{dk}{k} \frac{3}{(kr)^3)} [\sin kr - kr \cos kr]. \tag{4.43}$$

having first linearized the two power-law power spectrum. In order to minimize computation time, this integration was carried out once to high accuracy, and the results recorded. The MICF at arbitrary redshift was found by scaling the linear MICF as per linear theory, non-linearizing the resulting MICF, and then modifying this for bias. This was related to the correlation function through

$$\xi(r,z) = \frac{d[r^3 \bar{\xi}(r,z)]}{d[r^3]}, \tag{4.44}$$

which was integrated through Limber's equation to determine the angular correlation function.

Figures 4.8 and 4.9 show the model predictions for the angular correlation function of the APM galaxies, limited to $b_J \leq 20$. Model 'A' was used for the redshift-magnitude relation, since this model was chosen by BE93 specifically for this survey.

4.5 Comparison With Observations

The first stage of comparison of models with data is to look at the amplitude of the correlation function at fixed angle. The observations suggest that an angle of $\theta = 30''$ is an appropriate choice, being well within the power-law regime. Figure 4.10 shows $A_w =$

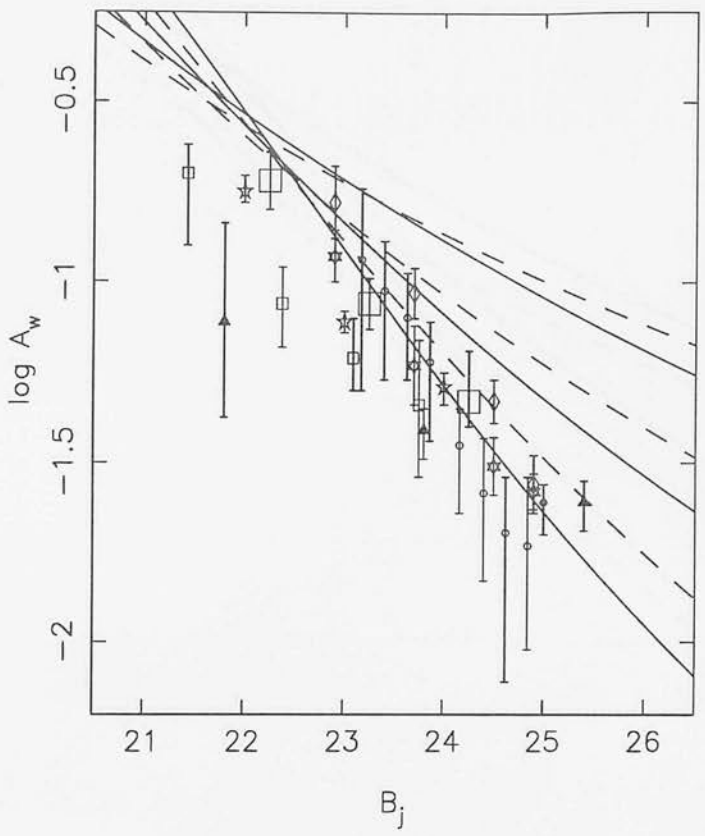

Figure 4.10: Angular correlation amplitude against limiting magnitude. The solid lines show the $\Omega = 1$ CDM model discussed in the text, the dashed lines the two power-law empirical fit. Each pair of solid and dashed lines is calculated from one of the redshift distribution models; The highest is model A (lowest redshift), the lowest, model B (highest redshift), and the central pair is for model C (intermediate). The symbols are as for Figure 4.1, with the addition of Infante & Pritchett (1995), large squares.

$w(\theta = 30'')$ plotted against limiting magnitude for the $\Omega = 1$, $\Omega h = 0.255$, $\sigma_8 = 0.75$, $b = 1.15$ biased CDM model , discussed above, for the three redshift magnitude relations described above. These are the solid lines; model A produces the highest amplitude at faint magnitudes, model B the lowest, with model C intermediate. The dashed lines show the empirical two power-law fit, for the same three redshift distribution models. Also shown in this figure are the data of Figure 4.1, with the correlation amplitudes of the J-limited surveys of IP95. Figure 4.11 shows the same data, with the CDM and empirical two power-law fits for $\Omega = 0.2$. Given the 25% error in the fitting of a two power-law model to the APM data, and the uncertainties in the bias model, again of order 25%, for $\Omega = 1$ CDM, the only conclusions to draw are that the deepest of the

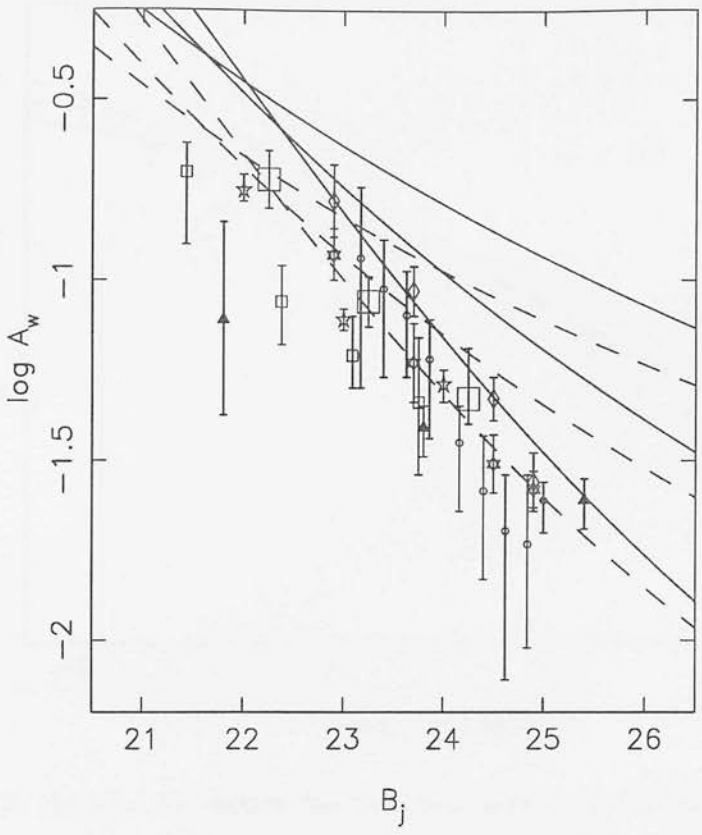

Figure 4.11: Angular correlation amplitude against limiting magnitude. The solid lines show the $\Omega = 0.2$ CDM model discussed in the text, the dashed lines the two power-law empirical fit. Each pair of solid and dashed lines is calculated from one of the redshift distribution models; The highest is model A (lowest redshift), the lowest, model B (highest redshift), and the central pair is for model C (intermediate). The symbols are as for Figure 4.1, with the addition of Infante & Pritchett (1995), large squares.

redshift distribution models, B, is necessary in order to fit the observed amplitudes. It is also apparent that at low limiting magnitude ($B \lesssim 22$), the correlation amplitude is lower than is predicted by even the highest redshift model (B). These data seem to break away from a smooth trend followed by the fainter limit data, and it is hard to see how any model could fit these two regions of data, and the APM data at the same time. The low limiting magnitude data exhibit large error bars, and some scatter, so the discrepancy may be due to observational effects.

Another observational feature of the angular correlation function of the FBGs is the approximately power-law behaviour exhibited over the range $0.001^\circ \leq \theta \leq 0.1^\circ$. Shown in Figures 4.12 and 4.13 are the angular correlation functions measured by IP95 for

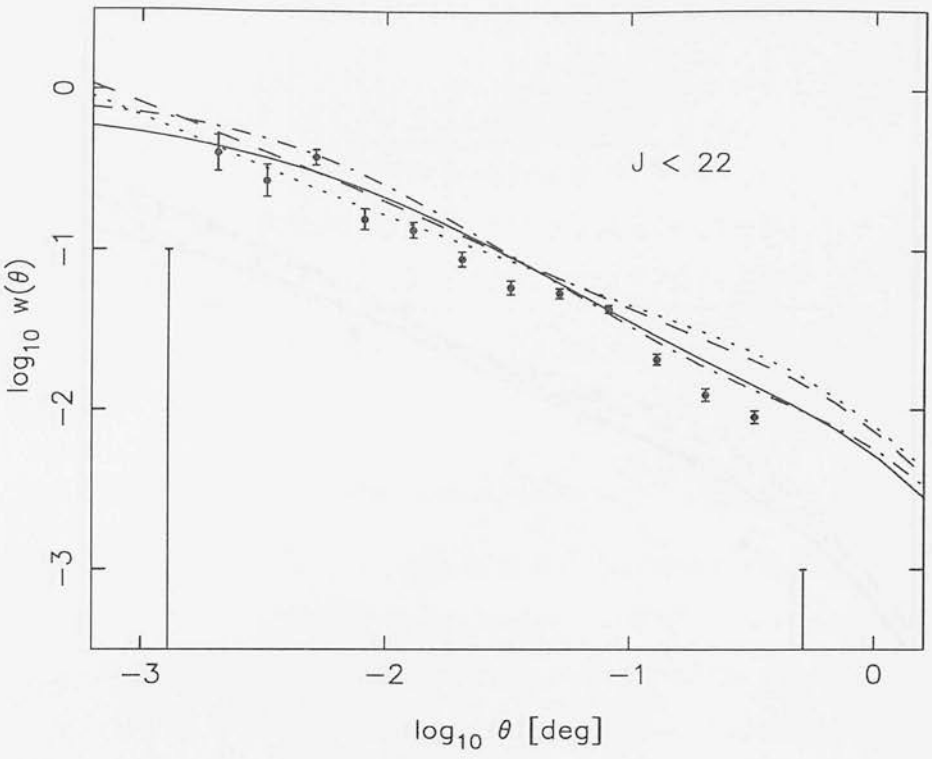

Figure 4.12: Angular correlation function from Infante & Pritchet (1995), limited to $J < 22$. The lines are: solid, $\Omega = 1$ CDM; dashed, $\Omega = 1$ two power-law fit; dot-dashed, $\Omega = 0.2$ CDM; dotted, $\Omega = 0.2$ two power-law.

galaxies in their surveys limited to $J \leq 22$ and $J \leq 24$, respectively. The drop off in the observed correlations seems likely to be due to the finite size of the surveys. Also shown are the predictions of the favoured power spectrum models: $\Omega = 1$, $b = 1.15$ CDM; $\Omega = 1$ two power-law fit; $\Omega = 0.2$, $\Omega h = 0.2$, $\sigma_8 = 0.2$ CDM; and $\Omega = 0.2$ two power-law fit. The slope of the correlation function in the power-law regime can be compared with the observations. An inspection of the data of IP95 suggests $-2.5 \leq \log_{10}\theta \leq -0.5$ as suitable limits. For each of the data points in this region, a value of $w(\theta)$ was calculated at the θ of the data point, and assigned the fractional error of the data point. A weighted least squares fit was then made for both the observational data and the simulated model data. The results are given in Table 4.1 for $\Omega = 1$ models, and in Table 4.2 for $\Omega = 0.2$. For clarity, the observational data are given in both tables.

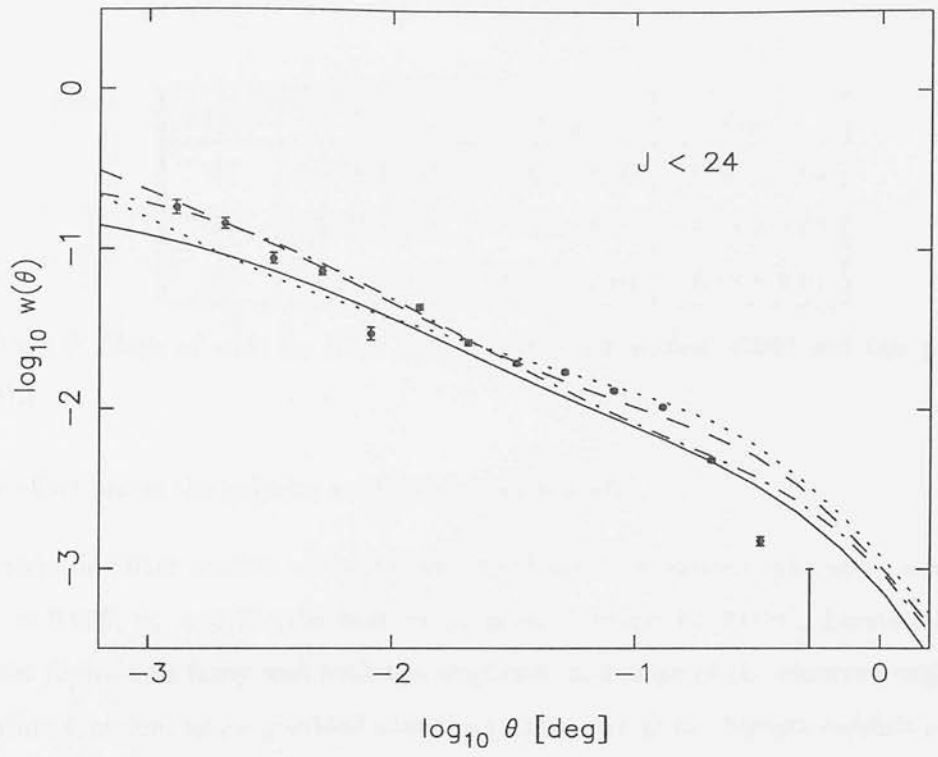

Figure 4.13: Angular correlation function from Infante & Pritchet (1995), limited to $J < 24$. The lines are: solid, $\Omega = 1$ CDM; dashed, $\Omega = 1$ two power-law fit; dot-dashed, $\Omega = 0.2$ CDM; dotted, $\Omega = 0.2$ two power-law.

4.6 Discussion

The angular correlation function arising from a spatial correlation function fitting the APM angular correlation function at median redshift 0.13, has been calculated for faint blue galaxies at a range of redshifts. It has been seen that if the model is to agree with the observations, the median redshift of the galaxies must be assumed to be at the deepest limit of the range allowed by observations. Due to the observational bias in favour of nearer objects, this is not surprising, and, indeed, an estimated correction for

J limit	$\delta_{\rm obs}$	$\delta_{\rm CDM}$	$\delta_{\rm 2PL}$
22	-0.78 ± 0.03	-0.74 ± 0.03	-0.66 ± 0.03
23	-0.72 ± 0.02	-0.71 ± 0.02	-0.66 ± 0.02
24	-0.65 ± 0.01	-0.66 ± 0.01	-0.65 ± 0.01

Table 4.1: Slope of $w(\theta)$ for IP95 data and $\Omega = 1$ models, CDM and two power-law (2PL).

J limit	$\delta_{\rm obs}$	$\delta_{\rm CDM}$	$\delta_{\rm 2PL}$
22	-0.78 ± 0.03	-0.83 ± 0.03	-0.56 ± 0.03
23	-0.72 ± 0.02	-0.79 ± 0.02	-0.53 ± 0.02
24	-0.65 ± 0.01	-0.74 ± 0.01	-0.49 ± 0.01

Table 4.2: Slope of $w(\theta)$ for IP95 data and $\Omega = 0.2$ models, CDM and two power-law (2PL).

this effect places the galaxies at the necessary redshift.

Einstein-de Sitter models are better able to fit the observations than open models. An $\Omega h = 0.255$, $\sigma_8 = 0.75$ (the best fit parameters found by PD94), Einstein-de Sitter model reproduces fairly well both the amplitude and slope of the observed angular correlation function, again provided that the galaxies are at the highest redshift suggested by observations. The slopes calculated for the CDM $\Omega = 1$ model agree well with the observations of IP95, which cannot be said for all the other models. In particular, both two power-law models produce slopes too flat to agree with the data. The scatter in the $w(\theta)$ data at both these magnitudes is much greater than the estimated errors of IP95, suggesting that either the angular correlation function exhibits many features, or, more likely, that the errors are significantly under-estimated (as indeed the authors admit). Thus, the fit of a power-law to the data is somewhat unreliable. However, many authors, such as Neuschaefer & Windhorst (1995), as well as IP95, comment on a flattening of the slope of $w(\theta)$ as one looks at progressively fainter magnitudes. This effect is reproduced most strongly by the CDM models, in particular the $\Omega = 1$, and poorly by the two power-law models, although the slope of the angular correlation function will be quite sensitive to the bias model used, particularly a power-law scheme. The effect of non-zero vacuum energy on the angular correlation function has not been calculated: this would be a worthwhile extension, particularly if the deficit between observed $\Omega_{\rm m} = \approx 0.2$ and the closure density is made up by the vacuum energy.

The most uncertain quantity in all these calculations is the redshift of the FBGs. It is to be hoped that more accurate surveys will in the near future determine this, and so make the study of the angular correlation function of faint galaxies a clear test of clustering model. However, with the observational measurements available at present,

a non-linear model of clustering evolution can be made to fit both the APM and the FBG angular correlation function approximately, and with the small discrepancy in the direction expected given observational selection effects. It is not necessary to assume that the FBGs are any different from the present epoch L^* galaxies, on the basis of the angular correlation function.

The conclusion, though, is this: the non-linear evolution model used here predicts a significantly lower amplitude than the simple models used by previous authors, and while further observational work (of the redshift distribution) is needed to establish firmly that the non-linear model can explain the observations, the case for the FBGs comprising a different population of galaxies is shown to be without foundation. Any calculations of the angular correlation function of the FBGs must include some model for bias, and thus further uncertainties, and so the result here must be considered in the light of this. However, a non-linear treatment of clustering evolution will produce a lower amplitude than the simple model of Efstathiou *et al.* (1991) for most reasonable bias schemes, so even given the uncertainties in bias, the postulation of a new population of galaxies is unjustified.

Chapter 5

CONCLUSIONS

This thesis has been concerned with tests of the models of large-scale structure formation in the context of the scenario in which structure forms through gravitationally dominated evolution of primordial density perturbations. The origin of these density perturbations is a matter for speculation; although models such as Inflation predict a form for the primordial spectrum (roughly scale-invariant, $P(k) \propto k$), as it arises from quantum fluctuations; the amplitude of the spectrum is undetermined. Furthermore, such models have yet to be firmly established empirically. Other models exist, such as cosmic strings perturbing the density field as they pass through it. One feature of such models is that, unlike the Inflationary model where the primordial density perturbations are Gaussian, the perturbations produced are expected to be non-Gaussian. Detecting non-Gaussian features of the density field is difficult; the Central Limit Theorem shows that observations of counts-in-cells may resemble a Gaussian. Detailed predictions of power spectra are not made by these models, and so the models are very hard to test. The Gaussian, scale-invariant model makes testable predictions, and for this reason, and also by virtue of its simplicity, it is adopted as the working hypothesis for this work.

Prior to redshift $z \sim 100$, the growth of density perturbations in influenced not only by gravity, but also by other physical processes. The effects of these processes on the perturbation spectrum depends on the types of matter involved, but are well understood for a number of models. The Hot Dark Matter model, in which the matter density is

dominated by neutrinos, is unable to agree with observations, producing too little power on scales smaller than about 50Mpc. The Cold Dark Matter model meets with considerably more success, producing power spectra at least 'in the right ball-park', although the particles making up the CDM (axions, WIMPS, etc.) are purely speculative. Hybrid models, called Mixed Dark Matter models, are able to improve slightly on the CDM model, but at the expense of introducing further free parameters. Because there are other unknown factors, such as bias, redshift-space distortions, and, prior to this work, non-linear evolution, it is not clear that the MDM model is needed.

Once gravitation becomes dominant in the evolution of structure, a simple linearization of the equations of fluid mechanics is able to model the growth of structure well, for scales on which the amplitude of the power spectrum is small compared to unity. Attempts have been made to study analytically the evolution of perturbations beyond this regime, the most successful of which is the Zel'dovich approximation (described in Chapter 1), which is able to model evolution a little further than linear theory, to the point where perturbations are slightly non-linear. Second-order perturbation theory has been applied to the equations of fluid mechanics (Baugh & Efstathiou, 1994). The predictions were compared with N-body simulations, and found to agree for spectra which were just going non-linear; beyond this, the approximation failed. N-body simulations have been used extensively in the study of models of large-scale structure, permitting a linear power-spectrum to be evolved into a non-linear one in a conceptually simple, but practically complex, way. If one assumes that the simulations are accurately modelling the effects of gravity, the major drawback is then the time taken to carry out large simulations (of order days). The simulations are also limited in that they cannot be used to evolve a spectrum backwards in time, to recover the linear spectrum, and are restricted in the resolution obtainable by the finite computing resources available. A comprehensive test and comparison of the various N-body algorithms (PM, P^3M, AP^3M, tree-codes) has not to date been carried out; doubts remain about whether the algorithms approximating Newtonian gravitational interactions and the integration of the equations of motion are reliable.

In Chapter 2, a semi-analytical approach was developed to the modelling of the non-linear evolution of density perturbations. The original work of Hamilton *et al.* (1991,

HKLM) used analytical models (linear theory, and the stable clustering hypothesis) to determine the behaviour of the model in the linear and highly non-linear regimes, and then made use of N-body simulations to determine the behaviour in-between. The original work considered the mean interior correlation function, $\bar{\xi}(r)$, for an Einstein-de Sitter cosmology. It was shown here that the formalism could also be made to work for the dimensionless power spectrum, $\Delta^2(k)$, a much more commonly used measure. The model was extended to cover open cosmologies, making use of linear theory and further N-body simulations. Since observational measurements of the cosmological density parameter suggest $0.1 \lesssim \Omega \lesssim 1.0$, it is important to be able to model non-linear evolution in an open cosmology. The model was found to work well even for highly non-linear spectra; a significant improvement. Since the observed spectrum of galaxy clustering extends well into the non-linear regime, the range of data against which models of structure formation can be tested is greatly extended. The model is also semi-analytical in the sense that, when converting a linear spectrum to a non-linear one (or vice versa) the simple analytic expressions relating scales and power must be solved iteratively. Although it is not possible to carry out such a conversion analytically, the iterations may be performed on a computer in a matter of seconds, which is clearly a great improvement on the hours or days needed to perform N-body simulations. Another major advantage of this technique over N-body simulations is that it can be used to reconstruct a linear spectrum. It is usual in science to test a model by making predictions that can be compared with observations. In structure formation, no compelling model exists that can be used to make such a comparison; it is clearly useful to be able to remove non-linear effects from the observed power spectrum in order to learn about the linear spectrum, which should contain information about the nature of the matter in the Universe (e.g. CDM or MDM). The hypothesis of a scale-invariant primordial spectrum was also tested in Chapter 2, although the need to extrapolate through an order of magnitude or more made this approximate. It was found that within the uncertainties, the observed power spectrum on large scales is consistent with a scale-invariant spectrum normalized to the COBE results. Another important result for structure formation was that the linear spectrum, after effects of bias and redshift-space distortions had been accounted for, was found to be consistent with a CDM spectrum if $\Omega h = 0.25$. This value for Ωh is surprisingly low, implying $h = 0.25$ if $\Omega = 1$, and $h = 1.25$ if $\Omega = 0.2$. An Einstein-de Sitter cosmology,

where $h = 0.75$, the mid-range of observational estimates, requires $\Omega h = 0.75$. One interpretation is that $\Omega < 1$, and that the CDM model is acceptable. Another is that $\Omega = 1$, but that the CDM model is incorrect. Clearly, this work is just one model-dependent estimate of Ωh; it is to be hoped that current uncertainties regarding Ω and h, and combination thereof will be resolved soon, allowing a clear interpretation of this result to be made.

Given that much is known about the observed, non-linear, spectrum of mass fluctuations today, models for the formation of structure must be made to agree with this. In particular, N-body simulations designed to measure some quantity other than the power spectrum must reproduce the observed spectrum at the final output time. Previously, it has not been possible to fix the final power spectrum of N-body simulations, making these studies spurious. This can now be done using the non-linear evolution model of this work, and Chapter 3 (discussed below) describes the application of this technique to the simulation of galaxy clusters.

However, the non-linear evolution model is far from being confirmed beyond doubt. Other workers have also studied the model of HKLM, and carried out N-body simulations. Mo, Jain, & White (1995, MJW) have proposed a model based on structure formation in a Gaussian random field. Since linear theory and the stable clustering hypothesis determine the behaviour of the non-linear growth function, which they find to be (in the dimensionless power spectrum form)

$$\Phi_{\rm NL}(x) = x\left(\frac{1+2x^2-0.6x^3-1.5x^{3.5}+x^4}{1+0.0037x^3}\right)^{1/2}, \tag{5.1}$$

MJW propose the following modification to the HKLM method:

$$\frac{\Delta^2_{\rm NL}(k_{\rm NL})}{B(n)} = \Phi_{\rm NL}\left[\frac{\Delta^2_{\rm L}(k_{\rm L})}{B(n)}\right]. \tag{5.2}$$

The function $B(n)$ they determine from the analytical model for gravitational clustering of Mo & White (1994), and scale to fit the N-body data, finding

$$B(n) = 0.795 \times \left[\frac{\Gamma\left(\frac{17+n}{10+2n}\right)}{\Gamma\left(\frac{11+n}{10+2n}\right)}\right]^{-(5+n)}. \tag{5.3}$$

The model of MJW has been plotted in the Figures 2.3 and 2.6 of Chapter 2, alongside the HKLM model and the N-body data of this work. It is apparent that this N-body data fails to support the model of MJW, although the steepening of Φ_{NL} is also observed in the data, but to a much lesser extent. The reasons for this disagreement are unclear. It could arise from differences in the analysis procedure used to determine the growth function from the power spectra. For instance, in the original HKLM work, the normalization of the mean interior correlation function was not known, and was adjusted to fit the non-linear function, although this cannot entirely explain the differences in shape. Inspection of the data of MJW for $\bar{\xi}$ shows that even for $\bar{\xi}_{NL} \sim 10^{-2}$, the N-body data do not reach the linear theory asymptote. In order to understand the differences between the two sets of data, and avoid profitless speculation, it would be necessary to examine the power spectrum data and analysis techniques in detail. It is hoped that further cooperation with MJW will permit this. A curious feature of the theoretical basis of the MJW model is that mass shells are required to virialize at their radius of maximum expansion to within a few percent. The model is based upon the assumption of spherical symmetry; it would be informative to measure this virialization quantity in the N-body simulations to see the effect of asymmetries, although this was done for the simulations used by HKLM, and the virialization radius found to be 0.55 of the turn-around radius.

Another, more worrying, possibility, which has already been touched upon in this Chapter, is that one or more of the N-body algorithms is flawed. The use of these codes has grown greatly in recent years as ever more powerful computers have become available, and a thorough test of the codes is overdue. The simplest test to perform would be to compare the force calculated by each code for a given ensemble of particles. The true force could be determined by performing a direct sum (if this is only done once, rather than many times, as in a simulation, the processing time would not be prohibitively high), although it is not clear how best to obtain an ensemble of particles for this test. The evolved output of one of the codes could be used, but if the code is miscalculating small separation forces, it will also miscalculate the positions. This effect would likely reduce the small scale correlations, which is precisely where the force evaluation should be tested. Another possibility would be to distribute the particles randomly, thus ensuring some small scale power, although such a spectrum would be very different from any

that one would want to simulate. The time integration should also be tested, but this involves the accuracy of the force evaluation. It would be difficult to find a reference for this test. If a sufficiently small number of particles were used, a direct sum force evaluation could be used to eliminate worries about the force evaluation, but then the small number of particles would reduce the statistical weight of the results. The effect of the size of the time-step can be found readily by changing the step size, by factors of two, for example. A comprehensive test of the codes would be difficult, but never-the-less, an attempt at such a study would provide valuable information on the accuracy of N-body codes, and lend weight to the results derived from such methods.

The non-linear evolution model can also be compared with the second order perturbation theory. It is, in principle, straightforward to perform the necessary integrals numerically (see Baugh & Efstathiou, 1994). In both the non-linear model and second order perturbation theory, the leading term in an expansion in $\Delta_{\rm L}^2$ should be simply $f_{\rm NL} = \Delta_{\rm L}^2$, to agree with linear theory. The second-order term, absent from the HKLM version, but present in the MJW version (for the power spectrum, but, curiously, not the mean interior correlation function formalism) and in the version presented here, could be calculated, and compared with the three fitting formulae. While such a comparison would not be the final word, it would shed some light on a complex process.

If the N-body data of this work are confirmed, it would be advantageous to incorporate some form of slope dependence into the non-linear evolution function, $f_{\rm NL}$, along the lines of the MJW modification, but less strong. At present, such a fit would be purely empirical, although further study may reveal theoretical motivations as well. This, however, would introduce another difficulty, namely that the slope dependence is itself dependent on Ω. It is not clear at this time why this should be so. It should be noted, as well, that further work must be done to investigate the breakdown of the model for steep ($n = 0.0$ and $n = -0.5$) spectra in low Ω cosmologies. Only two simulations were carried out for vacuum energy models; clearly, there is scope for further work here. Again, provided the N-body codes are authenticated, it would be helpful to perform several realisations of each simulation in order to get an average result and quantify statistical variations. The technique could be further tested against spectra other than power-laws: an obvious choice is the CDM spectrum. MJW claim that a generalized

spectrum should be non-linearized as a power-law with slope

$$n_{\rm eff} \equiv \left[\frac{{\rm d}\ln P_{\rm L}(k_{\rm L})}{{\rm d}\ln k_{\rm L}}\right]_{k_0=1/r_0}, \tag{5.4}$$

where r_0 is the radius of the top-hat window in which the *r.m.s.* mass fluctuation is unity, which could be readily tested.

The non-linear evolution model has made it possible to specify the final power spectrum of an N-body simulation, by linearizing the spectrum, and using it as the initial power spectrum. In this way, N-body simulations were carried out in Chapter 3, resulting in spectra close to the canonical power-law spectrum with slope $n = -1.2$, for both Einstein-de Sitter and open cosmological models. It is very important to remove first order (i.e. power spectrum) differences if one wishes to study quantities that depend on higher order moments of the density perturbations, such as the structure of galaxy clusters. One of the guiding principles of scientific experimentation is that only one variable should be changed at a time. Previous work, such as that by Crone *et al.* (1994) failed in this respect; it was not possible determine the linear power spectrum that would evolve to become a power-law at later times, prior to the development of the non-linear growth model of this work. As a consequence, it was not clear that the differences in mean density profiles found by Crone *et al.*, which they claimed were due to the different cosmological models used, were in fact due to this, or due to differences in the final power spectrum. In Chapter 3, this uncertainty was resolved; the mean density profile of galaxy clusters depends on Ω independently of any power spectrum dependence. The important observational consequence of this is that models which match the observed power spectrum predict different mean density profiles for different values of Ω, and so an observational measurement of mean profile could provide a new measurement of Ω. The mean profiles of Chapter 3 were calculated using approximately 40 simulated profiles. Since the uncertainties in observational profiles will be larger than those estimated for the simulated profiles here, many more clusters would need to be observed in order to get a comparable level of accuracy. Such an observational project is not currently possible, although much work is being done on the use of the gravitational lensing properties of clusters to study their structure and mass (Kaiser & Squires, 1993; Fahlman *et al.*, 1994; Broadhurst, Taylor, & Peacock, 1995). Once techniques to infer

density profiles are available, the considerable effort needed to measure a large number of profiles would be justified by the determination of a new measure of Ω. The simulated clusters could also be used to quantify the effects of Ω upon the shapes of clusters, and the degree of substructure within them.

The simulations of galaxy clusters here considered only gravitationally dominated dark matter, taking no account of the effects of gas dynamics on the dark matter. Within the year, it is expected that a Smoothed Particle Hydrodynamics (SPH) version of the AP^3M code will become publicly available (Couchman, Thomas, & Pearce 1995). With this code, it will be possible to repeat the simulations here, but with gas dynamics included, although further free parameters will be introduced, relating to the gas component, such as temperature, density, and mass relative to the dark matter. X-ray observations of the intra-cluster gas provide estimates of these quantities, but the dependence of the density profiles on these is, of course, unknown. The dark matter profiles can be transformed to light profiles, if the biasing scheme is well understood. The power-law bias, considered in Chapter 4, where

$$\left(\frac{\rho_{\rm G}}{\bar{\rho}_{\rm G}}\right) \propto \left(\frac{\rho_{\rm DM}}{\bar{\rho}_{\rm DM}}\right)^{b}, \tag{5.5}$$

would clearly result in light profiles steeper by a factor b than the dark matter profiles. If $b \approx 1.2$ for Einstein-de Sitter models, then the mean density profile slope will be steepened to approximately the slope for $\Omega = 0.2$. Then to determine Ω from the slopes would require prior knowledge of the bias (and so probably Ω), so light profiles are not likely to be of much use. Although an observational measurement of light profiles appears straight-forward, the problems of finding the centre of the cluster, and identifying objects that are just line-of-sight associations, make such an observation difficult. It seems, then, that the best hope of using this result to determine Ω lies with the gravitational lens work.

The low amplitude of the angular correlation function of the Faint Blue Galaxies (FBGs) cannot be reconciled with the observed present epoch correlation function by the models of structure evolution available prior to this work. For this reason, it has been suggested that the FBGs comprise a population distinct from the nearby optically-selected galaxies

of, for example, the APM survey.The angular correlation function of the FBGs provides information on the correlation function at higher redshift than any redshift survey, albeit averaged over a range of redshift. For this reason, it is important that a model of structure formation be able to account for it. Using the non-linear evolution model, it was found in Chapter 4 that the angular correlation function of the FBGs is consistent with that of the low redshift APM survey, provided that the FBGs lie at the upper limit of the allowed uncertainty in their redshift distribution. This is the single most significant uncertainty; the FBGs can only be said to be of the same nature as nearby optical galaxies if the redshift distribution of the FBGs is high. Further observational work is needed to determine this; if it were found that the FBGs are at a lower redshift than is needed, some explanation for the low amplitude would be needed (such as that the intrinsically weakly clustered FBGs formed away from peaks in the density field, and subsequently evolved into something else that is not identified today as an FBG). Another, lesser, but still significant, source of uncertainty in the model predictions of the angular power spectrum comes from the process of biasing, which is still not well understood. Work is being pursued on the problem of bias, as discussed in Chapters 1 and 4, but much uncertainty remains.

To conclude, then, the scenario in which structure forms from a scale-invariant power spectrum and then grows through gravitational instability and physical processes dependent on the nature of the matter, is still the most successful at explaining observations of large-scale structure. The predictive power of these models has been greatly enhanced by the model of non-linear evolution developed here. Furthermore, the range of data available for comparison is extended by these techniques. It is not possible yet to determine the exact composition of the matter in the Universe; it seems likely that a significant Cold Dark Matter component exists, maybe with a smaller amount of Hot Dark Matter. The total matter density is also uncertain; a new observational test of this quantity has been put forward here. Major difficulties persist in the study of large-scale structure even when non-linear evolution is understood, principally the lack of understanding of the processes leading to galaxy formation (bias).

REFERENCES

Alcock, C., Akerlof, C. W., Allsman, R. A., Axelrod, T. S., Bennett, D. P., Chan, S., Cook, K. H., Freeman, K. C., Grlest, K., Marshall, S. L., Park, H-S., Perlmutter, S., Peterson, B. A., Pratt, M. R., Quinn, P. J., Rodgers, A. W., Stubbs, C. W., & Sutherland, W., Nature, 1993, 365, 621.

Auborg, E., Bareyre, P., Brehlin, S., Gros, M., Lachleze-Rey, M., Laurent, B., Lesquoy, E., Magneville, C., Milsztajn, A., Moscoso, L., Queinnec, F., Rich, J., Spiro, M., Vigroux, L., Zylberajch, S., Ansarl, R., Cavalier, F., Moniez, M., Beaulieu, J-P., Ferlet, R., Grison, Ph., Vidal-Mdjar, A., Guibert, J., Moreau, O., Tajahmady, F., Maurice, E., Prevot, L., & Gry, C, 1993, Nature, 365, 623.

Babul A., Postman M., 1990, ApJ, 359, 280.

Baganoff, F. K., & Malkan, M. A., 1995, ApJ, 444, L13.

Bahcall, N., 1977, Ann. Rev. Astr. Ap., 15, 505.

Bardeen, J. M., Bond, J. R., & Efstathiou, G., 1987, ApJ, 321, 28.

Bardeen, J. M., Bond, J. R., Kaiser, N., Szalay, A. S., 1986, ApJ, 304, 15.

Barnes, J. E., & Hut, P., 1986, Nature, 324, 446.

Baugh, C. M., 1994, Ph.D Thesis, Univ. of Oxford.

Baugh, C. M., & Efstathiou, G., 1993, MNRAS, 265, 145.

Baugh, C. M., & Efstathiou, G., 1994, MNRAS, 270, 183.

Bertschinger, E., 1985a, ApJS, 58, 1.

Bertschinger, E., 1985b, ApJS, 58, 39.

Bertschinger, E., 1987, ApJ, 323, L103.

Binney, J., & Tremaine, S. D., 1987, 'Galactic Dynamics', Princeton.

Boesgaard, A., & Steigman, G., 1985, Ann. Rev. Astr. Ap., 23, 319.

Bond J.R., Couchman H.M.P., 1988, in Coley A., Dyer C.C., Tupper B.O.J., eds, Proc.

Second Canadian Conference on General Relativity & Relativistic Astrophysics. (World Scientific, Singapore), p385.

Bond, J. R., & Efstathiou, G., 1984, ApJ, 285, L45.

Bond, J. R., & Szalay, A. S., 1983, ApJ, 274, 443.

Bower R.G., Coles P., Frenk C.S., White S.D.M., 1993, ApJ, 405, 403.

Broadhurst, T. J., Ellis, R. S., Glazebrook, K. G., 1992, Nat., 355, 55.

Broadhurst, T. J., Ellis, R. S., Shanks, T., 1988, MNRAS, 235, 827.

Broadhurst, T. J., Taylor, A. N., & Peacock, J. A., 1995, ApJ, 438, 49.

Carroll, S. M., Press, W. H., & Turner, E. L., ARA&A, 30, 499.

Colless, M. M., Ellis, R. S., Taylor, K., Hook, R. N., 1990, MNRAS, 244, 408.

Colless, M. M., Ellis, R. S., Broadhurst, T. J., Taylor, K., Peterson, B. A., 1993, MNRAS, 261, 10.

Crone, M. M., Evrard, A. E., Richstone, D. O., 1994, ApJ, in press.

Couchman, H. M. P., 1991, ApJ, 368, L23.

Couchman, H. M. O., Thomas, P. A., & Pearce, F. R., 1995, preprint.

Davis, M., & Peebles, P. J. E., 1983, Ann. Rev. Astr. Ap., 21, 109.

Dekel, A., 1994, Ann. Rev. Astr. Ap., 32.

Dekel A., Bertschinger E., Yahil A., Strauss M.A., Davis M., Huchra J.P., 1993, ApJ, 412, 1.

Dekel, A., Kowitt, M., & Shaham, J., 1981, ApJ, 250, 561.

Doroshkevich, A. G., 1970, Astrophysica, 6, 320.

Efstathiou, G., 1995, MNRAS, 272, L25.

Efstathiou, G., Ellis, R. S., & Peterson, B., 1988, MNRAS 232, 431.

Efstathiou, G., Frenk, C. S., White, S. D. M., & Davis, M., 1988, MNRAS, 235, 715.

Einasto J., Joeveer M., Saar E., 1980, MNRAS, 193, 353.

Evrard, A. E., Mohr, J. J., Fabricant, D. G., & Geller, M. J., 1993, ApJ, 419, L9.

Faber, S. M., and Gallagher, J. S., 1979, Ann. Rev. Astr. Ap., 17, 135.

Fahlman, G., Kaiser, N., Squires, G., Woods, D., 1994, ApJ, 437, 56.

Feldman H.A., Kaiser N., Peacock J.A., 1994, ApJ, in press.

Fillmore, J. A., & Goldreich, P., 1984, ApJ, 281, 1.

Fisher K.B., Davis M., Strauss M.A., Yahil A., Huchra J.P., 1993, ApJ, 402, 42.

Fitchett, M. & Webster, R., 1987, ApJ, 317, 653.

Forman, W. & Jones, C., 1982 ARA&A, 20, 547.

Freedman, W. L., Madore, B. F., Mould, J. R, Hill, R., Ferrarese, L., Kennicutt, R. C. Jr., Saha, A., Stetson, P. B., Graham, J. A., Ford, H., Hoessel, J. G., Huchra, J., Hughes, S. M., Illingworth, G. D., 1994, Nature, 371, 757.

Gamow, G., 1946, Phys. Rev., 70, 527.

Glazebrook, K., Ellis, R., Colless, M., Broadhurst, T., Allington-Smith, J., & Tanvir, N., 1995, MNRAS, 273, 157.

Gott, J. R., 1973, ApJ, 186, 481.

Gott, J. R., 1975, ApJ, 201, 296.

Gramann M., Cen R., Bahcall N., 1993, ApJ, 419, 440.

Gunn, J. E., 1977, ApJ, 218, 592.

Gunn, J. E., & Gott, J. R. III, 1972, ApJ, 176, 1

Guth, A., 1981, Phys. Rev., D23, 347.

Hawkins, M. R. S., 1993, Nature, 366, 242.

Hockney, R. W., & Eastwood, J. W., 1988, "Computer Simulations Using Particles", IOP Publishing, Bristol.

Hoffman, Y., 1988, ApJ, 328, 489.

Hoffman, Y., & Shaham, J., 1985, ApJ, 297, 16.

Hubble, E., 1925, Observatory, 48, 139.

Infante, L., & Pritchet, C. J., 1994, preprint.

Irvine, W. M., 1961, Local Irregularities in a Universe Satisfying the Cosmological Priciple, Ph.D. thesis, Harvard University.

Jones, H. R. A. J., 1995, Ph.D. Thesis, University of Edinburgh.

Kaiser, N., 1984, ApJ, 284, L9.

Kaiser, N., & Squires, G., 1993, ApJ, 404, 441.

van Kampen, E., 1994, Ph.D. Thesis, Leiden University.

Knieb, J.-P., Ellis, R. S., Smail, I., Couch, W. J., & Sharples, R. M., submitted to Nature.

Knieb, J.-P., Mathez, G., Fort, B., Mellier, Y., Soucail, G., Longaretti, P.-Y., 1994, A&A, 286, 701.

Kofman L., Gnedin N., Bahcall N., 1993, ApJ, 413, 1.

Lahav O., Lilje P.B., Primak J.R., Rees M.J., 1991, MNRAS, 251, 128.

Layzer, D., 1963, A Preface to Cosmology. I. The Energy Equations and the Virial Theorem for Cosmic Distributions, ApJ, 138, 174

Lightman, A. P., & Schechter, P. L., 1990, ApJS, 74.

Loveday J., Efstathiou G., Peterson B.A., Maddox S.J., 1992, ApJ, 400, L43.

Loveday, J., Maddox, S. J., Efstathiou, G., Peterson, B. A., 1995, ApJ, 442, 457.

McNally, S. J., & Peacock, J. A., 1995, MNRAS, accepted for publication.

Majewski, S. R., 1992, ApJS, 78, 87.

Mann, R. G., Heavens, A. F., & Peacock, J. A., 1993, MNRAS, 263, 798.

Mo, H. J., Jain, B., and White, S. D. M., 1995, preprint.

Mo, H.J., Jing, Y.P., Börner, G., 1993b, MNRAS, 264, 825.

Mo, H.J., Peacock, J.A., Xia, X.Y., 1993a, MNRAS, 260, 121.

Mo, H. J., & White, S. D. M., 1994, MNRAS, submitted.

Ostriker, J. P., & Peebles, P. J. E., 1973, ApJ., 186, 467.

Peacock J.A., 1991, MNRAS, 253, 1P.

Peacock J.A., 1992, in Martinez V., Portilla M., Sáez D., eds, New insights into the Universe, Proc. Valencia summer school (Springer, Berlin), p1.

Peacock, J. A., & Dodds, S. J., 1994, MNRAS, 267, 1020.

Peacock, J. A., & Heavens, A. F., 1985, MNRAS, 217, 805.

Peacock J.A., Nicholson D., 1991, MNRAS, 253, 307.

Peacock J.A., West M.J., 1992, MNRAS, 259, 494 .

Peebles, P. J. E., 1980, "The Large-Scale Structure of the Universe",Princeton University Press.

Peebles, P. J. E., 1990, in "Clusters of Galaxies", ed. Oegerle, Fitchett & Danly, CUP.

Peebles, P. J. E., 1993, "Principles of Physical Cosmology", Princeton Univ. Press.

Penzias, A. A., & Wilson, R. W., 1965, ApJ, 142, 419.

Pierce, M. J., Welch, D. L., McClure, R. D., van den Bergh, S., Racine, R., Stetson, P. B., 1994, Nature, 371, 385.

Prestage, R. M., 1985, Ph.D. thesis, University of Edinburgh.

Pryor, C. P., 1982, Ph.D. thesis, Harvard University.

Quinn, P. J., Salmon, J. K. & Zurek, W. H. 1986, Nature, 322, 329.

Richstone, D., Loeb, A., & Turner, E. L., 1992, ApJ, 393, 477.

Rindler, W., 1977, "Essential Relativity", Springer-Verlag, Berlin.

Rivolo, R., and Yahil, A., 1982, ApJ, 251, 477.

Sachs R.K., Wolfe A.M., 1967, ApJ, 147, 73

Saunders W., Rowan-Robinson M., Lawrence A., 1992, MNRAS, 258, 134.

Shandarin, S. F., & Zeldovich, Ya. B., 1989, Rev. Mod. Phys., 61, 185.

Smith M.S., Kawano L.H., Malaney R.A., 1993, ApJS, 85, 219

Strauss M.A., Davis M., Yahil Y., Huchra J.P., 1992, ApJ, 385, 421.

Steidel, C., & Sargent, W. L. W., 1987, ApJ Letters, 318, L11.

Sunyaev R.A., Zeldovich Ya.B., 1972, Comments Ap. Space Sci., 4, 173

Tyson, J. A., 1988, AJ, 96, 1.

Vogeley M.S., Park C., Geller M., Huchra J.P., 1992, ApJ, 391, L5.

Wagoner, R. V., Fowler, W. A., & Hoyle, F., 1967, ApJ 148, 3.

Warren, M. S., Quinn, P. J., Salmon, J. K., & Zurek, W. H., 1992, ApJ, 399, 405.

Weinberg S., 1972, Gravitation and Cosmology. Wiley, New York

West, M. J., Dekel, A. & Oemler, A., 1987, ApJ, 316,1.

White, S. D. M., Efstathiou, G., & Frenk C. S., 1993, MNRAS, 262, 1023.

White, S. D. M., Huchra, J., Latham, D., and Davis, M., 1983, MNRAS, 203, 701.

White, S. D. M., Navarro, J. F., Evrard, A. E., & Frenk, C. S., 1993, Nature, 366, 429.

White, S. D. M., 1990, in "Physics of the Early Universe", ed. Peacock, Heavens & Davies, Scottish Universities Summer School in Physics.

Wolf, A. M., 1989, in "The Epoch of Galaxy Formation" (ed. Frenk, C. S., *et al.*).

Zeldovich, Ya. B., 1970, A&A, 5, 84.

Zwicky, F., 1933, Helv. Phys. Acta, 6, 110.

ACKNOWLEDGEMENTS

I would like to thank: my supervisors, John Peacock and Alan Heavens; Hugh Couchman for the use of his AP^3M code; Chris Pritchet and Karl Glazebrook for giving me access to their data in electronic form; Eelco van Kampen, Richard Bower, and Andy Taylor, for advice and assistance; Harvey MacGillivray for allowing me to use the SuperCosmos AXP 3000/600; and especially Bob Mann for kindly proof-reading my thesis.

PUBLISHED PAPER

Peacock J.A., & Dodds, S. J., 1994, MNRAS, 267, 1020.

Reconstructing the Linear Power Spectrum of Cosmological Mass Fluctuations

Mon. Not. R. Astron. Soc. **267**, 1020–1034 (1994)

Reconstructing the linear power spectrum of cosmological mass fluctuations

J. A. Peacock[1] and S. J. Dodds[2]

[1]*Royal Observatory, Blackford Hill, Edinburgh EH9 3HJ*
[2]*Institute for Astronomy, University of Edinburgh, Blackford Hill, Edinburgh EH9 3HJ*

Accepted 1993 November 24. Received 1993 November 24; in original form 1993 August 11

ABSTRACT

We describe an attempt to reconstruct the initial conditions for the formation of cosmological large-scale structure, under the assumption of gravitational instability in a Gaussian density field. Information on the power spectrum of the primordial fluctuations is provided by a variety of autocorrelation and cross-correlation analyses on samples of different classes of galaxy and galaxy clusters. These results differ from the desired linear power spectrum because of three modifying effects: bias, non-linear evolution and redshift-space distortions. We show how the latter two effects can be corrected for analytically, allowing the linear mass spectrum to be recovered provided that the bias is independent of scale for a given class of galaxy. We argue that this is a good assumption for large scales, which is well verified in practice.

We apply this method to eight independent data sets, and obtain excellent agreement in the estimated linear power spectra for wavelengths $\lambda \gtrsim 10\,h^{-1}$Mpc, given the following conditions. First, the relative bias factors for Abell clusters, radio galaxies, optical galaxies and *IRAS* galaxies must be in the ratios $b_A : b_R : b_O : b_I = 4.5 : 1.9 : 1.3 : 1$, to within 6 per cent rms. Secondly, the data require a significant degree of redshift-space distortion: $\Omega^{0.6}/b_I = 1.0 \pm 0.2$. Thirdly, low values of Ω and bias are disfavoured because non-linear evolution would spoil the agreement in shape between galaxy and cluster power spectra. The amplitude of the preferred linear power spectrum is only weakly dependent on Ω and agrees well at large wavelengths with the normalization demanded by the *COBE* data for a scale-invariant primordial spectrum, provided that $\Omega = 1$ and gravity-wave anisotropies are negligible. In this case, the shape of the spectrum is extremely well described by a CDM transfer function with an apparent value of the fitting parameter $\Omega h = 0.25$. Tilted models, for which inflation requires a large gravity-wave contribution to the *COBE* data, predict too little power at 100-Mpc wavelengths.

Key words: galaxies: clustering – cosmology: theory – large-scale structure of Universe.

1 INTRODUCTION

The simplest hypothesis for the origin of the large-scale structure of the Universe is that it is the result of the operation of gravitational instability on small initial density perturbations. On grounds of economy, these are often assumed to have the random-phase character common in noise processes, and hence to form a Gaussian random field. This has been the standard picture for structure formation for the half century since the pioneering studies of Lifshitz, given added motivation more recently by inflationary theories in which the initial perturbations are supplied by quantum fluctuations at early times.

If this picture is correct, the only quantity needed for a complete statistical description of the cosmological density field is the power spectrum of the fluctuations at some early time (or its linear-theory extrapolation to the present). Observationally, much progress has been made in recent years towards the goal of determining the power spectrum, fulfilling the programme outlined by Peebles (1973). New generations of deep redshift surveys have allowed the clustering of various classes of galaxy to be determined up to the contribution from wavelengths of several hundred Mpc. In parallel, new analysis techniques have been developed in order to extract the long-wavelength portion of the power spectrum more sensitively (e.g. Feldman, Kaiser & Peacock 1994 [FKP] and references therein).

The intention of this paper is to compare various recent determinations of galaxy clustering, and to see if there exists a single consistent picture for the underlying mass fluctuations. It is an updated version of a previous attempt in this direction (Peacock 1991), but with several important improvements in

addition to a great increase in quantity of data. In essence, there are three filters that cause the observed clustering properties of galaxies to depart from the desired linear mass power spectrum.

(i) Non-linear evolution. On small scales, perturbation theory fails and the mass power spectrum departs in a complicated way from a linear extrapolation of the initial conditions.

(ii) Redshift-space effects. Because 3D data sets use redshift as a radial coordinate, the apparent density field that results is distorted through the existence of peculiar velocities. Even for perfect data, the redshift-space power spectrum is not the same as that in real space.

(iii) Bias. The fact that different species of galaxy follow the mass distribution with different degrees of fidelity is a major problem in relating observations to theory. To correct for bias in principle requires a detailed model for how the effect arises.

None of these effects was handled very thoroughly in previous work. The issue of bias is the most difficult, and is really only tractable on large scales where the degree of bias can be assumed constant. It is now possible to have a better idea of where this approximation is valid, and we discuss this issue in Section 2. Previously, non-linear distortions were either ignored or treated by comparing non-linear data with an evolved N-body model. However, thanks to the insight of Hamilton et al. (1991; HKLM), it is possible to correct the data for the effects of non-linearities. We discuss their method in Section 3 and give a number of generalizations. Redshift-space distortions have usually been treated by a simple scaling of amplitude analysed by Kaiser (1987), but this is inapplicable on small scales. We give an improved analysis in Section 4.

Given a method for treating the practical distortions of power spectra, there are two possible approaches. There is an honourable tradition which states that it is better to apply any corrections to the theory under test, and to compare the modified model with the raw data. Nevertheless, we shall do the opposite and estimate the linear spectrum by correcting the data. This has two advantages: no model is needed, and the power spectrum can be found empirically; by comparing the various estimates, we can then see directly if all data sets are consistent with each other. In Section 5, we assemble the most recent power-spectrum data and apply the above tools to deduce the linear power spectrum. This empirical reconstruction is compared with a variety of a priori models in Section 6, and the main points of the paper are summarized in Section 7.

2 GALAXY AND CLUSTER CORRELATIONS IN GAUSSIAN MODELS

2.1 Evidence for Gaussian fluctuations

Since a good part of the analysis in this paper rests on the assumption of a Gaussian density field, we should start by considering the evidence that this is a good approximation.

The evidence has to be gathered on large scales, because non-linear evolution inevitably induced non-Gaussian statistics on small scales, whatever the initial statistics. The most direct test was carried out by FKP, who looked at the distribution of power measured for individual modes in a power-spectrum analysis of the *IRAS* QDOT redshift survey. For a Gaussian field, such modes should have power values that are independently exponentially distributed. This was found to be the case out to the limit of the statistics – powers of about 10 times the mean. This is not a complete test of the Gaussian hypothesis: it is equivalent to asking in real space whether the one-point density distribution is Gaussian. Further information is provided by higher-order k-space correlations which test for independence of the modes. Nevertheless, it is worth recalling that there have been suggestions that even this lowest-order test is badly violated. On the basis of a pencil-beam redshift survey, Broadhurst et al. (1990) and Szalay et al. (1991) have suggested that there is gross non-Gaussian behaviour on large scales, based on the existence of strong quasi-periodic power at a few wavelengths. There is no need to repeat here the counter-arguments given by Kaiser & Peacock (1991); it should suffice to note that the QDOT sample is deep enough that it encompasses several of the suggested periods in a large number of independent directions, yet no non-Gaussian signature is detected.

Any initial Gaussian nature of the field is completely erased on very small scales, but on intermediate scales the field develops a skewness which can be analysed perturbatively (Peebles 1980). The observed degree of skewness appears to be in accord with this prediction (Gaztañaga 1992; Bouchet et al. 1993), which gives further support to the Gaussian hypothesis. This is not a definitive test, since most bias mechanisms will induce skewness; what is observed is a mixture of this effect with primordial skewness, plus the effects of gravitational evolution. Nevertheless, simple Gaussian models without a strong degree of bias do account for the data well.

A variety of other tests have been suggested, including the topology of isodensity surfaces (Hamilton, Gott & Weinberg 1986; Coles & Plionis 1991; Moore et al. 1992) and the one-point distribution of the velocity field (Nusser & Dekel 1993; Kofman et al. 1994). It is fair to say that none of these methods has produced any evidence against primordial Gaussian statistics. However, as usual in statistics, it is necessary to choose the null hypothesis with care. It is certainly the case that not all tests are necessarily very powerful; the central limit theorem means that a variety of non-Gaussian processes may yield nearly Gaussian behaviour in experiments where limited resolution averages over different regions of space (Scherrer 1992). Thus some of the more popular models based on topological singularities (strings, textures etc.) may still be allowed by existing data (e.g. Gooding et al. 1992). However, it will be interesting to see such theories confronted with the FKP result, particularly as such statistics will become more demanding as data sets increase in size.

For the present, it is enough to note that there is empirical reason to believe that the statistics of the large-scale density field are close to Gaussian. If this is so, then there are consequences for the clustering of galaxy systems, as discussed below. As we will see, these predictions are verified in practice, which is one further piece of supporting evidence for the Gaussian picture.

2.2 Bias in galaxy and cluster correlations

In a Gaussian model, the correlations of different classes of galaxy system can be directly related to the underlying density field, with the power spectra being proportional on large scales:

$$\Delta^2(k) = b^2\,\Delta^2_{\rm mass}(k). \quad (1)$$

Here and below, we shall use a dimensionless notation for the power spectrum designed to minimize uncertainties from differing Fourier conventions. In words, Δ^2 is the contribution to the fractional density variance per bin of $\ln k$; in the convention of Peebles (1980), this is

$$\Delta^2(k) \equiv \frac{{\rm d}\sigma^2}{{\rm d}\ln k} = \frac{V}{(2\pi)^3}\,4\pi k^3\,|\delta_k|^2. \quad (2)$$

The justification for the above relation is the assumption, introduced by Kaiser (1984), Peacock & Heavens (1985) and Bardeen et al. (1986; BBKS), that the sites of massive objects such as clusters can be identified at early times as high peaks in the linear density field. Such a scheme might be termed Lagrangian bias, and b is called a bias parameter. This is rather sloppy: biased galaxy formation usually means the situation where light does not trace mass in the Universe, but clusters would still be more correlated than the mass even if the galaxy distribution followed the mass exactly. However, this usage is too firmly embedded in the literature to make it worth fighting; we will therefore describe the enhanced correlations of clusters as bias.

As the density field evolves, the initial statistical clustering in Lagrangian space is supplemented as dynamics moves objects from their initial sites. Owing to the equivalence principle, all objects move in the same way, so that the overall observed clustering in Eulerian space is

$$1 + \delta_{\rm Euler} = (1 + \delta_{\rm Lagrange})\,(1 + \delta_{\rm dynamics}). \quad (3)$$

In the linear regime, we therefore have

$$\delta_{\rm Lagrange} = (b - 1)\delta_{\rm dynamics}. \quad (4)$$

Bond & Couchman (1988) showed how this decomposition could be used to compute exact total correlations, under the assumption that the dynamical evolution obeyed the Zeldovich (1970) approximation. Mann, Heavens & Peacock (1993) applied this method to the calculation of cluster correlations. In practice, the statistical contribution tends to dominate for scales larger than the filter size used to define clusters (a few Mpc); the cluster distribution has not undergone strong dynamical evolution, and most clusters are close to their original sites.

Although the idea of Lagrangian bias was borrowed by BBKS from its cluster origins and applied as a model for biased galaxy formation, it may be more fruitful to think of galaxy bias in a purely Eulerian way, where the density of galaxies is some function of the final mass density. This has long been advocated by Einasto and collaborators, with galaxy formation being suppressed in low-density regions (Einasto, Jôeveer & Saar 1980). More recently, studies of the operation of dissipation in numerical simulations have produced a more direct physical justification for relating the galaxy and mass density fields through a single non-linear function (Cen & Ostriker 1992).

These contrasting views of the origin of cluster and galaxy bias lead to rather different approaches when attempting to use clustering data to infer the mass fluctuations. For clusters, the statistical bias is dominant, and we may assume that the clusters reflect mainly the initial conditions. Conversely, it is reasonable to believe that galaxies come close to tracing the mass. Many studies have indicated that different classes of galaxy follow the same 'skeleton' of voids, filaments, walls and clusters, while differing most markedly in regions of high density (e.g. Babul & Postman 1990; Strauss et al. 1992). This last effect may not be so important: despite having densities differing by factors of close to 10 in rich clusters, we shall see below that *IRAS* and optical galaxies have bias factors within about 30 per cent of each other. This is analogous to the findings of Cen & Ostriker (1992): even though their model has a highly non-linear dependence of galaxy density on mass density for high densities, the power spectra are proportional on most scales, even down to the point where $\Delta^2(k) \sim 1$. In any case, it is important to keep in mind that we are not interested in exactly how a given class of galaxy does or does not follow the density field: a variety of different bias schemes could give the same galaxy power spectrum, even though the light distributions would be model dependent.

The above discussion motivates the assumptions that we shall use below to make estimates of the linear power spectrum. We shall adopt the extreme approximations that the cluster distribution contains information only about the linear power spectrum, whereas the galaxy distribution mainly measures the non-linear density field:

$$\Delta^2_{\rm C} = b^2_{\rm C}\Delta^2_{\rm L}, \quad (5)$$

$$\Delta^2_{\rm G} = b^2_{\rm G}\Delta^2_{\rm NL}. \quad (6)$$

A further way of understanding this distinction is to consider the following illustrative model, in which we populate the Universe with identical spherical protocluster perturbations. At some critical time, these will turn round and virialize, producing a large excess of small-scale power in the non-linear density field. However, at this time, the cluster centres will still be weakly perturbed: the existence of the small-scale power is what allows us to say that clusters are present, but there is no reason to expect this power to manifest itself in many close pairs of cluster centres. Ultimately, our hypothesis must submit to the test of numerical simulation, but for the present it should certainly be closer to the truth to say that clusters respond to the linear power spectrum, rather than to the non-linear one.

Although the above bias factors are calculable given a specific bias model, we shall treat them as unknowns to be determined from the data. It is clear that the assumption of constant bias factors cannot be exact, and will certainly break down at small scales. To some extent, the domain of validity can be found empirically, by seeing whether it is possible to make a consistent picture in this way from all the available data. In practice, we shall use data at wavenumbers $k \lesssim 0.6\,h\,{\rm Mpc}^{-1}$, i.e. wavelengths $\lambda \gtrsim 10\,h^{-1}\,{\rm Mpc}$ (as usual, $h \equiv H_0/100\,{\rm km\,s^{-1}\,Mpc^{-1}}$), so we are only dealing with the large-scale mass distribution.

There is a third way in which the mass power spectrum may be inferred, which is to use cross-correlation data from two catalogues, in addition to the respective autocorrelations. In this case, it is not so obvious whether we measure more nearly the linear or non-linear correlations. In practice, we shall use data on large enough scales that the distinction will not be so important; we therefore assume a relation to linear theory

$$\Delta^2_{\rm CG} = b_{\rm C} b_{\rm G}\Delta^2_{\rm L}. \quad (7)$$

This provides a useful consistency test of our assumptions: the cluster-galaxy cross-correlation should be the geometrical mean of the separate autocorrelations.

3 NON-LINEAR EVOLUTION OF POWER SPECTRA

To implement the above assumptions requires some way of relating linear and non-linear power spectra; until recently, this would have required N-body modelling. However, in a marvelous piece of alchemy, Hamilton et al. (1991; HKLM) gave a universal analytical formula for accomplishing the linear $\leftrightarrow$ non-linear mapping. The conceptual basis of their method can be understood with reference to the spherical collapse model. For $\Omega = 1$ (the only case they considered), a spherical clump virializes at a density contrast of order 100 when the linear contrast is of order unity. The trick now is to think about the density contrast in two distinct ways. To make a connection with the statistics of the density field, the correlation function $\xi(r)$ may be taken as giving a typical clump profile. What matters for collapse is that the integrated overdensity reaches a critical value, so one should work with the volume-averaged correlation function $\bar{\xi}(r)$. A density contrast of $1+\delta$ can also be thought of as arising through collapse by a factor $(1+\delta)^{1/3}$ in radius, which suggests that a given non-linear correlation $\bar{\xi}_{\rm NL}(r_{\rm NL})$ should be thought of as resulting from linear correlations on a linear scale

$$r_{\rm L} = [1+\bar{\xi}_{\rm NL}(r_{\rm NL})]^{1/3} r_{\rm NL}. \tag{8}$$

This is one part of the HKLM procedure. The second part, having translated scales as above, is to conjecture that the non-linear correlations are a universal function of the linear ones:

$$\bar{\xi}_{\rm NL}(r_{\rm NL}) = f_{\rm NL}[\bar{\xi}_{\rm L}(r_{\rm L})]. \tag{9}$$

The asymptotics of the function can be deduced readily. For small arguments $x \ll 1$, $f_{\rm NL}(x) \simeq x$; the spherical collapse argument suggests $f_{\rm NL}(1) \simeq 10^2$. Following collapse, $\bar{\xi}_{\rm NL}$ depends on scale factor as a^3 (stable clustering), whereas $\bar{\xi}_{\rm L} \propto a^2$; the large-$x$ limit is therefore $f_{\rm NL}(x) \propto x^{3/2}$. HKLM deduced from numerical experiments that the exact coefficient is

$$f_{\rm NL}(x) \rightarrow 11.68\, x^{3/2} \tag{10}$$

and obtained a numerical fit that interpolated between these two regimes, in a manner that empirically showed negligible dependence on power spectrum.

To use this method in the present application, we need two generalizations: we need to make the method work with power spectra, and we need the analogous results with $\Omega \neq 1$. In principle, the translation between $\bar{\xi}(r)$ and $\Delta^2(k)$ is straightforward, but it is not so easy to obtain stable numerical results. One route is to use the relations between $\bar{\xi}(r)$ and $\xi(r)$:

$$\bar{\xi}(r) = \frac{3}{r^3}\int_0^r \xi(x)\, x^2\, {\rm d}x, \tag{11}$$

$$\xi(r) = \frac{{\rm d}\,[r^3\,\bar{\xi}(r)]}{{\rm d}[r^3]}, \tag{12}$$

followed by the Fourier relations between $\xi(r)$ and $\Delta^2(k)$:

$$\xi(r) = \int_0^\infty \Delta^2(k)\,\frac{\sin kr}{kr}\,\frac{{\rm d}k}{k}, \tag{13}$$

$$\Delta^2(k) = \frac{2k^3}{\pi}\int_0^\infty \xi(r)\,\frac{\sin kr}{kr}\,r^2\,{\rm d}r. \tag{14}$$

This approach is not so attractive. To obtain the non-linear power spectrum from the linear one requires two numerical integrations, followed by differentiation, followed by one further integration. It is possible to do a little better by manipulating the above equations to relate $\Delta^2(k)$ and $\bar{\xi}(r)$ directly:

$$\bar{\xi}(r) = \int_0^\infty \Delta^2(k)\,\frac{{\rm d}k}{k}\,\frac{3}{(kr)^3}[\sin kr - kr\cos kr], \tag{15}$$

$$\Delta^2(k) = \frac{2k^3}{3\pi}\int_0^\infty \bar{\xi}(r)\,r^2\,{\rm d}r\,\frac{1}{(kr)}[\sin kr - kr\cos kr], \tag{16}$$

where the last relation holds provided that $\bar{\xi}(r) \rightarrow 0$ faster than r^{-2} at large r (i.e. a spectrum which asymptotically has $n > -1$, a valid assumption for spectra of practical interest). This looks better, since there are now only two integrations required, and furthermore efficient methods exist for dealing with integrations with sin and cos weightings in the integrand. However, because the window function consists of the difference of two such terms, life is still not so easy: evaluation of the two parts of the integral separately gives a result as a difference of two large numbers, which is thus generally of low accuracy. The most satisfactory practical procedure seems to be a mixture of the two possibilities: (i) evaluate a table of $\bar{\xi}_{\rm L}(r)$ values for a given linear power spectrum by evaluating the oscillatory integral directly; (ii) transform to a table of $\bar{\xi}_{\rm NL}(r)$ values using the HKLM procedure; (iii) fit splines to the result and differentiate to get $\xi_{\rm NL}(r)$; (iv) Fourier transform to get $\Delta^2_{\rm NL}(k)$. The accuracy of the result can be improved in the final step by transforming $\xi_{\rm NL}(r) - \xi_{\rm L}(r)$, which vanishes rapidly at large r, and then adding $\Delta^2_{\rm L}(k)$ to the answer.

The above process is still rather time-consuming and inelegant; it would be much better to make the HKLM method work directly in terms of power spectra, and this is usually possible. The main idea is that $\bar{\xi}(r)$ can often be thought of as measuring the power at some effective wavenumber: it is obtained as an integral of the product of $\Delta^2(k)$, which is often a rapidly rising function, and a window function which cuts off rapidly at high k. The answer can be approximated by replacing the exact window function by the Gaussian which is equivalent to second order in k:

$$\bar{\xi}(r) = \Delta^2(k_{\rm eff}), \tag{17}$$

$$k_{\rm eff} = \left[\frac{([n+1]/2)\,!}{2}\right]^{1/(n+3)}\frac{\sqrt{10}}{r}, \tag{18}$$

where n is the effective power-law index of the power spectrum. This approximation is within a few per cent of the exact integration provided that $n \lesssim 0$. The effective wavenumber is insensitive to n, and is within 20 per cent of $2.4/r$ over the range $-2 < n < 0$. In most circumstances, it is therefore an excellent approximation to use the HKLM formulae directly to scale wavenumbers and powers:

$$\Delta^2_{\rm NL}(k_{\rm NL}) = f_{\rm NL}[\Delta^2_{\rm L}(k_{\rm L})], \tag{19}$$

$$k_{\rm L} = [1+\Delta^2_{\rm NL}(k_{\rm NL})]^{-1/3} k_{\rm NL}. \tag{20}$$

Even better, it is not necessary that the number relating $1/r$ and $k_{\rm eff}$ be a constant over the whole spectrum. All that matters is that the number can be treated as constant over the limited range $r_{\rm NL}$ to $r_{\rm L}$. This means that the deviations of the above formulae from the exact transformation of the HKLM procedure

are only noticeable in cases where the power spectrum deviates markedly from a smooth monotonic function, or where either the linear or non-linear spectra are very flat ($n \lesssim -2$). Even this is not obviously a problem, since the HKLM procedure itself is not exact and does not work so well for flat spectra, $n \lesssim -2$ (A.S. Hamilton, private communication). Our approximation is illustrated in Fig. 1, which shows the result of non-linear evolution on spectra with and without a short-wavelength cutoff. Whether the HKLM method actually applies to the first situation is an interesting question which we hope to investigate elsewhere. Other cases where our approximation would fail include power spectra with the oscillations characteristic of pure baryon models. However, since the data studied here reveal no trace of such sharp features in the power spectrum, we may use the direct approximation for the non-linear evolution of the power spectrum with confidence.

It remains to generalize the result from the $\Omega = 1$ model considered by HKLM. This can be done partly analytically. The argument that leads to the $f_{\rm NL}(x) \propto x^{3/2}$ asymptote in the non-linear transformation is just that linear and non-linear correlations behave as a^2 and a^3 respectively following collapse. If collapse occurs at high redshift, then $\Omega = 1$ may be assumed at that time, and the non-linear correlations still obey the a^3 scaling to low redshift. All that has changed is that the linear growth is suppressed by some Ω-dependent factor $g(\Omega)$. It then follows that the large-x asymptote of the non-linear function is

$$f_{\rm NL}(x) \to 11.68\,[g(\Omega)]^{-3}\,x^{3/2}. \qquad (21)$$

According to Carroll, Press & Turner (1992), the growth factor may be approximated almost exactly by

$$g(\Omega) = \frac{5}{2}\Omega_{\rm m}\left[\Omega_{\rm m}^{4/7} - \Omega_{\rm v} + (1+\Omega_{\rm m}/2)(1+\Omega_{\rm v}/70)\right]^{-1}, \qquad (22)$$

where we have distinguished matter (m) and vacuum (v) contributions to the density parameter explicitly. We shall generally use Ω without a subscript to mean $\Omega_{\rm m}$ hereafter.

To interpolate between the expected non-linear asymptote and the linear regime, numerical experiments are necessary. We therefore wrote a PM N-body code, which was used to evolve a variety of initial spectra to a final state of given $\Omega_{\rm m}$ and $\Omega_{\rm v}$; typically 64^3 particles and a 128^3 mesh were used. At a later stage of the investigation, we were able to check our results with the superior resolution provided by the AP^{3}M code of Couchman (1991). It was also possible to compare with low-density cold dark matter (CDM) models published by Davis et al. (1985) and Kauffmann & White (1992). Our conclusion is that a near-universal behaviour analogous to that of HKLM does appear to exist for low-density models, at least for the linear spectra with power-law indices $-2 < n < 0$ that we were able to test. We have produced the following fitting formula for the generalized $f_{\rm NL}$. This is designed to match the HKLM expression almost exactly in the $\Omega = 1$ limit, and to describe the main features of the alterations encountered in low-density models. The accuracy is approximately 10 per cent in terms of the deduced linear power $\Delta_{\rm L}^2$ corresponding to a given $\Delta_{\rm NL}^2$, over the range $0.3 \lesssim g(\Omega) \lesssim 1$.

$$f_{\rm NL}(x) = x\left[\frac{1 + 0.2\beta x + (Ax)^{\alpha\beta}}{1 + ([Ax]^{\alpha} g^3(\Omega)/[11.68x^{1/2}])^{\beta}}\right]^{1/\beta}, \qquad (23)$$

where the parameters are $A = 0.84[g(\Omega)]^{0.2}$, $\alpha = 2/[g(\Omega)]$, and $\beta = 2g(\Omega)$. This fit says that the transition region between the linear and non-linear regimes is dominated by an $f_{\rm NL} \propto x^{1+\alpha}$ power law, which becomes very steep for low-density models. This steepening has long been familiar from N-body models, and the apparent power-law nature of the spectrum can been used as an argument against low-density models. We shall end up making a rather similar argument here.

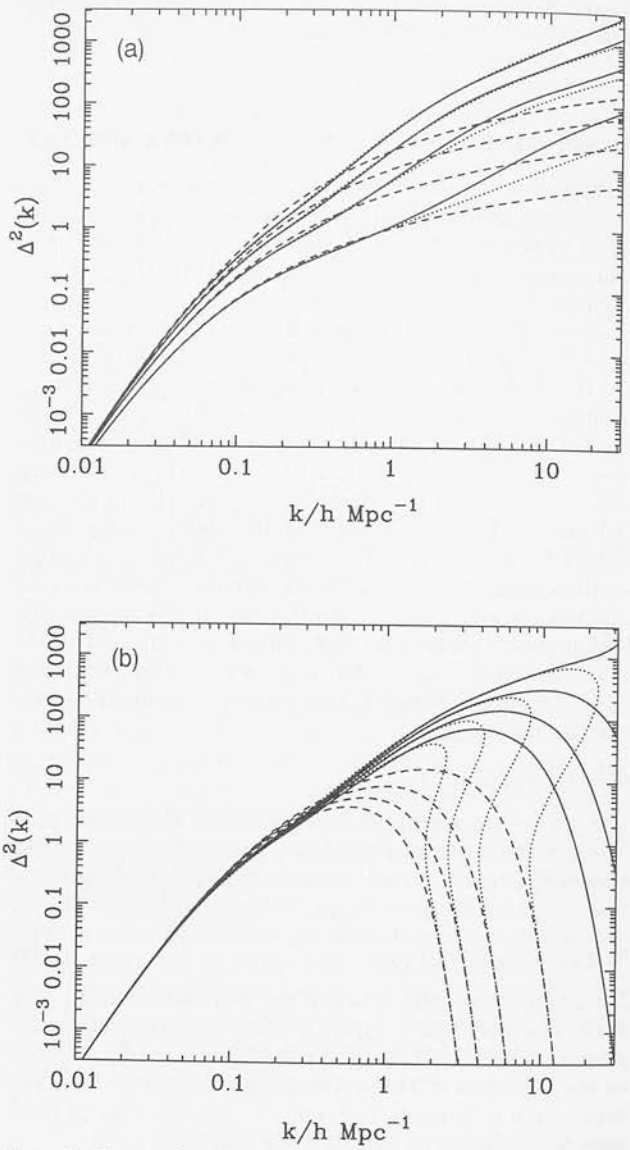

Figure 1. The non-linear evolution of power spectra according to the HKLM method, and the approximate direct alternative presented here. The dashed lines show the input linear power spectra, the solid lines show the result of numerically integrating the HKLM method and the one-step solution is shown dotted. Panel (a) shows a variety of *COBE*-normalized CDM models (with $\Omega h = 0.2, 0.3, 0.4, 0.5$); while (b) shows Ωh=0.5 CDM filtered with different Gaussian windows ($R_{\rm f} = 0.25, 0.5, 0.75, 1\ h^{-1}$ Mpc), approximating the effect of warm dark matter. As expected, our method fails at very high k, where the linear CDM spectra become very flat and the linear WDM spectra cutoff, but is otherwise excellent. Note that the effect of the WDM cutoff is only felt at very large k: WDM is not the explanation for the shape of the power spectrum around $k = 0.1h$.

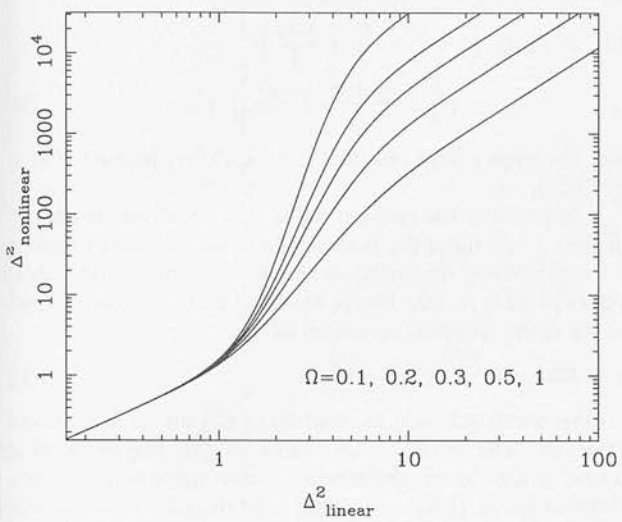

Figure 2. The generalization of the HKLM function relating non-linear power to linear power (or $\bar{\xi}$, as in the original method). The lowest curve is the original HKLM function for $\Omega = 1$; low densities give a greater non-linear response. We show the fitting formula for open models only, but what matters in general is just the Ω-dependent linear growth suppression factor.

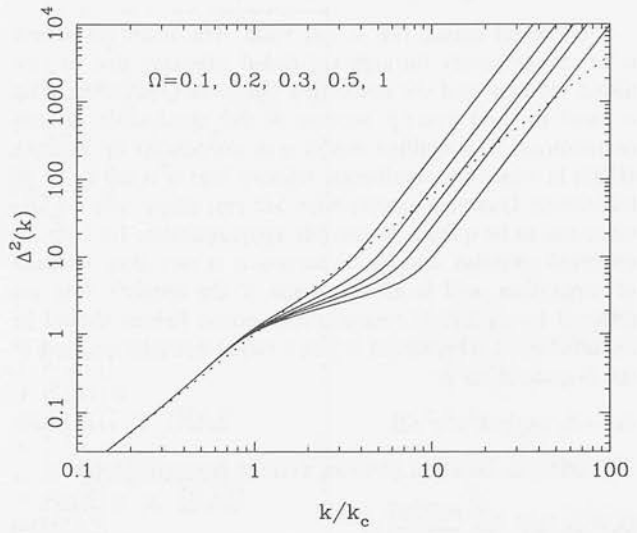

Figure 3. The inverse of the generalized HKLM procedure, as applied to a power-law power spectrum (shown dotted) $\Delta^2(k) = (k/k_c)^{1.8}$ (in correlation-function terms, $r_0 = 0.945/k_c$). Open models with $\Omega = 1$, 0.5, 0.3, 0.2, 0.1 are considered. Note that the effects of non-linearities in this case are rather small for high densities, but for low densities the required linear initial conditions are very flat for $k \gtrsim k_c$. This flat case is one where our approximate inversion of the HKLM procedure will not be perfect (cf. Fig. 1); nevertheless, any errors will be small in comparison with the systematic feature in the power spectrum required around $\Delta^2 \sim 1$. It clearly requires something of a conspiracy to achieve a scale-free non-linear spectrum in a low-density model.

It is useful to have an analytical expression for the inverse function, and the following agrees with the exact inverse of our formula to within a typical maximum error of a few per cent over the range of interest:

$$f_{\rm NL}^{-1}(y) = y\left[\frac{1+(By^{\gamma-1/3}[g^3(\Omega)/11.68]^{2/3})^{\delta}}{1+0.2\delta y+(By^{\gamma})^{\delta}}\right]^{1/\delta}, \qquad (24)$$

where $B = 0.96[g(\Omega)]^{0.07}$, $\gamma = 1.03 - 0.39[g(\Omega)]^{0.5}$, and $\delta = 5[g(\Omega)]^{0.3}$. A plot of the Ω-dependent non-linear function is shown in Fig. 2. We show only models with zero vacuum energy, since the above reasoning shows that all that matters is the linear growth-suppression factor $g(\Omega)$. Note that, for spatially flat vacuum-dominated models, the growth suppression is rather more modest (roughly $g(\Omega) = \Omega^{0.2}$) than in models with zero vacuum energy (roughly $g(\Omega) = \Omega^{0.7}$). Our results (and those of HKLM) apply only to initial conditions with Gaussian statistics. It is an interesting question to what extent the method will also apply to non-Gaussian models, and we hope to investigate this elsewhere. Some idea of the likely degree of universality may be gained from the non-Gaussian models studied by Weinberg & Cole (1992). They found that the non-linear power spectrum was very similar for a range of initial models, with the exception only of those that were strongly skew-negative. It therefore seems likely that mildly non-Gaussian models such as cosmic strings should be treated correctly by the method we have given.

We now have the required means of deducing the initial conditions that correspond to a given observed non-linear mass spectrum. As an example, we show in Fig. 3 the initial conditions required to create the canonical correlation function $\bar{\xi}(r) = (r/r_0)^{1.8}$; i.e. $\Delta^2(k) = (k/k_c)^{1.8}$, where $k_c = 1.058/r_0$. For low-density models, the initial conditions require an enormous 'bite' to be taken out of the spectrum for k between k_c and several times k_c. The reconstructed spectrum tends to be very flat and close to $\Delta^2(k) = 1$ over a large range of wavenumber. Conversely, for $\Omega = 1$ the effects of non-linearities are not very severe in this case until we reach $\Delta^2(k) \gtrsim 10$. These differences will be important when we come to linearize the observed data.

4 REDSHIFT-SPACE DISTORTIONS

With the exception of surveys where angular data are deprojected to obtain an estimate of the spatial power spectrum, three-dimensional clustering data generally involve redshift surveys where the radii are distorted by peculiar velocities. There are two effects to consider. On large scales, a linear analysis should be valid and we have the anisotropic effect noted by Kaiser (1987):

$$\delta_k \to b\,\delta_k\,(1 + f\mu^2/b), \qquad (25)$$

where μ is the cosine of the angle between the wavevector and the line of sight. The function $f(\Omega) \simeq \Omega^{0.6}$ is the well-known velocity-suppression factor due to Peebles, which is in practice a function of $\Omega_{\rm m}$ only, with negligible dependence on the vacuum density (Lahav et al. 1991). The anisotropy arises because mass flows from low-density regions on to high-density sheets, and the apparent density contrast of the pattern is thus enhanced in redshift space if the sheets lie near the plane of the sky. If we average this anisotropic effect by integrating over a uniform distribution of μ, the net boost to the power spectrum is

$$|\delta_k|^2 \to b^2 |\delta_k|^2 \left(1 + \frac{2}{3}[f/b] + \frac{1}{5}[f/b]^2\right). \quad (26)$$

On small scales, this is not valid. The main effect here is to reduce power through the radial smearing due to virialized motions and the associated 'finger-of-God' effect. This is hard to treat exactly because of the small-scale velocity correlations. A simplified model was introduced by Peacock (1992) in which the small-scale velocity field is taken to be an incoherent Gaussian scatter with 1D rms dispersion σ. This turns out to be quite a reasonable approximation, because the observed pairwise velocity dispersion is a very slow function of separation, and is all the better if the redshift data are afflicted by significant measurement errors (which should be included in σ). This model is just a radial convolution, and so the k-space effect is

$$\delta_k \to \delta_k \exp[-k^2\mu^2\sigma^2/2]. \quad (27)$$

This effect in isolation gives an average isotropic factor of

$$|\delta_k|^2 \to |\delta_k|^2 \frac{\sqrt{\pi}}{2} \frac{\mathrm{erf}\,(k\sigma)}{k\sigma} \quad (28)$$

and produces only mild damping (one power of k at large k).

Some workers (e.g. Fisher et al. 1992; Kofman, Gnedin & Bahcall 1993) have combined the above two effects simply by multiplying the two power correction factors to achieve a total distortion. However, this is not correct: both terms are anisotropic in k space and they interfere before averaging: $\langle A^2B^2\rangle \neq \langle A^2\rangle\langle B^2\rangle$. For the present paper, it is also interesting to consider the case of cross-correlation where each of two catalogues gives a different measure of the same underlying density field. The model for the effect in k space of cross-correlation is then the product of two separate factors of the above form:

$$|\delta_k|^2 \to b_1 b_2 |\delta_k|^2 (1 + f\mu^2/b_1)(1 + f\mu^2/b_2) \times \exp[-k^2\mu^2(\sigma_1^2 + \sigma_2^2)/2]. \quad (29)$$

The overall effect is obtained by averaging over μ, and looks more complicated than it really is:

$$|\delta_k|^2 \to b_1 b_2 |\delta_k|^2 \, G(y, \alpha_1, \alpha_2), \quad (30)$$

where

$$y^2 \equiv k^2(\sigma_1^2 + \sigma_2^2)/2, \quad (31)$$

$$\alpha \equiv f(\Omega)/b, \quad (32)$$

$$G(y, \alpha_1, \alpha_2) = \frac{\sqrt{\pi}}{8} \frac{\mathrm{erf}\, y}{y^5} [3\alpha_1\alpha_2 + 2(\alpha_1 + \alpha_2)y^2 + 4y^4] - \frac{\exp(-y^2)}{4y^4} [\alpha_1\alpha_2(3 + 2y^2) + 2(\alpha_1 + \alpha_2)y^2]. \quad (33)$$

This simplifies a little in the case of autocorrelations, where indices 1 and 2 are equivalent. The interesting aspect of this formula is that the linear boost is lost at large k, where the result is independent of Ω (as is obvious from the anisotropic form: the main contribution at large k comes from small μ). The true damping at large k is thus more severe than would be obtained by multiplying the power corrections prior to angular averaging. The simulations of Gramann, Cen & Bahcall (1993) show a good level of agreement with the above formula in the autocorrelation case. The result is reassuringly insensitive to the assumed form for the small-scale velocity distribution function; if we take an exponential instead of a Gaussian, we find the same result at small k:

$$G(y, \alpha_1, \alpha_2) \simeq \left(1 + \frac{\alpha_1 + \alpha_2}{3} + \frac{\alpha_1\alpha_2}{5}\right) - \left(\frac{1}{3} + \frac{\alpha_1 + \alpha_2}{5} + \frac{\alpha_1\alpha_2}{7}\right) y^2, \quad (34)$$

and the large-y limit becomes $G \to \pi/(2^{3/2}y)$ instead of $G \to \pi^{1/2}/(2y)$.

In practice, the relevant value of σ to choose is approximately $1/\sqrt{2}$ times the pairwise dispersion $\sigma_\parallel$ seen in galaxy redshift surveys. According to the most recent compilation of velocity results by Mo, Jing & Börner (1993b), this corresponds to the figure (adopted hereafter) of

$$\sigma \simeq 300 \ \mathrm{km\,s^{-1}}. \quad (35)$$

To this, we should add in quadrature any errors in measured velocities. The relatively low value of this dispersion is of course a significant problem for some high-density models. Gramann et al. (1993) argue that redshift-space power spectra of CDM models fit observation very well, mainly because the predicted pairwise dispersion is so high in these models. As we shall see below, such an unrealistically large dispersion would spoil the agreement between data sets in real and in redshift space.

5 POWER-SPECTRUM RECONSTRUCTION

5.1 Data

We now apply the above tools to some of the more recent results on the clustering power spectrum. We shall consider eight distinct sets of data, which fall into several distinct classes.

(i) Real-space clustering of galaxies. Baugh & Efstathiou (1993) have applied a deprojection procedure to the angular clustering of the APM galaxy survey to infer the non-linear power spectrum of optically selected galaxies without redshift-space distortions. This paper considers the large-scale power spectrum, and we have thus used the APM data at $k < 1\,h\,\mathrm{Mpc^{-1}}$ only. To allow comparison with other data sets, we have also set a lower limit of $k > 0.015\,h\,\mathrm{Mpc^{-1}}$.

(ii) Redshift-space clustering of galaxies. We consider three data sets: FKP for *IRAS* galaxies (the QDOT sample); Loveday et al. (1992) for the Stromlo/APM survey; Vogeley et al. (1992) for the CfA survey. The last paper quotes results for two separate subsets; we have adopted a straight mean of the two sets of data. We have not used the *IRAS* data of Fisher et al. (1993), which are systematically lower than those of FKP. As discussed by FKP, this seems most likely to be a local sampling effect. In any case, it is the deeper QDOT sample used by FKP which also appears in cross-correlation analyses (see iv below).

(iii) Redshift-space clustering of groups and clusters of galaxies. We use the power spectrum for $R \geq 1$ Abell clusters from Peacock & West (1992) and also radio galaxies from Peacock & Nicholson (1991), on the assumption that the strongly enhanced clustering of these latter objects may be attributed to their location in moderately rich environments.

(iv) We also use the cross-correlation between *IRAS* galaxies and Abell clusters or radio galaxies from Mo, Peacock & Xia (1993a).

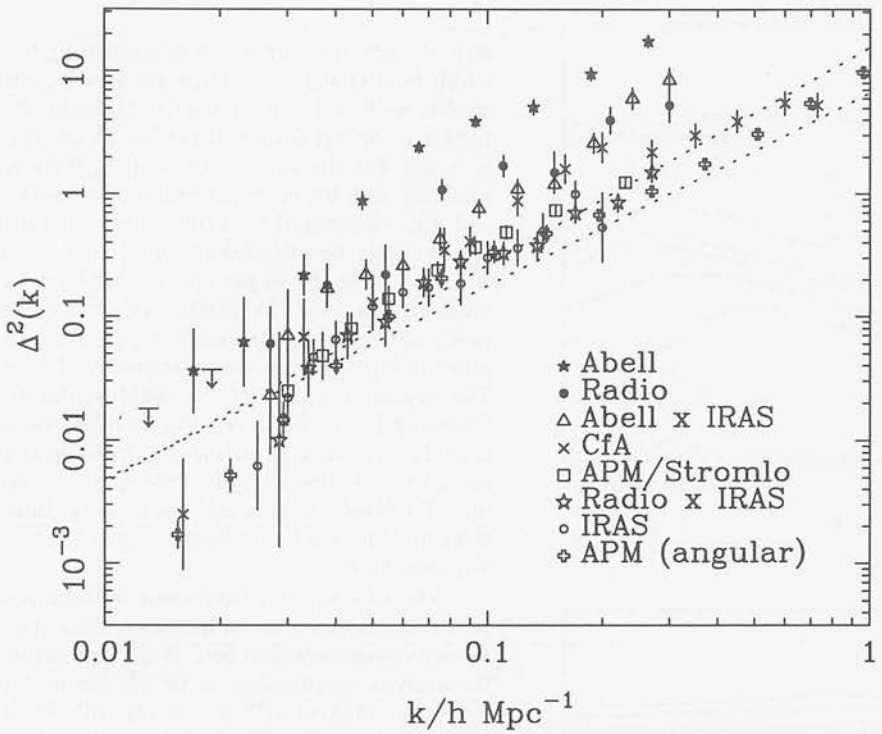

Figure 4. The raw power-spectrum data used in this analysis. All data with the exception of the APM power spectrum are in redshift space. The two lines shown for reference are the transforms of the canonical real-space correlation functions for optical and *IRAS* galaxies ($r_0 = 5$ and 3.78 h^{-1} Mpc and slopes of 1.8 and 1.57 respectively).

Not all of the above data are available directly in power-spectrum form. In cases where what is published is a cell variance or a measure of $\bar{\xi}(r)$, we have used the notion of an effective wavenumber, as discussed above and in Peacock (1991). The treatment of errors requires some discussion. Only FKP give a full realistic error covariance matrix for their data; the other data sets give errors ranging from Poisson estimates to field-to-field errors, but with no discussion of the independence of the measurements at different k. For consistency, we have therefore used a fraction of the FKP data, spaced widely enough to be roughly independent. Any imprecision in this procedure, plus unrecognized systematics, will become apparent when the various data sets are compared with each other.

The raw power-spectrum data are plotted in Fig. 4. There is a wide range of power measured, ranging over perhaps a factor 20 between the real-space APM galaxies and the rich Abell clusters. We now have to see to what extent these measurements are all consistent with one Gaussian power spectrum for mass fluctuations.

5.2 Implications for bias and Ω

The reconstruction analysis has available eight data sets containing 91 distinct $k-\Delta^2$ pairs. The modelling has available five free parameters in the form of Ω and the four bias parameters for Abell clusters, radio galaxies, optical galaxies and *IRAS* galaxies (b_A, b_R, b_O, b_I). We optimized the model by making independent determinations of $\Delta^2_L(k)$ for each data set and then comparing them. This was done in practice by dividing the range $0.01 < k < 0.1\ h\,\mathrm{Mpc}^{-1}$ into 20 bins, and evaluating a weighted mean power and a χ^2 for each bin. The likelihood of the model is given in terms of the summed χ^2 values:

$$\mathscr{L} \propto \exp -\chi^2/2. \tag{36}$$

At this stage, the question arises of whether the errors are realistic, which may be judged from whether the overall χ^2 matches the number of degrees of freedom: in fact, it does not. A procedure that ensures the required match is to add some constant rms error ϵ in quadrature to the existing errors. In practice,

$$\epsilon = 23 \text{ per cent} \tag{37}$$

is required for the best-fitting model. Such a fudge is unsatisfactory and indicates a failure of understanding of the data errors. However, there are grounds for suspecting that some of the published errors are too low, so ϵ is not a surprisingly large correction. There may be excessive democracy here, in that the formally most accurate data sets are penalized most strongly by this procedure. On the other hand, these may be the ones most likely to 'detect' small residual systematics; it seems conservative to distribute the blame for any small disagreement uniformly. One might also query whether this correction should be applied at all k; for many models, the disagreement is worst at high k. We shall stick with the simplest procedure, since the quoted errors are usually much larger at low k.

Of our free parameters, only two are really important: Ω and a measure of the overall level of fluctuations. We take the *IRAS* bias parameter to play this latter role. Once these two

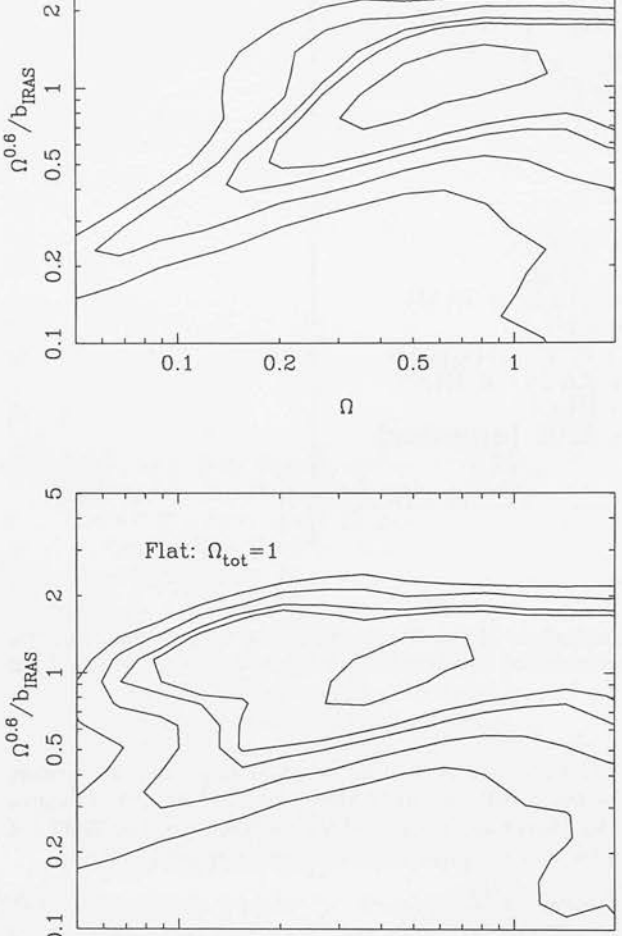

Figure 5. Contours of relative likelihood based on the degree of agreement of the various estimates of linear power spectra. At each (Ω, b_I) point, the other bias factors have been optimized. We distinguish the cases $\Omega_v = 0$ (open) and $\Omega_m + \Omega_v = 1$ (flat). Contours are plotted at what would be the 50, 90, 95, 99, 99.5 per cent confidence levels in a two-dimensional Gaussian (i.e. $\Delta \ln \mathscr{L} = 0.69$, 2.3, 3.0, 4.6, 5.3).

are specified, the other bias parameters are well determined – principally from the data at small k, where we are in the linear regime. The best-fitting values depend only very slightly on the two controlling parameters, and for all allowed models are close to

$$b_A : b_R : b_O : b_I = 4.5 : 1.9 : 1.3 : 1, \tag{38}$$

to within 6 per cent rms. We now show likelihood plots for the remaining two parameters, Ω and b_I. Contours of likelihood are displayed in Fig. 5, distinguishing the cases $\Omega_v = 0$ (open) and $\Omega_m + \Omega_v = 1$ (flat). Two main features are visible on these plots: the data appear to demand a significant degree of redshift-space distortion, with the optimal model having

$$\frac{\Omega^{0.6}}{b_I} = 1.0 \pm 0.2 \tag{39}$$

in both cases (rms error). Models satisfying this constraint in which both Ω and b_I are large are allowed, corresponding to models well in the linear regime. However, low-bias models appear to be less favoured: for low Ω, the best models have $b_I \simeq 0.8$. For the case of flat models, there is a certain bimodality, with the preferred values of b_I for $\Omega = 0.1$ being 0.8 and 0.25. However, the heavily antibiased branch of solutions can probably be excluded on other grounds, and we ignore it hereafter. At the 90 per cent confidence level, this analysis requires $\Omega > 0.14$. The various reconstructions of the linear power spectrum for the case $\Omega = b_I = 1$ are shown superimposed in Fig. 6, and display an impressive degree of agreement. This argues very strongly that what we measure with galaxy clustering has a direct relation to mass fluctuations, rather than the large-scale clustering pattern being an optical illusion caused by non-uniform galaxy-formation efficiency (Bower et al. 1993). If this were the case, the spectrum inferred from clusters should have a very different shape at large scales, contrary to observation.

The detection of redshift-space distortions is based largely on the inclusion of the APM survey, since it is the only real-space measurement used here. If this data set is removed from the analysis, small values of $\Omega^{0.6}/b_I$ are no longer excluded. An upper limit at $\Omega^{0.6}/b_I \lesssim 2$ can still be set; this comes primarily from the cross-correlation data. In real space, the cross-correlation should be the geometric mean of the two autocorrelation results. Because of the different effects of the redshift-space mapping, however, this is no longer true when redshift-space distortions become large. The observed cross-correlations thus set a limit to how strong the distortion can be. Some independent confidence in the detection of non-zero distortion can be gained from the work of Saunders, Rowan-Robinson & Lawrence (1992). They deduced the real-space correlation function for *IRAS* galaxies: $\xi(r) = (r/r_0)^{-\gamma}$, with $r_0 = 3.78 \pm 0.14\, h^{-1}$Mpc and $\gamma = 1.57 \pm 0.03$. If we convert this to a power spectrum, it lies lower than the QDOT results of FKP by a factor 1.61 ± 0.26 over the range $0.05\, h < k < 0.15\, h$ Mpc^{-1}. This corresponds to $\Omega^{0.6}/b_I = 0.75 \pm 0.25$, in good agreement with the figure deduced above, and provides independent evidence for the detection of significant redshift-space distortion. This lower degree of real-space clustering is also in agreement with our ratio of 1.3 between optical and *IRAS* bias factors. The Saunders et al. figure for r_0 predicts $r_0 = 5.3\, h^{-1}$Mpc for optically selected galaxies in real space, which is very close to the canonical value. *IRAS* galaxies have a slightly smaller value of γ, but this only produces an important change in relative power on scales rather smaller than those probed here.

The conclusion that models with $\Omega^{0.6}/b_I \simeq 1$ and low Ω are not allowed stems from the effect of non-linearities: the true level of mass fluctuations in such models would be very high. Moreover, a decrease of Ω increases the effect of non-linearities, as discussed above; this trend is less marked for the flat models, which is why low densities are not so strongly excluded in that case. It is easy to see how this conclusion arises by referring to Fig. 6. This shows that the linear power spectra inferred from galaxy and cluster data agree down to $k \simeq 0.3\, h\,$Mpc^{-1}, where $\Delta^2 \simeq 1$ in the best-fitting case. If we assume a higher normalization, the effect of non-linearities in this case is to add

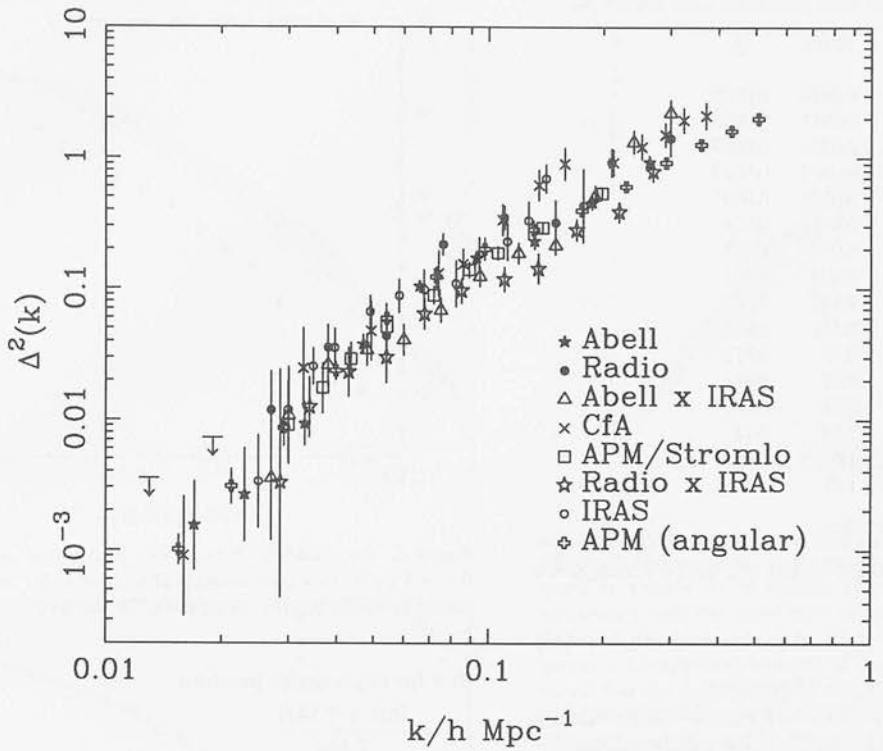

Figure 6. The power-spectrum data from Fig. 4, individually linearized assuming $\Omega = b_{\rm I} = 1$. There is an excellent degree of agreement, particularly in the detection of a break around $k = 0.03h$.

power, so the linear reconstruction from galaxy data would become very flat at high k (cf. Fig. 3). However, this would disagree with the cluster data, which would still indicate a steep power spectrum, since we have assumed that the clusters give the linear result directly. This is a general problem with highly evolved models: since non-linearities change the shape of the power spectrum at $\Delta^2 \simeq 1$, and especially so for low densities, it requires something of a conspiracy for the non-linear power spectrum to be a featureless power law (see Gott & Rees 1975). However, on the present assumptions, extreme non-linear evolution should steepen the galaxy correlations faster than those for clusters, and yet they empirically have much the same slope. The easiest way of understanding this is to say that the degree of non-linearity is only mild. This is certainly an issue which merits further investigation, and a detailed simulation of cluster formation in a highly non-linear low-density model would be most valuable. In the meantime, it is interesting to note that the constraints we have drawn here on density and bias are very similar to those obtained in a completely independent way by the POTENT group in their analysis of the peculiar-velocity field (Dekel et al. 1993).

Table 1 gives the final data for the mean reconstructed power spectrum, for the case $\Omega = b_{\rm I} = 1$. The data have been averaged in bins of width 0.1 in $\log_{10}$(wavenumber) and the errors quoted are standard errors. These numbers are plotted in Fig. 7, and will be compared with models in the next section; as will be shown there, the data are consistent with a smooth and featureless power spectrum, despite the small size of the errors. One of the pleasant features of our result is that the power spectrum is only weakly dependent on model parameters. For $\Omega = 1$, the power is not so sensitive to b, because in redshift space (the majority of the data) we measure

$$\Delta_z^2 \propto b^2 \left(1 + \frac{2}{3}[f/b] + \frac{1}{5}[f/b]^2\right). \tag{40}$$

The overall power correction factor thus scales only as $b^{10/7}$ for b close to unity. This can be used to rescale our 'standard' result to some other desired value of b, given $\Omega = 1$. For low densities, an empirical formula for the scaling of the linear mass spectrum in the present analysis is

$$\Delta_{\rm L}^2 \propto \Omega^{-0.3}. \tag{41}$$

It is convenient to be able to compare the results here with another common measure of the amplitude of linear mass fluctuations. This is σ_8: the linear-theory rms density contrast when averaged over spheres of radius $8\,h^{-1}$ Mpc:

$$\sigma_R^2 = \int \Delta^2(k)\,\frac{{\rm d}k}{k}\,\frac{9}{(kR)^6}[\sin kR - kR\cos kR]^2. \tag{42}$$

The squared window function weighting the power spectrum is very close to a Gaussian $W_k^2 = \exp[-k^2R^2/5]$, and so σ_R^2 is just $\Delta^2(k)$ at some effective wavenumber:

$$\sigma_R^2 = \Delta^2(k_R), \tag{43}$$

$$k_R = \left[\frac{([n+1]/2)\,!}{2}\right]^{1/(n+3)}\frac{\sqrt{5}}{R}, \tag{44}$$

where n is the effective power-law index of the power spectrum. As before, this approximation is within a few per cent of the exact integration provided that $n \lesssim 0$. On the scales of

Table 1. The linear power-spectrum data, assuming $\Omega = b_I = 1$. To scale the data to other values of these parameters, see Section 5.2.

$k/h\,\mathrm{Mpc}^{-1}$	$\Delta^2(k)$	$\pm$
0.014	0.0010	0.0003
0.018	0.0013	0.0008
0.022	0.0032	0.0009
0.028	0.0087	0.0023
0.035	0.0196	0.0037
0.045	0.0312	0.004
0.056	0.052	0.008
0.071	0.107	0.011
0.089	0.146	0.017
0.112	0.211	0.027
0.141	0.33	0.033
0.178	0.43	0.051
0.224	0.73	0.095
0.282	1.14	0.13
0.355	1.63	0.27
0.447	1.61	0.41

interest, the effective index is close to -1.5 and so the effective wavenumber for σ_8 is $k = 0.20$. Using the above scalings, we get

$$\sigma_8 = 0.75\,\Omega^{-0.15}, \tag{45}$$

with a formal rms uncertainty of 13 per cent.

The significance of $8\,h^{-1}$ Mpc as a normalization scale is that σ_8 is of order unity and thus its value can be probed by observations of weakly non-linear structures such as galaxy clusters. White, Efstathiou & Frenk (1993) discuss this constraint, and deduce $\sigma_8 = 0.57\,\Omega^{-0.56}$ for spatially flat models (although the scaling should be very similar for open models), to within a tolerance of roughly ± 10 per cent. The precise meaning of their uncertainty is hard to quantify, but it seems intended to give hard limits, rather than an rms. The agreement with our results is very good; the Ω dependence is steeper, but the disagreement in σ_8 is only a factor 1.4 even for $\Omega = 0.2$.

6 POWER-SPECTRUM DATA AND MODELS

6.1 CDM-like models

It is interesting to ask if the power spectrum contains any features, or whether it is consistent with a single smooth curve. In fact, a variety of simple models describe the data from Table 1 very well within the errors. Consider the fitting formula used by Peacock (1991), which is just a break between two power laws:

$$\Delta^2(k) = \frac{(k/k_0)^\alpha}{1 + (k/k_c)^{\alpha-\beta}}. \tag{46}$$

This works well, with

$$k_0 = 0.29 \pm 0.01\ h\,\mathrm{Mpc}^{-1}, \tag{47}$$

$$k_1 = 0.039 \pm 0.002\ h\,\mathrm{Mpc}^{-1}, \tag{48}$$

$$\alpha = 1.50 \pm 0.03, \tag{49}$$

$$\beta = 4.0 \pm 0.5. \tag{50}$$

A value of $\beta = 4$ corresponds to a scale-invariant spectrum at large wavelengths.

A more physical alternative is the CDM power spectrum, which is $\Delta^2(k) \propto k^{n+3} T_k^2$. We shall use the BBKS approximation for the transfer function:

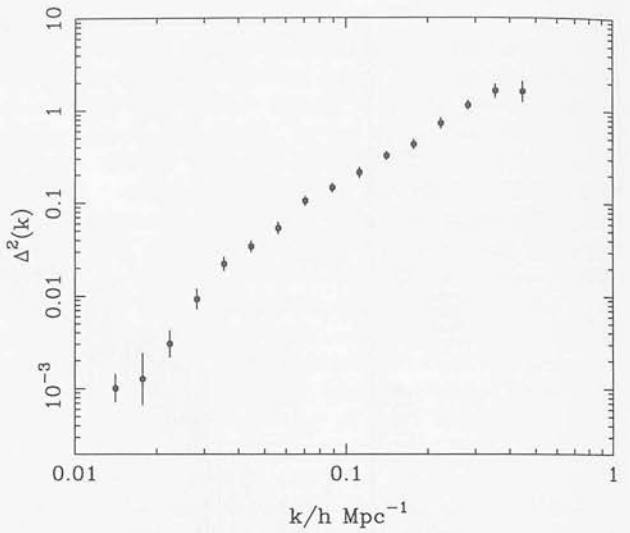

Figure 7. The linearized data of Fig. 6, averaged over bins of width 0.1 in $\log_{10} k$. This plot assumes $\Omega = b_I = 1$; for lower densities the power increases slightly, as described in the text.

$$T_k = \frac{\ln(1 + 2.34q)}{2.34q} \times [1 + 3.89q + (14.1q)^2 + (5.46q)^3 + (6.71q)^4]^{-1/4}, \tag{51}$$

where $q \equiv k/[\Omega h^2\ \mathrm{Mpc}^{-1}]$. Since observable wavenumbers are in units of $h\,\mathrm{Mpc}^{-1}$, the shape parameter is the apparent value of Ωh. This scaling applies for models with zero baryon content, but there is an empirical scaling that can account for the effect of baryons, and which deserves to be more widely known. Fig. 8 shows a compilation of CDM transfer functions taken from Holtzman (1989). When plotted against $k/\Omega h^2$, there is a strong dependence on baryon density: high baryon content mimics low CDM density. If we instead use the scaling

$$T_k(k) = T_{\mathrm{BBKS}}(k/[\Omega h^2 \exp(-2\Omega_{\mathrm{B}})]), \tag{52}$$

then all the curves lie on top of one another to a few per cent tolerance. We shall henceforth use the term 'Ωh' to refer to the BBKS fitting parameter, on the understanding that it means the combination $\Omega h \exp(-2\Omega_{\mathrm{B}})$. Our results will hence differ slightly from those of Efstathiou, Bond & White (1992), who defined a parameter Γ which is almost Ωh. Unfortunately, they scaled to a 'standard' CDM model with $\Omega_{\mathrm{B}} = 0.03$, with the result that $\Gamma = 1.06\Omega h$.

Fitting of the CDM model to our data also results in a satisfactory χ^2 and requires the parameters

$$\Omega h = 0.255 \pm 0.017 + 0.32(1/n - 1), \tag{53}$$

in agreement with many previous arguments suggesting that a low-density model is needed. The fit of this and other models is illustrated in Fig. 9. For any reasonable values of h and baryon density, a high-density CDM model is not viable. Even a high degree of 'tilt' in the primordial spectrum (Cen et al. 1992) does not help reach the required $\Omega h \simeq 0.75$. The alternatives are to retain the CDM model, but assume that some piece of unknown physics has produced a transfer function that looks like a low-density model, or to adopt a low density, or to go for

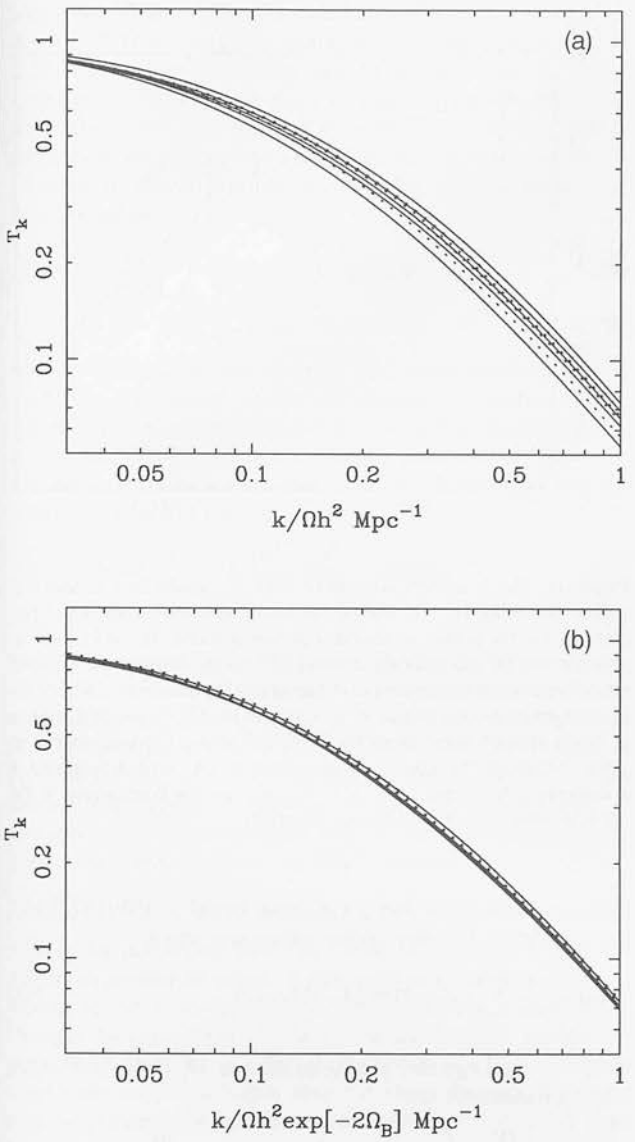

Figure 8. A set of CDM transfer functions, using the fitting formulae of BBKS for zero baryon content, and those of Holtzman (1989) for $\Omega_B = 0.01, 0.03, 0.05, 0.1$. Models with $h = 1$ are shown as solid lines, $h = 0.5$ are dotted. When plotted (panel a) against $k/\Omega h^2$, the varying baryon content causes variations in the curves, with higher Ω_B producing greater suppression of power. However, this can be scaled away (panel b) by plotting against the combination $k/[\Omega h^2 \exp(-2\Omega_B)]$. In these terms, the CDM transfer function has a universal shape, which can be described by the zero-baryon formula of BBKS. The scaling becomes noticeably imperfect for $\Omega_B \gtrsim 0.3$, but is very good for the models plotted here.

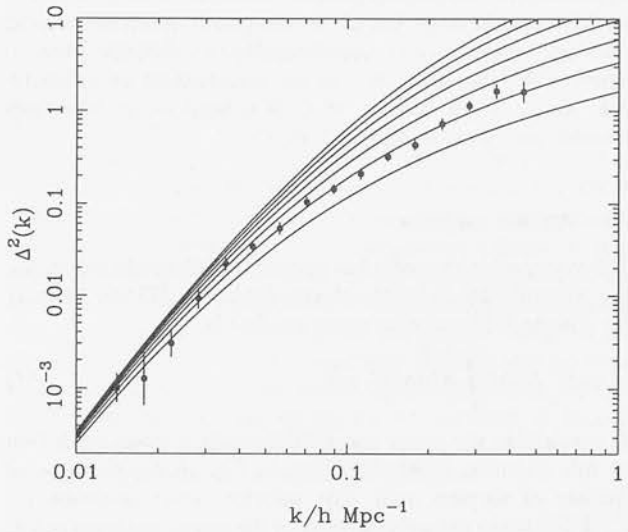

Figure 9. The averaged linear power-spectrum data of Fig. 7, compared to various CDM models. These assume scale-invariant initial conditions, with the same large-wavelength normalization. Different values of the fitting parameter $\Omega h = 0.5, 0.45, \ldots 0.25, 0.2$ are shown; power is an increasing function of Ωh, so that the 'standard' $\Omega h = 0.5$ model has the highest power, whereas $\Omega h = 0.2$ has the lowest. The best-fitting model has $\Omega h = 0.25$ and a normalization which is 1.5σ higher than *COBE* if $\Omega = 1$ and gravity-wave anisotropies are negligible ($\epsilon = 3.25 \times 10^{-5}$).

something else entirely. As far as low densities are concerned, note that the popular choice of $\Omega = 0.2$ (e.g. Kauffmann & White 1992) will overshoot and yield too low values of Ωh. More viable alternatives with high density are either mixed dark matter (MDM: Holtzman 1989; van Dalen & Schaefer 1992; Taylor & Rowan-Robinson 1992; Davis, Summers & Schlegel 1992; Klypin et al. 1993; Pogosyan & Starobinsky 1993), or non-Gaussian pictures such as cosmic strings + hot dark matter, where the lack of a detailed prediction for the power spectrum helps ensure that the model is not yet excluded (Albrecht & Stebbins 1992). Mixed dark matter seems rather ad hoc, but may be less so if it is possible to produce both hot and cold components from a single particle, with a Bose condensate playing the role of the cold component (Madsen 1992; Kaiser, Malaney & Starkman 1993). However, the shape of the MDM spectrum is not very close to the spectrum deduced here: it bends much more sharply, and is very flat on small scales. At the quasi-linear scale $k = 0.2\,h$ Mpc^{-1}, the local power-law index for the MDM model is about $n = -2.2$, as opposed to our empirical value $n \simeq -1.5$. If the good fit of a low-density CDM transfer function is taken literally, then perhaps this is a hint that the epoch of matter–radiation equality needs to be delayed. An approximate doubling of the number of relativistic degrees of freedom would suffice – but this would do undesirable violence to primordial nucleosynthesis: any such boost would have to be provided by a particle that decays after nucleosynthesis. The apparent value of Ωh depends on the mass and lifetime of the particle roughly as

$$\Omega h|_{\rm apparent} = \Omega h\ [1 + (m_{\rm keV}\tau_{\rm years})^{2/3}]^{-1/2} \qquad (54)$$

(Bardeen, Bond & Efstathiou 1987; Bond & Efstathiou 1991), so a range of masses is possible. Apart from making the observed large-scale structure, such a model yields a small-scale enhancement of power which could lead to early galaxy formation. Whether the required particle physics is at all plausible remains to be seen, but the model is arguably the most attractive of those currently available.

An important general lesson to be drawn from this section is the lack of large-amplitude features in the power spectrum.

This is a strong indication that collisionless matter is deeply implicated in forming large-scale structure. Purely baryonic models contain large bumps in the power spectrum around the Jeans length prior to recombination ($k \sim 0.03\,\Omega h^2$ Mpc^{-1}), whether the initial conditions are isocurvature or adiabatic (e.g. section 25 of Peebles 1993). It is hard to see how such features can be reconciled with the data.

6.2 Peculiar velocities

The mass power spectrum has a direct application in predicting the cosmological peculiar-velocity field. The 3D rms velocity for clumps averaged over some window is

$$\sigma_v^2 = H^2 f(\Omega)^2 \int \Delta^2(k)\, \frac{\mathrm{d}k}{k^3}\, W_k^2, \tag{55}$$

so we can use the power spectrum to make a direct prediction of this quantity, which is shown in Fig. 10 for the case of spheres of varying radii. The velocity power spectrum ($\propto k^{-2}\Delta^2(k)$) peaks around the break in the power spectrum at $k \simeq 0.03\,h$ Mpc^{-1}, and so the predicted velocities decline rapidly for spheres which filter out this scale.

For $\Omega = 1$, the predicted velocities are very reasonable. If we model the Local Group as a sphere of radius $5\,h^{-1}$ Mpc, the 3D rms is 680 km s^{-1}, as against the observed 600 km s^{-1} one-point local measurement (the answer is very insensitive to the size used to define the Local Group). Fig. 10 also shows the deduced velocities from the POTENT group (Bertschinger et al. 1990) for spheres of radius 40 and 60 h^{-1}Mpc, which also agree well. However, the predictions are completely inconsistent with the velocity of 842 km s^{-1} for the local sphere out to $150\,h^{-1}$Mpc claimed by Lauer & Postman (1993). The predicted 3D rms for this scale is only 140 km s^{-1}. Even if we allow that their weighting scheme might reduce the effective radius of their sphere (they weight each radial shell equally), there remains a qualitative discrepancy. If this result were to be confirmed, it would probably indicate a large feature in the power spectrum on scales beyond those probed here ($k \lesssim 0.01\,h$ Mpc^{-1}).

The empirical power spectrum deduced here thus seems to agree extremely well with large-scale velocity data. The crucial test for $\Omega = 1$ models, however, has often been the small-scale velocity dispersion. The preferred low-Ωh model predicts a pairwise dispersion at $1\,h^{-1}$ Mpc separation of about $\sigma_\parallel = 550$ km s^{-1} (Mann 1993), which is interestingly close to more recent observational data (Mo et al. 1993b).

6.3 CMB anisotropies

We now relate the measurement of mass fluctuations on scales of several hundred Mpc to those implied on larger scales from the measurement of cosmic microwave background (CMB) fluctuations by the *COBE* team (Smoot et al. 1992). This is a subject which has advanced rapidly since the original detection, with a more widespread appreciation of the possible contribution of gravitational waves to the anisotropy (following the original insight of Starobinsky 1985). We therefore distinguish explicitly between scalar and tensor contributions to the CMB fluctuations by using appropriate subscripts. The former category are those described by the Sachs–Wolfe effect, and are gravitational potential fluctuations that relate directly

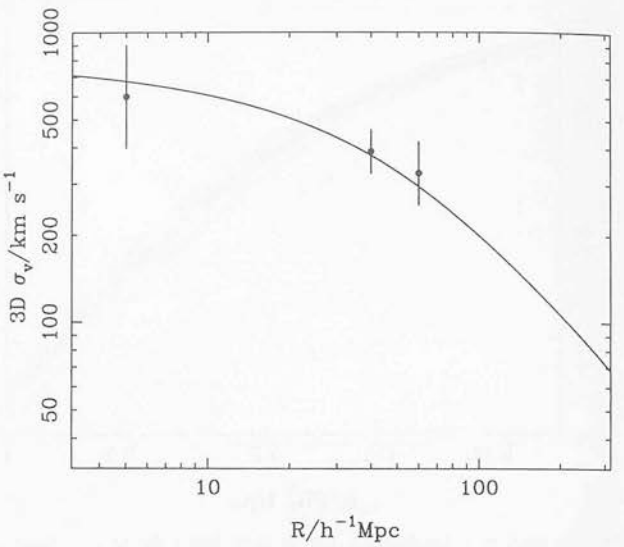

Figure 10. The predicted 3D rms velocity of spheres as a function of radius, assuming $\Omega = 1$. This is based on the two-power-law fitting formula for the power spectrum. For low densities the velocities are reduced, but by less than the normal $\Omega^{0.6}$ factor, because the inferred mass fluctuations rise in that case (see text). The plotted points are the Local Group motion assigned to a radius of $5\,h^{-1}$Mpc, and motion of larger spheres taken from the POTENT group (Bertschinger et al. 1990). Although the Local Group motion is very well determined, it is assigned a fractional error of $6^{-1/2}$ to allow for fluctuations in the 3D rms velocity seen by different observers.

to mass fluctuations. For a Gaussian beam of FWHM 2.35σ, the correlation function of the microwave sky is

$$C_s(\theta) = \frac{1}{4\pi} \sum_\ell (2\ell + 1)\, W_\ell^2\, C_\ell\, P_\ell(\cos\theta), \tag{56}$$

where P_ℓ are Legendre polynomials, and $W_\ell = \exp(-\ell^2\sigma^2/2)$. The coefficients C_ℓ are

$$C_\ell = 16\pi\, \frac{\Omega^2}{g^2(\Omega)} \int (k[2c/H_0])^{-4} \Delta^2(k)\, j_\ell^2(kR_\mathrm{H})\, \frac{\mathrm{d}k}{k}, \tag{57}$$

where j_ℓ are spherical Bessel functions (see Peebles 1982). The length R_H is the present comoving horizon size

$$R_\mathrm{H} = \frac{2c}{\Omega H_0} \quad \text{(open)} \tag{58}$$

$$\simeq \frac{2c}{\Omega^{0.4} H_0} \quad \text{(flat)} \tag{59}$$

(Vittorio & Silk 1991) and the function $g(\Omega)$ is the linear growth suppression factor relative to $\Omega = 1$, as discussed earlier. These formulae strictly apply only to spatially flat models, since the notion of a scale-free spectrum is imprecise in an open model. Nevertheless, since the curvature radius subtends an angle of $\Omega/[2(1-\Omega)^{1/2}]$, normalization to *COBE* in an open model should not be a very bad approximation until we reach $\Omega \lesssim 0.2$. We shall therefore ignore this uncertainty in what follows. We also ignore corrections to the first few multipoles which arise through the time dependence of the gravitational potential in flat vacuum-dominated models (Kofman et al. 1993).

In the case of the *COBE* measurements, the simplest and most robust datum is just the sky variance convolved to 10° FWHM, i.e. $C_S(0)$ in the above expression with $\sigma = 4.^\circ25$. This can be converted into an integral over the power spectrum multiplied by a window function that is a sum over Bessel functions. In practice, it is convenient to have a simpler expression for the window, and it turns out that this can be achieved to almost perfect accuracy by using a small-angle approximation:

$$C_S(0) = \frac{\Omega^2}{g^2(\Omega)} \int 4(k[2c/H_0])^{-4}\Delta^2(k)\, W^2(kR_H)\, \frac{dk}{k}, \quad (60)$$

$$W^2(y) = [1 - j_0^2(y) - 3j_1^2(y)]\, F(y\sigma)/(y\sigma), \quad (61)$$

where $F(x)$ is Dawson's integral. The terms involving Bessel functions correspond to the subtraction of monopole and dipole terms. The window function is relatively sharply peaked and so the *COBE* variance essentially picks out the power at a given scale. For the case of $\sigma = 0.0742$ (FWHM of 10°), the result is very well fitted by

$$C_S(0) = 1.665\, \frac{\Omega^2}{g^2(\Omega)}\, [4(k_S[2c/H_0])^{-4}\Delta^2(k_S)], \quad (62)$$

$$k_S R_H = 7.29 + 2.19(n-1). \quad (63)$$

The observed value is $C^{1/2}(0) = 1.10 \pm 0.18 \times 10^{-5}$ (Smoot et al. 1992). For scale-invariant spectra, this corresponds to an rms quadrupole of $Q_{rms} = 15.0 \pm 2.5\ \mu$K. For $\Omega = 1$, this translates to a normalization of $\epsilon = 2.6 \pm 0.4 \times 10^{-5}$ in the notation of Peacock (1991). How well does this amplitude match on to the clustering observed at 100-Mpc wavelengths? If we stick to asymptotically scale-invariant spectra, the agreement is very good. The CDM fit shown in Fig. 9 requires

$$\epsilon = 3.25 \pm 0.18 \times 10^{-5}. \quad (64)$$

This is slightly higher than the *COBE* measurement, but well within experimental error. If the large-scale normalization is forced to be $\epsilon = 2.6 \times 10^{-5}$, the best-fitting CDM shape changes to $\Omega h = 0.31$. In fact, a more detailed analysis of the *COBE* data by Wright et al. (1994) yields a preferred amplitude somewhat higher than the above simple calculation, and in extremely good agreement with the fit derived from Fig. 9.

For a more general comparison, it is convenient to define a reference datum at the largest scale where our data are still accurate. From Table 1, we take this to be $\Delta^2(k = 0.028h) = 0.0087 \pm 0.0023$. At this point, there is still some curvature in the power spectrum: the $\Omega h = 0.25$ transfer function is $T_k = 0.61$ and the effective transfer function defined by the two-power-law formula is $T_k = 0.80$. We shall adopt a compromise T_k=0.70 and hence deduce

$$\Delta^2(k = 0.028h) = 0.018 \pm 0.0023 \quad (65)$$

as our best estimate of the true level of any primordial power-law fluctuations on these scales (subject to scalings as above if $\Omega \neq 1$). We can now use our earlier discussion of the *COBE* data to predict this small-scale fluctuation, ignoring for the moment any gravity-wave contribution. The answer is

$$\Delta^2(k = 0.028h) = 0.014 \exp[3.2(n-1)]\, \Omega^{-0.7} \quad \text{(open)} \quad (66)$$

$$= 0.014 \exp[3.2(n-1)]\, \Omega^{-1.6} \quad \text{(flat)}. \quad (67)$$

Thus, if we adopt $\Omega = 1$, there is a very good agreement with scale-invariance: $n = 1.08 \pm 0.04$. Conversely, tilted models do not match large and small scales very well: for $n = 0.7$, the predicted power near 100 Mpc is too small by a factor 3. Things get worse if gravity waves are included: a prediction of many inflationary models is that

$$\frac{C_\ell^G}{C_\ell^S} \simeq 6(1-n) \quad (68)$$

(e.g. Liddle & Lyth 1992; Lidsey & Coles 1992; Lucchin, Matarrese & Mollerach 1992; Souradeep & Sahni 1992), which decreases the predicted small-scale power by a further factor 2.8 for $n = 0.7$, making a total mismatch of a factor 8. It is inconceivable that our analysis of the 100-Mpc-scale power could be in error by this amount. Thus, although tilted models may be attractive in removing the one-degree 'bump' in the predicted microwave sky (Crittenden et al. 1993) and allowing consistency with intermediate-scale CMB experiments, it seems implausible that this can be the correct solution, at least if $\Omega = 1$. To allow a tilted model with $n = 0.7$, we need $\Omega \simeq 0.06$ and 0.3 respectively in the open and flat cases.

7 SUMMARY

We have analysed a compilation of recent measures of galaxy clustering, under the assumption of underlying Gaussian mass fluctuations. We have presented new methods for dealing analytically with the modifying effects of non-linear evolution and redshift-space distortions, and their effect on the power spectrum. Application of these methods to the data leads to a consistent determination of the linear mass spectrum, with the following properties.

(i) The relative bias factors for Abell clusters, radio galaxies, optical galaxies and *IRAS* galaxies must be in the ratios $b_A : b_R : b_O : b_I = 4.5 : 1.9 : 1.3 : 1$, to within 6 per cent rms.

(ii) The data require a significant degree of redshift-space distortion: $\Omega^{0.6}/b_I = 1.0 \pm 0.2$.

(iii) Low values of Ω and bias are disfavoured because non-linear evolution would spoil the agreement in shape between galaxy and cluster power spectra. Both this and the previous conclusion are in good agreement with independent studies based on peculiar-velocity fields.

(iv) The linear power spectrum is smooth and featureless, and is well described by a zero-baryon CDM model with $\Omega h = 0.25$.

(v) The amplitude of 100-Mpc power matches well to that inferred from *COBE* provided that the primordial spectrum was close to scale-invariant. Tilted models that postulate a dominant gravity-wave CMB component are difficult to reconcile with our data.

ACKNOWLEDGMENTS

SJD is supported by a SERC research studentship. We thank Hugh Couchman for the use of his AP^{3}M code, Carlton Baugh for communicating the APM power-spectrum data, and Guinevere Kauffmann & Simon White for providing N-body data.

REFERENCES

Albrecht A., Stebbins A., 1992, Phys. Rev. Lett., 69, 2615
Babul A., Postman M., 1990, ApJ, 359, 280

Bardeen J.M., Bond J.R., Kaiser N., Szalay A.S., 1986, ApJ, 304, 15 (BBKS)
Bardeen J.M., Bond J.R., Efstathiou G., 1987, ApJ, 321, 28
Baugh C.M., Efstathiou G., 1993, MNRAS, 265, 145
Bertschinger E., Dekel A., Faber S.M., Dressler A., Burstein D., 1990, ApJ, 364, 370
Bond J.R., Couchman H.M.P., 1988, in Coley A., Dyer C.C., Tupper B.O.J., eds, Proc. Second Canadian Conference on General Relativity & Relativistic Astrophysics. World Scientific, Singapore, p.385
Bond J.R., Efstathiou G., 1991, Phys. Lett. B, 265, 245
Bouchet F.R., Strauss M.A., Davis M., Fisher K.B., Yahil A., Huchra J.P., 1993, ApJ, 417, 36
Bower R.G., Coles P., Frenk C.S., White S.D.M., 1993, ApJ, 405, 403
Broadhurst T.J., Ellis R.S., Koo D.C., Szalay A.S., 1990, Nat, 343, 726
Carroll S.M., Press W.H., Turner E.L., 1992, ARA&A, 30, 499
Cen R., Ostriker J.P., 1992, ApJ, 399, L113
Cen R., Gnedin N.Y., Kofman L.A., Ostriker J.P., 1992, ApJ, 399, L11
Coles P., Plionis M., 1991, MNRAS, 250, 75
Couchman H.M.P., 1991, ApJ, 368, L23
Crittenden R., Bond J.R., Davis R.L., Efstathiou G., Steinhardt P.J., 1993, Phys. Rev. Lett., 71, 324
Davis M., Efstathiou G., Frenk C.S., White S.D.M., 1985, ApJ, 292, 371
Davis M., Summers F.J., Schlegel D., 1992, Nat, 359, 393
Dekel A., Bertschinger E., Yahil A., Strauss M.A., Davis M., Huchra J.P., 1993, ApJ, 412, 1
Efstathiou G., Bond J.R., White S.D.M., 1992, MNRAS, 258, 1P
Einasto J., Jôeveer M., Saar E., 1980, MNRAS, 193, 353
Feldman H.A., Kaiser N., Peacock J.A., 1994, ApJ, in press (FKP)
Fisher K.B., Davis M., Strauss M.A., Yahil A., Huchra J.P., 1993, ApJ, 402, 42
Gaztañaga E., 1992, ApJ, 398, L17
Gooding A.K., Park C., Spergel D.N., Turok N., Gott J.R., III, 1992, ApJ, 393, 42
Gott J.R., III, Rees M.J., 1975, A&A, 45, 365
Gramann M., Cen R., Bahcall N., 1993, ApJ, 419, 440
Hamilton A.J.S., Gott J.R., III, Weinberg D.H., 1986. ApJ, 309, 1
Hamilton A.J.S., Kumar P., Lu E., Matthews A., 1991, ApJ, 374, L1 (HKLM)
Holtzman J.A., 1989, ApJS, 71, 1
Kaiser N., 1984, ApJ, 284, L9
Kaiser N., 1987, MNRAS, 227, 1
Kaiser N., Peacock J., 1991, ApJ, 379, 482
Kaiser N., Malaney R.A., Starkman G.D., 1993, Phys. Rev. Lett., 71, 1128
Kauffmann G., White S.D.M., 1992, MNRAS, 258, 511
Klypin A., Holtzman J., Primak J., Regős E., 1993, ApJ, 416, 1
Kofman L., Gnedin N., Bahcall N., 1993, ApJ, 413, 1
Kofman L., Gelb J., Bertschinger E., Nusser A., Dekel A., 1994, ApJ, in press
Lahav O., Lilje P.B., Primak J.R., Rees M.J., 1991, MNRAS, 251, 128
Lauer T.R., Postman M., 1993. Proc. Milan meeting on observational cosmology
Liddle A.R., Lyth D., 1992, Phys. Lett. B, 291, 391
Lidsey J.E., Coles P., 1992, MNRAS, 258, 57P
Loveday J., Efstathiou G., Peterson B.A., Maddox S.J., 1992, ApJ, 400, L43
Lucchin F., Matarrese S., Mollerach S., 1992, ApJ, 401, 49
Madsen J., 1992, Phys. Rev. Lett., 69, 571
Mann R.G., 1993, PhD thesis, University of Edinburgh
Mann R.G., Heavens A.F., Peacock J.A., 1993, MNRAS, 263, 798
Mo H.J., Peacock J.A., Xia X.Y., 1993a, MNRAS, 260, 121
Mo H.J., Jing Y.P., Börner G., 1993b, MNRAS, 264, 825
Moore B. et al., 1992, MNRAS, 256, 477
Nusser A., Dekel A., 1993, ApJ, 405, 437
Peacock J.A., 1991, MNRAS, 253, 1P
Peacock J.A., 1992, in Martinez V., Portilla M., Sáez D., eds, New insights into the Universe, Proc. Valencia summer school. Springer, Berlin, p.1
Peacock J.A., Heavens A.F., 1985, MNRAS, 217, 805
Peacock J.A., Nicholson D., 1991, MNRAS, 253, 307
Peacock J.A., West M.J., 1992, MNRAS, 259, 494
Peebles P.J.E., 1973, ApJ, 185, 413
Peebles P.J.E., 1980, The Large-Scale Structure of the Universe. Princeton Univ. Press, Princeton, NJ
Peebles P.J.E., 1982, ApJ, 263, L1
Peebles P.J.E., 1993, Principles of physical cosmology. Princeton Univ. Press, Princeton, NJ
Pogosyan D.Yu., Starobinsky A.A., 1993, MNRAS, 265, 507
Saunders W., Rowan-Robinson M., Lawrence A., 1992, MNRAS, 258, 134
Scherrer R.J., 1992, ApJ, 390, 330
Smoot G.F. et al., 1992, ApJ, 396, L1
Souradeep T., Sahni V., 1992, Mod. Phys. Lett., 7, 3541
Starobinsky A.A., 1985, Sov. Astron. Lett., 11, 133
Strauss M.A., Davis M., Yahil Y., Huchra J.P., 1992, ApJ, 385, 421
Szalay A.S., Ellis R.S., Koo D.C., Broadhurst T., 1991, in Holt S.S., Bennett C.L., Trimble V., eds, After the first three minutes, Proc. AIP Conf. 222. AIP, New York, p.261
Taylor A.N., Rowan-Robinson M., 1992, Nat, 359, 396
van Dalen A., Schaefer R.K., 1992, ApJ, 398, 33
Vittorio N., Silk J., 1991, ApJ, 385, L9
Vogeley M.S., Park C., Geller M., Huchra J.P., 1992, ApJ, 391, L5
Weinberg D.H., Cole S., 1992, MNRAS, 259, 652
White S.D.M., Efstathiou G., Frenk C.S., 1993, MNRAS, 262, 1023
Wright E.L. et al., 1994, COBE preprint 93–06, ApJ, in press
Zeldovich Ya.B., 1970, A&A, 5, 84

This paper has been produced using the Blackwell Scientific Publications LaTeX style file.